INTERNATIONAL DOCTORAL
SCHOOL OF THE USC

Luigi
Bellafronte

PhD Thesis

Precision physics at High Luminosity LHC and future colliders

Santiago de Compostela, 2023

Doctoral Programme in Nuclear and Particles Physics

USC
UNIVERSIDADE
DE SANTIAGO
DE COMPOSTELA

DOCTORAL THESIS

PRECISION PHYSICS AT HIGH LUMINOSITY LHC AND FUTURE COLLIDERS

Luigi Bellafronte

INTERNATIONAL PHD SCHOOL OF THE UNIVERSITY OF SANTIAGO DE COMPOSTELA

PHD PROGRAMME IN NUCLEAR AND PARTICLES PHYSICS

SANTIAGO DE COMPOSTELA

2023

USC
UNIVERSIDADE
DE SANTIAGO
DE COMPOSTELA

DECLARATION BY THE THESIS AUTHOR

Mr/ Ms. **Luigi Bellafronte**

Thesis Title: **Precision physics at High Luminosity LHC and future colliders**

I submit my thesis, following the appropriate procedure to the Regulations and declare that:

1) The thesis covers the results of the elaboration of my work.
2) If this is the case, the thesis refers to the collaborations within this work.
3) I confirm that the thesis does not incur in any kind of plagiarism from other authors nor works submitted by me in order to obtain other titles.
4) The thesis is the final version submitted for its defence and both the printed version and the electronic version provide the same content.

And I agree to submit the Documentary Commitment of supervision in the event that the original version is not deposited at the School.

In **Santiago de Compostela**, **25th August 2023**.

Electronic signature

USC
UNIVERSIDADE
DE SANTIAGO
DE COMPOSTELA

SUPERVISOR/TUTOR AUTHORISATION

Mr/Ms **Pier Paolo Giardino**

As: **Supervisor**

Thesis title: **Precision physics at High Luminosity LHC and future colliders**

STATES:

That this thesis corresponds to the work carried out by Mr/Ms **Luigi Bellafronte**, under my supervision/tutoring and hereby authorise its presentation, taking into account that it meets all the relevant requirements stated in the Doctoral Studies Regulations of the USC, and as its director/ tutor it does not incur in the causes of abstention established in the 40/2015 Law.

In **Santiago de Compostela**, **24 August 2023**

Electronic signature

USC
UNIVERSIDADE
DE SANTIAGO
DE COMPOSTELA

SUPERVISOR/TUTOR AUTHORISATION

Mr/Ms **Néstor Armesto Pérez**

As: **Tutor**

Thesis title: **Precision physics at High Luminosity LHC and future colliders**

STATES:

That this thesis corresponds to the work carried out by Mr/Ms **Luigi Bellafronte**, under my supervision/tutoring and hereby authorise its presentation, taking into account that it meets all the relevant requirements stated in the Doctoral Studies Regulations of the USC, and as its director/ tutor it does not incur in the causes of abstention established in the 40/2015 Law.

In **Santiago de Compostela**, **28 August 2023**

Electronic signature

USC
UNIVERSIDADE
DE SANTIAGO
DE COMPOSTELA

ENG	ITA
And he to me: «This mount is such, that	*Ed elli a me: «Questa montagna è tale,*
it is always wearisome at the start below;	*che sempre al cominciar di sotto è grave;*
but the more a man proceeds, the less it hurts.	*e quant'om più va sù, e men fa male.*
And, when it shall seem so mild,	*Però, quand'ella ti parrà soave*
that going up shall be as gentle	*tanto, che sù andar ti fia leggero*
as in a boat to go down the tide,	*com'a seconda giù andar per nave,*
then at this pathway's ending you will be;	*allor sarai al fin d'esto sentiero;*
there to repose your panting breath expect.	*quivi di riposar l'affanno aspetta.*
No more I answer, and this I know for true.»	*Più non rispondo, e questo so per vero».*
~~Pier Paolo talking with Luigi about the PhD thesis~~	~~Pier Paolo parlando con Luigi della tesi di dottorato~~
Virgilio talking with Dante about how hard it was to climb Purgatory	Virgilio rispondendo a Dante su quanto fosse difficile scalare il Purgatorio

Dante Alighieri
Divina Commedia, Purgatorio, Canto IV

USC
UNIVERSIDADE DE SANTIAGO DE COMPOSTELA

Contents

Acknowledgements **10**

Resumo **11**

Resumen **13**

Summary **15**

Objectives and Methodology **17**

1 Introduction **19**

2 Standard Model **23**
2.1 Gauge Fields . . . 23
2.2 Non-abelian Higgs mechanism: the Electroweak interactions . . . 24
2.2.1 SM fermion couplings to the gauge bosons . . . 27
2.3 Mass terms in the SM . . . 28
2.3.1 Custodial symmetry . . . 31
2.4 Beyond tree level . . . 32
2.4.1 Regularization . . . 33
2.4.2 Dirac Algebra . . . 34
2.4.3 Kramer scheme . . . 35
2.5 Renormalization . . . 36
2.5.1 $\overline{MS}$ . . . 37
2.5.2 OS . . . 37

3 Higgs production from gluon fusion **39**
3.1 Overview . . . 40
3.1.1 Kinematic . . . 42
3.2 Method . . . 43
3.2.1 Pade approximant . . . 45
3.3 The p_T and HE expansions vs the exact results at LO . . . 48
3.4 Merging the p_T and HE expansions at NLO . . . 50
3.5 Conclusions . . . 54

USC UNIVERSIDADE DE SANTIAGO DE COMPOSTELA

4 Standard Model Effective Field Theory **57**
4.1 EFT . . . 58
4.2 HEFT . . . 59
4.3 SMEFT . . . 60
4.4 Warsaw basis . . . 60
4.4.1 Complete set of dimension-6 operator . . . 61
4.4.2 Dimension 5 operators . . . 61
4.4.3 Single-fermionic-current operator classification . . . 65
4.4.4 Four-fermion operator classification . . . 68
4.5 SMEFT couplings . . . 68
4.5.1 Higgs sector . . . 69
4.5.2 EW gauge sector . . . 70
4.6 Fermion sector . . . 70
4.7 Effects on observables . . . 71

5 Electroweak precision observables **73**
5.1 Overview . . . 74
5.2 Notation . . . 75
5.2.1 EWPOs . . . 76
5.3 Scenarios . . . 78
5.3.1 Flavor Assumptions: $U(3)^5$ . . . 78
5.3.2 Flavor Assumptions: MFV . . . 79
5.3.3 Flavor Assumptions: $U(2)^5$ . . . 80
5.3.4 Flavor Assumptions: Third Generation Centric . . . 81
5.3.5 Flavor Assumptions: Third Generation Phobic . . . 81
5.3.6 Flavor Assumptions: Third Generation Phobic + $U(2)^5$ . . . 82
5.3.7 Flavor Assumptions: Flavorless Scenario . . . 83
5.4 NLO calculations . . . 83
5.4.1 Real contributions . . . 85
5.4.2 Virtual contributions . . . 86
5.4.3 UV counterterms . . . 86
5.4.4 M_W calculation . . . 88
5.5 Results . . . 89
5.6 Future perspectives . . . 94
5.6.1 Results . . . 98
5.7 Conclusions . . . 102

6 Drell Yan process **105**
6.1 Overview . . . 105
6.2 Notation . . . 106
6.3 LO DY calculations . . . 107
6.4 SMEFT NLO DY calculations:
Virtual contributions . . . 109

USC UNIVERSIDADE DE SANTIAGO DE COMPOSTELA

6.5 SMEFT NLO DY calculations: Real Contributions . . . 113
6.6 Phenomenology . . . 115

7 Results and Conclusions **119**

A **121**
A.1 SMEFT . . . 121
A.2 Drell Yan . . . 122
A.3 EWPOs . . . 124

Bibliography **128**

List of publications **145**

Permissions of content reuse **147**

Resumo da tese (en galego) **149**

USC UNIVERSIDADE DE SANTIAGO DE COMPOSTELA

Acknowledgements

Questa tesi non è solo il risultato dei miei studi, ma è anche e soprattutto merito del supporto delle persone che mi sono state accanto in questo cammino. Anche se un po' complicato, cercherò di ringraziarle tutte (sperando di non dimenticare nessuno) scrivendo questa sezione alternando italiano e inglese.

Il protocollo impone per prima cosa di ringraziare il proprio advisor, solitamente per la disponibilità, i suggerimenti, le discussioni, etc. Nel mio caso, ringraziare Pier Paolo solo per questo sarebbe estremamente riduttivo. In questi tre anni, tutte le conoscenze e le competenze che ho acquisito non sarebbero state possibili senza il suo aiuto. Alcuni periodi del dottorato sono stati molto difficili e aver avuto una guida come lui è il motivo per cui questa tesi è finita e io sono qui oggi a scrivere questi ringraziamenti. Lavorare con lui è stata una immensa opportunità di apprendimento e di crescita, ed è il tipo di mentore che tutti dovrebbero avere.

During this journey, I had the privilege to work and interact with many excellent researchers. I would like to thank my university tutor Nestor, for his help and suggestions during these years. I am grateful to my collaborators Giuseppe, Sally, Ramona and Marco for the many interesting and helpful discussions; without your contributions this work would not have been possible.

Ringrazio i miei genitori, per tutto l'affetto e il sostegno che mi hanno dato anche in questo percorso; siete sempre voi la parte migliore di me. Ringrazio Dario, per esserci sempre, specialmente quando ne ho più bisogno. Ringrazio Emanuele, per l'immenso aiuto durante le varie fasi del dottorato e per le nostre *brevi* chiamate domenicali. Ringrazio gli amici di una vita Francesca, Massimo, Nanni, Klando, Fabio, Lallo e Giacomo; il vostro supporto è stato prezioso, in particolare quello degli ultimi due (loro sanno perché). Infine, vorrei ringraziare gli amici che ho conosciuto a Pisa e con cui nonostante la distanza riusciamo a tenerci in contatto: Stefano, Davide, Vittoria, Luca e Marco.

I can not acknowledge all the wonderful people I had the pleasure to meet at the IGFAE in these few lines, but I feel obliged to mention some of them. Thanks to Ricardo, for his invaluable assistance with all bureaucracy issues and not. Thanks to Miguel, for his great help with the documents translation. Thanks to my office mates Praveen and Xoán for the mutual encouragement and support during these years spent in Celda 2 of the *Covacha*. Thanks to Sam for his sincere friendship and the many drinks together. Thanks to Sara for the never ending discussions on so many topics. Finally, thanks to Clara, Marti, Arnau, Sibylle and Niels; I have been so lucky meet all of them.

USC
UNIVERSIDADE DE SANTIAGO DE COMPOSTELA

Resumo

O Modelo Estándar (SM) da física de partículas é o marco teórico actual que describe, a nivel fundamental, as interaccións entre partículas elementais. A construción de colisionadores de alta enerxía o Large Hadron Collider(LHC) no CERN, o maior acelerador de partículas construído ata o de agora, permitiu que os científicos probasen os seus modelos a escalas de enerxía cada vez maiores. Nos últimos anos, o LHC centrou cada vez máis a súa atención nas medidas de precisión dos procesos do SM, xa que xogan un papel crucial na exploración da nova física. A énfase na física de precisión tamén motivou o desenvolvemento da actualización de alta luminosidade (HL) do LHC e a proposta de novas máquinas de alta precisión, como o FCC-ee. Neste contexto, o esforzo teórico debe igualar o traballo experimental, porque as medidas precisas requiren dunha precisión igual nas predicións do SM. Este argumento tamén se aplica ás teorías máis alá do Modelo Estándar (BSM) e vólvese especialmente relevante no caso das Teorías de Campo Efetivas (EFTs), onde as correccións de orde superior poden ter un impacto significativo nos límites da nova física. O enfoque principal deste tese é o cálculo preciso dos procesos no SM e no marco da Teoría Efetiva do Modelo Estándar (SMEFT), incluíndo gg-HH, produción de Drell Yan qq-ll e observables electrofebles. Finalmente, o obxectivo é facer predicións precisas que poidan ser probadas nos colisionadores do futuro, como o HL LHC e o FCC-ee. O estudo desta área é moi importante e proporciona información crucial sobre a estrutura da nova física máis alá do SM.

USC
UNIVERSIDADE DE SANTIAGO DE COMPOSTELA

USC
UNIVERSIDADE
DE SANTIAGO
DE COMPOSTELA

Resumen

El Modelo Estándar (SM) de la física de partículas es el marco teórico actualmente establecido que describe, a nivel fundamental, las interacciones entre las partículas elementales. La construcción de colisionadores de alta energía como el Large Hadron Collider (LHC) en el CERN, el acelerador de partículas más grande jamás construido, ha permitido a los científicos probar sus modelos a escalas de energía cada vez más altas. En los últimos años, el LHC ha centrado cada vez más su atención en las mediciones precisas de los procesos del SM, ya que desempeñan un papel crucial en la exploración de la nueva física. El énfasis en la física de precisión también ha motivado el desarrollo de la actualización de alta luminosidad (HL) del LHC y la propuesta de nuevas máquinas de alta precisión, como el FCC-ee. En este contexto, el esfuerzo teórico debe igualar el trabajo experimental, porque las mediciones precisas requieren una precisión igual en las predicciones del SM. Este argumento también se aplica a las teorías más allá del Modelo Estándar (BSM) y se vuelve especialmente relevante en el caso de las Teorías de Campo Efectivas (EFT), donde las correcciones de orden superior pueden tener un impacto significativo en los límites de la nueva física. El enfoque principal de este tesis es el cálculo preciso de los procesos en el SM y en el marco de la Teoría Efectiva del Modelo Estándar (SMEFT), incluyendo gg-HH, producción de Drell Yan qq-ll y observables electrodébiles. Finalmente, el objetivo es hacer predicciones precisas que puedan ser probadas en futuros colisionadores, como el HL LHC y el FCC-ee. El estudio de esta área es muy importante y proporciona información crucial sobre la estructura de la nueva física más allá del SM.

USC
UNIVERSIDADE DE SANTIAGO DE COMPOSTELA

USC
UNIVERSIDADE
DE SANTIAGO
DE COMPOSTELA

Summary

The Standard Model (SM) of particle physics is the currently established theoretical framework which describes, at a fundamental level, interactions among elementary particles. The construction of high-energy colliders such as the Large Hadron Collider (LHC) at CERN, the largest particle accelerator ever built, allowed scientists to test their models at increasingly high energy scales. In recent years, the LHC has increasingly focused its attention on the precise measurements of SM processes, as they play a crucial role in the exploration of new physics. The emphasis on precision physics has also motivated the development of the high luminosity (HL) LHC upgrade, and the proposal of new high precision machines such as the FCC-ee. In this context, the theoretical effort has to match the experimental work, because precise measurements require an equal precision of the SM predictions. This argument applies also to theories Beyond the Standard Model (BSM), and it becomes particularly relevant in the case of Effective Field Theories (EFTs), where higher-order corrections can significantly impact the bounds on new physics. The main focus of this thesis is the precision calculation of processes in the SM and Standard Model Effective Field Theory (SMEFT) framework, including $gg \to HH$, Drell Yan production $qq \to ll$, and electroweak observables. Finally, the ultimate goal is to make accurate predictions that can be tested on future colliders, such as HL LHC and Fcc-ee. The study of this area is very important, and it gives crucial information on the structure of new physics beyond the SM.

USC
UNIVERSIDADE DE SANTIAGO DE COMPOSTELA

USC
UNIVERSIDADE
DE SANTIAGO
DE COMPOSTELA

Objectives and Methodology

The main goal of this thesis is to test physical phenomena at LHC and future colliders by providing accurate calculations of sensitive observables.

Historically, precise calculations of observables have played a crucial role in our search to understand the Nature. Indeed, they allowed us to rigorously test the theories formulated to comprehend the universe. For this reason, in this thesis we calculated the perturbative corrections to SM and SMEFT processes that are phenomenologically relevant for physics at the LHC and future colliders. These include:

- The NLO correction to the production of a pair of H bosons and HZ bosons from gluon fusion. The calculation of these processes is extremely important for the experimental measurement of the Higgs properties and it used to measure the Higgs width. In particular, the double higgs production is significantly relevant because of the triple Higgs coupling involved in the calculation.

- The calculation of EWPOs at the next-to-leading order (NLO) QCD and electroweak expansions of the SMEFT with an arbitrary flavor structure for the fermion operators. Numerical NLO SMEFT fits to EWPOs are expected to have a strong dependence on the assumed flavor structures and we will check this using various popular assumptions for flavor symmetries.

- Drell Yan production in the SM EFT at NLO; this process is very important to detect new physics signals and precise theoretical predictions in the effective field theory are crucial. The effects of four fermions operators on this amplitude is a new challenge and it will give us essential knowledge on the structure of the BSM physics, in particular on the flavour structure.

All the required the calculations are performed analytically. Indeed while there are purely numerical methods that could be used, hybrid numerical/analytical techniques are generally more flexible and easier to adapt to broader uses, such as EFTs, than the purely numerical ones. Furthermore, they are computationally less intensive, making them better suited to build efficient Monte Carlo generators. For these reasons analytical calculations are more convenient to our aims.

USC
UNIVERSIDADE
DE SANTIAGO
DE COMPOSTELA

Methodology

As explained, the main objective of this thesis is the study of precision physics in the SM and its extensions. This involve the application of tools for the precise calculation of processes relevant for the phenomenology of the LHC and future colliders.

To achieve our goals we use public and private codes implemented in the software Mathematica. The relevant amplitudes for the scattering or the decay in analysis are generated with FeynArts [1] and we use Feyncalc, LiteRed and Fire [2, 3, 4] to reduce the amplitudes into a combination of Master Integrals (MI). Feynman integrals are calculated through standard methods when possible and through the energy expansions techniques when necessary. At one loop level we use the Passarino-Veltman functions as basis for the MI and the analytical evaluations is done through FeynHelpers [5]. We use the *Padé Approximants* to improve the convergence of energy expansions to allow us to extend the validity of these techniques to regions of the phase space where these approaches should otherwise fail. This method is applied to physical processes such as $gg \to HZ$ and $gg \to HH$ in order to improve the accuracy of the results obtained in [6, 7] and allowing us to match with the results of [8]. In this way we are able to make a prediction at every point of the parameter space with high precision.
The problems arising by the presence of γ^5 and several Dirac nmatrices are treated with Kreimer's regularization scheme [9], a powerful tool that preserves the chiral symmetry of the Standard Model in all bare perturbative calculations. All the SMEFT calculations are done in the Warsaw basis with the FeynArts model file obtained from [10]. Finally, we use plots and bar diagrams to present our phenomenological results.

USC UNIVERSIDADE DE SANTIAGO DE COMPOSTELA

Chapter 1

Introduction

The investigation of the natural phenomena has been one of the driving forces behind scientific advancement. Regarding particle physics, this pursuit has led to the development of the Standard Model (SM), an outstanding successful framework that describes and classifies the elementary particles and their interactions. This culminated with the discovery of the Higgs boson in 2012 [11, 12], marking a further essential step towards a satisfactory understanding of the mechanism underlying the electroweak-symmetry breaking (EWSB). Nevertheless, even with its triumphs, the SM leaves numerous theoretical and experimental questions unanswered. Examples of the latter include neutrino oscillations and dark matter. From a theoretical point of view, we can mention the hierarchy of the fermion masses, the mystery of the origin of the Higgs potential and the inclusion of gravity (beyond the classical level) in the SM framework.
In this context, particle colliders have played a crucial role in shaping our understanding of the fundamental laws of the universe. The construction of high-energy colliders such as Tevatron, LEP and the Large Hadron Collider (LHC) at CERN, the largest particle accelerator ever built, allowed scientists to test their models at increasingly high energy scales driving discoveries and confirming theories. After the discovery of the Higgs boson, none of the measured observables indicated clearly the energy scale of physics beyond the Standard Model (BSM). Indeed, only events predicted by the SM have been seemingly detected at particle colliders.

In recent years the precise measurement of SM processes has taken a prominent role as a fundamental instrument in the search of new physics. Anomalies in precision measurements, like deviations from expected values, can be an indirect indication of new phenomena. Indeed, through off-shell and loop effects, we can observe the influence of new particles without directly producing them.

In general, the phenomena we are looking for have very low probability of occurring, making the detection process demanding. This aspect is particularly relevant in precision physics, since the measurement of small variations from the expected predictions requires large amount of data. One of the central motivations behind the planned high luminosity (HL) LHC upgrade [13] is the development of the capabilities of the LHC

USC
UNIVERSIDADE DE SANTIAGO DE COMPOSTELA

as a precision machine. Increasing luminosity facilitates the generation of more data, which not only enables a more comprehensive examination of established mechanisms but, as already mentioned, opens also the door to the observation of unexpected new phenomena.

For instance, the upcoming HL LHC is projected to generate a minimum of 15 million Higgs bosons annually, a significant increase compared to the about three million collected during the LHC operation in 2017 [14]. This enhancement will allow us to put more stringent constraints on many SM parameters. In this context, gluon fusion, which is already the most relevant production mechanism [15, 16] for Higgs physics, will be even more significant. It plays an important role in double-Higgs production, $gg \to HH$, and it is also relevant in the production of a Higgs boson in association with a Z boson, $gg \to ZH$. These two scatterings are very important for Higgs physics. The first one receives contributions from the Higgs trilinear interaction, one of few SM couplings still not measured. The second one is one of main channel for ZH and it allows to study Higgs decays to bottom quarks, a tricky process to observe in hadronic colliders due to QCD background. For this reason, in this thesis we studied the next-to-leading-order (NLO) virtual contributions for these processes.
Indeed, the experimental effort needs to be complemented by an equivalent level of theoretical work. This is essential because, in order for the measurements to hold importance, our SM predictions have to match the precision of experimental results.

This reasoning also applies to theories beyond the SM, and it is specially important when considering Effective Field Theories (EFT). Indeed, without relying on a specific BSM model, an extension of the SM with higher-dimensional operators provides an important way to describe indirect BSM phenomena. One of the most commonly used method to study new physics effects is the Standard Model Effective Field Theory (SMEFT), which mantains the same field composition and symmetries as the SM. In this context, investigating the properties of massive electroweak gauge bosons (W and Z bosons) has significant potential for indirect searches of BSM physics. We can divide in two classes the processes that have been studied to explore this direction. The first one includes the multi-boson processes at high-energy colliders; the second one involves the fermion scattering processes mediated by s- or t-channel W/Z bosons, also known as the Electroweak Precision Observables (EWPOs). In this thesis we focus on the latter.

In the last decades, EWPOs have offered clear indications that the SM accurately describes physics at the EW scale, since they are sensitive to modifications of the gauge-boson–fermion couplings and of the gauge-bosons masses. In recent years the analysis of these measurements has been extended also beyond the the SM framework. Indeed, within the SMEFT approach, the comparison of EWPOs with theoretical predictions can put significant bounds on the coefficients associated with new physics. In this context, at leading order (LO) in SMEFT numerous studies have been performed, extracting limits on the coefficients of dimension-6 operators from global fits on EWPOs and other

USC UNIVERSIDADE DE SANTIAGO DE COMPOSTELA

observables [17, 18, 19, 20]. Given these considerations, it is reasonable to consider extending the calculations to the next-to-leading-order (NLO). In this thesis, we calculated the NLO contributions both in QCD and EW considering an arbitrary flavor structure for the fermion operators. As we will see in the following, these calculations allow us not only to study the impact of the NLO corrections on the LO coefficients, but they would also give us the possibility to constrain coefficients that do not appear at tree level.
Regarding the study of the EWPOs, we must also notice that it is one of the motivations behind the planned construction of many future colliders [21]. Indeed, the investigation of these observables at e^+e^- colliders has the advantages deriving from the clean and controlled initial state, whereas other colliders such as LHC are affected by large systematic uncertainties due to parton distributions functions and other QCD effects. Therefore, colliders such as the International Linear Collider (ILC) [22, 23, 24] and the Future Circular Collider-ee (Fcc-ee) [25, 26], can potentially have a better sensitivity for EWPOs than hadron colliders. As discussed in [21], projected statistical and systematic uncertainties of these future colliders are expected to improve the accuracy of the current experimental values. Considered this, using our EWPOs results, we performed an analysis with these expected error values.

Another relevant process we can mention for indirect searches of BSM physics, is the Drell-Yan scattering. In particular, the neutral Drell-Yan process, where $pp \to Z/\gamma \to l^+l^-$, has had fundamental importance in confirming the predictions of the SM and has had different applications. For example, it has been useful to explore new physics scenarios, such as the presence of high-mass Z' bosons. The current SM results perfectly align with experimental data [27, 28], suggesting that BSM physics, within DY production, either appears at high energy scale or it has extremely weak coupling, making the detection a difficult challenge for current experimental setups.
The upcoming HL-LHC upgrade is expected to significantly impact the study of the Drell-Yan process. Indeed, increasing the luminosity will increase the number of events being produced and a larger statistical sample will allow for more precise measurements. Additionally, although HL-LHC will operate approximately at the same hadronic energy (~ 14 TeV) of the current LHC, the increase in luminosity will allow us to explore higher collision energies at partonic level. Indeed, LHC accelerates protons but the actual collisions occur between quarks and gluons. These internal particles hold only a portion of the proton energy, making high-energy collisions rare. Therefore, a straightforward approach to increase the number of such collisions is to increase the collision rate or, in other words, boost the luminosity of the collider. In the SMEFT framework, new physics phenomena might manifest as partonic energy scales rise, demanding precise SMEFT calculations that are beyond the current SM outcomes of the Drell Yan process. For this reason, we calculated NLO contributions for this scattering with the aim of studying the associated high energy distribution.

This thesis is divided as follows. In Chapter 2 we provide a brief review of the SM, including regularization and renormalization procedures. In Chapter 3, we analyze the

USC
UNIVERSIDADE DE SANTIAGO DE COMPOSTELA

SM virtual corrections to Higgs production via $gg \to HH$ and $gg \to ZH$ at the NLO level; in particular, we demonstrate that it is possible to cover the entire region of the phase space by merging two complementary expansions present in literature [29, 30]. In Chapter 4, we discuss the EFT method, focusing on the Warsaw basis of SMEFT. This basis is used as theoretical framework employed for calculations in Chapters 5 and 6. In Chapter 5, within SMEFT, we present results for EWPOs at the NLO both in QCD and EW considering an arbitrary flavor structure for the fermion operators. Additionally, assuming specific flavor scenarios, we perform fits to EWPOs including also analyses with projected uncertainties from future colliders. In Chapter 6, we provide analytical NLO QCD and electroweak contributions for the neutral Drell-Yan process, with all dimension-6 operators in the SMEFT framework. Finally, in Chapter 7 we present our results and conclusions.

USC UNIVERSIDADE DE SANTIAGO DE COMPOSTELA

Chapter 2

Standard Model

The Standard Model (SM) of particle physics is a comprehensive framework that describes the fundamental particles of the universe and their interactions [1]. It is the result of half a century of experimental observations and theoretical work, and it stands as one of the most successful and tested theories in modern physics. The components of the SM are essentially three: the fermionic matter, the gauge bosons and the Higgs boson. The way in which these particles interact each others is described through the SM Lagrangian:

$$\mathcal{L}^{SM} = -\frac{1}{4}F_{\mu\nu}F^{\mu\nu} + |D_\mu\phi|^2 + \mu^2\phi^\dagger\phi - \frac{\lambda}{2}(\phi^\dagger\phi)^2 + i\bar{\mathcal{F}}\not{D}\mathcal{F} + \left(y\bar{\mathcal{F}}_L\phi\mathcal{F}_R + h.c\right). \quad (2.1)$$

In this chapter, we will analyse and discuss each piece of 2.1. First we will start reviewing the gauge field strength tensors and their derivative. Then, we will discuss in some detail how the Higgs mechanism works in the case of a non-abelian gauge symmetry, i.e. in the SM case. Focusing on the fermion sector, we will study the problem of generating masses for quarks and leptons and their interactions with the Higgs and gauge bosons. Recall that, in the SM, one is not allowed to introduce renormalizable mass terms in the Lagrangian. Indeed, since the left- and right-handed components carry different gauge quantum numbers and such a term would violate the gauge symmetry. Finally, we will discuss the regularization and renormalization procedures, analyzing some of the methods we will use in this thesis.

2.1 Gauge Fields

In [31, 32, 33], combining two of the fundamental forces, Glashow, Weinberg and Salam (GWS) introduced the Electroweak interactions (EW) in their modern form. Instead, the strong interaction, was a more collective work, but nevertheless it is possible to recognize as fathers of the modern Quantum Chromodynamics (QCD), Murray Gell-Mann, George Zweig, Oscar W.Greenberg, Moo-Young Han and Yoichiro Nambu [34,

[1] excluding gravity

USC UNIVERSIDADE DE SANTIAGO DE COMPOSTELA

35, 36, 37]. All together, their work established that the fundamental vector fields of the SM are associated with the non-abelian gauge group

$$G_{\rm SM} \equiv SU(3)_C \otimes SU\,(2)_W \otimes U(1)_Y. \tag{2.2}$$

The covariant derivative of a field belonging to a generic representation of this group is defined as:

$$D_\mu = (\partial_\mu - igW_\mu^a \tau^a - ig' B_\mu Y - ig_s T^A G_\mu^A) \tag{2.3}$$

where G_μ^i, $i = 1, \ldots, 8$, W_μ^i, $i = 1, 2, 3$, B_μ are the gauge bosons of $SU(3)_C$,$SU(2)_W$,$U(1)_Y$ respectively, and $Y = \frac{1}{2}\mathbf{1}_{2\times 2}$, $\tau^a = \frac{\sigma^a}{2}$, $a = 1, 2, 3$, with σ^a being the customary Pauli matrices. The gauge field tensors and their covariant derivatives are:

$$\begin{aligned}
G^A_{\mu\nu} &= \partial_\mu G^A_\nu - \partial_\nu G^A_\mu - g_s f^{ABC} G^B_\mu G^C_\nu\,, & (D_\rho G_{\mu\nu})^A &= \partial_\rho G^A_{\mu\nu} - g_s f^{ABC} G^B_\rho G^C_{\mu\nu}\,,\\
W^I_{\mu\nu} &= \partial_\mu W^I_\nu - \partial_\nu W^I_\mu - g\epsilon^{IJK} W^J_\mu W^K_\nu\,, & (D_\rho W_{\mu\nu})^I &= \partial_\rho W^I_{\mu\nu} - g\epsilon^{IJK} W^J_\rho W^K_{\mu\nu}\,,\\
B_{\mu\nu} &= \partial_\mu B_\nu - \partial_\nu B_\mu\,, & D_\rho B_{\mu\nu} &= \partial_\rho B_{\mu\nu}
\end{aligned} \tag{2.4}$$

where f^{ABC} and ϵ^{IJK} are the structure constants of $SU(3)_C$ and $SU(2)_W$. Since they are completely anti-symmetric by definition, it is easy to see that all the gauge fields tensors are anti-symmetric in the Lorentz indices. The associated kinetic Lagrangian is:

$$\mathcal{L} = -\frac{1}{4} G^A_{\mu\nu} G^{A\mu\nu} - \frac{1}{4} W^I_{\mu\nu} W^{I\mu\nu} - \frac{1}{4} B_{\mu\nu} B^{\mu\nu} \tag{2.5}$$

Finally, we define the dual tensors as:

$$\widetilde{X}_{\mu\nu} = \frac{1}{2}\epsilon_{\mu\nu\rho\sigma} X^{\rho\sigma} \tag{2.6}$$

where X can be G^A. W^I or B. Other terms that can be included in the Lagrangian are:

$$\begin{gathered}
\widetilde{G}^A_{\mu\nu} G^A_{\mu\nu}\\
\widetilde{W}^I_{\mu\nu} W^I_{\mu\nu}
\end{gathered} \tag{2.7}$$

these terms show topological quantum effects that we will not explore in this thesis, since the Feynman rules and the equations of the motion result independent of them.

2.2 Non-abelian Higgs mechanism: the Electroweak interactions

The construction of the EW part of the SM requires the application of the Higgs mechanism to the non-abelian gauge group $G_{\rm SM} \equiv SU\,(2)_W \otimes U(1)_Y$. In order to break this symmetry spontaneously, we introduce a scalar field $\phi = (\phi^+, \phi^0)^T$ which is a doublet of $SU(2)_W$, and we assign it an hypercharge $+\frac{1}{2}$ under the $U(1)_Y$ so that the complete gauge transformation is

$$\phi \to e^{i\alpha^a \tau^a} e^{i\frac{\beta}{2}} \phi. \tag{2.8}$$

USC UNIVERSIDADE DE SANTIAGO DE COMPOSTELA

If the field ϕ acquires a vacuum expectation value (VEV) of the form:

$$\langle 0|\phi|0\rangle = \frac{1}{\sqrt{2}}\begin{pmatrix}0\\ v\end{pmatrix}, \tag{2.9}$$

then a gauge transformation with

$$\alpha^1 = \alpha^2 = 0 \quad \alpha^3 = \beta \tag{2.10}$$

leaves the VEV invariant. This means that the theory will contain one massless gauge boson, corresponding to the generator that preserves the vacuum. This matches the expectation that only one gauge boson remains massless in the EW interactions, corresponding to the photon. The remaining three generators become massive by virtue of the Higgs mechanism. In order to show this, we write the covariant derivative acting on ϕ as:

$$D_\mu\phi = (\partial_\mu - igW_\mu^a\tau^a - ig'B_\mu Y)\phi\,. \tag{2.11}$$

Then, we consider the following renormalizable Lagrangian:

$$\mathcal{L}_H = |D_\mu\phi|^2 + \mu^2\phi^\dagger\phi - \frac{\lambda}{2}(\phi^\dagger\phi)^2. \tag{2.12}$$

For $\mu^2 > 0$, $\lambda > 0$ the potential has a global minimum for

$$v = \left(\frac{2\mu^2}{\lambda}\right)^{\frac{1}{2}}, \tag{2.13}$$

which means that spontaneous symmetry breaking occurs, as expected.

In order to study the fluctuations around the vacuum, we parametrize the field ϕ as

$$\phi = e^{i\frac{\theta_a(x)}{v}\tau^a}\begin{pmatrix}0\\ \frac{v+h(x}{\sqrt{2}})\end{pmatrix}, \tag{2.14}$$

where θ_a and h are real scalar fields.
Using the gauge symmetry, it is possible to reabsorb the matrix $e^{i\frac{\theta_a(x)}{v}\tau^a}$ and then reduce ϕ to a field with one physical degree of freedom. Working in the unitary gauge the kinetic term of the Lagrangian becomes:

$$\frac{1}{2}\partial_\mu h\partial^\mu h + \frac{1}{2}\frac{v^2}{4}\Big(1+\frac{h}{v}\Big)^2\Big[g^2(W_\mu^1)^2 + g^2(W_\mu^2)^2 + (-gW_\mu^3 + g'B_\mu)^2\Big]. \tag{2.15}$$

There are three massive vector bosons, which are defined as follows:

$$\begin{array}{rll} W_\mu^\pm = \frac{1}{\sqrt{2}}(W_\mu^1 \mp W_\mu^2) & \text{with square mass} & m_W^2 = g^2\frac{v^2}{4} \\ Z_\mu = \frac{1}{\sqrt{g^2+g'^2}}(gW_\mu^3 - g'B_\mu) & \text{with square mass} & m_Z^2 = (g^2+g'^2)\,\frac{v^2}{4}. \end{array}$$

USC UNIVERSIDADE DE SANTIAGO DE COMPOSTELA

The fourth vector field, orthogonal to Z^0_μ, remains massless

$$A_\mu = \frac{1}{\sqrt{g^2+g'^2}}(gW^3_\mu + g'B_\mu). \tag{2.16}$$

The covariant derivative can be rewritten in terms of these mass eigenstate fields as:

$$\begin{aligned} D_\mu = \partial_\mu - i\frac{g}{\sqrt{2}}(W^+_\mu\tau^+ + W^-_\mu\tau^-) - i\frac{1}{\sqrt{g^2+g'^2}}Z_\mu(g^2\tau^3 - g'^2Y) \\ - i\frac{gg'}{\sqrt{g^2+g'^2}}A_\mu(\tau^3+Y), \end{aligned} \tag{2.17}$$

where $\tau^\pm = (\tau^1 \pm i\tau^2)$. The last term of this equation shows that the massless gauge boson A_μ couples to the gauge generator $(\tau^3 + Y)$, as expected from equation (2.10). It is possible to identify this boson as the photon and the coefficient in front of the field as the electric charge of the electron:

$$e = \frac{gg'}{\sqrt{g^2+g'^2}}\,. \tag{2.18}$$

In order to simplify the notation, we define the weak mixing angle θ_W, to be the angle that appears in the change of basis from (W^3_μ, B_μ) to (Z_μ, A_μ):

$$\begin{pmatrix} Z \\ A \end{pmatrix} = \begin{pmatrix} \cos\theta_W & -\sin\theta_W \\ \sin\theta_W & \cos\theta_W \end{pmatrix} \begin{pmatrix} W^3 \\ B \end{pmatrix} \tag{2.19}$$

that is

$$\cos\theta_W = \frac{g}{\sqrt{g^2+g'^2}}, \qquad \sin\theta_W = \frac{g'}{\sqrt{g^2+g'^2}}. \tag{2.20}$$

Notice that all the gauge couplings can be described by the electric charge and this parameter. Indeed, defining the electric charge as

$$Q = \tau^3 + Y \tag{2.21}$$

we can rewrite the covariant derivative in equation (2.17) in the form

$$D_\mu = \partial_\mu - i\frac{g}{\sqrt{2}}(W^+_\mu\tau^+ + W^-_\mu\tau^-) - i\frac{g}{\cos\theta_W}Z_\mu(\tau^3 - \sin^2\theta_W Q) - ieA_\mu Q \tag{2.22}$$

where

$$g = \frac{e}{\sin\theta_W}. \tag{2.23}$$

Therefore all the couplings of all the weak bosons are described by two parameters

$$e \quad \text{and} \quad \theta_W.$$

USC UNIVERSIDADE DE SANTIAGO DE COMPOSTELA

The interactions involving Z and W will also involve the masses of these particles, which respect the relation

$$m_W = m_Z \cos\theta_W. \tag{2.24}$$

This means that all the effects of W and Z exchange process, at least at tree-level, can be written in terms of m_Z, e and θ_W.
It is also useful to define the parameter:

$$\rho \equiv \frac{m_W^2}{m_Z^2 \cos^2\theta_W} = 1. \tag{2.25}$$

The equation (2.25) is experimentally confirmed at the per mille level [38]. As we will see below, it is related to the so-called custodial symmetry of the SM. Whatever mechanism one introduces to study beyond the Standard Model (BSM) theories, is highly constrained to reproduce this result.

2.2.1 SM fermion couplings to the gauge bosons

Using the covariant derivative in equation (2.22) we can determine the couplings of the vector bosons to the SM fermions, once the quantum number of fermions fields are set. Taking in account the fact that (experimentally) the W boson couple only to left-handed quarks and leptons, we assign the left-handed SM fermions to doublets of $SU(2)_W$ while making the right-handed singlet under this group. Once the τ^3 value has been specified for each fermions, the value Y can be set using the electric charge operator. The right-handed fermions have $\tau^3 = 0$, so the hypercharge is equal to Q. In particular, the right-handed neutrino is completely uncharged, under the SM gauge group. Instead, for the left-handed field we have

$$l_L = \begin{pmatrix} \nu_e \\ e^- \end{pmatrix}_L, \qquad q_L = \begin{pmatrix} u \\ d \end{pmatrix}_L \tag{2.26}$$

and assigning $Y = -\frac{1}{2}$ to the lepton doublet and $Y = +\frac{1}{6}$ to the quark doublet, we reproduce the correct electric charge. Notice that, the left- and the right- handed fermions live in different fundamental representations of the SM gauge group, so an useful way to look at them is to think of these components as distinct particles.
The kinetic Lagrangian follows directly from the quantum numbers assignment and is

$$\mathcal{L} = i\bar{l}_L \not{D} l_L + i\bar{q}_L \not{D} q_L + i\bar{e}_R \not{D} e_R + i\bar{u}_R \not{D} u_R + i\bar{d}_R \not{D} d_R \tag{2.27}$$

where the covariant derivative is given by equation (2.22). We omitted the right-handed neutrino in the kinetic term since would have zero coupling both to $SU(2)$ and $U(1)$. Expanding the covariant derivative, the Lagrangian becomes

$$\mathcal{L} = i\bar{l}_L \not{\partial} l_L + i\bar{q}_L \not{\partial} q_L + i\bar{e}_R \not{D} e_R + i\bar{u}_R \not{\partial} u_R + i\bar{d}_R \not{\partial} d_R + \tag{2.28}$$

$$+ g(W_\mu^+ J_W^{\mu+} + W_\mu^- J_W^{\mu-} + Z_\mu J_Z^\mu) + eA_\mu J_{EM}^\mu \tag{2.29}$$

USC UNIVERSIDADE DE SANTIAGO DE COMPOSTELA

where

$$J_W^{\mu+} = \frac{1}{\sqrt{2}}(\bar{\nu}_L\gamma^\mu e_L + \bar{u}_L\gamma^\mu d_L) \tag{2.30}$$

$$J_W^{\mu-} = \frac{1}{\sqrt{2}}(\bar{e}_L\gamma^\mu \nu_L + \bar{d}_L\gamma^\mu u_L) \tag{2.31}$$

$$\begin{aligned} J_Z^\mu = \frac{1}{\cos\theta_W}\Big[&\bar{\nu}_L\gamma^\mu(\frac{1}{2})\nu_L \\ &+ \bar{e}_L\gamma^\mu(-\frac{1}{2} + \sin^2\theta_W)e_L + \bar{e}_R\gamma^\mu(\sin^2\theta_W)e_R \\ &+ \bar{u}_L\gamma^\mu(\frac{1}{2} - \frac{2}{3}\sin^2\theta_W)u_L + \bar{u}_R\gamma^\mu(-\frac{2}{3}\sin^2\theta_W)u_R \\ &+ \bar{d}_L\gamma^\mu(-\frac{1}{2} + \frac{1}{3}\sin^2\theta_W)d_L + \bar{d}_R\gamma^\mu(\frac{1}{3}\sin^2\theta_W)d_R\Big] \end{aligned} \tag{2.32}$$

$$J_{EM}^\mu = \bar{e}\gamma^\mu(-1)e + \bar{u}\gamma^\mu(+\frac{2}{3})u + \bar{d}\gamma^\mu(-\frac{1}{3})d \tag{2.33}$$

where in the EM current is written in the Dirac notation since the left and the right handed couplings are equal.
Notice that the J_W currents, mix the up and the down components of each left doublet.

2.3 Mass terms in the SM

In writing the Higgs field couplings to the fermions, we will first analyze the quark couplings to the Higgs field ϕ and then we will discuss to lepton case.
The six left-handed quarks are arranged into three doublet of $SU(2)_w$, as follows

$$q_L = \begin{pmatrix} u_i \\ d_i \end{pmatrix}_L = \left(\begin{pmatrix} u \\ d \end{pmatrix}_L, \begin{pmatrix} c \\ s \end{pmatrix}_L, \begin{pmatrix} t \\ b \end{pmatrix}_L \right) \tag{2.34}$$

having hypercharge $Y = +\frac{1}{6}$. On the other hand, the six right-handed quarks are singlets under $SU(2)_w$: the up-type quarks carry hypercharge $Y = \frac{2}{3}$, while the down-type ones have $Y = -\frac{1}{3}$:

$$u_R^i = \{u_R, c_R, t_R\}, \qquad d_R^i = \{d_R, s_R, b_R\} \tag{2.35}$$

Without assuming any flavour conservation (or any other additional symmetry), the most general, renormalizable, gauge invariant term that involves the fields Q_L^i, u_R^i, d_R^i and ϕ is:

$$\mathcal{L}_m = -\lambda_d^{ij}\bar{q}_L^i\phi d_R^i - \lambda_u^{ij}\bar{q}_L^i(i\sigma_2\phi^*)u_R^i + h.c \tag{2.36}$$

where λ_u^{ij} and λ_d^{ij} are generic 3×3 complex matrices. We can simplify the form of this Lagrangian by making a chiral transformation in flavour space. To find the appropriate transformations we notice that by squaring λ_u we obtain two Hermitian matrices $\lambda_u\lambda_u^\dagger$ and $\lambda_u^\dagger\lambda_u$. This can be diagonalized by defining the unitary matrices U_u and W_u

$$\lambda_u\lambda_u^\dagger = U_u D_u^2 U_u^\dagger \qquad \lambda_u^\dagger\lambda_u = W_u D_u^2 W_u^\dagger \tag{2.37}$$

USC UNIVERSIDADE DE SANTIAGO DE COMPOSTELA

where D_u^2 is a diagonal matrix with positive eigenvalues. Then we can write

$$\lambda_u = U_u D_u W_u^\dagger \tag{2.38}$$

where D_u is the diagonal matrix whose diagonal elements are the positive square-roots of the eigenvalues of D_u^2. By similar considerations we can write λ_d as

$$\lambda_d = U_d D_d W_d^\dagger \tag{2.39}$$

Notice that the unitary matrices $U_{u,d}$ and $W_{u,d}$ can still be multiplied on the right by the same phase matrix:

$$\begin{bmatrix} e^{i\alpha_1} & 0 & 0 \\ 0 & e^{i\alpha_2} & 0 \\ 0 & 0 & e^{i\alpha_3} \end{bmatrix} \tag{2.40}$$

without modifying the matrices $\lambda_{u,d}$.

We are now ready to make the change of variables with the following transformations

$$u_R^i = W_u^{ij} u_R^i \qquad d_R^i = W_d^{ij} d_R^i \,. \tag{2.41}$$

Since the right-handed quarks u_R^i and d_R^i do not couple to each other through the kinetic terms, the matrices W_u and W_d disappear from the theory.
Again, we perform the change of variables:

$$u_L^i = U_u^{ij} u_R^i \qquad d_L^i = U_d^{ij} d_L^i \,. \tag{2.42}$$

These transformations eliminate U_u and U_d from the terms in (2.37) that involve the lower component of the field ϕ. In unitary gauge only these terms survive. If we now define

$$m_u = \frac{v}{\sqrt{2}} D_u \qquad m_d = \frac{v}{\sqrt{2}} D_d \,, \tag{2.43}$$

in unitary gauge, the equation (2.37) becomes:

$$\mathcal{L}_m = -m_u^{ij} \bar{u}_L^i u_R^j (\, 1 + \frac{h}{v} \,) - m_d^{ij} \bar{d}_L^i d_R^j (\, 1 + \frac{h}{v} \,) + h.c \tag{2.44}$$

The transformations carried out in equation (2.42) have some implications in the kinetic Lagrangian, because u_L and d_L are mixed by the weak interactions.
The only relevant terms are the couplings of the left-handed quarks with the gauge bosons $W^\pm$:

$$\bar{u}_L \gamma^\mu d_L \to \bar{u}_L \gamma^\mu U_u^\dagger U_d d_L \,. \tag{2.45}$$

This means that the charge-changing weak interactions mix the three generations of u_L^i quarks with three generations of d_L^i quarks, through a unitary matrix:

$$V_{CKM} = U_u^\dagger U_d \tag{2.46}$$

where V_{CKM} is known as the Cabibbo-Kobayashi-Maskawa (CKM) mixing matrix.
In general, a unitary 3×3 matrix can be parametrized using six imaginary phases and

USC UNIVERSIDADE DE SANTIAGO DE COMPOSTELA

three rotation angles. Nevertheless, in our case we can still remove[2] five of this phases by performing a change of variables on the quark fields:

$$u^i_{L,R} \to e^{i\alpha_i} u^i_{L,R} \qquad d^i_{L,R} \to e^{i\beta_i} d^i_{L,R} \tag{2.47}$$

The final form of V_{CKM} will contain three rotation angle and one imaginary phase. The latter is responsible of the CP violation of weak interaction.
Finally, we discuss the Higgs coupling with the leptons. Like for the quarks sector we have 3 generations of leptons that correspond to three left-handed doublets

$$l_L = \begin{pmatrix} \nu_i \\ e_i \end{pmatrix}_L = \left(\begin{pmatrix} \nu_e \\ d \end{pmatrix}_L, \begin{pmatrix} \nu_\mu \\ \mu \end{pmatrix}_L, \begin{pmatrix} \nu_\tau \\ \tau \end{pmatrix}_L \right) \tag{2.48}$$

each one with hypercharge $Y = -\frac{1}{2}$, while there are only three right-handed singlet leptons and they have hypercharge $Y = -1$ (the charged leptons)

$$e^i_R = \{e_R, \mu_R, \tau_R\}. \tag{2.49}$$

We now write the Yukawa couplings involving the above fields and the field ϕ as

$$\mathcal{L}_m = -\lambda^{ij}_e \bar{l}^i_L \phi e^i_R + h.c. \tag{2.50}$$

Neglecting the right-handed neutrino we have only one coupling. Following the same steps we did for the quark sector, we can write

$$\lambda_e = U_e D_e W^\dagger_e \tag{2.51}$$

and make the change of variables

$$e^i_L \to U^{ij}_e e^j_L \qquad \nu^i_L \to U^{ij}_e \nu^j_L \qquad e^i_R \to W^{ij}_e e^j_R \tag{2.52}$$

In unitary gauge the Lagrangian (2.50) reads

$$\mathcal{L}_m = -m^{ij}_e \bar{e}^i_L e^j_R (\, 1 + \frac{h}{v}\,) + h.c \tag{2.53}$$

where we have defined the mass matrix

$$m_e = \frac{v}{\sqrt{2}} D_e \tag{2.54}$$

Notice that we have eliminated all the unitary matrices from the theory. In fact, since e^i_L and ν^i_L transform in the same way, the couplings with the gauge bosons $W^\pm$ are invariant under this transformation. The resulting lepton theory does not violate CP symmetry and further preserves the lepton number per each generation. This property is called *lepton universality*.

[2] This fact is related to equation (2.40).

USC UNIVERSIDADE DE SANTIAGO DE COMPOSTELA

CKM matrix and Wolfestein parametrization

The CKM matrix is a unitary 3×3 matrix defined on the quark generation space. It can be parameterized by three mixing angles and the CP-violating KM phase. Of the many possible conventions, a standard choice has become [39]:

$$V_{CKM} = \begin{pmatrix} c_{12}c_{13} & s_{12}c_{13} & s_{13}e^{-i\delta} \\ -s_{12}c_{23} - c_{12}s_{23}s_{13}e^{i\delta} & c_{12}c_{23} - s_{12}s_{23}s_{13}e^{i\delta} & s_{23}c_{13} \\ s_{12}s_{23} - c_{12}c_{23}s_{13}e^{i\delta} & -c_{12}s_{23} - s_{12}c_{23}s_{13}e^{i\delta} & c_{23}c_{13} \end{pmatrix} \tag{2.55}$$

where $s_{ij} = \sin\theta_{ij}$, $c_{ij} = \cos\theta_{ij}$ and δ is the phase responsible of the CP-violating phenomena. Notice that θ_{ij} can be chosen to lie in the first quadrant , so s_{ij},$c_{ij} \geq 0$. Since, it is known experimentally that

$$s_{13} \ll s_{23} \ll s_{12} \ll 1 \tag{2.56}$$

it is convenient to introduce another parametrization to exhibit this hierarchy; we define the four Wolfenstein parameters [40]:

$$\begin{aligned} \lambda &= s_{12} \\ A\lambda^2 &= s_{23} \\ A\lambda^3(\rho - i\eta) &= s_{13}e^{-i\delta} \end{aligned}$$

then, to λ^3 order we the CKM matrix reads:

$$V_{CKM} = \begin{pmatrix} 1 & 0 & 0 \\ 0 & 1 & 0 \\ 0 & 0 & 1 \end{pmatrix} + \begin{pmatrix} -\frac{\lambda^2}{2} & \lambda & A\lambda^3(\rho - i\eta) \\ -\lambda & -\frac{\lambda^2}{2} & A\lambda^2 \\ A\lambda^3(1 - \rho - i\eta) & -A\lambda^2 & 0 \end{pmatrix} + \mathcal{O}(\lambda^4) \tag{2.57}$$

and CP violation can be determined by measuring $\rho - i\eta$.

2.3.1 Custodial symmetry

Suppose to turn off the gauge couplings in equation (2.12). The field ϕ can be rearranged in a matrix fields Φ as

$$\Phi = (i\sigma_2\phi^*, \phi) = \begin{pmatrix} \phi_0^* & \phi_+ \\ -\phi_+^* & \phi_0 \end{pmatrix} \tag{2.58}$$

and we can rewrite the Lagrangian (2.12):

$$\mathcal{L}_h = \frac{1}{2}Tr[(\partial_\mu\Phi)^\dagger\partial^\mu\Phi] + \frac{\mu}{2}Tr[\Phi^\dagger\Phi] - \frac{\lambda}{2}Tr[(\Phi^\dagger\Phi)^2] \tag{2.59}$$

This Lagrangian is invariant under a global symmetry $SU(2)_L \otimes SU(2)_R$:

$$\Phi \to L\Phi R^\dagger \tag{2.60}$$

USC UNIVERSIDADE DE SANTIAGO DE COMPOSTELA

with $L \in SU(2)_L$ and $R \in SU(2)_R$.
The field Φ, because of the potential form, acquires a non vanishing VEV:

$$\langle \Phi \rangle \sim \begin{pmatrix} v & 0 \\ 0 & v \end{pmatrix} \tag{2.61}$$

This latter is still invariant under the subgroup $SU(2)_V \subset SU(2)_L \otimes SU(2)_R$, which corresponds to the transformations:

$$\Phi \to V \Phi V^\dagger \tag{2.62}$$

The global symmetry is spontaneously broken, with a breaking pattern $SU(2)_L \otimes SU(2)_R \to SU(2)_V$ and we have again that three Goldstone bosons emerge from the theory. Now, suppose to gauge the $SU(2)_L$ group. The Lagrangian is still invariant under the global $SU(2)_L \otimes SU(2)_R$ group and the Goldstone bosons, by the Higgs mechanism, can be "eaten" to give mass to the gauge fields. In this case the physical eigenstates would correspond to linear combination of the $SU(2)_L$ gauge fields, and the masses of the vector bosons would be exactly degenerate:

$$m_W^2 = m_Z^2 = \frac{g^2}{4} v^2 \tag{2.63}$$

where g is the gauge coupling of $SU(2)_L$.

In the SM, this scenario occurs when all the Yukawa couplings are identical and $g' \to 0$, resulting in the W and Z becoming exactly degenerate. The latter approximate symmetry is called *custodial symmetry* and it protects the parameter ρ from quantum corrections, giving the exact relation $\rho = 1$ at tree-level. Furthermore, assuming that the hypercharge corresponds to the third generator of $SU(2)_R$, T_R^3, it also explains why only m_Z receives a contribution from the hypercharge coupling g'. Finally, we notice that the top quark mass has an important role on the explicit breaking of the custodial symmetry. Indeed, being the heaviest elementary particle in the SM, the quark top introduces significant quantum corrections to the ρ parameter, causing a deviation (a few percent [41, 42]) from the LO value $\rho = 1$.

2.4 Beyond tree level

The Lagrangian we just built introduces a number of free parameters that are directly related to the physical observables. Indeed, at the Leading Order (LO) in the perturbation theory, the calculations involve only the simplest Feynman diagrams. The results are typically finite quantities and can be directly interpreted as physical observables. However, when higher-order corrections are taken into account, we have more complicated Feynman diagrams involved and loops of virtual particles come into play. The loops in Feynman diagrams introduce integrals over momenta of the virtual particles

USC UNIVERSIDADE DE SANTIAGO DE COMPOSTELA

and, when evaluated, can lead to divergent terms. An example of these integrals is:

$$\lambda \int \frac{d^4k}{(2\pi)^4} \frac{1}{k^2 + m^2} \sim \infty, \tag{2.64}$$

where λ is a dimensionless coupling. The presence of divergent integrals is an indication that the theory requires further treatment.

2.4.1 Regularization

In QFT, at fixed order in the perturbation theory, we can expect a finite number of integrals (divergent or not). Indeed, physical quantities contains sums, products and convolutions of them. However, as mentioned in the previous section, some of the integrals may be divergent, but this is not necessarily a an unsolvable problem. Indeed, if a single integral does not converge the reason may be that we isolated the integral from the rest of the theory. This may happen, for example, when we are considering non observable parameters, that are indeed not physical. In this case the divergence is not a problem, but it is just a matter of re-parametrization. A theory where all the divergences may be consistently removed in a finite number of steps is called *renormalizable*[3].
As first step towards the renormalization of a theory, we will briefly describes how to deal with integrals in the form (2.64). The idea is to introduce an artificial prescription to make our integral finite; an example is the introduction of a cut-off Λ:

$$\lambda \int_{|k|\leq\Lambda} \frac{d^4k}{(2\pi)^4} \frac{1}{k^2 + m^2} \sim \Lambda^2. \tag{2.65}$$

The parameter introduced is called *regulator* and the prescription for rendering divergent diagrams finite is called *regularization*. Of course in the limit $\Lambda \to \infty$ the integral is still divergent, but this trick allow us to postpone this operation until we have calculated quantities that are physically relevant. Indeed the presence of a divergence in a single integral is not an issue if, after a re-parametrization, the physical quantities admit the removal of the regulator, which in this scheme corresponds to the limit $\Lambda \to \infty$. Several regularization schemes were proposed in the literature, but the one that established itself to be the favourite strategy in theoretical particle physics is the *Dimensional Regularization*. This method preserves Lorentz and gauge invariance and has the useful characteristics of being applicable also on infrared divergences. The idea of dimensional regularization is very simple: we extend the 4-dimensional domain of definition of the analytical function into $D = 4 - 2\epsilon$ dimensions:

$$\lambda\mu^{4-D} \int \frac{d^Dk}{(2\pi)^D} \frac{1}{k^2 + m^2} \sim \frac{2}{4 - D} \sim \frac{1}{\epsilon}. \tag{2.66}$$

[3]In a series of papers of 1971-1972, G. t'Hooft and M. Veltman proved that the Electroweak Theory is renormalizable [43].

USC UNIVERSIDADE DE SANTIAGO DE COMPOSTELA

Notice that in D dimensions, the coupling λ has non–zero mass dimension $4-D$, so we replaced $\lambda \to \lambda\mu^{4-D}$. The *new* λ is dimensionless and μ is an arbitrary energy scale. As we can see, here ϵ plays the role of the *regulator*, the limit to consider is $\epsilon \to 0$ and the divergence manifest itself as a pole in ϵ.

2.4.2 Dirac Algebra

In general, to consistently evaluate the integrand in integrals of the form 2.66, we will need a generalisation of the metric and of the Dirac algebra to D dimensions. Some of the prescribed continuations of the Lorentz and Dirac algebra are very natural:

$$\begin{aligned} g^{\mu\nu}g_{\mu\nu} &= D, \\ \{\gamma^\mu, \gamma^\nu\} &= 2g^{\mu\nu}\ \mathbb{1}, \\ \gamma^\mu\gamma_\mu &= \frac{1}{2}g_{\mu\nu}\{\gamma^\mu, \gamma^\nu\} \\ &= g^{\mu\nu}g_{\mu\nu} = D. \end{aligned} \tag{2.67}$$

However other prescriptions are far more subtle and require a more careful explanation. Indeed, since Dimensional regularization was introduced, it was evident that dealing with chiral couplings was a complicated issue. The problem emerges because the usual 4-dimensional γ^5, defined as

$$\gamma^5 = -i\gamma^0\gamma^1\gamma^2\gamma^3, \tag{2.68}$$

does not have a canonical extension into D dimension. Indeed [43], we cannot expect to preserve the anticommutation relation

$$\{\gamma^\mu, \gamma^5\} = 0 \tag{2.69}$$

and, at the same time, handle the traces of the Dirac matrices with the usual mathematical rules. In a nutshell, as pointed out by D. Kramer [44] and 't Hooft-Veltman [43, 45], one has to decide between keeping the cyclic property of the trace (HVBM scheme) or keeping the anticommutation relation 2.69 of the γ^5 (Kramer scheme). Clearly, the scheme used has a relevant impact on the the Feynman rules and on the Dirac traces. In the HVBM scheme, the anticommutation rule 2.69 is abandoned and the γ^5 definition is extended to a -2ϵ -dimensional subspace:

$$\begin{aligned} \{\gamma^\mu, \gamma^5\} &= 0 \qquad 4 \text{ dimensions} \\ [\gamma^\mu, \gamma^5] &= 0 \qquad -2\epsilon \text{ dimensions.} \end{aligned} \tag{2.70}$$

HVBM scheme provides a natural treatment to handle Dirac traces. However, it has the significant drawback of violate the the chiral symmetry of the SM (hence of Ward Identity

USC UNIVERSIDADE DE SANTIAGO DE COMPOSTELA

) in all perturbative calculations involving chiral couplings. The solution proposed by Breitenlohner-Maison (BM in the HVBM scheme) involves the restoration of the chiral symmetry as part of the renormalization process. The idea is to introduce additional finite counterterms alongside the usual divergent ones. It is important to note that this restoration of chiral symmetry is not limited to interactions explicitly involving γ^5 but is expected for all interactions in the SM. Additionally, these finite counterterms need to be calculated beyond $O(\epsilon^0)$ to consistently restore chiral symmetry at higher perturbative orders. Thus, the renormalization procedure can be very demanding.
For this reason, we will use the Kramer scheme to deal with traces of Dirac matrices. Indeed, Kramer scheme does not need the introduction of any counterterm, simplifying substantially the calculation and, as we will see below, this procedure does not break the chiral symmetry of the SM. Nevertheless, it is important to mention that Kramer scheme has not been completely accepted and embraced as a preferable choice to HVBM and there are still doubts about its use beyond one loop [46, 47]. However, in this thesis we will use the Kramer scheme only for one loop calculations.

2.4.3 Kramer scheme

The rules for handling Dirac matrices in Kramer scheme are[44]:

- Anticommutation rules:

$$\begin{aligned} \{\gamma_\mu, \gamma_\nu\} &= 2g_{\mu\nu}\ \mathbb{1}, \\ \{\gamma_\mu, \gamma_5\} &= 0. \end{aligned} \tag{2.71}$$

- For the traces of Dirac matrices without γ_5:

$$\begin{aligned} &Tr[\gamma_{\mu 1}\gamma_{\mu 2}\dots\gamma_{\mu_{2n-1}}] = 0, \\ &Tr[\gamma_{\mu 1}\gamma_{\mu 2}\dots\gamma_{\mu_{2n}}] = 4\sum_\sigma (-1)^{sgn(\sigma)}\, g_{\mu_{i_1}\mu_{j_1}} g_{\mu_{i_2}\mu_{j_2}}\dots g_{\mu_{i_n}\mu_{j_n}}. \end{aligned} \tag{2.72}$$

- For the traces of Dirac matrices involving γ_5 we have:

$$\begin{aligned} &Tr[\gamma_{\mu 1}\gamma_{\mu 2}\dots\gamma_{\mu_{2n-1}}\gamma_5] = 0, \\ &Tr[\gamma_{\mu 1}\gamma_{\mu 2}\dots\gamma_{\mu_{2n}}\gamma_5] = 4i\sum_\sigma (-1)^{sgn(\sigma)}\, \epsilon_{\mu_{i_{n+1}}\mu_{i_{n+2}}\mu_{j_{n+1}}\mu_{j_{n+1}}} g_{\mu_{i_1}\mu_{j_1}}\dots g_{\mu_{i_{n+2}}\mu_{i_{n+2}}}, \end{aligned} \tag{2.73}$$

with

$$1 = i_1 < \dots < i_n + 2, \quad i_k < j_k,$$

where $\epsilon_{\mu_1\mu_2\mu_3\mu_4}$ is the 4-dimensional Levi-Civita tensor.

USC UNIVERSIDADE DE SANTIAGO DE COMPOSTELA

- It is forbidden to use cyclic property of the trace when an odd number of γ_5 is involved.
- If there is more than one diagram contributing to a given process, all the traces must be read starting at the same point[4].
- In the case where an anomalous axial current is involved, the trace of the anomalous graph must be read starting from an axial vector vertex, in order to fulfill the usual convention of conserved vector currents. In the case of multiple axial vector vertices a symmetric choice of the reading prescription must be used.

Notice that when one is computing Dirac traces with at most four Dirac gammas and γ_5, the Kramer scheme is equivalent to the Naive Dimensional Regularization (NDR). More details about the differences and the analogies between the schemes discussed are explained in [46].

2.5 Renormalization

We know briefly describe the renormalization procedure, following [48]. A practical way to carry out the renormalization is the so-called counterterm approach. The basic idea behind the counterterm approach is to introduce additional terms, known as counterterms, into the Lagrangian of the theory. First step, we have to replace the parameters of the Lagrangian with their *bare quantities* (in the following denoted with a "0" subscript), meaning that they cannot be directly interpreted as physical quantities. Then, the *bare quantities* are separated into two components: a finite renormalized part and a divergent counterterm or renormalization constant. Every bare parameter $\mathcal{K}_0$ is split as:

$$\mathcal{K}_0 = Z_{\mathcal{K}}\mathcal{K} = (1 + \delta_{\mathcal{K}})\mathcal{K}. \tag{2.74}$$

Then inserting this transformations into the classical Lagrangian we have

$$\mathcal{L}_0 = \mathcal{L} + \delta\mathcal{L} \tag{2.75}$$

where $\mathcal{L}$ is the same as the original Lagrangian but with bare quantities replaced by renormalized ones and $\delta\mathcal{L}$ is the counterterm Lagrangian. This latter groups all the potential UV terms and leads to an additional set of Feynman rules. After imposing the renormalization conditions on the renormalized quantities, we can obtain their numerical values using experimental inputs. The choice of the input observables and the renormalization conditions determine the *renormalization scheme*. The complexity of the theory together with arbitrariness in the choice of the 'best' renormalization scheme can make it difficult to compare and to follow different approaches. In the literature are present many different schemes [49]; depending on the physical process we are considering, it may be convenient to use a renormalization scheme rather than another.

[4] In the Drell Yan scattering, the fermion chains of the LO will provide us a natural reading point.

USC UNIVERSIDADE DE SANTIAGO DE COMPOSTELA

In this thesis we are using two renormalization schemes, the *modified Minimal Substraction* ($\overline{MS}$) scheme and the *On Shell* (OS) scheme.

2.5.1 $\overline{MS}$

The easiest way to introduce the $\overline{MS}$, is to start with his close relative, the MS scheme. In this approach, one simply removes ϵ poles in divergent quantities. The cancellation of the poles occurs through the renormalization constants Z defined in 2.74. Usually, tough, the divergences are followed by terms involving the Eulero-Mascheroni γ_{EM} constant and $\text{Log}(4\pi)$. Thus, it is convenient to absorb the divergent part plus these constants into the counterterms. To do this we can just redefine the pole as

$$\frac{1}{\epsilon} \longrightarrow \frac{1}{\epsilon} - \gamma_{EM} + \text{Log}(4\pi), \tag{2.76}$$

this prescription is called $\overline{MS}$. The characteristic of the $\overline{MS}$ scheme is that it normally puts the one-loop corrections in a particular simple form. However, despite the simplicity of the expressions, it takes some efforts to express the physical observables in terms of of the parameters. Finally, we notice that in $\overline{MS}$, the parameters have a residual dependence on the energy scale μ (introduced in 2.66) and thus this scheme is more suitable for dimensionless parameters, like Wilson coefficients and couplings.

2.5.2 OS

In the on shell scheme, the renormalization conditions are fixed by asking that, once we take the continuum limit, the renormalized quantities occur at some experimentally measured value. For example, for the electron, we constrain the renormalized propagator to have a pole at the physical mass, the pole mass $m_{e,\text{pole}}$. The conditions are:

$$\Sigma_R(m_{e,\text{pole}}) = 0, \quad \frac{d}{d\not{p}}\Sigma_R(\not{p})\bigg|_{\not{p}=m_{e,\text{pole}}} = 0 \tag{2.77}$$

where $\Sigma_R(\not{p})$ is the sum of the one particle irreducible Feynman diagrams, plus counterterm contributions. These equations apply to all orders in perturbation theory and they are known as *on shell renormalization conditions*. Clearly, to perform the on shell scheme, it is necessary to use physical observables as input parameters. Finally, we notice that in this renormalization scheme, the input parameters do not depend on the energy scale μ, because it is re-absorbed in the renormalization constants $Z_{\mathcal{K}}$.

For the SM parameters, since we are using dimension parameters as input, we use the OS scheme. Indeed, the renormalization conditions of this scheme are defined for external fields on their mass shell, giving us a direct physical interpretation of the renormalized parameters. Nevertheless, for $gg \to HH$ we will also explore the $\overline{MS}$ renormalization scheme for the top mass. Indeed, among the purposes of that calculation, there is also how the result is affected by the change of the renormalization scheme. Lastly, for

USC UNIVERSIDADE DE SANTIAGO DE COMPOSTELA

SMEFT parameters, since it is not possible to fix their renormalization condition with an experimental value, we use the $\overline{MS}$ scheme.

USC
UNIVERSIDADE DE SANTIAGO DE COMPOSTELA

Chapter 3

Higgs production from gluon fusion

At the Large Hadron Collider (LHC) gluon fusion is the most relevant production mechanism 3.1 for Higgs physics in single-Higgs production, $gg \to H$, and pair production, $gg \to HH$, and plays an important role in the production of a Higgs boson in association with a Z boson, $gg \to ZH$. Precise predictions for such processes are necessary in order to measure the properties of the Higgs boson accurately. Since the Higgs boson is a colorless particle, these processes are all loop-induced and mediated by a heavy particle, mainly the top quark. For over two decades, it has been well-established that QCD corrections to the Born result are very large and the perturbative expansion converges slowly (see for example [50, 51]). This implies that the knowledge of the higher-order QCD corrections is very important. However, the evaluation of these corrections is extremely challenging already at next-to-leading order (NLO), since it requires the computation of two-loop diagrams. In this chapter we are going to consider the virtual corrections to Higgs production via gluon fusion at the NLO level. It is is organized as follows. In section 3.1.1 we provide an overview of the the processes examined, before delving into more technical aspects of the calculation. In section 3.2 we introduce the different expansions as well as the method for combining them. In section 3.3 we validate the method at LO both at the level of form factors and at the level of the partonic cross section, with a focus on the $gg \to HH$ process. Finally, in section 3.4 we present the merging of the two expansions at NLO. In order to show the flexibility of our approach with respect to the modification of the input parameters, in the same section we present the result for the two-loop virtual contribution in $gg \to HH$ and $gg \to ZH$ for two different choices of the top quark mass, namely the on–shell and the $\overline{\text{MS}}$ mass.

USC UNIVERSIDADE DE SANTIAGO DE COMPOSTELA

This chapter is based on the following paper:

Gluon Fusion Production at NLO:

Authors

Luigi Bellafronte[a], Giuseppe Degrassi[b], Pier Paolo Giardino[a], Ramona Gröber[c], Marco Vitti[b]

(a) Instituto Galego de Física de Altas Enerxías, Universidade de Santiago de Compostela, 15782 Santiago de Compostela, Galicia-Spain
(b) Dipartimento di Matematica e Fisica, Università di Roma Tre and INFN, sezione di Roma Tre, I-00146 Rome, Italy
(c) Dipartimento di Fisica e Astronomia 'G. Galilei', Università di Padova and INFN, sezione di Padova, I-35131 Padova, Italy

Journal and Article Information

Journal name: Journal of High Energy Physics

Publisher: Springer Nature

ISSN: 1029-8479

Year of publication: 2022

DOI: 10.1007/JHEP07(2022)069

3.1 Overview

HH

Recalling the Higgs Lagrangian 2.12 and working in the unitary gauge, after the SSB the Higgs potential take the form:

$$\begin{aligned}\mathcal{L}_V &= -\mu^2 h^2 - \frac{\lambda}{2} v h^3 - \frac{1}{8}\lambda h^4 \\ &= -\frac{1}{2} m_h^2 - \sqrt{\frac{\lambda}{4}} m_h h^3 - \frac{1}{8}\lambda h^4,\end{aligned} \tag{3.1}$$

where

$$m_h = \sqrt{\lambda v} = 125.25 \text{ GeV}, \tag{3.2}$$

is the Higgs boson mass and the cubic and quartic terms are the Higgs self-interactions. Measuring the Fermi constant G_F defined as

$$G_\mu = \frac{v^2}{\sqrt{2}} = 1.1663787(6) \times 10^{-5} \text{GeV}^{-2}, \tag{3.3}$$

USC UNIVERSIDADE DE SANTIAGO DE COMPOSTELA

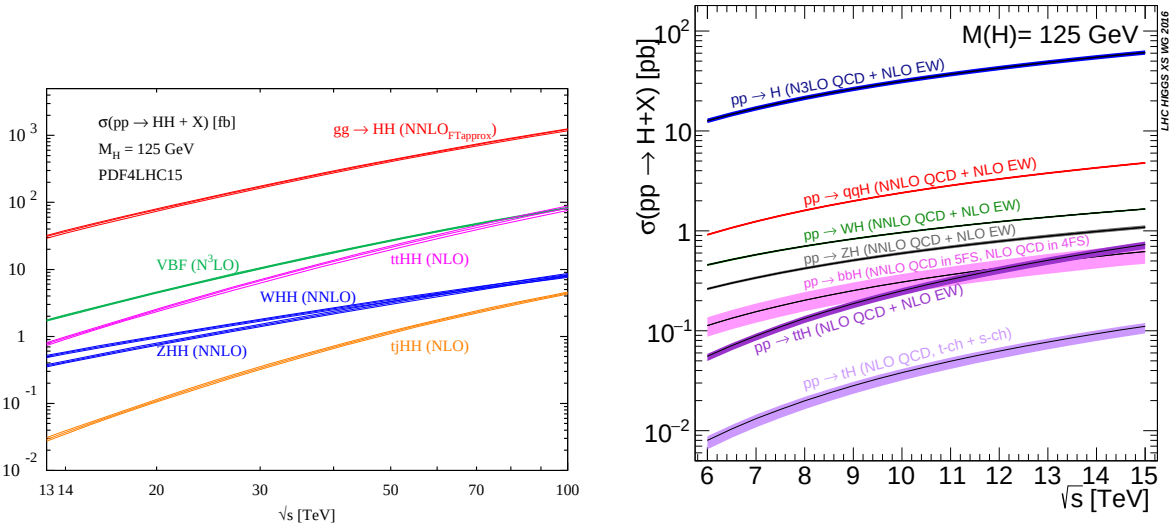

Figure 3.1: Theoretical SM predictions for double Higgs and single Higgs production at LHC [15, 16]

we find that the expected SM value for λ is :

$$\lambda_{SM} = \frac{m_h^2}{v^2} \simeq 0.26. \tag{3.4}$$

This parameter can be compared with his experimental counterpart λ_{exp} from collider experiments. Defining

$$\kappa_\lambda = \frac{\lambda_{exp}}{\lambda_{SM}} \tag{3.5}$$

we can measure how much the experimental value deviates from the SM value. Current bounds, at 95% of CL, from CMS and Atlas [52, 53] are:

$$\begin{aligned} -6.9 < \kappa_\lambda^{CMS} < 11.1 \\ -0.4 < \kappa_\lambda^{ATLAS} < 6.13 \end{aligned} \tag{3.6}$$

From these values, we see that the measurement of λ with high precision is a significant challenge and it is probably beyond the capabilities of the current LHC configuration. However, the upcoming HL-LHC and a potential FCC future collider can put more stringent bounds, since the expected range [54] at 95% CL is

$$-0.1 < \kappa_\lambda < 2.3 \ . \tag{3.7}$$

For this reason, precise predictions for the Higgs pair production becomes very important.

HZ

The process of associated VH production ($V = W, Z$) holds significant importance at the LHC and HL-LHC, because is one of the primary production modes of the Higgs

USC UNIVERSIDADE DE SANTIAGO DE COMPOSTELA

boson (see Fig 3.1). Anticipated experimental uncertainties for VH measurements are expected to reach the 5% level after the High-Luminosity phase. To ensure consistent comparisons with future measurements, considerable efforts are directed toward reducing the uncertainty in the theory prediction within the SM.

Different sources of theoretical uncertainty have varying impacts on the SM predictions for WH and ZH production. Specifically, the contribution from the scale uncertainty arising due to missing higher-order terms in perturbative calculations is not so relevant in the WH case, while it is most significant in the ZH prediction. This is because ZH production can occur via a quark-initiated process (similar to WH production) but also through the partonic channel $gg \to ZH$. The latter process is suppressed compared to $q\bar{q} \to ZH$ but it still contributes around O(10%) to the hadronic cross section. To reduce the impact of related scale uncertainties, improving the accuracy of the current prediction for $gg \to ZH$ is crucial. Indeed, although associated production is not as frequent as other production mechanisms, it provides a unique way to study the decay of the Higgs to a pair of bottom quarks, which is challenging to observe at an hadronic collider due to the many sources of QCD background. In this context, the study of the associated production was a key point for measuring the first $H \to b\bar{b}$ decay, providing also the best sensitivity for this process[55]. Finally we notice that $gg \to ZH$ is also relevant for New Physics (NP). Indeed, being sensitive for expample to both sign and magnitude of the top Yukawa coupling, it may be used for testing NP in this channel. Thus, improving our understanding of the SM prediction for the gluon-induced contribution is thus very significant, not only for precision measurements of ZH production but also for exploring New Physics in this channel.

3.1.1 Kinematic

The processes can be written as

$$g^a_\mu(p_1)\, g^b_\nu(p_2) \to 3(-p_3)\, 4(-p_4), \tag{3.8}$$

where 3 and 4 are two neutral[1] particles with masses m_3 and m_4, respectively. The Feynman amplitudes for these scatterings are given by

$$\begin{aligned}
\mathcal{A}_{HH} &= \frac{G_\mu}{\sqrt{2}} \frac{\alpha_S(\mu_R)}{2\pi} \hat{s}\, \delta_{ab} \epsilon^a_\mu(p_1) \epsilon^b_\nu(p_2) T_F \hat{\mathcal{A}}^{\mu\nu}_{HH}(p_1, p_2, p_3), \\
\mathcal{A}_{HZ} &= i\sqrt{2}\, \frac{m_Z G_\mu \alpha_S(\mu_R)}{\pi}\, \delta_{ab} \epsilon^a_\mu(p_1) \epsilon^b_\nu(p_2) \epsilon^*_\rho(p_3) \hat{\mathcal{A}}^{\mu\nu}_{HZ}(p_1, p_2, p_3)
\end{aligned} \tag{3.9}$$

where $\epsilon(p_i)$ is the polarisation vector of the i_{th} particle, G_μ is the Fermi constant, α_S is the QCD fine structure constant defined at the renormalization scale μ_R and $T_F = \frac{1}{2}$ is

[1] Dealing with neutral particles in the final state implies the absence of mixed top-bottom diagrams, as they would appear e.g. in $gg \to W^+W^-$ production, for which the proposed method cannot be straightforwardly applied.

USC UNIVERSIDADE DE SANTIAGO DE COMPOSTELA

the Dynkin index. For the double higgs production we have:

$$\mathcal{A}^{\mu\nu}_{HH} = A^{\mu\nu}_1 F_1 + A^{\mu\nu}_2 F_2 \tag{3.10}$$

where F_1 and F_2 are the form factors associated to the spin-0 and spin-2 projectors, respectively. For the HZ production we have:

$$\mathcal{A}^{\mu\nu\rho}_{HZ} = \sum_i^7 \mathcal{P}^{\mu\nu\rho}_i A_{iHZ} \tag{3.11}$$

where $\mathcal{P}_i$ are a basis of orthonormal projectors and A_{iHZ} are the associated scalar form factors. In both the processes, they depend only on scalar quantities, namely the top quark mass m_t, the masses of the external particles and the partonic Mandelstam variables. Additionally, taking all momenta to be incoming, we define the partonic Mandelstam variables as

$$\hat{s} = (p_1 + p_2)^2, \qquad \hat{t} = (p_1 + p_3)^2, \qquad \hat{u} = (p_2 + p_3)^2, \tag{3.12}$$

and the transverse momentum p_T of the final-state particles can be written as

$$p_T^2 = \frac{\hat{t}\hat{u} - m_3^2 m_4^2}{\hat{s}}. \tag{3.13}$$

As suggested in refs. [29, 56], if the amplitude of the process is written in terms of (anti)symmetric form factors with respect to the exchange $\hat{t} \leftrightarrow \hat{u}$, then it is sufficient to discuss only the forward contribution to the cross section. Therefore, in the following we will always assume that $|\hat{t}| \leq |\hat{u}|$ and that

$$\hat{t} = -\frac{1}{2}\left(\hat{s} - m_3^2 - m_4^2 - \sqrt{\lambda(\hat{s}, m_3^2, m_4^2) - 4\hat{s}\, p_T^2}\right), \tag{3.14}$$

where $\lambda(a, b, c) = a^2 + b^2 + c^2 - 2ab - 2ac - 2bc$ is the Källén function.

3.2 Method

In general, the degree of difficulty in the evaluation of loop diagrams grows with the number of energy scales present in the diagram. In the case of single-Higgs production the relevant diagrams feature a triangular topology and, consequently, depend upon only two scales, namely the Higgs mass, m_H, and the top mass[2], m_t. In this case, the functional dependence of the result upon the top mass can be expressed in terms of one single variable, m_H^2/m_t^2. Due to this *simplified* one-scale situation, exact analytic results for the NLO corrections are available since many years [57, 58, 59, 60].

In the case of processes with two particles in the final state the situation is more complicated. Indeed these processes receive contributions not only from triangle diagrams,

[2] All the quarks but the top are assumed to be massless.

USC UNIVERSIDADE DE SANTIAGO DE COMPOSTELA

that can be calculated adapting the exact analytic results obtained for single-Higgs production, but also from box-topology diagrams. In pair production, $gg \to HH$, the box diagrams depend upon four scales, namely $\hat{s}$, $\hat{t}$, m_t, m_H, where $\hat{s}$, $\hat{t}$, and $\hat{u}$ are the Mandelstam variables which satisfy the condition

$$\hat{s} + \hat{t} + \hat{u} = 2\, m_H^2 \ . \tag{3.15}$$

Concerning associated production, $gg \to ZH$, a fifth energy scale is present, i.e. the mass of the Z vector boson, m_Z.

Exact analytic results for two-loop box diagrams with several energy scales cannot be derived with the present computational technology. Instead, usually two different strategies are followed in order to evaluate the two-loop box contribution in Higgs production via gluon fusion. a) A fully numerical exact evaluation [61, 62, 63, 64, 65]. b) An approximate analytic evaluation that takes advantage of hierarchies among the various energy scales present in the diagrams, in order to reduce the number of scales in the problem. Thus, its validity is restricted to specific regions of the phase space. The method used is based on the expansion of the diagrams in terms of ratios of small energy scales vs. large energy scales, in order to obtain a result that retains an exact dependence upon the large energy scales. Concerning the small ones, in order to simplify further the evaluation, expansions in term of ratios between small energy scales is often used.

The former strategy, although accurate, is very demanding from a computational point of view, requiring a high degree of optimization in order to obtain a result in a *reasonable*, although usually quite long, computer time. Furthermore, this approach is not very flexible with respect to the modification of the input parameters.

Strategy b) provides accurate results valid in specific regions of the phase space without requiring heavy computational work, i.e. in a short computer time. Examples of this approach of evaluating the two-loop box contribution are:

i) The infinite-top-mass limit [66, 67] refined by the inclusion of powers in the large top-mass expansion (LME) [68, 69, 70, 71]. Here, m_t is assumed to be the large energy scale while $\hat{s}$, $\hat{t}$, m_H, and in associated production also m_Z, are considered to be the small ones. Thus, the validity of this approach is restricted to phase-space regions where $\hat{s}/(4m_t^2) \leq 1$. The advantage of this approximation are the rather simple results, which can be expressed in terms of rational functions and logarithms of the kind $\log(m_t^2/\hat{s})$.

ii) The evaluation via an expansion in the transverse momentun, p_T, of the final-state particles [29, 56]. Here, $\hat{s}$ and m_t are assumed to be the large energy scale while m_H, m_Z and p_T, that can be traded for $\hat{t}$, are considered to be the small ones. The validity of this approach is restricted to phase-space regions where $|\hat{t}|/(4m_t^2) \lesssim 1$. The analytical complexity of this approach is higher than in i), as generalised polylogarithms and two elliptic integrals occur in the final results. The evaluation of the latter can be easily performed using the results of Ref. [72].

USC UNIVERSIDADE DE SANTIAGO DE COMPOSTELA

iii) The evaluation via a high-energy (HE) expansion [30, 73, 74]. Here $\hat{s}$, $\hat{t}$ are assumed to be the large energy scale while m_t, m_H and m_Z, with $m_t \gg m_H, m_Z$, are considered to be the small ones. The validity of this approach is restricted to phase-space regions where $|\hat{t}|/(4m_t^2) \gtrsim 1$. The HE expansion leads to analytical results that can be expressed in terms of harmonic polylogarithms.

iv) The evaluation via an expansion in terms of small external masses [75, 76, 77]. Here $\hat{s}$, $\hat{t}$, m_t are assumed to be the large energy scale while m_H and m_Z are considered to be the small ones. This approach basically covers the entire phase space of the considered processes. However, since the reduction of scales in this approach is minimal, one ends up with the evaluation of Master Integrals (MIs) that are much more complicated than those appearing in the i)–iii) cases. As a consequence the evaluation of the box contribution in any point of the phase space requires a longer computer time than in the approaches i)–iii).

As an alternative approach, refs. [78, 79] proposed to reconstruct the full result from its LME version, supplemented by the non-analytic part of the diagrams near the top threshold, via a conformal mapping and Padé approximants.

In [80] we propose an alternative way to derive the full top-mass dependence in Higgs production via gluon fusion, based on the merging of the p_T expansion in ii) with the HE expansion in iii) that individually are valid in complementary regions of the phase space. Since the numerical evaluations of the two expansions are quite fast from a computational point of view, our proposal allows a fast evaluation of the virtual corrections to Higgs production via gluon fusion that is accurate in the entire phase space.

The key point of our analysis is to extend the fixed-order results both in the p_T expansion [29, 56] and in the HE expansion [73, 74] up to or beyond their border of validity, i.e. $\hat{t} \simeq 4m_t^2$, in order to merge the two analytic approximations. This is done by constructing a [1/1] Padé approximant for the p_T-result and a [6/6] Padé approximant for the HE-result. We point out that the extension of the HE expansion via Padé approximants has been already considered in refs. [73, 74].

3.2.1 Pade approximant

In the forward regime, the validity of both the p_T and HE expansions is limited by the condition

$$|\hat{t}| \simeq 4m_t^2, \tag{3.16}$$

i.e. for any fixed value of $\hat{s}$, the p_T expansion provides reliable results when $|\hat{t}| \lesssim 4m_t^2$ while the HE expansion is accurate for $|\hat{t}| \gtrsim 4m_t^2$, if the fixed $\hat{s} > 4m_t^2$. However, we find that in the vicinity of the point $|\hat{t}| = 4m_t^2$ the fixed-order results in the p_T expansion and in the HE expansion are both divergent (see fig. 3.2). As a consequence, a straightforward combination of the p_T-expanded and the HE-expanded results cannot allow for an accurate description of the above region, and this fact prevents a full coverage

USC UNIVERSIDADE DE SANTIAGO DE COMPOSTELA

of the phase space. We point out that this situation does not change substantially when higher orders in both the expansions are computed.

Alternatively, the convergence of the expanded results can be improved by considering the respective Padé approximants. Indeed, starting from a given Taylor expansion of an exact function $f(x)$ around $x = 0$ up to the first r terms

$$f(x) \simeq \sum_{k=0}^{r-1} c_k x^k, \tag{3.17}$$

it is possible to construct the associated Padé approximant, defined as

$$[m/n](x) = \frac{p_0 + p_1 x + \cdots + p_m x^m}{1 + q_1 x + \ldots q_n x^n}, \tag{3.18}$$

provided that $m + n + 1 = r$. Specifically, by Taylor-expanding the r.h.s. of eq. (3.18), the $\{p_i, q_j\}$ coefficients of the Padé approximant can be written in terms of the c_k ones known from eq. (3.17), by solving a system of linear equations. Usually, $[m/n]$ Padé approximants such that $m = n$ give the best improvement in the convergence of the original Taylor expansion, and we consider only these combinations in our study. In the p_T-expanded results, at NLO, only the first three terms in eq. (3.17) are known and therefore we are limited to construct a [1/1] Padé approximant (we will refer to this as the p_T-Padé). Instead the availability of many terms in the HE-expansion results allows to consider several $[n/n]$ approximants (defined as HE-Padé).

When calculating the p_T-Padé, care is to be taken in the treatment of the expansion parameters. As discussed in refs.[29, 56], not only the p_T but also the masses of the external particles are understood as small parameters. Since these are all treated on the same footing with respect to the large scales set by $\hat{s}$ and m_t, we can write the general expression for a p_T-expanded form factor F in the amplitude in terms of a scaling parameter x

$$F(x) = \sum_{N=0}^{2} x^N \sum_{i+j+k=N} c_{ijk}\ (p_T^2)^i (m_3^2)^j (\Delta_m)^k \equiv \sum_{N=0}^{2} x^N c_N \tag{3.19}$$

where m_3 is interpreted as m_H and m_Z for $gg \to HH$ and $gg \to ZH$, respectively, and $\Delta_m = (m_4^2 - m_3^2)/2$ is included only for the ZH case (see ref. [56]). Starting from eq. (3.19) we can then obtain the corresponding [1/1] Padé approximant with respect to the limit $x \to 0$

$$[1/1](x) = \frac{p_0 + p_1 x}{1 + q_1 x}, \tag{3.20}$$

with

$$p_0 = c_0 \qquad p_1 = c_1 - \frac{c_0 c_2}{c_1} \qquad q_1 = -\frac{c_2}{c_1},$$

and subsequently set $x = 1$ in eq. (3.20).

We want to clarify a possible source of ambiguity concerning the limit of validity of the p_T expansion. Indeed, while in the previous works we suggested that this expansion

USC UNIVERSIDADE DE SANTIAGO DE COMPOSTELA

is valid for $p_T^2 \lesssim 4m_t^2$, as the comparison at LO between the p_T-expanded and exact result seems to indicate, in this paper we follow a more conservative approach and we consider as limit of validity for the p_T expansion $|\hat{t}| \lesssim 4m_t^2$. Additionally, we checked that the same complementarity for the p_T and HE expansions can be observed when choosing $p_T^2 = 4m_t^2$ as limit of validity.

We now discuss the procedure adopted to construct the Padé approximants from the HE expansion. Following the prescription of ref. [81] (see also [82, 83]), we initially arrange the various orders $F^{(i)}$ of the HE expansion for a given form factor as follows

$$F(x) = F^{(0)} + \sum_{l=1}^{L} \left(F^{(2l-1)} m_t^{(2l-1)} + F^{(2l)} m_t^{(2l)} \right) x^l = \sum_{l=0}^{L} d_l x^l, \tag{3.21}$$

where orders related to odd powers of m_t are grouped with the orders related to the next even power. Then, we construct $[n/n]$ approximants in x with $2n = L$ from eq. (3.21) using the analytic expressions available in [84, 85], and setting $x = 1$. We remark that our Padé approximants are obtained in a fully symbolic way, whereas in refs. [81, 82] all the kinematical quantities are fixed to the respective numerical values before the Padés are constructed in x. Furthermore, in comparison to refs.[81, 74], we only studied $[n/n]$ HE-Padés up to $n = 6$. In those references Padés with $n > 6$ were also considered in order to extrapolate the results in the region $|\hat{t}| < 4m_t^2$, for a fixed $\hat{s}$, and characterize the relative uncertainties of different $[m/n]$ Padés. In our case, because the region $|\hat{t}| < 4m_t^2$, is more accurately described by the results of the p_T expansion, we find that a [6/6] HE-Padé is more than enough to perform the merging with the p_T-result and, at the same time, to describe accurately the high-energy region.

The p_T-Padé and the HE-Padé extend the range of validity of each expansion beyond its limit. As discussed in the next section, the p_T and the HE Padés are accurate enough to bridge the gap around the phase-space region $|\hat{t}| \simeq 4m_t^2$. Then, an accurate approximation of the exact result for any phase-space point $(\hat{s}, \hat{t})$ can be obtained by choosing as switching point between the Padé-improved expansions any point in the region $|\hat{t}| \sim 4m_t^2$. For simplicity we choose to use the p_T-Padé when $|\hat{t}| < 4m_t^2$ and the HE-Padé when $|\hat{t}| \geq 4m_t^2$, for any fixed value of $\hat{s}$. We recall that in our discussion we just consider the forward region $|\hat{t}| \leq |\hat{u}|$, while the result in the complementary phase-space region is obtained using the symmetry of our form factors under $\hat{t} \leftrightarrow \hat{u}$. Noticing that, when $|\hat{t}| \leq |\hat{u}|$, the maximum absolute value of $\hat{t}$ as a function of $\hat{s}$ is given by $|\hat{t}|_{\max} = 1/2(\hat{s} - m_3^2 - m_4^2)$ our choice corresponds to using the p_T-Padé up to the partonic energy $\hat{s}_c = 8m_t^2 + m_3^2 + m_4^2$. In this energy region ($\sqrt{\hat{s}_c} \simeq 500$ GeV for $gg \to HH$ and $gg \to ZH$) at the LHC more than 2/3 of the hadronic cross section is concentrated.

USC UNIVERSIDADE DE SANTIAGO DE COMPOSTELA

3.3 The p_T and HE expansions vs the exact results at LO

In this section we assess the reliability of our merging procedure by studying how well the combination of the p_T-Padé and the HE-Padé can reproduce the exact LO results for HH and ZH production via gluon fusion. For the sake of simplicity, we discuss in detail only the $gg \to HH$ process, but we verified that similar conclusions can be drawn for $gg \to ZH$. We recall that the amplitude for $gg \to HH$ can be expressed as

$$A^{\mu\nu} = \frac{G_\mu}{\sqrt{2}} \frac{\alpha_S(\mu_R)}{2\pi} \delta_{ab} T_F \hat{s} [A_1^{\mu\nu} F_1 + A_2^{\mu\nu} F_2], \tag{3.22}$$

and that both triangle and box diagrams contribute to F_1

$$F_1 = F_\triangle \frac{3m_H^2}{\hat{s} - m_H^2} + F_\square, \tag{3.23}$$

whereas the F_2 form factor receives contribution only from boxes. Our goal is to improve the evaluation of the box contributions, therefore we focus on the discussion of $F_\square$ and F_2. The LO results for these form factors, denoted as $F_\square^{LO}$ and F_2^{LO}, are shown in fig. 3.2, for fixed values of the partonic center-of-mass energy.

Only large values of $\hat{s}$ are shown in fig. 3.2 because for small $\hat{s}$ values the p_T-expanded results are very accurate [29]. The p_T-expanded and HE-expanded results are represented by the blue and purple solid lines, respectively, and they deviate from the exact result, shown as a solid black line, at $|\hat{t}|/4m_t^2 \simeq 1$, as anticipated in the previous section. The light blue dashed line stands for the [1/1] p_T-Padé, while the pink dashed line represents the [6/6] HE-Padé. One can see that the Padé results show an improved convergence with respect to the fixed-order expansions. The bottom part of the plots in fig. 3.2 shows the ratio of the expanded and Padé results to the exact one. Indeed, fig. 3.2(a,b) shows that in the case of $F_\square^{LO}$ for $|\hat{t}|/4m_t^2 = 1$ the differences of the Padé results with respect to the exact prediction are negligible. For the F_2 form factor, whose contribution to the cross-section is much smaller than the one of the F_1 form factor, the difference is always below 5%, see fig. 3.2(c,d). We notice that, when comparing the accuracies of the Padé approximants, larger discrepancies can be attributed to the p_T-Padé. Indeed, being the latter a [1/1] Padé, it is expected to be a less refined approximation than the [6/6] HE-Padé. Still, in the case of $F_\square^{LO}$ the differences between the two Padé near $|\hat{t}|/4m_t^2 = 1$ are negligible. We also notice that, as $\hat{s}$ increases, larger values of $|\hat{t}|$ are allowed by the kinematics, and the relative importance of the HE expansion increases.

The improvement in convergence provided by the Padé approximants is such that the merging of the two results discussed in the previous section can reproduce the exact prediction with good accuracy for every value of $\hat{t}$, for any $\hat{s}$. While we refrain from showing more examples here, we note that we studied the behaviour of all the box contributions to $gg \to HH$ and $gg \to ZH$ at several values of $\hat{s}$. We explicitly checked that, among the various possibilites, a [6/6] HE-Padé is more than enough for an accurate merging. Furthermore, we observed that the value $|\hat{t}| = 4m_t^2$ is a good choice as a merging

USC UNIVERSIDADE DE SANTIAGO DE COMPOSTELA

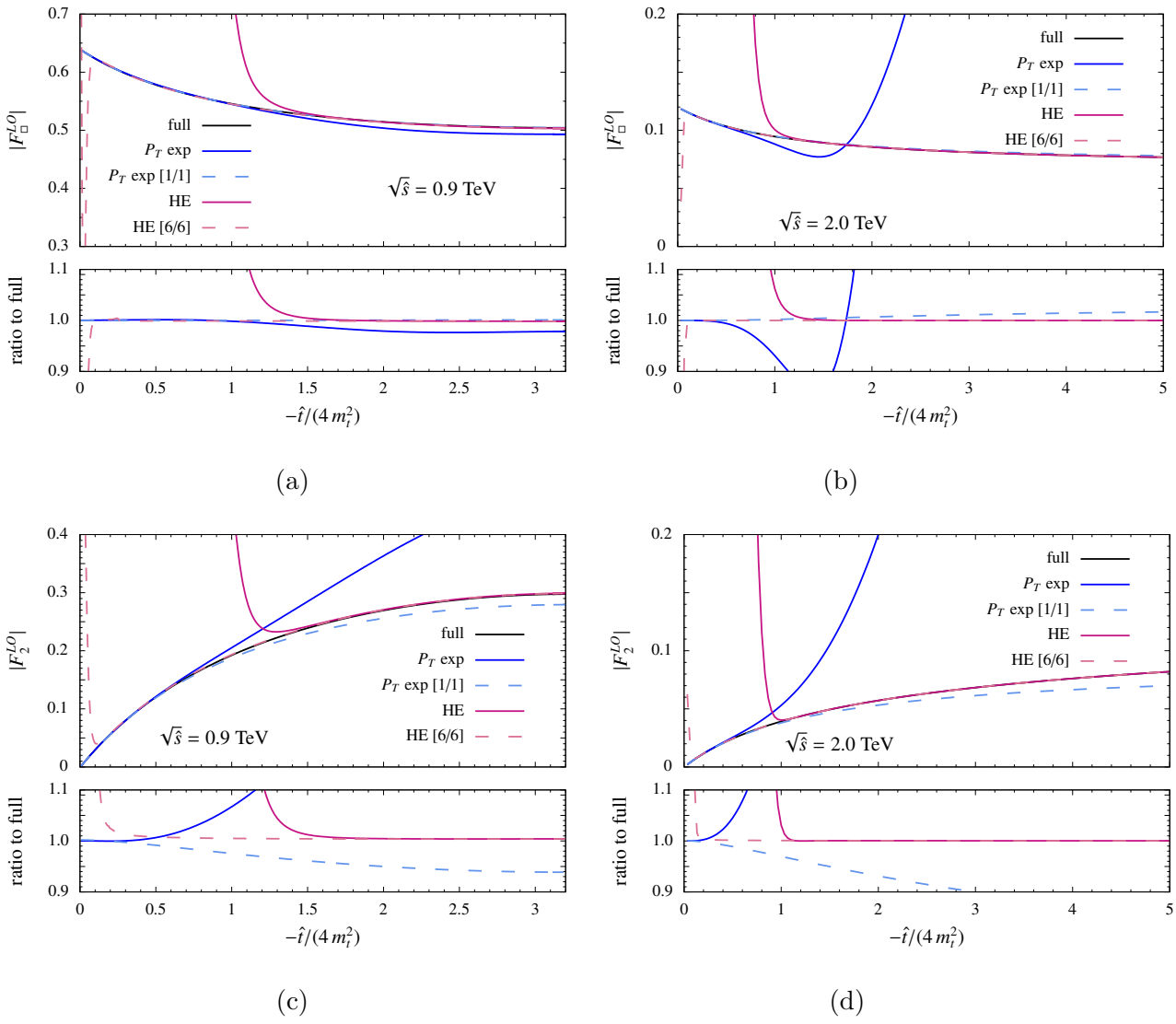

Figure 3.2: Modulus of the box form factors contributing to $gg \to HH$ at LO, for a fixed value of (a,c) $\sqrt{\hat{s}} = 0.9$ TeV and (b,d) $\sqrt{\hat{s}} = 2$ TeV. In the upper part of each plot, the exact prediction (solid black line) is shown together with the p_T and HE expansions (solid blue and purple lines, respectively) and with the [1/1] p_T and [6/6] HE Padé approximants (dashed light blue and pink lines, respectively). The bottom part of each plot shows the ratio of the above results to the exact prediction.

USC UNIVERSIDADE DE SANTIAGO DE COMPOSTELA

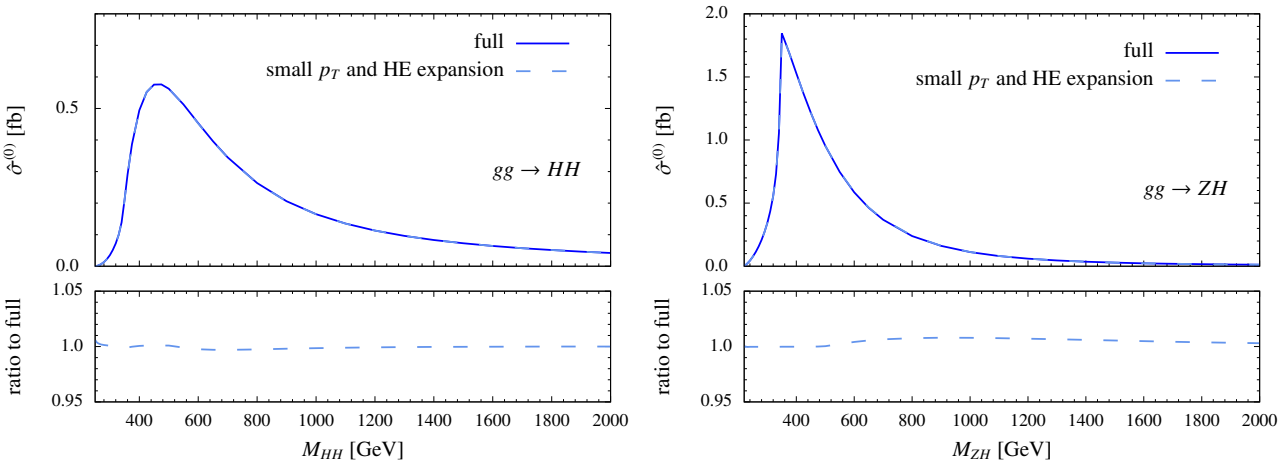

(a) (b)

Figure 3.3: Partonic cross section at LO for (a) $gg \to HH$ and (b) $gg \to ZH$. The upper part of each plot shows the exact prediction (solid line) together with the merging of the p_T and HE Padé approximants (dashed line). The bottom part of each plot shows the ratio of the merged result to the exact prediction.

point for the p_T and HE Padé approximants. The high level of accuracy of our merging method can be observed in fig. 3.3, where the partonic cross section at LO is shown for $gg \to HH$ and $gg \to ZH$. One can see that deviations of the combination of the p_T- and HE-Padé with respect to the exact prediction never exceed 1%.

3.4 Merging the p_T and HE expansions at NLO

In the previous section we showed that the merging of the p_T- and HE-Padé can accurately reproduce the exact LO prediciton. In this section we present the merging of the NLO p_T-expanded and HE-expanded results improved by the respective Padé approximants.

In fig. 3.4 the NLO contributions to $F_\square$ and F_2 are shown[3]. The relative behaviour of the various approximations is analogous to what we observed at LO. For low values of $|\hat{t}|$ the fixed-order and Padé-improved p_T-expanded results agree well. Increasing the value of $|\hat{t}|$ up to the merging region, $|\hat{t}| \sim 4m_t^2$, the p_T-Padé becomes close to the Padé-improved HE expansion. For values above $|\hat{t}| = 4m_t^2$ the p_T and HE Padé approximants show small deviations as expected. The NLO study shows the same qualitative behaviour as the LO one. This makes us confident that the proposed merging procedure works well also at NLO.

[3] $F_\square^{NLO}$ and F_2^{NLO} are the form factors as defined in eq. (3.22) but do not contain the double triangle diagrams that can be expressed in terms of products of one-loop integrals and as such are computed analytically in exact top-mass dependence [70].

USC UNIVERSIDADE DE SANTIAGO DE COMPOSTELA

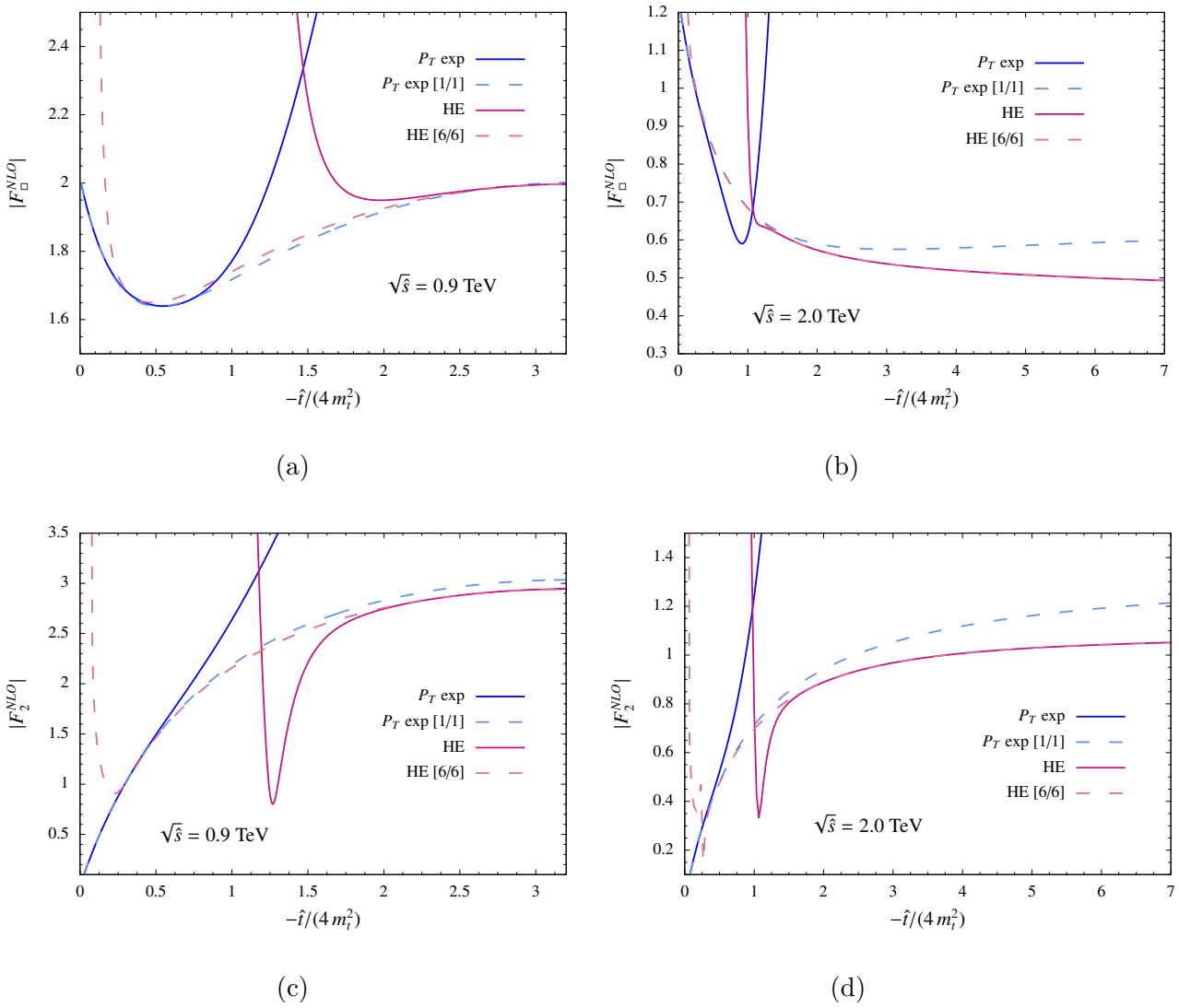

Figure 3.4: Modulus of the box form factors contributing to $gg \to HH$ at NLO, for a fixed value of (a,c) $\sqrt{\hat{s}} = 0.9$ TeV and (b,d) $\sqrt{\hat{s}} = 2$ TeV. The p_T and HE expansions are shown as solid blue and purple lines, respectively, while the [1,1] p_T- and [6,6] HE-Padé are shown as dashed light blue and pink lines, respectively.

USC UNIVERSIDADE DE SANTIAGO DE COMPOSTELA

M_{HH} [GeV]	$\hat{t}$ [GeV^2]	$\mathcal{V}_{fin}^{Pade}$	$\mathcal{V}_{fin}^{grid}$
280.9	$-7.783 \cdot 10^3$	$9.548 \cdot 10^{-6}$	$9.410 \cdot 10^{-6}$
411.4	$-6.627 \cdot 10^4$	$4.520 \cdot 10^{-4}$	$4.510 \cdot 10^{-4}$
586.96	$-6.925 \cdot 10^4$	$4.930 \cdot 10^{-4}$	$4.943 \cdot 10^{-4}$
716.55	$-1.816 \cdot 10^5$	$4.430 \cdot 10^{-4}$	$4.298 \cdot 10^{-4}$
1048.93	$-2.133 \cdot 10^5$	$2.952 \cdot 10^{-4}$	$3.104 \cdot 10^{-4}$
1855.32	$-1.678 \cdot 10^6$	$2.497 \cdot 10^{-4}$	$2.498 \cdot 10^{-4}$

Table 3.1: Comparison of various numerical values of $\mathcal{V}_{fin}$ taken from the grid of ref. [86] with our Padé construction.

We now compare our evaluation of the virtual corrections for the di-Higgs production process[4] with the numerical result provided as a grid in ref. [86]. This reference summarizes the work of ref. [81], where the numerical calculation in exact top-mass dependence of ref. [62] was supplemented by the result in the HE expansion of ref. [73]. The comparison is done on the quantity

$$\Delta\hat{\sigma}_{virt} = \int_{\hat{t}_-}^{\hat{t}_+} \frac{\alpha_s}{32\pi^2} \frac{1}{\hat{s}^2} \mathcal{V}_{fin} d\hat{t}, \tag{3.24}$$

where the finite part of the virtual corrections $\mathcal{V}_{fin}$ is defined as in ref. [78]. The results are shown in fig. 3.5. We note that $\mathcal{V}_{fin}$ depends on the choice of the IR subtraction, this is why in the lower panel of fig. 3.5 the difference between the expanded results and the numerical grid of ref. [81] is shown (divided by the Born result), a quantity that is independent of the IR subtraction term. The grid of ref. [86] shows very good agreement with our results at every invariant mass, except for the first few bins at low M_{HH}. The reason is a large uncertainty of the numerical grid on the low M_{HH} bins, that are described by only a few points in the numerical grid due to their small contribution to the total cross section. For moderate and large M_{HH} we observe differences below 1% in the ratio between our results and the ones of ref. [81]. We confirm these findings by comparing our results for $\mathcal{V}_{fin}$ with the values given in the grid [86] for various points at fixed $(M_{HH}, \hat{t})$. We find a good agreement, as can be inferred from table 3.1 for some representative values. We notice that in the region where both expansions perform less well we see differences of a few percent, although the latter will be reduced in $\Delta\hat{\sigma}_{virt}$ due to the integration over $\hat{t}$.

Finally, we show that our merging approach is flexible with respect to the modification of the input parameters by computing the virtual corrections for various renormalisation schemes of the top quark mass. It was noted in refs. [63, 64] that the di-Higgs production process suffers from a large uncertainty associated to the renormalisation

[4]We note that for ZH production no public code including the results of the full computation [65] is currently available. Hence we refrain from making any comparisons for ZH production.

USC UNIVERSIDADE DE SANTIAGO DE COMPOSTELA

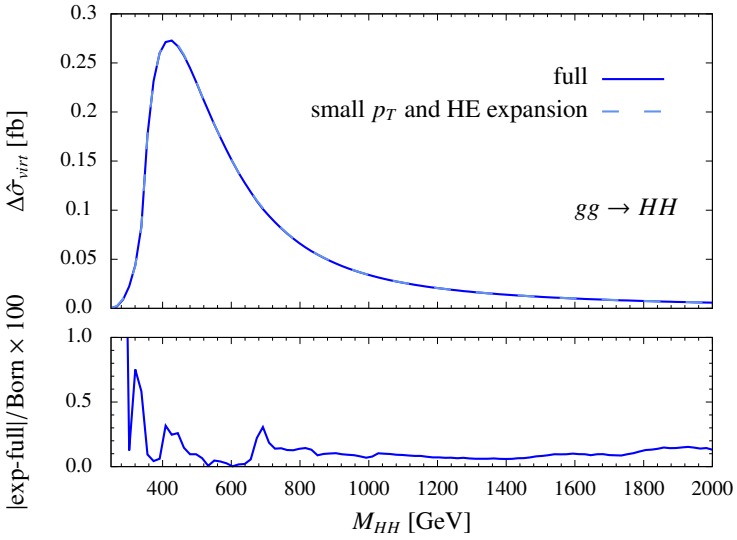

Figure 3.5: Upper pannel: $\Delta\hat{\sigma}_{virt}$ using the numerical grid provided in ref. [81] (dark blue line) and our combination of HE expansion and small p_T expansion (light blue dashed line). The lower panel shows the absolute value of the difference between the two results, normalized to the partonic LO cross section.

scheme of the top quark mass. In particular, an uncertainty on the NLO cross section between $+4\%$ and -18% [87] is related to the change from the on-shell renormalisation scheme to the $\overline{\text{MS}}$ scheme for the top mass, with the latter evaluated at different values of the renormalisation scale (m_t, M_{HH} and $M_{HH}/4$). The results presented so far have been calculated using the on-shell scheme for the top mass, however the form factors in the $\overline{\text{MS}}$ scheme can be obtained by simply shifting our result according to:

$$F_i^{NLO,\overline{\text{MS}}} = F_i^{NLO,\text{OS}} - \frac{1}{4}\frac{\partial F_i^{LO}}{\partial m_t^2}\Delta_{m_t^2} \tag{3.25}$$

with $i = \Delta, \square, 2$ and

$$\Delta_{m_t^2} = 2m_t^2 C_F \left[-4 + 3\log\left(\frac{m_t^2}{\mu^2}\right)\right] . \tag{3.26}$$

Notice that the numerical values for the top quark mass have to be adjusted to their $\overline{\text{MS}}$ values, which we evaluate following refs. [88, 89]. Since the LO results are available analytically, we can first build the Padé approximants of the p_T- or HE-expanded $F_i^{NLO,\text{OS}}$ form factors and then calculate the shift to the the $\overline{\text{MS}}$ scheme using the full LO form factors in eq. (3.25). Alternatively, we can use the expanded LO form factors to perform the shift in eq. (3.25) order by order in the p_T-expanded and the HE-expanded results, and then build Padé approximants on the $F_i^{NLO,\overline{\text{MS}}}$ form factors. The difference between these two approaches turns out to be well below the 0.5 permille level everywhere except near the top-mass threshold where the difference is at the percent level. For the

USC UNIVERSIDADE DE SANTIAGO DE COMPOSTELA

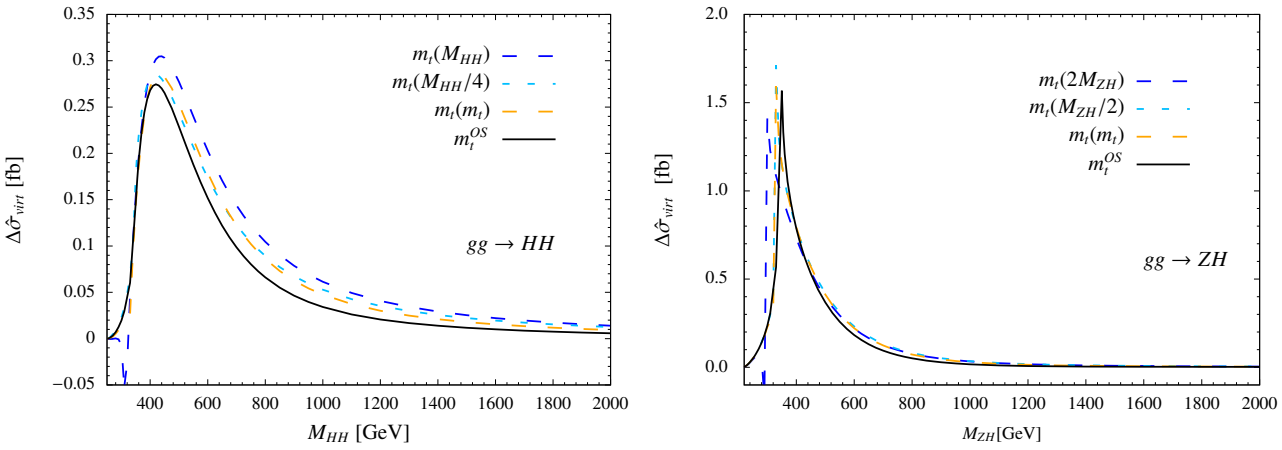

(a) (b)

Figure 3.6: The integrated virtual corrections in different renormalisation schemes for the top quark mass for (a) $gg \to HH$ and (b) $gg \to ZH$. The dashed lines show $\Delta\hat{\sigma}_{virt}$ in the $\overline{\text{MS}}$ scheme using the top quak mass evaluated at different choices of the renormalisation scale, while the black solid line shows the on-shell result.

$gg \to ZH$ process, the shift to the $\overline{\text{MS}}$ scheme can be applied in analogy to eq. (3.25) on the associated form factors[5]. For the triangle contributions we always use the results available in full top-mass dependence.

We present our results in fig. 3.6. We observe that indeed the $\Delta\hat{\sigma}_{virt}$ show a non-negligible dependence on the renormalisation scheme for the top quark mass. This holds true both for $gg \to HH$ and for $gg \to ZH$. In particular, for $gg \to ZH$ we see a shift of the maximal value of the differential $\Delta\hat{\sigma}_{virt}$, which is associated to the lower top quark mass value. This may point to a significant uncertainty related to the top-mass scheme also in the case of $gg \to ZH$. We notice, however, that the effects observed in fig. 3.6 are likely to be partially compensated by similar modifications in the LO cross section and by the inclusion of the real-emission corrections at NLO. Therefore, we use fig. 3.6 only as an illustration of the flexibility of the merging method discussed in this paper, and we leave a full assessment of the effects due the change of the top-mass renormalization scheme to a future work. For the same reason we refrain from providing a full comparison with ref. [87] for $gg \to HH$.

3.5 Conclusions

In this chapter, we combined an expansion in small p_T with a HE expansion for the processes $gg \to HH$ and $gg \to ZH$ and we showed that this combination leads to results that describe the whole phase space of the considered processes with high accuracy. The

[5]The $\Delta\hat{\sigma}_{virt}$ for $gg \to ZH$ was defined as in ref. [56].

USC UNIVERSIDADE DE SANTIAGO DE COMPOSTELA

expansion in small p_T is valid for $|\hat{t}| \lesssim 4m_t^2$, while the HE expansion is valid for $|\hat{t}| \gtrsim 4m_t^2$ and $\hat{s} > 4m_t^2$. For a successful combination of the two expansion methods, we extended the validity range of both expansions making use of simple Padé approximants. This allowed us to describe also the region $|\hat{t}| \simeq 4m_t^2$ very accurately. We verified our method first at LO, where exact analytic results are available. At the level of the differential partonic cross section, the difference with the results in exact top quark mass dependence never exceeded 1% for any of the M_{HH} bins. In a second step, we compared our results with a numerical grid containing the results of a computation in exact top quark mass dependence for the $gg \to HH$ process [81]. Also at NLO we could verify the good numerical accuracy of our approach, observing differences below 1% for the invariant mass bins where the numerical accuracy of the grid is assumed to be sufficiently high. We have also shown that in our analytic calculation the top quark mass renormalisation scheme can be easily changed. This shows the great flexibility of our analytic approach with respect to the numerical one. With a running time of well below 1 s per phase-space point our results can be well implemented in a fast and versatile Monte Carlo program.

USC UNIVERSIDADE DE SANTIAGO DE COMPOSTELA

USC
UNIVERSIDADE
DE SANTIAGO
DE COMPOSTELA

Chapter 4

Standard Model Effective Field Theory

The SM successfully describes the fundamental particles and their interactions and it has been extensively tested and confirmed by experiments [90]. However, it is widely believed that the SM is not a complete description of nature. In this context, the SM is considered as an effective theory emerging from a more fundamental and comprehensive theory at higher energies. Indeed, there are several experimental and theoretical indications that point towards the existence of new particles, new interactions, and more in general of New Physics (NP). Examples include the hierarchy problem, the existence of dark matter and the neutrino masses.
The search for NP beyond the SM has been one of the main drives behind the construction of the LHC and it is still one of its main aims. Fundamental information on the characteristics of the NP can be obtained at the LHC and its future High Luminosity (HL) upgrade through "indirect searches", that is through the precise measurement of physical processes, whether or not new particles are directly produced at the LHC. Constraints from direct searches indicate that NP degrees of freedom, if present, would probably appear at scales much above the EW scale. Therefore, NP properties could be studied in the framework of the Effective Field Theories (EFT), which is an incredibly powerful tool for the study of physical processes in theories where a hierarchy between lighter and heavier degrees of freedom is present. Indeed, if we know the full theory but we are interested only on physical processes at a certain scale of energy Λ , we can use an EFT to parametrize the effect of states with masses much larger than Λ in terms of local operators of the lighter states. This is a powerful feature of EFT, since it allows us to focus only on the relevant degrees of freedom and interactions, and therefore simplify the computations. On the other hand, if the physics at the heavy scale is unknown, EFT can be used to parametrize our ignorance of the complete model and to obtain information on the underlying UV theory, through the precise measurement of the interactions between the light states.
An extension of the SM that follows this approach is the Standard Model Effective Field Theory (SMEFT), in which all the SM fields (Higgs boson, top quark, etc.) are considered *light*. The SMEFT offers a reliable way to study the properties of BSM physics

USC UNIVERSIDADE DE SANTIAGO DE COMPOSTELA

without the need of specifying a concrete UV model. Indeed, in the SMEFT, the interactions between SM fields are modified with respect to their SM value, and precise measurements of these interactions can inform us on the properties of the BSM that cause the modifications. It is important to point out that also heavy resonances that are are beyond the reach of direct searches at colliders can still affect the interaction between SM fields and appear in indirect searches. For this reason the bounds obtained from global fits of the SMEFT operators provide a unique and versatile map from experiment to theory.
In this chapter we are are going to talk about the EFT method and the main characteristics of the SMEFT, explaining the virtues and the limits of this framework. In particular we will focus on the so-called *Warsaw basis* for SMEFT operators.

4.1 EFT

An Effective Field Theory can be defined as a Quantum Field Theory (QFT) that does not strictly limit to the appearance of dimension 4 operators. However, imposing this requirement, we have to deal with a significant issue: the number of counterterms needed to absorb the UV divergences that come from radiative corrections becomes infinite. This presents a problem that requires further examination. To better understand this point, we can analyze it from a mathematical and physics perspective.

From a mathematical perspective, the problem is clear. If a dimension 5 operator is added to a theory, it will generate dimension 6 operators at 1 loop. Consequently, to cancel the arising UV divergences, one has to include dimension 6 operators in the theory. However, this will generate dimension 7 operators, and the process continues indefinitely.

The physical viewpoint introduces a different aspect to this discussion. When we are performing the renormalization our goal is to cancel UV divergences by redefining the parameters of the theory. But in doing this, we are implying that our loop calculations include all relevant physics up to the UV scale, making our theory valid at all energy scales. This is a very powerful hypothesis.

Relaxing this assumption, we can impose that our theory is valid up to a certain cutoff scale, denoted as Λ. As we approach the scale Λ, a new theory may emerge. However, even if we don't have a full knowledge of the entire theory, we can still attempt to incorporate its effects. This can allow us to employ operators with $D > 4$, transforming our QFT into an EFT. Nevertheless, the problem of how we calculate quantum corrections still remains. To fix this issue we have to redefine our concept of renormalizability. When we are using an EFT, we initially set the order of negative powers of the cutoff scale Λ we wish to include, e.g Λ^{-2}. We then incorporate all operators up to that power in our Lagrangian, including operators with $D \geq 4$, e.g up to dim-6 in the case Λ^{-2}. Therefore, when we are evaluating a loop integral, we expand it as a series in $\frac{1}{\Lambda}$ at amplitude level and retain terms only up to the chosen power, discarding possible terms that may arise from double insertion of operators. By following this procedure, only a finite number

USC UNIVERSIDADE DE SANTIAGO DE COMPOSTELA

of operators are generated and only a finite number of counterterms is necessary. This procedure is effective but relies on certain assumptions to be meaningful. To ensure the validity of this approach, one must assume that contributions from higher-dimensional operators and double insertions of operators are much smaller than single insertions. In this context, we can take the SM as an example. Let's assume that the cut-off for the SM is $\Lambda = 1$ TeV

$$\begin{aligned} \text{dim-6 operator:} \quad & C_{\text{dim}-6}\frac{v^2}{\Lambda^2} \sim \frac{C_{\text{dim}-6}}{16} \\ \text{two dim-6 operators:} \quad & C^2_{\text{dim}-6}\frac{v^2}{\Lambda^4} \sim \frac{C^2_{\text{dim}-6}}{16^2} \\ \text{dim-8 operator:} \quad & C_{\text{dim}-8}\frac{v^4}{\Lambda^4} \sim \frac{C_{\text{dim}-8}}{16^2} \end{aligned} \tag{4.1}$$

where C_{dim} is the Wilson coefficient of the operator and v is the Higgs vev that we used to make the contribution adimensional[1]. By applying this rescaling, we obtain the conditions $C_{\text{dim}-6} \ll 16$ and $C_{\text{dim}-8} \ll C_{\text{dim}-6}$. These conditions appear reasonable, but it is important to note that the Wilson coefficients are not couplings themselves. Therefore, they can have large values without necessarily indicating the need for non-perturbative new physics.

4.2 HEFT

As mentioned in the Introduction, the calculations performed in the thesis are carried out in the SM and its most common EFT extension, the SMEFT framework. However, we notice that there is another common strategy to build an EFT extension to the SM, called Higgs Effective Field Theory (HEFT). In this approach, unlike SMEFT where the Higgs is the usual SM doublet, the Higgs field is considered to be a singlet under $G_{SM} = SU(2)_W \times U(1)_Y$, while the Goldstone bosons, resulting from the symmetry breaking process, arrange themselves in a non-linear representation of G_{SM} :

$$U = \exp(2i\frac{\phi^j T^j}{v}). \tag{4.2}$$

Although we will not delve into this method in the thesis, we think it is relevant to mention alternative frameworks to the one employed in this work. Overall, the main distinctions between HEFT and SMEFT lie in the energy scale, degrees of freedom and the scope of applicability for describing BSM physics.

In general HEFT includes SMEFT, thus all NP signals can be detected within this framework. However, in the limit $\Lambda \gg v$, HEFT is equivalent to SMEFT [91], but the

[1] v is the scale of the SM interactions, so it is logical to use this parameter.

USC UNIVERSIDADE DE SANTIAGO DE COMPOSTELA

calculations are more complex and complicated. Therefore, assuming $\Lambda \sim$ TeV, we can use SMEFT instead of HEFT to simplify the calculations, while still capturing the full range of BSM physics effects.

4.3 SMEFT

The concept of the Standard Model Effective Field Theory (SMEFT) has been developed and studied by many researchers in the field of particle physics. It is probably not possible to attribute its invention to a single individual or group. Indeed this approach has been built upon the foundations of EFT and the understanding of the SM. Various physicists have contributed to the development and exploration of SMEFT, including [92, 93, 94].
The SMEFT Lagrangian is constructed as an expansion in higher dimension operators, with the $SU(3) \times SU(2) \times U(1)$ gauge symmetry unbroken,

$$\mathcal{L} = \mathcal{L}_{SM} + \Sigma_{k=5}^{\infty} \Sigma_{a=1}^{n} \frac{C_a^k}{\Lambda^{k-4}} \mathcal{O}_a^k \,. \tag{4.3}$$

where the operators of mass-dimension k, $\mathcal{O}_a^k$, are constructed from SM fields and all of the effects of the beyond the SM (BSM) physics reside in the coefficient functions, C_a^k.

The focus of most of SMEFT research has been on dimension-6 operators and more recently on dimension-8. This is due to the fact that these operators provide the dominant contributions and it is commonly assumed that any new physics would initially manifest itself through a dimension-6 operator. Indeed, at dimension 5, only one operator arises and it introduces lepton number violation and yields Majorana masses for neutrinos. The stringent constraints on this type of violation needs either very high energy scales or very small coefficients to fit the experimental limits. See Appendix A.1 for a further discussion.

4.4 Warsaw basis

At dimension 6 in the SMEFT framework, as discussed in [95], there is a possibility of redundancy among the operators. In this context, redundancy refers to the presence of operators that can be related to each other through equations of motion (EOM), integration by parts (IBP), field redefinitions or underlying symmetries. Indeed, certain combinations of operators may lead to the same physical effects or have equivalent contributions to observables. As a result, including all possible operators in the analysis may lead to overcounting or redundant descriptions of the same physics. To address this issue, it is common to apply techniques such as the IBP or the EOM to build an operator basis. These methods help to systematically identify the independent structures and construct a minimal set of operators to catch the relevant BSM physics. Indeed, by removing redundant operators, we can obtain a more efficient and concise description

USC UNIVERSIDADE DE SANTIAGO DE COMPOSTELA

of the theory, facilitating the calculations and improving the comprehensibility of the results. Lastly, we notice that the identification of redundant operators requires meticulous consideration of the symmetries, fields content, and interactions of the theory. For this reason, the choice of operator basis plays a crucial role in determining the appropriate set of independent operators in SMEFT.
The most used operator basis in the SMEFT framework is the Warsaw basis, introduced by [96]. This basis choice has many advantages:

- Renormalization group investigation.

The Warsaw basis has been already studied in the context of the renormalization group and the associated RGEs have been completely calculated [97, 98, 99] at one loop order. This allows to perform calculations at NLO in this basis without the need for a change of basis which would also involve a SM field redefinition.

- FeynRules implemented in Mathematica.

The complete set of Feynman rules for the Warsaw basis have been derived in R_ξ gauges [100] and the final theory is expressed in a basis characterized by SM-like propagators for all physical and unphysical fields. Furthermore, in [101], the authors made publicly available a Mathematica code working with the *FeynRules* package, allowing automatic SMEFT amplitude calculations.

- Comparison of results.

The Warsaw basis is the currently most commonly used basis in SMEFT framework. Using the same basis in physics is useful to facilitate communication, promoting consistency and avoiding confusion between researchers.

4.4.1 Complete set of dimension-6 operator

The EFT we are building has to follow only two constraints: the operators must respect the gauge and the Lorentz symmetries. Additional requirements, such as CP conservation and/or the absence of operators that violate baryon symmetry, can be imposed. However, it should be noted that by imposing these conditions, one is already making specific assumptions about the underlying BSM physics. In the next sections, following [96], we perform the classification of all possible dimension-6 operators using the same notation introduced in 2.2.

4.4.2 Dimension 5 operators

For our analysis, it is convenient to initially consider only the left-handed fermions $\psi \in l, e_c, q, u_c, d_c$ as fundamental fields, using the charge conjugates of the $SU(2)_W$ - singlet fermions. Within this convention, there are three possibilities for the fermionic

USC UNIVERSIDADE DE SANTIAGO DE COMPOSTELA

currents [2]: $\psi_1\bar{\gamma}_\mu\psi_2, \psi_1^T\bar{C}\psi_2, \psi_1 C\bar{\sigma}_{\mu\nu}\psi_2$. By considering bosonic objects with the appropriate number of Lorentz indices and remembering that $X_{\mu\nu}$[3] is antisymmetric, complete sets of building blocks for for this class of operators can be easily determined for each fermionic current. For dimension 5 we have:

$$\begin{aligned} \psi_1\bar{\gamma}_\mu\psi_2 : &\quad (\phi D) \\ \psi_1^T\bar{C}\psi_2 : &\quad (\phi^2, D^2) \\ \psi_1 C\bar{\sigma}_{\mu\nu}\psi_2 : &\quad (X, D^2) \end{aligned} \tag{4.4}$$

where ϕ is the Higgs field and D is the SM covariant derivative. Recalling the hypercharges assigned in 2.2, we see that the currents involving C can never have hypercharge 0 while for the vector currents it can never be equal to $\pm\frac{1}{2}$. This means that the classes $(X, D^2, \phi D)$ can be discarded. Thus the only class we must consider is $\psi^2\phi^2$. The hypercharge of the Higgs product, if it is not 0, can be ± 1. The only fermionic current that can cancel it is the one built out of two lepton doublets. Therefore the only possibility is:

$$\epsilon_{jk}\epsilon_{mn}\phi^j\phi^m(l_p^k)^T C l_r^n \equiv (\widetilde{\phi}^\dagger l_p)^T C(\widetilde{\phi}^\dagger l_r)^T. \tag{4.5}$$

This operators violates lepton number conservation and, after eletroweak symmetry breaking, it generates neutrino masses and lepton mixings.

Bosonic Operators

For purely bosonic operators, due to constraints from the $SU(2)_W$ gauge group, it is necessary to have an even number of Higgs fields ϕ and an even number of covariant derivatives D so that all Lorentz indices must be contracted. Thus, the only potential field contents for dimension-6 bosonic operators are $X^3, X^2\phi^2, X^2D^2, X\phi^4, XD^4, X\phi^2D^2$, ϕ^6, ϕ^4D^2 and ϕ^2D^4. It is possible to demonstrate that all these operators can be reduced by the EOM (or symmetries considerations) to operators containing fermions or to classes $X^3, X^2\phi^2, \phi^6$ and ϕ^4D^2. The class $X\phi^4$ cannot appear because there is not any other object that can be used to contract the Lorentz indices. XD^4 can be moved in X^2D^2 because all possible contractions (including those with $\epsilon_{\mu\nu\rho\sigma}$) lead to the appearance of at least one invariant derivative commutator $[D_\mu, D_\nu] \sim X_{\mu\nu}$, which places it in the X^2D^2 class. For our classification, since we are interested to $\mathcal{O}(\frac{1}{\Lambda^2})$, the EOMs can be derived directly from the SM Lagrangian. We have:

$$\begin{aligned} (D_\mu D^\mu\phi)^j &= m^2\phi^j - \lambda(\phi^\dagger\phi)\phi^j - \bar{e}\lambda_e^\dagger l^j + \epsilon_{jk}\bar{q}^k\lambda_u u - \bar{d}\lambda_d^\dagger q^j, \\ (D^\rho G_{\rho\mu})^A &= g_s(\bar{q}\gamma_\mu T^A q + \bar{u}\gamma_\mu T^A u + \bar{d}\gamma_\mu T^A d), \\ (D^\rho W_{\rho\mu})^I &= \frac{g}{2}(\phi^\dagger i\overleftrightarrow{D}_\mu^I\phi + \bar{l}\gamma_\mu\tau^I l + \bar{q}\gamma_\mu\tau^I q), \\ (D^\rho B_{\rho\mu}) &= g'Y_\phi\phi^\dagger i\overleftrightarrow{D}_\mu\phi + g'\sum_{\psi\in\{l,e,q,u,d\}} Y_\psi\bar{\psi}\gamma_\mu\psi. \end{aligned} \tag{4.6}$$

[2] up to Lorentz indices

[3] We recall that $X_{\mu\nu}$ refers to the gauge field tensor and can be equal to $W^I_{\mu\nu}, G^A_{\mu\nu}$ or $B_{\mu\nu}$.

USC UNIVERSIDADE DE SANTIAGO DE COMPOSTELA

Furthermore, we define

$$\phi^\dagger i \overleftrightarrow{D}_\mu \phi \equiv \phi^\dagger (D_\mu \phi) - i(D_\mu \phi)^\dagger \phi \qquad \text{and} \qquad \phi^\dagger i \overleftrightarrow{D}^a_\mu \phi \equiv \phi^\dagger \tau^a D_\mu \phi - i(D_\mu \phi)^\dagger \tau^a \phi.$$

In this work, we have organized the operator classes in such a way that those with fewer covariant derivatives are considered "lower classes". Following [96], we will see that it is possible to reduce operators from higher to lower classes. If classes have an equal number of derivatives, the ordering is determined by the number of X tensors, with lower classes having fewer X tensors. We begin with the class of operators that can be reduced to lower class:

- $\phi^2 D^4$
  Here, we can consider only operators where all the derivatives act on a single ϕ field, because other possibilities are equivalent up to total derivatives. Contributions involving $\epsilon_{\mu\nu\rho\sigma}$ can be disregarded, because they result in terms in the form $[D_\mu, D_\nu] \sim X_{\mu\nu}$, which corresponds to lower classes. Similarly, the ordering of the covariant derivatives acting on ϕ can be chosen arbitrarily. We can take advantage of this freedom to use $D_\mu D^\mu \phi$ as the "building blocks" of the operators considered. This allows us to move this class to lower classes through the EOM 4.6.

- $\phi^2 X D^2$
  In this class, we consider X being potentially dual and we ignore $\epsilon_{\mu\nu\rho\sigma}$. Indices of X need to be contracted with both derivatives, thus we have to consider three cases: (i) Each derivative acts on a different ϕ field. We can eliminate this possibility through integration by parts, neglecting total derivatives. (ii) Both derivatives act on a single object. This results again in $[D_\mu, D_\nu] \sim X_{\mu\nu}$ leading to the $\phi^2 X^2$ class. (iii) One derivative acts on X and the other on ϕ. By EOM we can move to lower classes $\phi^4 D^2$ and $\psi^2 \phi D$.

- $X^2 D^2$
  For this class, similarly to the $\phi^2 D^4$, we can focus our attention only on operators where all the derivatives act on a single tensor. The case where both the derivatives are contracted with $\epsilon_{\mu\nu\rho\sigma}$ or with a single tensor is excluded because $[D_\mu, D_\nu] \sim X_{\mu\nu}$. Therefore, we allow the tensor X to be dual and ignore $\epsilon_{\mu\nu\rho\sigma}$ otherwise. In the case where each derivative is contracted with a different tensor, we use $[D_\mu, D_\nu] \sim X_{\mu\nu}$ to change the order their order and through EOM we we can move it to lower class. The only possibility is that the derivatives are contracted with themselves $\widetilde{X}^{\mu\nu} D^\rho D_\rho X_{\mu\nu}$. However, using the Bianchi identity

$$\widetilde{X}^{\mu\nu} D^\rho D_\rho X_{\mu\nu} = -\widetilde{X}^{\mu\nu} (D^\rho D_\mu X_{\nu\rho} + D^\rho D_\nu X_{\rho\mu}) \tag{4.7}$$

  and again using $[D_\mu, D_\nu] \sim X_{\mu\nu}$ and EOM we can reduce this case to the lower class.

We can now review the operators appearing in table 4.1:

USC UNIVERSIDADE DE SANTIAGO DE COMPOSTELA

- X^3
  Here we have the first class of operators appearing in the Warsaw basis. We denote X, Y, Z the possible different tensors that may appear in this class. We allow them to be dual, thus we forget about $\epsilon_{\mu\nu\rho\sigma}$ otherwise. The only possible non vanishing and independent contraction of Lorentz indices reads $X^{\nu}_{\mu}Y^{\rho}_{\nu}Z^{\mu}_{\rho}$. Indeed, all the three tensors must be different because $X_{\alpha\mu}X_{\beta\nu}Z^{\mu\nu}g^{\alpha\beta}$ is zero by the antisimmetry of Z. Furthermore, neither of the two tensors can be dual, as $X^{\nu}_{\mu}\widetilde{X}^{\rho}_{\nu} = -\frac{1}{4}\delta^{\rho}_{\mu}X_{\alpha\beta}\widetilde{X}_{\alpha\beta}$ is symmetric while Z is antisymmetric. The only possibility is that to get a gauge singlet from three different tensors, we have to use the structure constants f^{ABC} and ϵ^{IJK}.

- $X^2\phi^2$
  The Higgs combinations can be singlets or triplets of $SU(2)_W$. Hypercharge conditions further constrain the forms of these products to be written as $\phi^\dagger\phi$ and $\phi^\dagger\tau^I\phi$. In total we have eight possible operators, as listed in table 4.1.

- ϕ^6
  Hypercharge constraints imply that exactly three of the Higgs fields must be complex conjugate. As in the previous case, we can consider tensor products of singlets and triplets of $SU(2)_W$. The combination of three triplets can only result in an overall singlet if it is fully antisymmetric. However, since all the triplets are identical, this combination evaluates to zero. Two triplets and one singlet is a possible combination $(\phi^\dagger\tau^I\phi)(\phi^\dagger\tau^I\phi)(\phi^\dagger\phi)$, but due to the equation

$$\tau^I_{jk}\tau^I_{mn} = 2\delta_{jn}\delta_{mk} - \delta_{jk}\delta_{mn} \tag{4.8}$$

  it results equals to $(\phi^\dagger\phi)^3$. Hence, we have only one independent operator in this class.

- ϕ^4D^2
  As in the other cases, the hypercharge constrains two Higgs fields to complex conjugated. Considering that the two derivatives must be contracted, they have to act on two different ϕ fields, or the EOM leads the operator to lower classes. If the derivatives act on two conjugated or two unconjugated fields, we can eliminate those possibilities by IBP. On the other hand, if one derivative acts on a conjugated field and the other on an unconjugated field, our $SU(2)_W$ tensor product contains four distinct fundamental representations, indicating the presence of exactly two independent singlets.

USC UNIVERSIDADE DE SANTIAGO DE COMPOSTELA

X^3		ϕ^6 and $\phi^4 D^2$		$\psi^2\phi^3$	
Q_G	$f^{ABC}G_\mu^{A\nu}G_\nu^{B\rho}G_\rho^{C\mu}$	Q_ϕ	$(\phi^\dagger\phi)^3$	$Q_{e\phi}$	$(\phi^\dagger\phi)(\bar{l}'_p e'_r \phi)$
$Q_{\widetilde{G}}$	$f^{ABC}\widetilde{G}_\mu^{A\nu}G_\nu^{B\rho}G_\rho^{C\mu}$	$Q_{\phi\Box}$	$(\phi^\dagger\phi)\Box(\phi^\dagger\phi)$	$Q_{u\phi}$	$(\phi^\dagger\phi)(\bar{q}'_p u'_r \widetilde{\phi})$
Q_W	$\varepsilon^{IJK}W_\mu^{I\nu}W_\nu^{J\rho}W_\rho^{K\mu}$	$Q_{\phi D}$	$\left(\phi^\dagger D^\mu\phi\right)^*\left(\phi^\dagger D_\mu\phi\right)$	$Q_{d\phi}$	$(\phi^\dagger\phi)(\bar{q}'_p d'_r \phi)$
$Q_{\widetilde{W}}$	$\varepsilon^{IJK}\widetilde{W}_\mu^{I\nu}W_\nu^{J\rho}W_\rho^{K\mu}$				
$X^2\phi^2$		$\psi^2 X\phi$		$\psi^2\phi^2 D$	
$Q_{\phi G}$	$\phi^\dagger\phi\, G^A_{\mu\nu}G^{A\mu\nu}$	Q_{eW}	$(\bar{l}'_p\sigma^{\mu\nu}e'_r)\tau^I\phi W^I_{\mu\nu}$	$Q_{\phi l}^{(1)}$	$(\phi^\dagger i\overleftrightarrow{D}_\mu\phi)(\bar{l}'_p\gamma^\mu l'_r)$
$Q_{\phi\widetilde{G}}$	$\phi^\dagger\phi\,\widetilde{G}^A_{\mu\nu}G^{A\mu\nu}$	Q_{eB}	$(\bar{l}'_p\sigma^{\mu\nu}e'_r)\phi B_{\mu\nu}$	$Q_{\phi l}^{(3)}$	$(\phi^\dagger i\overleftrightarrow{D}^a_\mu\phi)(\bar{l}'_p\tau^I\gamma^\mu l'_r)$
$Q_{\phi W}$	$\phi^\dagger\phi\, W^I_{\mu\nu}W^{I\mu\nu}$	Q_{uG}	$(\bar{q}'_p\sigma^{\mu\nu}T^A u'_r)\widetilde{\phi}\, G^A_{\mu\nu}$	$Q_{\phi e}$	$(\phi^\dagger i\overleftrightarrow{D}_\mu\phi)(\bar{e}'_p\gamma^\mu e'_r)$
$Q_{\phi\widetilde{W}}$	$\phi^\dagger\phi\,\widetilde{W}^I_{\mu\nu}W^{I\mu\nu}$	Q_{uW}	$(\bar{q}'_p\sigma^{\mu\nu}u'_r)\tau^I\widetilde{\phi}\, W^I_{\mu\nu}$	$Q_{\phi q}^{(1)}$	$(\phi^\dagger i\overleftrightarrow{D}_\mu\phi)(\bar{q}'_p\gamma^\mu q'_r)$
$Q_{\phi B}$	$\phi^\dagger\phi\, B_{\mu\nu}B^{\mu\nu}$	Q_{uB}	$(\bar{q}'_p\sigma^{\mu\nu}u'_r)\widetilde{\phi}\, B_{\mu\nu}$	$Q_{\phi q}^{(3)}$	$(\phi^\dagger i\overleftrightarrow{D}^a_\mu\phi)(\bar{q}'_p\tau^I\gamma^\mu q'_r)$
$Q_{\phi\widetilde{B}}$	$\phi^\dagger\phi\,\widetilde{B}_{\mu\nu}B^{\mu\nu}$	Q_{dG}	$(\bar{q}'_p\sigma^{\mu\nu}T^A d'_r)\phi\, G^A_{\mu\nu}$	$Q_{\phi u}$	$(\phi^\dagger i\overleftrightarrow{D}_\mu\phi)(\bar{u}'_p\gamma^\mu u'_r)$
$Q_{\phi WB}$	$\phi^\dagger\tau^I\phi\, W^I_{\mu\nu}B^{\mu\nu}$	Q_{dW}	$(\bar{q}'_p\sigma^{\mu\nu}d'_r)\tau^I\phi\, W^I_{\mu\nu}$	$Q_{\phi d}$	$(\phi^\dagger i\overleftrightarrow{D}_\mu\phi)(\bar{d}'_p\gamma^\mu d'_r)$
$Q_{\phi\widetilde{W}B}$	$\phi^\dagger\tau^I\phi\,\widetilde{W}^I_{\mu\nu}B^{\mu\nu}$	Q_{dB}	$(\bar{q}'_p\sigma^{\mu\nu}d'_r)\phi\, B_{\mu\nu}$	$Q_{\phi ud}$	$i(\widetilde{\phi}^\dagger D_\mu\phi)(\bar{u}'_p\gamma^\mu d'_r)$

Table 4.1: Dimension-6 operators other than the four-fermion ones (from [96]). For brevity we suppress fermion chiral indices L, R.

4.4.3 Single-fermionic-current operator classification

For this class of operators it is convenient to use the same notation introduced in 4.4.2. Again, by similar considerations, we have three possible fermionic currents. They are:

$$\begin{aligned} \psi_1\bar{\gamma}_\mu\psi_2: &\quad (XD, \phi^2 D, D^3) \\ \psi_1^T\bar{C}\psi_2: &\quad (\phi^3, \phi D^2) \\ \psi_1 C\bar{\sigma}_{\mu\nu}\psi_2: &\quad (X\phi, \phi D^2) \end{aligned} \tag{4.9}$$

For scalar and tensor fermionic currents, we notice that the numer of higgs fields is always odd. As a result, these currents must form isospin doublets. Using the standard notation with right-handed singlets, these currents are represented by $\bar{\psi}_1\psi_2$ and $\bar{\psi}_1\sigma_{\mu\nu}\psi_2$. Similarly, vector currents combine with an even number of Higgs fields, thus they can only form isospin singlets or triplets. With this consideration, no vector currents with C enter into our considerations, even if the isospin singlets are taken as right-handed. Therefore , we can go back to the standard notation in the following discussion. As for the bosonic case, we will use the EOM 4.6 and as well as the classical EOM for fermions

$$i\not{D}l = \lambda_e e\phi, \qquad i\not{D}e = \lambda_e\phi^\dagger l, \qquad i\not{D}q = \lambda_u u\widetilde{\phi} + \lambda_d d\phi, \qquad i\not{D}u = \lambda_u^\dagger\widetilde{\phi}^\dagger q, \qquad i\not{D}d = \lambda_d^\dagger\phi^\dagger q. \tag{4.10}$$

USC UNIVERSIDADE DE SANTIAGO DE COMPOSTELA

Furthermore, we will need to recall the identities:

$$\gamma_\mu\gamma_\nu = g_{\mu\nu} - i\sigma_{\mu\nu}, \qquad \gamma_\mu\gamma_\nu\gamma_\rho = g_{\mu\nu}\gamma_\rho + g_{\nu\rho}\gamma_\mu - g_{\rho\mu}\gamma_\nu - \epsilon_{\mu\nu\rho\sigma}\gamma^\rho\gamma_5. \tag{4.11}$$

As in the previous section, we start with the operators that can be reduced to lower classes:

- $\psi^2 D^3$
  Here, three covariant derivatives are contracted with the vectorial current $\bar{\psi}\gamma_\mu\psi$. As discussed for the classes ϕ^2D^4 and X^2D^2, we can eliminate derivatives acting on $\bar{\psi}$ "by parts" and choose the ordering of the derivatives acting on ψ. By choosing the ordering as $\bar{\psi}D_\mu D^\mu \not{D}\psi$, we can reduce by EOM to lower classes.

- $\psi^2\phi D^2$
  In this class, we consider scalar and tensorial currents. Derivatives acting on $\bar{\psi}$ can be removed "by parts". The cases $\bar{\psi}\sigma^{\mu\nu}\psi D_\mu D_\nu\phi$ and $\phi\bar{\psi}\sigma^{\mu\nu}D_\mu D_\nu\psi$ can be moved to lower classes recalling that $[D_\mu, D_\nu] \sim X_{\mu\nu}$. We still have 4 possible combinations:

  $$\bar{\psi}\psi D_\mu D^\mu\phi,\ \phi\bar{\psi}D_\mu D^\mu\psi,\ (D_\mu\phi)\bar{\psi}\sigma^{\mu\nu}D_\nu\psi,\ (D_\mu\phi)\bar{\psi}D^\mu\psi.$$

  The cases $\bar{\psi}\psi D_\mu D^\mu\phi$ and $\phi\bar{\psi}D_\mu D^\mu\psi \sim \phi\bar{\psi}\not{D}\not{D}\psi$ can be reduced to lower classes by EOM; $(D_\mu\phi)\bar{\psi}\sigma^{\mu\nu}D_\nu\psi$ can be moved to the last case recalling that $\sigma_{\mu\nu} = -i(g_{\mu\nu} - \gamma_\mu\gamma_{nu})$. Considering that:

  $$\begin{aligned} 2(D_\mu\phi)\bar{\psi}D^\mu\psi &= (D_\mu\phi)\bar{\psi}\gamma^\mu\not{D}\psi + (D_\mu\phi)\bar{\psi}\not{D}\gamma^\mu\psi \\ &= -\bar{\psi}\overleftarrow{\not{D}}\gamma_\mu\psi D^\mu\phi - \bar{\psi}\gamma^\mu\gamma^\nu\psi D_\mu D_\nu\phi + \dots \end{aligned} \tag{4.12}$$

  where the " $\dots$ " stands for a total derivative and lower classes. Finally, using the EOM and recalling the relation 4.11, we can move it to lower classes.

- $\psi^2 XD$
  Similarly to other cases, we assume that X can be dual and neglect $\epsilon_{\mu\nu\rho\sigma}$ otherwise. Since we are dealing with a vectorial current, recalling that X is antisymmetric, the derivative must be contracted with X. If it acts on X, we can move it to lower classes (for the usual tensor) through EOM or we can use the Bianchi identity $D^\rho\widetilde{X}_{\rho\mu} = 0$ (for the dual tensor). The only remaining expression to be considered is $X^{\mu\nu}\bar{\psi}\gamma_\mu D_\nu\psi$. It is reduced to lower classes as follows:

  $$\begin{aligned} X^{\mu\nu}\bar{\psi}\gamma_\mu D_\nu\psi = \frac{1}{2}X^{\mu\nu}\bar{\psi}(\gamma_\mu\gamma_\nu\not{D} + \gamma_\mu\not{D}\gamma_\nu)\psi = \frac{1}{2}X^{\mu\nu}\bar{\psi}(\gamma_\mu\gamma_\nu\not{D} - \not{D}\gamma_\mu\gamma_\nu)\psi + X^{\mu\nu}\bar{\psi}\gamma_\mu D_\nu\psi \\ \implies \frac{1}{4}X^{\mu\nu}\bar{\psi}(\gamma_\mu\gamma_\nu\not{D} - \not{D}\gamma_\mu\gamma_\nu)\psi = \frac{1}{4}X^{\mu\nu}\bar{\psi}\gamma_\mu\gamma_\nu\not{D}\psi + \frac{1}{4}X^{\mu\nu}\overleftarrow{\bar{\psi}\not{D}}\gamma_\mu\gamma_\nu\psi + \\ + \frac{1}{4}D^\rho X^{\mu\nu}\bar{\psi}\gamma_\rho\gamma_\mu\gamma_\nu\psi + \dots \end{aligned} \tag{4.13}$$

USC UNIVERSIDADE DE SANTIAGO DE COMPOSTELA

In the last equation the first two terms are reduced to lower classes through EOM. For the last term we have:

$$D^\rho X^{\mu\nu}\bar{\psi}\gamma_\rho\gamma_\mu\gamma_\nu\psi = 2\bar{\psi}\gamma_\mu\psi D^\rho X^{\mu\nu} - i\epsilon_{\rho\mu\nu\sigma}\bar{\psi}\gamma^\sigma\gamma_5\psi D^\rho X^{\mu\nu}. \tag{4.14}$$

In both the cases (X dual or not), using EOM and Bianchi identity, we can move this terms to lower classes.

We continue our review discussing the other operators appearing in table 4.1:

- $\psi^2\phi^3$
  The fermion current must take the form of an isospin doublet and color singlet, like the Yukawa in the SM. The number of conjugated and un-conjugated scalar fields in ϕ^3 is fixed for each of the fermion currents due to hypercharge constraints. As a result, the only possibilities for this class are the Yukawa terms multiplied by $\phi^\dagger\phi$.

- $\psi^2 X\phi$
  In this case we have to consider only tensorial currents. Again, to respect hypercharge constraints, the fermion current must be analogous to the SM Yukawa couplings. For each tensor field $X_{\mu\nu}$, there is only one possible contraction with each fermionic current. The dual tensors $\tilde{X}$ would not yield any new results, due to the identities:

$$\epsilon_{\alpha\beta\mu\nu}\sigma^{\mu\nu} = 2i\sigma_{\alpha\beta}\gamma_5 \text{ and } \gamma_5\psi_{L,R} = \mp\psi_{L,R}. \tag{4.15}$$

- $\psi^2\phi^2 D$
  If the derivative acts on any of the fermion fields, its contraction with the vector current leads to equations of motion (EOMs) and brings us to the previously discussed lower class $\psi^2\phi^3$. Therefore, we can just consider the case where the derivative act on the scalar fields. The Higgs fields combined can give isospin singlets or triplets and color singlets. The fermion currents must obey to the same selection rules, allowing for precisely the currents listed in table 4.1, with the exception of the $u\gamma_\mu d$ current, which requires Hermitian conjugation. The number of conjugated and unconjugated Higgs fields is determined by hypercharge conditions. We begin by removing derivatives by using integration by parts on one of the scalars. We then form isospin singlets or triplets from products of ϕ_1 and $D_\mu\phi_2$ according to the structure of the corresponding fermion currents. At this point, we obtain operators that differ from those in table 4.1 only by the presence of D instead of $\overset{\leftrightarrow}{D}$. The point is that the operator without $\overset{\leftrightarrow}{D}$, are not Hermitian and we have to verify if the h.c. are independent from them or not. Notice that this issue does not occur for all the other operators (also for $Q_{\phi ud}$), since they are Hermitian by construction. For the remaining seven operators, considering the symmetric combination we have:

$$\phi^\dagger(D_\mu + \overset{\leftarrow}{D}_\mu)\phi\bar{\psi}\gamma_\mu\psi = \partial_\mu(\phi^\dagger\phi)\phi\bar{\psi}\gamma_\mu\psi = (\phi^\dagger\phi)\phi\bar{\psi}(\not{D} + \overset{\leftarrow}{\not{D}})\psi \tag{4.16}$$

USC UNIVERSIDADE DE SANTIAGO DE COMPOSTELA

and we can move them lower classes by EOM. The review on single-fermion-current operators is completed.

4.4.4 Four-fermion operator classification

Four-fermion operators are numerous but straightforward to classify. First, similar to the previous section, we consider only left-handed fermions $\psi \in l, e^c, q, u^c, d^c$. Besides trivial outcomes involving products of two zero-hypercharge currents (indicated in 4.2 as $(\bar{L}L)(\bar{L}L), (\bar{R}R)(\bar{R}R), (\bar{L}L)(\bar{R}R),$), we have only a few other possible field contents:

$$(\bar{l}\bar{e}^c d^c q), (q u^c q d^c), (l e^c q u^c), (qqql), (d^c u^c u^c e^c), (qq\bar{u}^c\bar{e}^c), (ql\bar{u}^c\bar{d}^c) \tag{4.17}$$

and the associated hermitian conjugate. The first three cases generate B-Conserving operators while the other four generate B-violating ones. We start by considering the expressions with two ψ and two $\bar{\psi}$. In this case, by spin considerations, we have only one single pairing; looking at the $SU(2)_W$ quantum numbers, we see that there are two doublets and two singlets fields, meaning that we can have only one singlet. Finally, including also the colour indices, we have

$$\begin{aligned} \bar{3} \otimes 3 &= 8 \oplus 1 && \text{B-conserving} \\ 3 \otimes 3 \otimes 3 &= 10 \oplus 8 \oplus 8 \oplus 1 && \text{B-violating} \end{aligned} \tag{4.18}$$

thus we have only one operator for each of three considered cases. In Table 4.2, they are indicated as $Q_{ledq}, Q_{duq}, Q_{qqu}$, using the standard right-hand notation. In the other four cases in 4.17, we have four left handed fermions. Again, by applying spin constraints and Fierz identities, we can eliminate redundant cases. Finally, taking into account isospin and color index contractions, we finalize the construction of the four-fermion operators. It can be readily confirmed that the listed operators form a complete basis for four-fermion operators, as discussed in [96].

4.5 SMEFT couplings

In SMEFT, similarly to what happens in the SM, the weak gauge bosons and the fermions acquire mass due to the SSB mechanism. However, unlike in the SM, to identify the physical degrees of freedom one needs to perform an extra intermediate step involving field rescalings, since SSB also affects the canonical normalization of the kinetic terms. This applies also to the SM fermions where, before the usual diagonalization of the Yukawa couplings, we need to redefine the SM fields and couplings. This process is accurately described in [100] and it involves several steps that we will not report entirely in this thesis, but we will just show the main results.

USC UNIVERSIDADE DE SANTIAGO DE COMPOSTELA

$(\bar{L}L)(\bar{L}L)$		$(\bar{R}R)(\bar{R}R)$		$(\bar{L}L)(\bar{R}R)$	
Q_{ll}	$(\bar{l}'_p\gamma_\mu l'_r)(\bar{l}'_s\gamma^\mu l'_t)$	Q_{ee}	$(\bar{e}'_p\gamma_\mu e'_r)(\bar{e}'_s\gamma^\mu e'_t)$	Q_{le}	$(\bar{l}'_p\gamma_\mu l'_r)(\bar{e}'_s\gamma^\mu e'_t)$
$Q_{qq}^{(1)}$	$(\bar{q}'_p\gamma_\mu q'_r)(\bar{q}'_s\gamma^\mu q'_t)$	Q_{uu}	$(\bar{u}'_p\gamma_\mu u'_r)(\bar{u}'_s\gamma^\mu u'_t)$	Q_{lu}	$(\bar{l}'_p\gamma_\mu l'_r)(\bar{u}'_s\gamma^\mu u'_t)$
$Q_{qq}^{(3)}$	$(\bar{q}'_p\gamma_\mu\tau^I q'_r)(\bar{q}'_s\gamma^\mu\tau^I q'_t)$	Q_{dd}	$(\bar{d}'_p\gamma_\mu d'_r)(\bar{d}'_s\gamma^\mu d'_t)$	Q_{ld}	$(\bar{l}'_p\gamma_\mu l'_r)(\bar{d}'_s\gamma^\mu d'_t)$
$Q_{lq}^{(1)}$	$(\bar{l}'_p\gamma_\mu l'_r)(\bar{q}'_s\gamma^\mu q'_t)$	Q_{eu}	$(\bar{e}'_p\gamma_\mu e'_r)(\bar{u}'_s\gamma^\mu u'_t)$	Q_{qe}	$(\bar{q}'_p\gamma_\mu q'_r)(\bar{e}'_s\gamma^\mu e'_t)$
$Q_{lq}^{(3)}$	$(\bar{l}'_p\gamma_\mu\tau^I l'_r)(\bar{q}'_s\gamma^\mu\tau^I q'_t)$	Q_{ed}	$(\bar{e}'_p\gamma_\mu e'_r)(\bar{d}'_s\gamma^\mu d'_t)$	$Q_{qu}^{(1)}$	$(\bar{q}'_p\gamma_\mu q'_r)(\bar{u}'_s\gamma^\mu u'_t)$
		$Q_{ud}^{(1)}$	$(\bar{u}'_p\gamma_\mu u'_r)(\bar{d}'_s\gamma^\mu d'_t)$	$Q_{qu}^{(8)}$	$(\bar{q}'_p\gamma_\mu T^A q'_r)(\bar{u}'_s\gamma^\mu T^A u'_t)$
		$Q_{ud}^{(8)}$	$(\bar{u}'_p\gamma_\mu T^A u'_r)(\bar{d}'_s\gamma^\mu T^A d'_t)$	$Q_{qd}^{(1)}$	$(\bar{q}'_p\gamma_\mu q'_r)(\bar{d}'_s\gamma^\mu d'_t)$
				$Q_{qd}^{(8)}$	$(\bar{q}'_p\gamma_\mu T^A q'_r)(\bar{d}'_s\gamma^\mu T^A d'_t)$

$(\bar{L}R)(\bar{R}L)$ and $(\bar{L}R)(\bar{L}R)$		B-violating	
Q_{ledq}	$(\bar{l}'^j_p e'_r)(\bar{d}'_s q'^j_t)$	Q_{duq}	$\varepsilon^{\alpha\beta\gamma}\varepsilon_{jk}\left[(d'^\alpha_p)^T\mathbb{C}u'^\beta_r\right]\left[(q'^{\gamma j}_s)^T\mathbb{C}l'^k_t\right]$
$Q_{quqd}^{(1)}$	$(\bar{q}'^j_p u'_r)\varepsilon_{jk}(\bar{q}'^k_s d'_t)$	Q_{qqu}	$\varepsilon^{\alpha\beta\gamma}\varepsilon_{jk}\left[(q'^{\alpha j}_p)^T\mathbb{C}q'^{\beta k}_r\right]\left[(u'^\gamma_s)^T\mathbb{C}e'_t\right]$
$Q_{quqd}^{(8)}$	$(\bar{q}'^j_p T^A u'_r)\varepsilon_{jk}(\bar{q}'^k_s T^A d'_t)$	Q_{qqq}	$\varepsilon^{\alpha\beta\gamma}\varepsilon_{jn}\varepsilon_{km}\left[(q'^{\alpha j}_p)^T\mathbb{C}q'^{\beta k}_r\right]\left[(q'^{\gamma m}_s)^T\mathbb{C}l'^n_t\right]$
$Q_{lequ}^{(1)}$	$(\bar{l}'^j_p e'_r)\varepsilon_{jk}(\bar{q}'^k_s u'_t)$	Q_{duu}	$\varepsilon^{\alpha\beta\gamma}\left[(d'^\alpha_p)^T\mathbb{C}u'^\beta_r\right]\left[(u'^\gamma_s)^T\mathbb{C}e'_t\right]$
$Q_{lequ}^{(3)}$	$(\bar{l}'^j_p\sigma_{\mu\nu}e'_r)\varepsilon_{jk}(\bar{q}'^k_s\sigma^{\mu\nu}u'_t)$		

Table 4.2: Four-fermion operators (from [96]). For brevity we suppress fermion chiral indices L, R.

4.5.1 Higgs sector

We define the Higgs doublet as

$$\phi = \begin{pmatrix} \varphi^+ \\ \frac{1}{\sqrt{2}}(v + h + i\varphi^0) \end{pmatrix}, \tag{4.19}$$

where h, φ^+ and φ^0 are the Higgs and Goldstone bosons, and v is the electroweak vev. Due to the contribution of $Q_\phi, Q_{\phi\Box}$ and $O_{\phi D}$ the corrected vev and the Higgs mass are:

$$\begin{aligned} v &= \sqrt{\frac{2\mu^2}{\lambda}} + \frac{3\mu^3}{\sqrt{2}\lambda^{5/2}}C_\phi, \\ m_h^2 &= \lambda - (3C_\phi - 2\lambda C_{\phi\Box} + \frac{\lambda}{2}C_{\phi D})v^4. \end{aligned} \tag{4.20}$$

where C_j is the Wilson coefficient of the operator of O_j.

USC UNIVERSIDADE DE SANTIAGO DE COMPOSTELA

4.5.2 EW gauge sector

The gauge couplings are redefined as:

$$\begin{aligned}\bar{g} &= \frac{g}{1 - C_{\phi W} v^2}, \\ \bar{g}' &= \frac{g'}{1 - C_{\phi B} v^2}, \\ \bar{g_Z} &= \sqrt{\bar{g}^2 + \bar{g}'^2}\left(1 + \frac{\epsilon \bar{g} \bar{g}'}{\bar{g}^2 + \bar{g}'^2}\right),\end{aligned} \tag{4.21}$$

with

$$\epsilon \equiv C_{\phi W B} v^2. \tag{4.22}$$

The masses read:

$$\begin{aligned}m_W &= \frac{1}{2} \bar{g} v, \\ m_Z &= \frac{1}{2} \bar{g_Z} v \left(1 + \frac{1}{4} C_{\phi D} v^2\right), \\ m_A &= 0.\end{aligned} \tag{4.23}$$

We notice that, as expected from gauge invariance, the photon remains massless.

4.6 Fermion sector

The Yukawa couplings read:

$$\begin{aligned}\lambda'_\nu &= -v^2 C_{\nu\nu}, & \lambda'_e &= \frac{v}{\sqrt{2}}\left(\lambda_e - C_{e\phi} \frac{v^2}{2}\right), \\ \lambda'_u &= \frac{v}{\sqrt{2}}\left(\lambda_e - C_{u\phi} \frac{v^2}{2}\right), & \lambda'_d &= \frac{v}{\sqrt{2}}\left(\lambda_e - C_{d\phi} \frac{v^2}{2}\right).\end{aligned} \tag{4.24}$$

To diagonalize the Yukawa we can use the same procedure as in the SM for the charged fermions, while for the neutrino we have:

$$U_{\nu_L}^T \lambda'_\nu U_{\nu_L} = M_\nu = \mathrm{diag}(m_{\nu_e}, m_{\nu_\mu}, m_{\nu_\mu}). \tag{4.25}$$

We stress that without fermion SM-singlets (e.g. right hand neutrino) in the SMEFT spectrum, neutrinos cannot acquire mass as Dirac particles. Finally, we mention that in the Majorana case, all interactions that include neutrinos intrinsically violate lepton number. Clearly, these effects are dependent on neutrino masses and in general they result in small or negligible corrections to the amplitudes.

USC UNIVERSIDADE DE SANTIAGO DE COMPOSTELA

4.7 Effects on observables

An important feature of dimension-6 operators is that they are related to the precision observables of the SM, thus they have an important impact on new physics search. For example, we can consider the custodial symmetry of the SM. First, we introduce a new parameter $\hat{\rho}$ (related to to 2.25):

$$\hat{\rho} \equiv \frac{g^2 m_Z^2}{(g^2 + g'^2) m_W^2} = \frac{g^2 m_Z^2}{g_Z^2 m_W^2}. \tag{4.26}$$

Then, we add the SMEFT modifications

$$\hat{\rho} = \frac{(g^2 + \Delta g^2) m_Z^2}{(g_Z^2 + \Delta g_Z^2) m_W^2} = \frac{\bar{g}^2 m_Z^2}{\bar{g_Z}^2 m_W^2} \tag{4.27}$$

where to simplify the notation, we introduced the barred quantities. m_Z and m_W are the masses of the gauge bosons redefined in 4.23, and we have seen that their relation to the gauge couplings changes. At LO we have:

$$m_W = \frac{\bar{g} v}{2} \quad \text{and} \quad m_Z = \frac{\bar{g_Z} v}{2} + \bar{g_Z} \Delta m_Z \tag{4.28}$$

where Δm_Z is generated by the operator

$$Q_{\phi D} = (\phi^\dagger D^\mu \phi)^* (\phi^\dagger D_\mu \phi) \sim \frac{v^4}{16} \bar{g_Z}^2 Z^\mu Z_\mu \tag{4.29}$$

and the term $Z^\mu Z_\mu$ modify the Z mass. Therefore we have:

$$\hat{\rho} = \frac{\bar{g}^2 m_Z^2}{\bar{g_Z}^2 m_W^2} = 1 + \frac{\Delta m_Z}{v^2} \sim 1 + C_{\phi D}. \tag{4.30}$$

From equation 4.30, due to the direct influence of $C_{\phi D}$, it is clear that careful consideration is required in theoretical calculations and experimental analyses of the $\hat{\rho}$ parameter. As we we will see this argument can be extended to many precision observables of the SM.

USC UNIVERSIDADE DE SANTIAGO DE COMPOSTELA

USC
UNIVERSIDADE
DE SANTIAGO
DE COMPOSTELA

Chapter 5

Electroweak precision observables

Historically, electroweak precision observables (EWPOs) provided strong evidence that the SM describes physics at EW scale. Similarly, in the SMEFT approach, comparisons of EWPOs with theoretical predictions severely constrain the coefficients associated to the new physics. Predictions for observables are typically made at the lowest order in the QCD and electroweak expansions in the SMEFT and often ignore the effects of flavor. In this chapter, we present results for electroweak precision observables at the next-to-leading order QCD and electroweak expansions (NLO) of the SMEFT with an arbitrary flavor structure for the fermion operators. Numerical NLO SMEFT fits to EWPOs have a strong dependence on the assumed flavor structures and we demonstrate this using various popular assumptions for flavor symmetries. The chapter is organized as follows. In section 5.1 we present an overview of the current state of EWPOs calculations, including flavor assumptions. In Section 5.2, we review the SMEFT framework and the role of flavor assumptions. Here we construct the general form of the 2-fermion and 4-fermion coefficients that occur in the one-loop computations of EWPOs corresponding to different flavor anzatz . We describe the NLO electroweak and QCD renormalization of EWPOs in detail in Section 5.4 with emphasis on the roles of the 2- and 4-fermion operators. Section 5.5 contains phenomenology results and demonstrates the important role of flavor assumptions in the SMEFT fits[102]. We see that even including more general flavor assumptions than earlier analyses, many blind directions remain in the fits. Finally, in Section 5.6 we study future perspectives considering projected uncertainties from future colliders.

USC UNIVERSIDADE DE SANTIAGO DE COMPOSTELA

This chapter is based on the following paper:

The Importance of Flavor in SMEFT Electroweak Precision Fits

Authors

Luigi Bellafronte[a], Sally Dawson[b], Pier Paolo Giardino[a],

(a) Instituto Galego de Física de Altas Enerxías, Universidade de Santiago de Compostela, 15782 Santiago de Compostela, Galicia-Spain
(b) High Energy Theory Group, Department of Physics, Brookhaven National Laboratory, Upton, NY 11973, USA

Journal and Article Information

Journal name: Journal of High Energy Physics

Publisher: Springer Nature

ISSN: 1029-8479

Year of publication: 2023

DOI: 10.1007/JHEP05(2023)208

5.1 Overview

The high luminosity (HL) LHC program will greatly improve our knowledge of the allowed possibilities for physics beyond the Standard Model (SM). In the absence of the discovery of a new particle, the SMEFT is the tool of choice for describing new physics effects and provides a point of comparison with SM predictions[103, 100]. As discussed in chapter 4, the SMEFT Lagrangian at dimension-6 is

$$\mathcal{L} = \mathcal{L}_{SM} + \Sigma_{a=1}^{n} \frac{C_a}{\Lambda^2} \mathcal{O}_a \,, \tag{5.1}$$

where $\mathcal{O}_a$ are the dimension-6 operators in the Warsaw basis and C_a are the associated coefficient functions. In a UV complete model, these coefficients will be predicted at the high scale Λ [104, 105, 106, 107]. The comparison between the SMEFT and the SM predictions thus requires SM predictions to the highest possible accuracy, along with SMEFT calculations beyond the leading order (LO). LO calculations in the SMEFT are automated[108, 109] as are NLO QCD SMEFT calculations [110], but electroweak corrections must be performed on a case by case basis. There exist numerous global fits comparing SMEFT predictions with electroweak precision, di-boson, Higgs, and top quark observables[111, 112, 113, 114, 18]. However, given the large number of SMEFT operators, it is impossible to do a fully general fit. The SMEFT theory predictions thus encode various assumptions, including the termination of the SMEFT expansion at some order in $1/\Lambda^2$, the loop order of the QCD and electroweak expansions, and the flavor

USC UNIVERSIDADE DE SANTIAGO DE COMPOSTELA

structure of fermion operators, among others. Understanding the uncertainties inherent in these assumptions is crucial for interpreting SMEFT fits[115].

The assumptions about the flavor structure introduce significant model dependence into the SMEFT predictions. It is straightforward to implement a general flavor structure for the tree level predictions for observables[116, 117, 118, 119, 120, 121, 122] and the one-loop $\overline{MS}$ renormalization of the dimension-6 coefficient functions is known for an arbitrary flavor structure[97, 98, 99]. The one-loop next-to-leading order (NLO) electroweak predictions for physical observables, however, typically involve a large number of 4-fermion and 2-fermion operators with potentially complicated flavor structures. In addition, the fermion operators introduce new subtleties in the renormalization procedure. Existing calculations of the one-loop electroweak corrections to EWPO, Higgs, and di-boson data do not include the most general flavor structure for the 2- quark and 4-quark operators in the loops[123, 124, 125, 126, 127, 128, 129]. Here, we present a generalization of previous NLO SMEFT calculation of EWPOs [130, 131, 132] which included 4-fermion operators, but not 2-fermion operators, to allow for an arbitrary flavor structure. The corrections to the EWPOs from 4-fermion operators in the $U(3)^5$ symmetric case are in [128]. The role of flavor assumptions in fits to top and bottom quark data has been extensively examined in the literature and those analyses are complementary to that presented here[133, 134, 135, 132].

We set the CKM matrix to be diagonal, which implies that only operators containing pairs of identical flavor fermions contribute. We further work to linear order in the SMEFT coefficients and set all masses other than the top quark to be 0. We want to remark that these two conditions constrain the light fermion Yukawa couplings to be zero, without additional assumptions, since the SMEFT operators that would induce a modification to the SM Yukawas do not interfere with the SM amplitudes at linear order.

5.2 Notation

Retaining only the dimension-6 operators, we calculate observables, O_b, to one-loop as an expansion in $\frac{1}{\Lambda^2}$ and keep only the linear terms since the SMEFT is renormalizable order by order in powers of $\frac{1}{\Lambda^2}$,

$$O_b = O_{b,SM} + \Sigma_{a=1}^{n} \frac{C_a}{\Lambda^2} \beta_{ab}, \tag{5.2}$$

where β_{ab} is process dependent and depends on the kinematic invariants and the input parameters, and $O_{b,SM}$ is the SM prediction. We use the Feynman rules from Ref. [100], with general flavor structures for the 2- and 4-fermion operators, although we assume that the CKM matrix is diagonal, which has implications for the fermion structures of the operators that contribute to our calculation, as we will see. Furthermore, we assume that the SMEFT does not introduce new sources of CP violation, that is we assume the coefficients of all the operators to be real.

USC UNIVERSIDADE DE SANTIAGO DE COMPOSTELA

$\mathcal{O}_{ll}[ijkl]$	$(\bar{l}_i\gamma_\mu l_j)(\bar{l}_k\gamma^\mu l_l)$	$\mathcal{O}_{\phi WB}$	$(\phi^\dagger\tau^a\phi)\,W^a_{\mu\nu}B^{\mu\nu}$	$\mathcal{O}_{\phi D}$	$\left(\phi^\dagger D^\mu\phi\right)^*\left(\phi^\dagger D_\mu\phi\right)$
$\mathcal{O}_{\phi e}[ij]$	$(\phi^\dagger i\overleftrightarrow{D}_\mu\phi)(\bar{e}_{Ri}\gamma^\mu e_{Rj})$	$\mathcal{O}_{\phi u}[ij]$	$(\phi^\dagger i\overleftrightarrow{D}_\mu\phi)(\bar{u}_{Ri}\gamma^\mu u_{Rj})$	$\mathcal{O}_{\phi d}[ij]$	$(\phi^\dagger i\overleftrightarrow{D}_\mu\phi)(\bar{d}_{Ri}\gamma^\mu d_{Rj})$
$\mathcal{O}^{(3)}_{\phi q}[ij]$	$(\phi^\dagger i\overleftrightarrow{D}^a_\mu\phi)(\bar{q}_i\tau^a\gamma^\mu q_j)$	$\mathcal{O}^{(1)}_{\phi q}[ij]$	$(\phi^\dagger i\overleftrightarrow{D}_\mu\phi)(\bar{q}_i\tau^a\gamma^\mu q_j)$	$\mathcal{O}^{(3)}_{\phi l}[ij]$	$(\phi^\dagger i\overleftrightarrow{D}^a_\mu\phi)(\bar{l}_i\tau^a\gamma^\mu l_j)$
$\mathcal{O}^{(1)}_{\phi l}[ij]$	$(\phi^\dagger i\overleftrightarrow{D}_\mu\phi)(\bar{l}_i\tau^a\gamma^\mu l_j)$				

Table 5.1: Dimension-6 operators contributing to the Z and W pole observables of this study at tree level. $i, j, k, l = 1, 2, 3$ are generation indices.

Our goal is the dimension-6 SMEFT calculation of NLO QCD and NLO electroweak corrections to electroweak precision observables (EWPOs) with arbitrary flavor structures for the operators involving fermions. The technical details are in the next section and in the following sub-sections we discuss the effects of flavor on the predictions.

5.2.1 EWPOs

In complete generality, the Warsaw basis contains 2499 baryon number conserving dimension-6 operators. Much of the proliferation of operators is associated with the flavor structure. Of course, most of the flavor structures will not contribute to a given observable and we begin by considering EWPOs at tree level. The Z and W boson pole observables that we consider are,

$$\begin{aligned} &M_W, \Gamma_W, \Gamma_Z, \sigma_h, R_e, R_\mu, R_\tau, R_s, R_c, R_b, A_e, A_\mu, A_\tau, \\ &A_s, A_c, A_b, A_{e,FB}, A_{\mu,FB}, A_{\tau,FB}, A_{FB,s}, A_{FB,c}, A_{FB,b}\,. \end{aligned} \tag{5.3}$$

Note that we do not use the effective mixing angle in our fits, since it is derived from the asymmetries.

The operators that contribute to the EWPOs at LO are comprised of two bosonic operators with no flavor structure ($O_{\phi WB}$ and $O_{\phi D}$) and 8 fermionic operators, of which there are 7 operators with 2 fermionic indices (the 2-fermion operators), and 1 operator with 4 fermionic indices (the 4-fermion operator). The explicit forms of the operators that appear at LO are reported in Table 5.1. These operators change the couplings of the Z and W bosons to fermions, and explicit predictions for the measured quantities of Eq. 5.3 are given in Appendix A of Ref. [124]. The only 4-fermion operator that is relevant for EWPOs at LO is $\mathcal{O}_{ll}[ijkl]$ which has the symmetry $\mathcal{O}_{ll}[ijkl] = \mathcal{O}_{ll}[klij]$ and only $\mathcal{O}_{ll}[2112] = \mathcal{O}_{ll}[1221]$ contributes to the observables of Eq.5.3. The indices $(i, j, k, l = 1, 2, 3)$ refer to the fermion generation.) Dimension-6 operators involving the electron and the muon give contributions to the decay of the μ, changing the relation between the vev, v, and the Fermi constant G_μ,

$$G_\mu \equiv \frac{1}{\sqrt{2}v^2} - \frac{1}{\sqrt{2}\Lambda^2}C_{ll}[1221] + \frac{1}{\sqrt{2}\Lambda^2}\left(C^{(3)}_{\phi l}[11] + C^{(3)}_{\phi l}[22]\right). \tag{5.4}$$

At NLO, the EWPOs of Eq. 5.3 receive contributions from 22 additional operators (which are defined in Ref. [124]), which we classify according to the number of fermions:

USC UNIVERSIDADE DE SANTIAGO DE COMPOSTELA

- 4 bosonic operators:
$$\mathcal{O}_{\phi B},\ \mathcal{O}_{\phi W},\ \mathcal{O}_{\Box}\,,\mathcal{O}_{W}\,. \tag{5.5}$$

- 2 2-fermion operators:
$$\mathcal{O}_{uB}[ij],\ \mathcal{O}_{uW}[ij]\,. \tag{5.6}$$
Notice that only $\mathcal{O}_{uB}[33]$ and $\mathcal{O}_{uW}[33]$ contribute to the EWPOs at NLO if all fermions except the top are massless.

- 16 4-fermion operators:
$$\begin{aligned}&\mathcal{O}_{ed}[ijkl],\ \mathcal{O}_{ee}[ijkl],\ \mathcal{O}_{eu}[ijkl],\ \mathcal{O}_{lu}[ijkl]\,,\mathcal{O}_{ld}[ijkl],\ \mathcal{O}_{le}[ijkl],\\ &\mathcal{O}^{(1)}_{lq}[ijkl],\ \mathcal{O}^{(3)}_{lq}[ijkl]\mathcal{O}_{qe}[ijkl]\,,\mathcal{O}^{(1)}_{qd}[ijkl]\,,\mathcal{O}^{(3)}_{qq}[ijkl]\,,\mathcal{O}^{(1)}_{qq}[ijkl]\,,\\ &\mathcal{O}^{(1)}_{qu}[ijkl]\,,\mathcal{O}^{(1)}_{ud}[ijkl]\,,\mathcal{O}_{uu}[ijkl]\ \,,\mathcal{O}_{dd}[ijkl]\,.\end{aligned} \tag{5.7}$$
Five of the NLO-generated 4-fermion operators have a flavor symmetry,
$$\mathcal{O}_{ee}[ijkl],\ \mathcal{O}^{(3)}_{qq}[ijkl],\ \mathcal{O}^{(1)}_{qq}[ijkl]\,,\mathcal{O}_{uu}[ijkl],\ \mathcal{O}_{dd}[ijkl]\equiv\mathcal{O}_Y[ijkl]=\mathcal{O}_Y[klij]. \tag{5.8}$$

It is convenient to categorize the operators according to their dependence on the flavor since only specific structures contribute to the EWPOs at NLO:

- A) 2-fermion operators: $\mathcal{O}_X[ij]\equiv\mathcal{O}_{\phi e}[ij]$, $\mathcal{O}_{\phi u}[ij]$, $\mathcal{O}_{\phi d}[ij]$, $\mathcal{O}^{(3)}_{\phi q}[ij]$, $\mathcal{O}^{(1)}_{\phi q}[ij]$, $\mathcal{O}^{(3)}_{\phi l}[ij]$, $\mathcal{O}^{(1)}_{\phi l}[ij]$, $\mathcal{O}_{uB}[ij]$, $\mathcal{O}_{uW}[ij]$. We consider the CKM matrix to be diagonal which has the consequence that the coefficients of the operators in Class A have diagonal flavor structures:
$$C_X[ij]=E^{(i)}_X\delta_{ij},\quad i,j=1,2,3, \tag{5.9}$$
resulting in 3 independent coefficients for each operator. Notice that the operator $\mathcal{O}_{\phi u}[33]$ first contributes to the EWPOs at NLO. Furthermore, as noted above, $\mathcal{O}_{uB}[ij]$ and $\mathcal{O}_{uW}[ij]$ enter in our calculations only with coefficients $C_{uB}[33]$ and $C_{uW}[33]$ respectively. Together there are 23 independent coefficients in Class A.

- B) 4-fermion operators involving only identical fermion representations: $\mathcal{O}_Y[ijkl]\equiv\mathcal{O}_{ee}[ijkl]$, $\mathcal{O}^{(3)}_{qq}[ijkl]$, $\mathcal{O}^{(1)}_{qq}[ijkl]$, $\mathcal{O}_{uu}[ijkl]$, $\mathcal{O}_{dd}[ijkl]$, $\mathcal{O}_{ll}[ijkl]$. Since they stem from the combination of two fermion currents belonging to identical representations once we require that the CKM matrix is the unit matrix, there are only two ways flavor is allowed to "flow" through these operators: $\mathcal{O}_Y[iijj]$ and $\mathcal{O}_Y[ijji]$. Furthermore, these operators are subject to the flavor symmetry in Eq. 5.8, resulting in the coefficients having the flavor structure,
$$\begin{aligned}&C_Y[iiii]=F^{(i)}_Y,\ C_Y[iijj]=A^{(ij)}_Y,\ C_Y[ijji]=B^{(ij)}_Y,\\ &A^{(ji)}_Y=A^{(ij)}_Y,\ B^{(ji)}_Y=B^{(ij)}_Y,\quad i\neq j\,\&\,i,j=1,2,3,\end{aligned} \tag{5.10}$$

USC UNIVERSIDADE DE SANTIAGO DE COMPOSTELA

resulting in 9 independent coefficients for each operator. However, the flavor structure of $\mathcal{O}_{ee}[ijkl]$ is further constrained by the Fiertz identity $(\overline{e}_i\gamma^\mu e_j)(\overline{e}_k\gamma^\mu e_l) = (\overline{e}_i\gamma^\mu e_l)(\overline{e}_k\gamma^\mu e_j)$, which imposes the equality $A_{ee}^{(ij)} = B_{ee}^{(ij)}$, reducing the number of independent coefficients for $\mathcal{O}_{ee}[ijkl]$ to 6. The only coefficient of Class B that does not contribute to the EWPOs at NLO is $C_{uu}[3333]$. In total, we have 50 independent coefficients in Class B contributing.

- C) 4-fermion operators with 2 different fermion representations: $\mathcal{O}_Z[ijkl] \equiv \mathcal{O}_{ed}[ijkl]$, $\mathcal{O}_{eu}[ijkl]$, $\mathcal{O}_{lu}[ijkl]$, $\mathcal{O}_{ld}[ijkl]$, $\mathcal{O}_{le}[ijkl]$, $\mathcal{O}_{lq}^{(1)}[ijkl]$, $\mathcal{O}_{lq}^{(3)}[ijkl]$, $\mathcal{O}_{qe}[ijkl]$, $\mathcal{O}_{qd}^{(1)}[ijkl]$, $\mathcal{O}_{qu}^{(1)}[ijkl]$, $\mathcal{O}_{ud}^{(1)}[ijkl]$. For these operators, our choice of a diagonal CKM matrix requires that the flavor must flow only in one way: $\mathcal{O}_Y[iijj]$. Therefore, the coefficients of these operators have the flavor structure:

$$C_Z[iijj] = D_Z^{(ij)}, \quad i,j = 1,2,3, \tag{5.11}$$

with no further restrictions, corresponding to 9 independent coefficients for each operator, for a total of 99 independent coefficients in Class C that contribute to the observables of Eq. 5.3 at NLO.

In the most general flavor case, we see that EWPOs computed to NLO receive contributions from 178 independent coefficients: 6 from bosonic operators, 23 from 2-fermion operators, and 149 from 4-fermion operators. We next consider different flavor assumptions for the fermionic operators in order to reduce the number of operators that need to be considered. The flavor assumptions we consider are $U(3)^5$, minimal flavor violation (MFV), $U(2)^5$, third generation centric, third generation phobic, third generation phobic + $U(2)^5$, and a flavorless structure. We will discuss each of these assumptions in detail in the following sub-sections.

5.3 Scenarios

5.3.1 Flavor Assumptions: $U(3)^5$

In the absence of Yukawa couplings, the SM fermions have a global $U(3)^5$ symmetry,

$$G_3 \equiv U(3)_q \times U(3)_l \times U(3)_u \times U(3)_d \times U(3)_e\,. \tag{5.12}$$

The introduction of Yukawa interactions in the SM Lagrangian preserves a global hypercharge symmetry $U(1)_Y$, a baryonic symmetry $U(1)_B$, and three leptonic symmetries, $U(1)_e$ $U(1)_\mu$ and $U(1)_\tau$.

Our first approximation when imposing flavor symmetries on SMEFT predictions is to assume that the dimension-6 SMEFT coefficients have the G_3 symmetry of the (Yukawa-less) SM. This symmetry prevents the generation of the operators $\mathcal{O}_{uW}[33]$ and $\mathcal{O}_{uB}[33]$ since they carry a left-right fermionic current.

Under G_3, the other operators in Class A respect the form

$$\text{Class A}: \quad C_X[ii] = E_X, \quad i = 1,2,3, \tag{5.13}$$

USC UNIVERSIDADE DE SANTIAGO DE COMPOSTELA

All the 2-fermion operators that contribute to the EWPOs automatically have the structure of Eq. 5.13, and there are 7 real coefficients in this class, consistent with the counting of Ref. [119].

Regarding the operators of Class B, both contractions of fermion indices

$$(\overline{f}_i\gamma^\mu f_i)(\overline{f}_j\gamma^\mu f_j), \qquad (\overline{f}_i\gamma^\mu f_j)(\overline{f}_j\gamma^\mu f_i), \tag{5.14}$$

are invariant under $U(3)^5$, so the coefficients of Class B reduce to

$$\begin{aligned}\text{Class B}: \quad & C_Y[iiii] = A_Y + B_Y,\ C_Y[iijj] = A_Y,\ C_Y[ijji] = B_Y, \\ & i \neq j \,\&i,j = 1,2,3.\end{aligned} \tag{5.15}$$

Remembering that $B_{ee} = A_{ee}$, there are 11 independent coefficients in Class B.

Finally, the operators in Class C have the structure

$$\text{Class C}: \quad C_Z[iijj] = D_Z \quad i,j = 1,2,3, \tag{5.16}$$

for a total of 11 independent coefficients also in Class C. In total, if we impose a G_3 symmetry on the SMEFT Lagrangian, we are left with 29 independent coefficients contributing to the EWPOs at one loop.[1]

5.3.2 Flavor Assumptions: MFV

The Yukawa couplings break the $U(3)^5$ global symmetry in the SM. If we assume that this is the *only* source of breaking of the G_3 symmetry, we are led to the MFV scenario[2][136]. The SM Yukawa couplings are considered as $U(3)^5$ auxiliary fields with the transformations,

$$\begin{aligned} Y_u &\sim (3,1,\overline{3},1,1) \\ Y_d &\sim (3,1,1,\overline{3},1) \\ Y_e &\sim (1,3,1,1,\overline{3})\,. \end{aligned} \tag{5.17}$$

It is always possible to choose a basis such that Y_u, Y_d, and Y_e are diagonal matrices. We remind the reader that we have assumed that the CKM matrix is diagonal and the only non-zero fermion mass is assumed to be the top quark mass, M_t. The coefficients of the operators containing at least 2 top quarks are modified, while the other coefficients retain the G_3 structure. Our implementation of the MFV scenario with a massless b quark is equivalent to a global $U(2)_q \times U(3)_l \times U(2)_u \times U(3)_d \times U(3)_e$ symmetry.

In Class A, the only operators with a flavor structure that depends on the third generation fermions are $\mathcal{O}_{\phi u}$, $\mathcal{O}^{(3)}_{\phi q}$, $\mathcal{O}^{(1)}_{\phi q}$, $\mathcal{O}_{uW}$ and $\mathcal{O}_{uB}$.

$$\begin{aligned}\text{Class A}: \quad & C_X[\alpha\alpha] = E_X,\ C_X[33] = E^{(3)}_X, && \mathcal{O}_X \equiv \mathcal{O}_{\phi u}\,, \mathcal{O}^{(3)}_{\phi q},\ \mathcal{O}^{(1)}_{\phi q}, && \alpha = 1,2 \\ & C_{\tilde{X}}[ii] = E_{\tilde{X}}, && \mathcal{O}_{\tilde{X}} \equiv \mathcal{O}_{\phi e},\ \mathcal{O}_{\phi d},\ \mathcal{O}^{(3)}_{\phi l}\,,\ \mathcal{O}^{(1)}_{\phi l}, && i = 1,2,3\,.\end{aligned}$$

[1] We note that the (RR)(RR) operator, $\mathcal{O}^{(8)}_{ud}$, does not contribute to EWPOs at one-loop, and so our counting of the $U(1)^5$ operators agrees with Ref. [118].

[2] Since we assume that the CKM matrix is diagonal, there is no flavor violation in our implementation of the MFV scenario.

USC UNIVERSIDADE DE SANTIAGO DE COMPOSTELA

Since for $\mathcal{O}_{uW}$ and $\mathcal{O}_{uB}$ only the $C_{uW}[33]$ and $C_{uB}[33]$ enter in our calculations, a total of 12 independent coefficients contribute to the EWPOs at NLO, in agreement with Table 9 of [119].

The operators in Class B involving charge $\frac{2}{3}$- quarks all have 4 u_R fields or 4 q_L fields. Retaining the contributions up to $\mathcal{O}(\frac{M_t^2}{v^2})$, the coefficients of $\mathcal{O}_{uu}$, $\mathcal{O}_{qq}^{(3)}$ and $\mathcal{O}_{qq}^{(1)}$ are subject to the following relations in the MFV scenario,

$$\begin{aligned}\text{Class B}: \quad & C_Y[1122] = C_Y[2211] = A_Y,\ C_Y[1221] = C_Y[2112] = B_Y \\ & C_Y[33\alpha\alpha] = C_Y[\alpha\alpha 33] = A_Y^{(3)},\ C_Y[3\alpha\alpha 3] = C_Y[\alpha 33\alpha] = B_Y^{(3)} \\ & C_Y[\alpha\alpha\alpha\alpha] = A_Y + B_Y,\ C_Y[3333] = 2(A_Y^{(3)} + B_Y^{(3)}) - A_Y - B_Y, \quad \alpha = 1,2\end{aligned}$$

which reduces the number of independent coefficients to 4 for each operator. The remaining operators in Class B satisfy the $U(3)^5$ relations of Eq. 5.15, thus resulting in 17 independent coefficients in Class B.

In Class C, the operators $\mathcal{O}_{lu}$, $\mathcal{O}_{qe}$, $\mathcal{O}_{qd}^{(1)}$, $\mathcal{O}_{eu}$, $\mathcal{O}_{ud}^{(1)}$, $\mathcal{O}_{lq}^{(1)}$ $\mathcal{O}_{lq}^{(3)}$ have 2 top quarks and they satisfy the relations:

$$\text{Class C}: \quad C_Z[\alpha\alpha ii] = D_Z,\ C_Z[33ii] = D_Z^{(3)}, \quad \alpha = 1,2,\ i = 1,2,3$$

and hence we have 2 independent coefficients for each operator.

The only operator in Class C with 2 charge- $\frac{2}{3}$ quarks contributing to EWPOs is $\mathcal{O}_{qu}^{(1)}$ which satisfies the relations,

$$\begin{aligned}\text{Class C}: \quad & C_{qu}^{(1)}[\alpha\alpha\beta\beta] = D_{qu^{(1)}},\ C_{qu}^{(1)}[3333] = D_{qu^{(1)}}^{(33)} \\ & C_{qu}^{(1)}[33\alpha\alpha] = D_{qu^{(1)}}^{(3)},\ C_{qu}^{(1)}[\alpha\alpha 33] = D_{qu^{(1)}}^{(\bar{3})}, \quad \alpha,\beta = 1,2,\end{aligned}$$

and hence there are 4 independent flavor structures for $C_{qu}^{(1)}$. The remaining operators in Class C, $\mathcal{O}_{ed}, \mathcal{O}_{ld}$ and $\mathcal{O}_{le}$, satisfy the $U(3)^5$ relations and contribute 1 independent operator each. Overall, we have 21 independent coefficients in Class C. Excluding the operators $\mathcal{O}_{qd}^{(8)}$, $\mathcal{O}_{qu}^{(8)}$, and $\mathcal{O}_{ud}^{(8)}$ which do not contribute to EWPOs at NLO, our counting is in agreement with Table 2 of [120] and Table 9 of [119].

5.3.3 Flavor Assumptions: $U(2)^5$

Here we consider a scenario where the new physics distinguishes between the 3^{rd} generation and the first 2 generations. The first 2 generations are assumed to have the global symmetry[118],

$$G_2 \equiv U(2)_q \times U(2)_l \times U(2)_u \times U(2)_d \times U(2)_e\,. \tag{5.18}$$

Since we consider only the top quark mass to be non-zero, the $U(2)^5$ symmetry is unbroken.

Using the classification of operators given in Sec. 5.3.1, the G_2 symmetry requires that operators of Class A have the form:

$$\begin{aligned}\text{Class A}: \quad & C_X[\alpha\alpha] = E_X, \\ & C_X[33] = E_X^{(3)}, \quad \alpha = 1,2.\end{aligned} \tag{5.19}$$

USC UNIVERSIDADE DE SANTIAGO DE COMPOSTELA

There are 16 independent coefficients in this class.

The Class B operators satisfy

$$\begin{aligned}\text{Class B}: \quad & C_Y[\alpha\alpha\beta\beta] = A_Y,\ C_Y[\alpha\beta\beta\alpha] = B_Y,\ C_Y[\alpha\alpha\alpha\alpha] = A_Y + B_Y,\\ & C_Y[\alpha\alpha 33] = C_Y[33\alpha\alpha] = A_Y^{(3)},\ C_Y[3\alpha\alpha 3] = C_Y[\alpha 33\alpha] = B_Y^{(3)},\\ & C_Y[3333] = F_Y^{(3)}, \qquad\qquad \alpha \neq \beta,\ \alpha,\beta = 1,2.\end{aligned}$$

so that each operator has 5 independent coefficients. As before, $\mathcal{O}_{ee}$ has an extra constraint coming from the Fierz identities, which reduces the number of independent coefficients to 3 for this operator. Therefore, since $\mathcal{O}_{uu}[3333]$ does not contribute, Class B has 27 coefficients contributing to EWPOs at NLO in total.

The Class C operators, $\mathcal{O}_C$, contain 2 different fermion representations and the $U(2)^5$ symmetry implies,

$$\begin{aligned}\text{Class C}: \quad & C_Z[\alpha\alpha\beta\beta] = D_Z,\ C_Z[3333] = D_Z^{(33)}\\ & C_Z[33\alpha\alpha] = D_Z^{(3)},\ C_Z[\alpha\alpha 33] = D_Z^{(\bar{3})}, \quad \alpha,\beta = 1,2.\end{aligned} \tag{5.20}$$

and there are 4 independent coefficients corresponding to each operator structure, for a total of 44 operators.

5.3.4 Flavor Assumptions: Third Generation Centric

In this scenario, only operators involving the 3^{rd} generation fermions are non-zero. An example of such a scenario might be a Z' boson that only interacts with the 3^{rd} generation. Operators of Class A in this scenario have the form:

$$\begin{aligned}\text{Class A}: \quad & C_X[\alpha\alpha] = 0,\\ & C_X[33] = E_X^{(3)}, \quad \alpha = 1,2.\end{aligned} \tag{5.21}$$

There are 9 real coefficients in this class.

The Class B and C operators satisfy

$$\begin{aligned}\text{Class B \& C}: \quad & C_{Y,Z}[\alpha\alpha\beta\beta] = C_Y[\alpha\beta\beta\alpha] = 0,\\ & C_{Y,Z}[\alpha\alpha 33] = C_{Y,Z}[33\alpha\alpha] = C_Y[3\alpha\alpha 3] = C_Y[\alpha 33\alpha] = 0,\\ & C_Y[3333] = F_Y^{(3)},\ C_Z[3333] = D_Z^{(3)}, \qquad\qquad \alpha,\beta = 1,2.\end{aligned}$$

For a total of 5 coefficients in Class B and 11 coefficients in Class C.

5.3.5 Flavor Assumptions: Third Generation Phobic

In this scenario, we assume that the new physics only couples to the 1^{st} 2 generations. An example of such a model can be found in [137]. We assume no further symmetry, but note that the operators contributing to EWPOs do not have an arbitrary flavor structure, as described at the beginning of this section.

USC UNIVERSIDADE DE SANTIAGO DE COMPOSTELA

Operator	$U(3)^5$	MFV	$U(2)^5$	3^{rd} gen specific	3^{rd} gen phobic	3^{rd} gen phobic + $U(2)^5$	Flavorless
Class A	7	12	16	9	14	7	9
Class B	11	17	27	5	23	11	6
Class C	11	21	44	11	44	11	11
Total	29	50	87	25	81	29	26

Table 5.2: Number of independent operators contributing to NLO predictions for EWPOs in various flavor scenarios.

The flavor structure of the operators of Class A is

$$\begin{aligned} \text{Class A}: \qquad & C_X[\alpha\alpha] = E_X^{(\alpha)}. \\ & C_X[33] = 0, \qquad \alpha = 1, 2, \end{aligned} \tag{5.22}$$

for a total of 14 independent coefficients.

For Class B we have

$$\begin{aligned} \text{Class B}: \qquad & C_Y[\alpha\alpha\alpha\alpha] = F_Y^{(\alpha)},\ C_Y[\alpha\alpha\beta\beta] = A_Y^{(\alpha\beta)},\ C_Y[\alpha\beta\beta\alpha] = B_Y^{(\alpha\beta)}, \\ & C_Y[\alpha\alpha 33] = C_Y[33\alpha\alpha] = C_Y[3\alpha\alpha 3] = C_Y[\alpha 33\alpha] = C_Y[3333] = 0, \\ & \alpha \neq \beta,\ \alpha, \beta = 1, 2, \end{aligned}$$

corresponding to 4 independent coefficients for each operator (3 for $\mathcal{O}_{ee}$), for a total of 23 coefficients in Class B.

Finally for Class C the available structures are

$$\begin{aligned} \text{Class C}: \qquad & C_Z[\alpha\alpha\beta\beta] = D_Z^{(\alpha\beta)} \\ & C_Z[\alpha\alpha 33] = C_Z[33\alpha\alpha] = C_Z[3333] = 0, \quad \alpha, \beta = 1, 2, \end{aligned} \tag{5.23}$$

which again gives 4 independent coefficients for each operator, for a total of 44 coefficients in Class C.

5.3.6 Flavor Assumptions: Third Generation Phobic + $U(2)^5$

As a specific case of the previous example, we consider a scenario where, after assuming that new physics couples only to the 1^{st} 2 generations, we further assume the existence of a $U(2)^5$ symmetry.

In this case, the flavor structure of the operators of Class A is

$$\begin{aligned} \text{Class A}: \qquad & C_X[\alpha\alpha] = E_X, \\ & C_X[33] = 0, \qquad \alpha = 1, 2, \end{aligned} \tag{5.24}$$

for a total of 7 independent coefficients.

USC UNIVERSIDADE DE SANTIAGO DE COMPOSTELA

For Class B we have

$$\begin{aligned}\text{Class B}: \quad & C_Y[\alpha\alpha\beta\beta] = A_Y, \quad C_Y[\alpha\beta\beta\alpha] = B_Y, C_Y[\alpha\alpha\alpha\alpha] = A_Y + B_Y, \\ & C_Y[\alpha\alpha 33] = C_Y[33\alpha\alpha] = C_Y[3\alpha\alpha 3] = C_Y[\alpha 33\alpha] = C_Y[3333] = 0, \\ & \alpha \neq \beta,\ \alpha, \beta = 1, 2, \end{aligned} \tag{5.25}$$

corresponding to 2 independent coefficients for each operator (1 for $\mathcal{O}_{ee}$), for a total of 11 coefficients in Class B.

Finally for Class C the available structures are

$$\begin{aligned}\text{Class C}: \quad & C_Z[\alpha\alpha\beta\beta] = D_Z \\ & C_Z[\alpha\alpha 33] = C_Z[33\alpha\alpha] = C_Z[3333] = 0, \quad \alpha, \beta = 1, 2, \end{aligned} \tag{5.26}$$

which again gives 1 independent coefficient for each operator, for a total of 11 coefficients in Class C.

5.3.7 Flavor Assumptions: Flavorless Scenario

This is the scenario employed in our previous calculations[130], where flavor plays no role and we simply drop all flavor indices. In this scenario, we assume that the operators have no flavor structure, that is we make the replacements,

$$C_{X,Y,Z}[\dots] = A_{X,Y,Z}\,. \tag{5.27}$$

Therefore in this case there are 26 coefficients that contribute.

We summarize the results of our discussion of flavor scenarios in Table 5.2. The number of operators contributing to EWPOs at NLO varies dramatically depending on the flavor structure and is significantly smaller than the 178 independent coefficients that contribute with no assumptions about flavor. We will see that these choices have large effects on the numerical results of fits to EWPOs.

5.4 NLO calculations

This section describes our calculational procedure for the NLO corrections to the electroweak precision observables. Some of the results can be obtained from our previous calculation[130] by generalizing the flavor structure of each observable. However, including a general flavor structure at NLO requires a new calculation for many of the flavor structures and observables. Therefore, we have performed the calculation in all generality and in this section we describe the details of the calculation and the assumptions that are implicit in the numerical results of the next section.

At tree level, the interactions are just the Z (and W) decays to 2 fermions shown in Fig. 5.1 and the effect of including the dimension-6 SMEFT contributions is to change

USC UNIVERSIDADE DE SANTIAGO DE COMPOSTELA

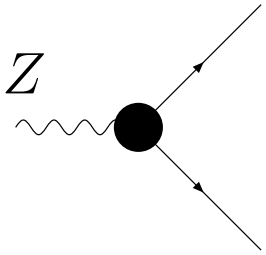

Figure 5.1: Z decays to fermions. The black circle represents the tree level SMEFT interaction.

the vector boson couplings to fermions. The tree level SMEFT couplings of fermions to the Z and W are given in terms of our input parameters (α, M_Z, G_μ),

$$\begin{aligned} L \equiv\ & 2M_Z\sqrt{\sqrt{2}G_\mu}\Big\{ Z_\mu\Big[g_L^{Zq}+\delta g_L^{Zq}\Big]\overline{q}\gamma_\mu q + Z_\mu\Big[g_R^{Zu}+\delta g_R^{Zu}\Big]\overline{u}_R\gamma_\mu u_R \\ & + Z_\mu\Big[g_R^{Zd}+\delta g_R^{Zd}\Big]\overline{d}_R\gamma_\mu d_R + Z_\mu\Big[g_L^{Zl}+\delta g_L^{Zl}\Big]\overline{l}\gamma_\mu l \\ & + Z_\mu\Big[g_R^{Ze}+\delta g_R^{Ze}\Big]\overline{e}_R\gamma_\mu e_R + Z_\mu\Big(\delta g_R^{Z\nu}\Big)\overline{\nu}_R\gamma_\mu\nu_R\Big\} \\ +\ & 2M_W[\alpha, M_Z, G_\mu]\sqrt{\frac{G_\mu}{\sqrt{2}}}\Big\{ W_\mu\Big[(1+\delta g_L^{Wq})\overline{u}_L\gamma_\mu d_L + \Big(\delta g_R^{Wq}\Big)\overline{u}_R\gamma_\mu d_R\Big] \\ & + W_\mu\Big[(1+\delta g_L^{Wl})\overline{\nu}_L\gamma_\mu e_L + \Big(\delta g_R^{W\nu}\Big)\overline{\nu}_R\gamma_\mu e_R\Big] + h.c.\Big\}, \end{aligned} \tag{5.28}$$

where at tree level,

$$\begin{aligned} g_R^{Zf} &= -s_W^2 Q_f \quad \text{and} \quad g_L^{Zf} = T_3^f - s_W^2 Q_f \\ s_W^2 &\equiv 1 - \frac{M_W^2[\alpha, M_Z, G_\mu]}{M_Z^2}, \end{aligned} \tag{5.29}$$

$T_3^f = \pm\frac{1}{2}$, and $M_W^2[\alpha, M_Z, G_\mu]$ is the mass of the W boson written in terms of the (α, M_Z, G_μ) input parameters as defined later in Sec. 5.4.4. Analytic expressions for the shifts in the couplings in terms of the Warsaw basis coefficients can be found in [138, 139].

We use the SMEFT Feynman rules of Ref. [100] as implemented in FeynRules [101] from which a FeynArts [140] model file is obtained. In this way, we are able to generate the relevant one-loop and real emission amplitudes, which include all the QCD and EW

USC UNIVERSIDADE DE SANTIAGO DE COMPOSTELA

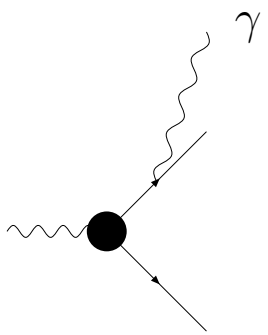

Figure 5.2: Z decays to 2 fermions, including real photon emission. The black circle represents the tree level SMEFT interaction.

corrections to the Z and W pole observables considered here. All the amplitudes are generated in R_ξ gauge, and the gauge invariance of the final results is verified explicitly. The results of the previous step are manipulated with FeynCalc [141, 142], which is also used to reduce the integrals that appear in terms of Passarino-Veltman integrals [143]. We retain only terms of $\mathcal{O}(v^2/\Lambda^2)$, since the SMEFT is renormalizable at fixed order in the (v^2/Λ^2) expansion[3] . As is the case of the pure SM results, the Feynman diagrams that contribute to the calculations are afflicted by both UV and IR divergences and we describe the regulation of these singularities below.

5.4.1 Real contributions

The decays of the Z and W bosons receive contributions from real photon and gluon emissions (as demonstrated generically in Fig. 5.2), which are necessary to cancel the IR divergences from the virtual contributions. From Fig. 5.2, it is clear that the flavor structure of the real emission diagrams is identical to that of the tree level result. Due to the complicated tensor structures of the SMEFT vertices, it is convenient to avoid integration over the final state 3-body phase space and therefore we use the method of Ref. [144], replacing the integration over the phase space with a loop integration. Specifically, we square the tree-level real amplitudes and then make use of the identity,

$$2i\pi\delta(p^2 - m^2) = \frac{1}{p^2 - m^2 + i0} - \frac{1}{p^2 - m^2 - i0}\,, \tag{5.30}$$

to build a correspondence between phase space integrals and the imaginary part of 2-loop integrals, which we calculate by rewriting them in terms of known master integrals [145, 146] using FIRE [147]. We notice that only the imaginary parts that correspond to a cut through all three particles in the final state contribute to the phase space integral, and thus particular attention has to be taken in isolating the correct imaginary part.

[3]Including terms resulting from squaring the LO EFT result would result in contributions of $\mathcal{O}(v^4/\Lambda^4)$, which is the same order as the dimension-8 terms we are neglecting, and hence would be inconsistent.

USC UNIVERSIDADE DE SANTIAGO DE COMPOSTELA

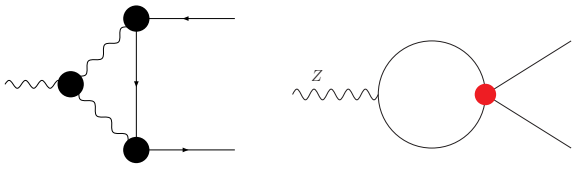

Figure 5.3: Sample virtual one-loop contributions to Z decays to 2 fermions. The black circles represent SMEFT insertions correcting the SM vertices, while the red circle denotes the dimension-6 4-fermion operators.

We then check that the results obtained with this technique reproduce the known results for the real photon and gluon contributions to the SM NLO results. Finally, we treat IR divergences in the real and virtual contributions by giving a small mass to photons and gluons, and then carefully taking the massless limit of the full result[148].

5.4.2 Virtual contributions

At LO, the amplitudes can be written in terms of the EW vacuum expectation value (v), the pole masses of the Z and W bosons, and the Wilson coefficients of SMEFT operators in Table 5.1. Tree level results for the observables of Eq. 5.3 are given in Appendix A of [130]. This reference also includes the NLO results in the case where the 2-fermion and 4-fermion operators are assumed to be independent of flavor. The virtual diagrams consist of the full set of one-loop EW and QCD diagrams with the SMEFT vertices. Contributions of special interest to the study of the flavor structure arise from the 4-fermion interactions shown in Fig. 5.3. In what follows, we do not assume any flavor structure for the 4 fermion operators, although as noted in Sec. 5.2, only certain flavor structures arise.

5.4.3 UV counterterms

To treat the UV divergences we use dimensional regularization in d dimensions so that the poles are written in terms of the regulator $\epsilon = (4-d)/2$, which are later canceled by adding appropriate counterterms.

Note that we chose to exactly cancel all the tadpole contributions, that is we put to zero from the beginning all the diagrams that contain tadpoles. This corresponds to identifying the renormalized vacuum with the (gauge-dependent) minimum of the renormalized Higgs potential[149]. Consequently, all intermediate quantities are in general gauge dependent and only the final physical observables are gauge independent. Therefore, the cancellation of the R_ξ gauge parameter is highly non trivial and a strong check of the correctness of the calculation.

Since we do not have direct measurements of the coefficients of the dimension-6 operators, we treat them as $\overline{MS}$ parameters by constructing renormalized coefficients,

USC UNIVERSIDADE DE SANTIAGO DE COMPOSTELA

$C_i(\mu)$, of the form

$$C_i(\mu) = C_{0,i} + \delta C_i = C_{0,i} - \frac{1}{2\hat{\epsilon}}\frac{1}{16\pi^2}\gamma_{ij}C_j, \tag{5.31}$$

where we define $\hat{\epsilon}^{-1} \equiv \epsilon^{-1} - \gamma_E + \log(4\pi)$. In the previous equation, μ is the renormalization scale, $C_{0,i}$ are the bare quantities, and γ_{ij} are the one-loop anomalous dimensions defined by the relation

$$\mu\frac{dC_i}{d\mu} = \frac{1}{16\pi^2}\gamma_{ij}C_j. \tag{5.32}$$

The complete set of anomalous dimensions for dimension-6 SMEFT operators in the Warsaw basis is in Refs. [97, 98, 99]. In general the γ_{ij} are not diagonal and 4 -fermion operators mix with 2-fermion and other operators under renormalization.

Regarding the SM input parameters, we use the on-shell (OS) scheme which defines the renormalized quantities in terms of measured observables, and specifically we choose $\{\alpha, G_\mu, M_Z\}$ as the independent inputs[139, 150].

The vacuum expectation value v is connected to the Fermi constant G_μ by the relation,

$$G_\mu + \frac{1}{\sqrt{2}\Lambda^2}C_{ll}[1221] - \frac{1}{\sqrt{2}\Lambda^2}(C^{(3)}_{\phi l}[11] + C^{(3)}_{\phi l}[22]) \equiv \frac{1}{\sqrt{2}v_0^2}(1+\Delta r), \tag{5.33}$$

where the C in Eq. 5.33 are the renormalized $C_i(\mu)$, v_0 is the unrenormalized minimum of the potential (where we use the notation '0' to denote the tree level relation), and Δr is extracted from the calculation of muon decay at 1-loop at zero momentum transfer. The result for Δr in terms of the dimension-6 coefficients is in Appendix D of [123].

For the mass of the Z boson, the relation between the bare and renormalized quantity is obtained from the formula

$$M_Z^2 = M_{0,Z}^2 - \Pi_{ZZ}(M_Z^2), \tag{5.34}$$

where $M_{0,Z}^2$ is the bare quantity and $\Pi_{ZZ}(M_Z^2)$ is the one-loop correction to the 2-point function for Z, which is reported analytically for the SMEFT in Refs. [151, 152]. It is also convenient to define the one-loop corrections to the W boson 2-point function $\Pi_{WW}(M_W^2)$ in a similar manner.

The relation between the bare and renormalized electromagnetic coupling α is

$$\alpha(M_Z) = \frac{\alpha}{1 - \Delta\alpha(M_Z)}\,, \tag{5.35}$$

where we derive $\Delta\alpha$ from the 1-loop SMEFT corrections to the $\gamma\bar{e}e$ vertex. Note that $\Delta\alpha$ receives non-perturbative corrections from diagrams involving light quarks that contribute to the vacuum polarization $\Pi^{(5)}_{\gamma\gamma}(0)$. To treat these contributions we use the hadronic contribution to $\Delta\alpha$ which is defined as

$$\Delta\alpha^{(5)}_{\rm had}(M_Z) = 4\pi\alpha\left(\Pi^{(5)}_{\gamma\gamma}(M_Z) - \Pi^{(5)}_{\gamma\gamma}(0)\right), \tag{5.36}$$

where $\Pi^{(5)}_{\gamma\gamma}(M_Z)$ is a perturbative correction obtained by calculating the same diagrams that contribute to $\Pi^{(5)}_{\gamma\gamma}(0)$. The value of the hadronic contribution to $\Delta\alpha$ is obtained

USC UNIVERSIDADE DE SANTIAGO DE COMPOSTELA

using dispersion relations and experimental data and we report it in Eq. 5.48 together with other inputs.

Finally, it is convenient to define the quantities

$$\Delta\rho \equiv \Pi_{WW}(M_W^2)/M_W^2 - \Pi_{ZZ}(M_Z^2)/M_Z^2 \quad \text{and} \tag{5.37}$$

$$\Delta r_W \equiv \Delta r + \Pi_{WW}(M_W^2)/M_W^2, \tag{5.38}$$

which will enter in some of the definitions in the following section.

5.4.4 M_W calculation

The relation between the mass of the W boson and the input parameters in the SM is given by the well-known formula

$$M_{W,SM}^2 = M_Z^2\left(1+\sqrt{1-\frac{4\pi\alpha(1+\Delta\bar{r}_{SM})}{\sqrt{2}M_Z^2 G_\mu}}\right), \tag{5.39}$$

where we use a slightly unusual notation to distinguish between the finite gauge-invariant $\Delta\bar{r}$ and the UV divergent gauge-dependent Δr. $\Delta\bar{r}_{SM}$ is obtained from the previous corrections:

$$\Delta\bar{r}_{SM} = \Delta\alpha_{SM} - \frac{\cos^2\theta_W}{\sin^2\theta_W}\Delta\rho_{SM} + \Delta r_{W,SM}, \tag{5.40}$$

where θ_W is the weak mixing angle, which is defined in the OS scheme as $\cos\theta_W \equiv M_W/M_Z$.

In the SMEFT, Eq. 5.39 is modified:

$$M_W^2 = M_Z^2\left(1+\sqrt{1-\frac{4\pi\alpha(1+\Delta\bar{r})}{\sqrt{2}M_Z^2 G_\mu}} - \frac{1}{16}\frac{1}{\sqrt{2}G_\mu\Lambda^2}\left(\frac{\cos\theta_W}{\cos 2\theta_W}\right)^3 (F_1G_1+F_2G_2)\right), \tag{5.41}$$

where

$$\begin{aligned}
\Delta\bar{r} &= \Delta\alpha - \frac{\cos^2\theta_W}{\sin^2\theta_W}\Delta\rho + \Delta r_W \\
&+ \frac{1}{\sqrt{2}G_\mu\Lambda^2}\left(-\frac{\cos\theta_W(\cos\theta_W C_{\phi D}+2\sin\theta_W C_{\phi WB})}{2\sin^4\theta_W}\Delta\rho_{SM}\right. \\
&+ \frac{\cos\theta_W(\cos\theta_W C_{\phi D}+4\sin\theta_W C_{\phi WB})}{2\sin^2\theta_W}\left(\Delta r_{W,SM} - \frac{\Pi_{WW,SM}(M_W^2)}{M_W^2}\right) \\
&+ \left.\frac{\cos^2\theta_W}{2\sin^2\theta_W}\delta C_{\phi D} + \frac{2\cos\theta_W}{\sin\theta_W}\delta C_{\phi WB}\right),
\end{aligned} \tag{5.42}$$

and we define

$$\begin{aligned}
G_1 &= \cos\theta_W C_{\phi D} + 4\sin\theta_W C_{\phi WB} + \sin\theta_W\tan\theta_W(2C_{\phi l}^{(3)}[11] + 2C_{\phi l}^{(3)}[22] - 2C_{ll}[1221]) \\
G_2 &= \cos\theta_W C_{\phi D} + 2\sin\theta_W C_{\phi WB} \\
F_1 &= 4 + 6\Delta r_{SM} + 2(2+\Delta r_{SM})\cos 4\theta_W - M_Z^2\frac{\partial\Delta r_{SM}}{\partial(M_W^2)}\sin 2\theta_W\sin 4\theta_W \\
F_2 &= -8\Delta r_{SM}\cos 2\theta_W.
\end{aligned} \tag{5.43}$$

USC UNIVERSIDADE DE SANTIAGO DE COMPOSTELA

It is convenient to rewrite Eq. 5.41 as,

$$M_W^2 = M_{W,SM}^2 + \frac{1}{\sqrt{2}G_\mu\Lambda^2} M_{W,EFT}^2 \tag{5.44}$$

where $M_{W,SM}^2$ is obtained from Eq. 5.39, and we separate the SM and EFT contributions. At NLO, the mass of the W boson is

$$M_{W,NLO} = \sqrt{M_{W,SM}^2 + \frac{1}{\sqrt{2}G_\mu\Lambda^2} M_{W,EFT}^2} \approx \sqrt{M_{W,SM}^2} + \frac{1}{\sqrt{2}G_\mu\Lambda^2} \frac{M_{W,EFT}^2}{2\sqrt{M_{W,SM}^2}}\,, \tag{5.45}$$

and we calculate $M_{W,SM}^2$ and $M_{W,EFT}^2$ at 1-loop. Note that the calculation of $M_{W,SM}^2$ and $M_{W,EFT}^2$ involve the mass of the W itself that enters through $\cos\theta_W$. In this case, we use the value of M_W obtained from Eq. 5.39 after putting $\Delta\bar{r} \to 0$. As the last step in our calculation, we replace the SM result from our calculation with the "best" theory result of Table 5.3, obtaining our final expression for the mass of the W boson:

$$M_{W,fin} = M_{W,\text{"best"}} + \frac{1}{\sqrt{2}G_\mu\Lambda^2} \frac{M_{W,EFT}^2}{2\sqrt{M_{W,SM}^2}}. \tag{5.46}$$

All the other observables that we include in our fit depend on the mass of the W boson in some way. In our numerical calculation of a generic observable, O, we use our best knowledge of M_W (Eq. 5.46) in the calculation of the LO contributions to O and $M_{W,NLO}$ in Eq. 5.45 in the calculation of the NLO contributions to O. Afterwards, we replace our SM result with the "best" theory results in table 5.3. Finally, our EWPOs are expressed as

$$O = O_{\text{"best"}} + O_{EFT,LO}|_{M_W \to M_{W,fin}} + O_{EFT,NLO}|_{M_W \to M_{W,NLO}}\,. \tag{5.47}$$

We close this section with a few remarks about the validity of our expansion. After renormalization, the amplitude is finite. We then square the amplitude and retain only terms that are linear in the SMEFT coefficients. In principle, we could retain the terms quadratic in the SMEFT coefficients as this is also finite. However, the quadratic contributions generically have the same counting in factors of $\frac{1}{16\pi^2}$ as does a 2-loop SMEFT contribution with 2 insertions of SMEFT coefficients interfering with the SM amplitude. Furthermore, the quadratic terms contain contributions from SMEFT operators that we have dropped because they don't interfere with the SM.[4]

5.5 Results

In this section, we show the effects of the flavor assumptions on global fits to EWPOs. We fit to the data given in Table 5.3 and we use the Particle Data Group review[153]

[4]The quadratic contributions corresponding to the square of the amplitude computed here can be obtained from the authors on request.

USC UNIVERSIDADE DE SANTIAGO DE COMPOSTELA

value for M_W. The column labelled "best" theory corresponds to predictions computed to the highest available order in perturbation theory. We take as our input parameters,

$$\begin{aligned} G_\mu &= 1.1663787(6) \times 10^{-5}\text{GeV}^{-2} \\ M_Z &= 91.1876 \pm .0021\text{GeV} \\ \frac{1}{\alpha} &= 137.035999139(31) \\ \Delta\alpha^{(5)}_{\text{had}} &= 0.02768 \pm 0.00009 \\ \alpha_s(M_Z) &= 0.1181 \pm 0.0011 \\ M_h &= 125.25 \pm 0.17 \text{ GeV} \\ M_t &= 172.69 \pm 0.5 \text{ GeV}\,. \end{aligned}$$

The SMEFT scale is always taken to be $\Lambda = 1$ TeV and the coefficient functions are evaluated at the renormalization scale $\mu = M_Z$.

Flavor blind predictions for EWPOs were presented in Ref. [132], which corresponds to the scenario labeled flavorless here.[5] In this section, we concentrate on the derivation of limits on SMEFT coefficients that are dependent on the assumed flavor scenario. Our limits are obtained by considering only one non-zero operator type, $\mathcal{O}[ijkl]$, at a time and imposing the flavor symmetries described in Sec. 5.2. The single parameter limits are marginalized over the other independent flavor structures. Before proceeding, we find it convenient to briefly describe the marginalization procedure we use to obtain our results. Assuming Gaussian uncertainties, we calculate the χ^2 function

$$\chi^2(\mathcal{C}) = \sum_{i,j}(O_i^{\text{exp}} - O_i^{\text{th}})\sigma_{ij}^{-2}(O_j^{\text{exp}} - O_j^{\text{th}}), \tag{5.48}$$

where O_i^{exp} and O_i^{th} are the experimental and theoretical values of a certain observable O_i respectively and σ_{ij}^2 is the covariance matrix. In general, we can write $\chi^2(\mathcal{C}) \equiv \chi^2(\bar{\mathcal{C}}, \hat{\mathcal{C}})$ as a function of coefficients $\bar{\mathcal{C}}$, which we are interested in finding the limits of, and coefficients $\hat{\mathcal{C}}$, which we want to marginalize over. As a first step, we find the values of $\hat{\mathcal{C}}$ that minimize χ^2 while keeping $\bar{\mathcal{C}}$ free. In other words, we find the $\hat{\mathcal{C}}_M(\bar{\mathcal{C}})$ that satisfy the system of equations

$$\left.\frac{\partial\chi^2}{\partial\hat{\mathcal{C}}}\right|_{\hat{\mathcal{C}}=\hat{\mathcal{C}}_M(\bar{\mathcal{C}})} = 0, \tag{5.49}$$

where we highlighted that the $\hat{\mathcal{C}}_M$ are defined as function of the free parameters $\bar{\mathcal{C}}$. We can now define,

$$\chi^2(\bar{\mathcal{C}}) \equiv \chi^2(\bar{\mathcal{C}}, \hat{\mathcal{C}} = \hat{\mathcal{C}}_M). \tag{5.50}$$

The new function $\chi^2(\bar{\mathcal{C}})$ is used to perform the necessary studies. More details on this procedure can be found in the literature (see for example [162, 163, 18]).

[5] The exact numerical results of this work differ slightly from Ref. [132] since we fit to an expanded set of measurements with slightly different numerical values for the inputs.

USC UNIVERSIDADE DE SANTIAGO DE COMPOSTELA

Measurement	Experiment	"Best" theory
Γ_Z(GeV)	2.4955 ± 0.0023	2.4943 ± 0.0006 [154, 155, 156]
R_e	20.804 ± 0.05	20.732 ± 0.009 [154, 155, 156]
R_μ	20.784 ± 0.034	20.732 ± 0.009 [154, 155, 156]
R_τ	20.764 ± 0.045	20.779 ± 0.009 [154, 155, 156]
R_b	0.21629 ± 0.00066	0.2159 ± 0.0001[154, 155, 156]
R_c	0.1721 ± 0.0030	0.1722 ± 0.00005[154, 155, 156]
σ_h	41.481 ± 0.033	41.492 ± 0.008[154, 155, 156]
A_e(from A_{LR} had	0.15138 ± 0.00216	0.1469 ± 0.0004 [156, 157]
A_e(from A_{LR} lep)	0.1544 ± 0.0060	0.1469 ± 0.0004 [156, 157]
A_e(from Bhabba pol)	0.1498 ± 0.0049	0.1469 ± 0.0004 [156, 157]
A_μ	0.142 ± 0.015	0.1469 ± 0.0004 [156, 157]
A_τ(from SLD)	0.136 ± 0.015	0.1469 ± 0.0004 [156, 157]
A_τ(τ pol)	0.1439 ± 0.0043	0.1469 ± 0.0004 [156, 157]
A_c	0.670 ± 0.027	0.66773 ± 0.0002[156, 157]
A_b	0.923 ± 0.020	0.92694 ± 0.00006[156, 157, 158]
A_s	0.895 ± 0.091	0.93563 ± 0.00004[156, 157]
$A_{e,FB}$	0.0145 ± 0.0025	0.0162 ± 0.0001 [156, 157]
$A_{\mu,FB}$	0.0169 ± 0.0013	0.0162 ± 0.0001 [156, 157]
$A_{\tau,FB}$	0.0188 ± 0.0017	0.0162 ± 0.0001 [156, 157]
$A_{b,FB}$	0.0996 ± 0.0016	0.1021 ± 0.0003 [156, 157, 158]
$A_{c,FB}$	0.0707 ± 0.0035	0.0736 ± 0.0003 [156, 157]
$A_{s,FB}$	0.0976 ± 0.0114	0.10308 ± 0.0003 [156, 157]
M_W(GeV) PDG World Ave	80.377 ± 0.012	80.357 ± 0.006[159, 160]
Γ_W(GeV)	2.085 ± 0.042	2.0903 ± 0.0003[161]

Table 5.3: Unless otherwise cited, experimental results are taken from Table 10.5 of the Particle Data Group[153]. The theory results include the full set of 2-loop contributions for the Z pole observables, along with higher order corrections when known. The theory predictions are computed using the formulae in the indicated references and our input parameters, and the theory errors include the parametric uncertainties on M_t and M_h[156], along with the estimated theory uncertainties described in the respective papers.

USC UNIVERSIDADE DE SANTIAGO DE COMPOSTELA

For example, we can study the χ^2 for the coefficient $C_{qq}^{(1)}$ in the MFV scenario. The χ^2 function is given by:

$$\begin{aligned}\chi^2_{\rm MFV}\big(C^{(1)}_{\rm qq}\big) = 21.0184 \; &- 0.183188\; C^{(1)}_{\rm qq}[1,1,2,2] + 0.00528431\; C^{(1)}_{\rm qq}[1,1,2,2]^2 \\ &- 0.193834\; C^{(1)}_{\rm qq}[1,1,3,3] + 0.00725802\; C^{(1)}_{\rm qq}[1,1,2,2]C^{(1)}_{\rm qq}[1,1,3,3] \\ &+ 0.120819\; C^{(1)}_{\rm qq}[1,1,3,3]^2 + 5.33703\; C^{(1)}_{\rm qq}[1,3,3,1] \\ &- 0.2973\; C^{(1)}_{\rm qq}[1,1,2,2]C^{(1)}_{\rm qq}[1,3,3,1] - 0.271204\; C^{(1)}_{\rm qq}[1,1,3,3]C^{(1)}_{\rm qq}[1,3,3,1] \\ &+ 4.19859\; C^{(1)}_{\rm qq}[1,3,3,1]^2 - 5.92823\; C^{(1)}_{\rm qq}[3,3,3,3] \\ &+ 0.163898\; C^{(1)}_{\rm qq}[1,1,2,2]C^{(1)}_{\rm qq}[3,3,3,3] + 0.0186148\; C^{(1)}_{\rm qq}[1,1,3,3]C^{(1)}_{\rm qq}[3,3,3,3] \\ &- 4.83774\; C^{(1)}_{\rm qq}[1,3,3,1]C^{(1)}_{\rm qq}[3,3,3,3] + 3.85299\; C^{(1)}_{\rm qq}[3,3,3,3]^2.\end{aligned} \tag{5.51}$$

Following the above procedure, to marginalize $C^{(1)}_{\rm qq}[1,1,2,2]$ and $C^{(1)}_{\rm qq}[3,3,3,3]$, we have

$$\begin{cases} \frac{\partial \chi^2_{\rm MFV}}{\partial C^{(1)}_{\rm qq}[1,1,2,2]} = 0 \\ \\ \frac{\partial \chi^2_{\rm MFV}}{\partial C^{(1)}_{\rm qq}[3,3,3,3]} = 0 \end{cases} \Longrightarrow \begin{aligned} C^{(1)}_{\rm qq}[1,1,2,2] \to 8.062020 \; &- 0.9688560\; C^{(1)}_{\rm qq}[1,1,3,3] \\ &+ 27.44810\; C^{(1)}_{\rm qq}[1,3,3,1] \\ \\ C^{(1)}_{\rm qq}[3,3,3,3] \to 0.597832 \; &+ 0.0181909\; C^{(1)}_{\rm qq}[1,1,3,3] \\ &+ 0.0439991\; C^{(1)}_{\rm qq}[1,3,3,1]. \end{aligned} \tag{5.52}$$

Setting the marginalized coefficients to their minimum we find:

$$\begin{aligned}\chi^2_{\rm MFV}(C^{(1)}_{\rm qq}[1,1,3,3], C^{(1)}_{\rm qq}[1,3,3,1]) = 18.5079 \; &- 0.124191 C^{(1)}_{\rm qq}[1,1,3,3] \\ &+ 0.117473 C^{(1)}_{\rm qq}[1,1,3,3]^2 + 0.048042 C^{(1)}_{\rm qq}[1,3,3,1] \\ &- 0.0711661\; C^{(1)}_{\rm qq}[1,1,3,3]C^{(1)}_{\rm qq}[1,3,3,1] + 0.012012 C^{(1)}_{\rm qq}[1,3,3,1]^2.\end{aligned} \tag{5.53}$$

The new χ^2, that now depends only on $C^{(1)}_{\rm qq}[1,1,3,3]$ and $C^{(1)}_{\rm qq}[1,3,3,1]$, is used to carry out the required analysis for the MFV scenario.

We begin by considering limits on the 2-fermion operators (Class A) that contribute to the Z and W boson observables listed in Eq. 5.3. Table 5.4 compares the LO and NLO results for the SMEFT coefficients in the $U(3)^5$, MFV, and 3^{rd} generation centric scenarios. We note that the $U(3)^5$ and flavorless scenarios are identical for the coefficients of the 2-fermion operators. The limits on flavor structures that are not listed in the table can be derived using the results of Section 5.2, although for clarity we list limits on some of the non-independent coefficients. The differences between the LO and NLO fits are in general quite small. The single parameter limits are compared graphically in Fig. 5.4 where we see differences up to factors of 2 between the various flavor assumptions.

The contributions of top quark loops to the 2-fermion operators have been studied in [164]. Table 3 of this reference presents the 95% CL single parameter limits on C_{uW}[33],

USC UNIVERSIDADE DE SANTIAGO DE COMPOSTELA

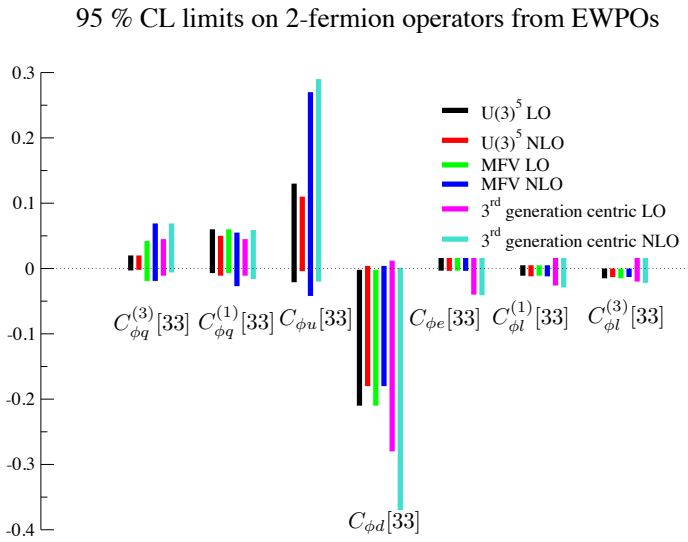

Figure 5.4: Limits on coefficients of 2-fermion operators in the $U(3)^5$ (LO in black, NLO in red), MFV (LO in green, NLO in blue) and 3^{rd} generation centric (LO in magenta, NLO in cyan) scenarios with a single non-zero operator and marginalizing over the other independent flavor structures of each operator.

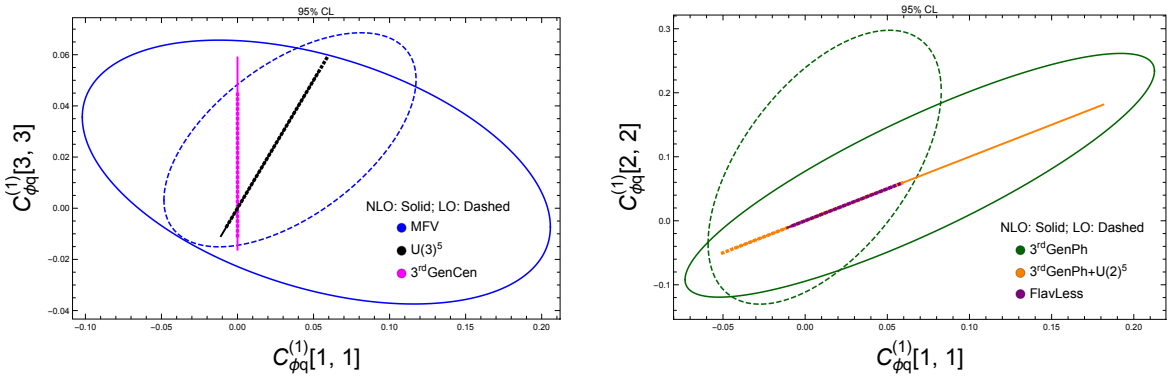

Figure 5.5: 95% CL limits on $C_{\phi q}^{(1)}[ij]$ under flavor assumptions described in the text. Results at LO are drawn with dashed lines, results at NLO are drawn with solid lines. **On the left** we present $C_{\phi q}^{(1)}[11]$ vs. $C_{\phi q}^{(1)}[33]$ in the $U(3)^5$ (black), MFV (blue) and 3^{rd} generation centric (magenta) scenarios. In these scenarios $C_{\phi q}^{(1)}[22] = C_{\phi q}^{(1)}[11]$. **On the right** we present $C_{\phi q}^{(1)}[11]$ vs. $C_{\phi q}^{(1)}[22]$ in the 3^{rd} generation phobic (green), 3^{rd} generation phobic + $U(2)^5$ (orange) and flavorless (violet) scenarios. In the first two scenarios $C_{\phi q}^{(1)}[33] = 0$, while in the flavorless scenario $C_{\phi q}^{(1)}[33] = C_{\phi q}^{(1)}[22] = C_{\phi q}^{(1)}[11]$. All other coefficients are set to 0.

$C_{uB}[33]$, $C_{\phi u}[33]$ and $C_{\phi q}^{(-)}[33] \equiv \frac{1}{2}(C_{\phi q}^{(1)}[33] - C_{\phi q}^{(3)}[33])$. Our results agree with these to $\sim 10 - 20\%$, which is consistent with the use of slightly different sets of data as input.

USC UNIVERSIDADE DE SANTIAGO DE COMPOSTELA

In Fig. 5.5 and in Figs. A.1-A.6 in the Appendix A.3, we show on the left hand side the limits on the 2-fermion operators in the $U(3)^5$, 3^{rd} generation specific, and MFV scenarios . On the right hand side of these plots we show the 3^{rd} generation phobic and 3^{rd} generation phobic + $U(2)^5$ scenarios, where the new physics only couples to the first and second generations, and the flavorless scenario. It is apparent that the limits one quotes on these operators is highly dependent on the assumed flavor scenario. It is interesting to note in Fig. 5.5, the large differences in the shapes of the LO and NLO fits in the MFV and 3^{rd} generation phobic scenarios and that the limits on the 3^{rd} generation phobic scenario are considerably weaker than in the other scenarios.

Tables 5.5 and 5.6 show the 95% CL limits on coefficients in the flavor schemes discussed in Sec. 5.2 for the Class B and Class C operators. In general, there is a strong dependence on the flavor scenario. This dependence is much larger than for the 2-fermion operator coefficients and the flavorless scenario gives much more stringent bounds for many coefficient functions than is the case in the other flavor scenarios.

The most precise limits are on C_{ll} and are shown in Fig. 5.6 for several flavor scenarios. It is clear that using the flavorless scenario gives limits that are factors of $\mathcal{O}(10-100)$ more precise than in the MFV or $U(3)^5$ scenarios for C_{ll}. This is understood from Eq. 5.4 where we see that the only flavor structure that contributes to G_μ is $C_{ll}[1221]$ and we observe that the limits on C_{ll} in the $U(2)^5$ scenario are the weakest. In Fig. 5.7, we show the strong correlation between $C_{ll}[1221]$ and $C_{ll}[3333]$ in the MFV scenario and between $C_{ll}[1221]$ and $C_{ll}[1122]$ in the $U(2)^5$ and 3^{rd} generation phobic scenarios. We note that there are only 2 independent C_{ll} coefficients.

Marginalized single parameter limits on the Class B operator coefficients $C_{qq}^{(1)}$ and $C_{qq}^{(3)}$ are shown in Fig. 5.8. The $U(3)^5$ and MFV results for these operators are within a factor of 2 of each other, while the 3^{rd} generation specific and 3^{rd} generation phobic scenarios are weakly constrained. Sample correlations between different flavor structures are shown in Fig. 5.9, demonstrating the sensitivity to the flavor assumptions of these fits.

The 4-fermion Class C operators can be studied individually, and marginalizing over the independent flavor structures gives the limits in Fig. 5.10. The limits obtained in the flavorless setup in this case also similar to those of the MFV and $U(3)^5$ flavor structures. The 3^{rd} generation specific and 3^{rd} generation phobic scenarios give weak bounds for these operators. In addition, there are large correlations between the different flavor structures, as illustrated in Fig. 5.11.

5.6 Future perspectives

As discussed in this chapter, the verification for consistency within the SM of EWPO is an important method, along with direct searches for new particles, to investigate the potential existence of BSM physics. Indeed, exploring the properties of massive electroweak gauge bosons (W and Z bosons) holds great promise for indirect BSM searches, as the interactions involving photons and gluons are subject to stringent constraints imposed by the unbroken gauge symmetries. In this context, the achievable precision of

USC UNIVERSIDADE DE SANTIAGO DE COMPOSTELA

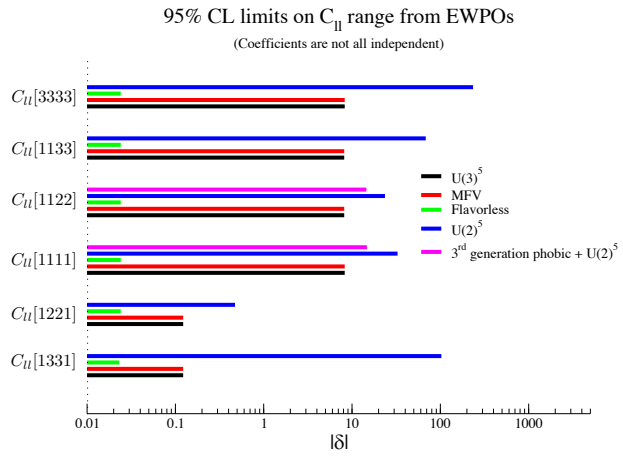

Figure 5.6: Limits on coefficients of $C_{ll}[ijkl]$ in various flavor scenarios, where $i, j, k, l = 1, 2, 3$. Only C_{ll} is taken to be non-zero in this figure, and the independent flavor structures not shown are marginalized over. Exact numbers are given in Table 5.5.

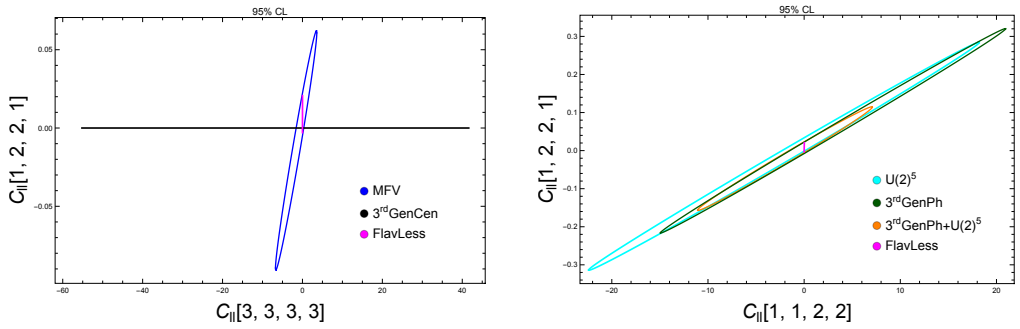

Figure 5.7: 95% CL limits on C_{ll} in various flavor scenarios with all other coefficients taken to be 0. **On the left** we present $C_{ll}[3333]$ vs. $C_{ll}[1221]$ in the MFV (blue), 3^{rd} generation centric (black) and flavorless (magenta) scenarios. **On the right** we present $C_{ll}[1122]$ vs. $C_{ll}[1221]$ in the $U(2)^5$ (cyan), 3^{rd} generation phobic (green), 3^{rd} generation phobic + $U(2)^5$ (orange) and flavorless (magenta) scenarios. All the independent flavor structures not present in the plots are marginalized over.

various future experiments has fundamental importance. Indeed, factors such as the statistical size of the data sample and the interplay between experimental and theoretical systematic uncertainties play a crucial role. In the report [21], an estimation of projected statistical and systematic uncertainties is proposed for various future linear colliders. In this section, using the data in Table 3 [21], we show the impact of projected future colliders errors (ILC-GigaZ and Fcc-ee) on the range of the bounds SMEFT coefficients, while also comparing them with the current values. We stress that the evaluations of systematic errors are rough estimates in terms of their magnitude. For a more accurate assessment, it would be necessary instrumentation details and other tools that are cur-

USC UNIVERSIDADE DE SANTIAGO DE COMPOSTELA

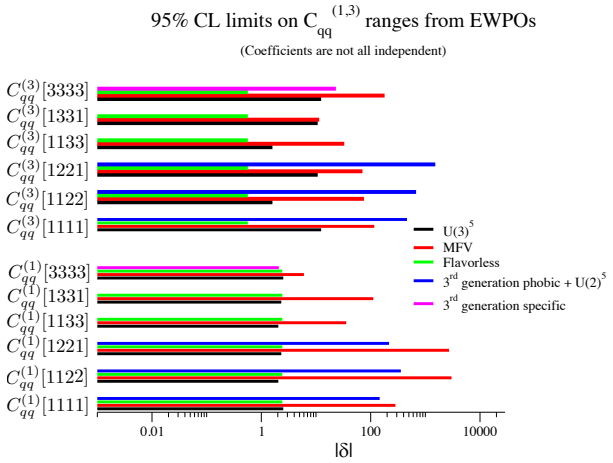

Figure 5.8: Limits on sample of coefficients of Class B 4-fermion operators in various flavor scenarios. δ is the range of the 95% confidence level limits. Only a single operator is taken to be non-zero and the flavor structures not shown are marginalized over. Exact numbers are given in Table 5.5.

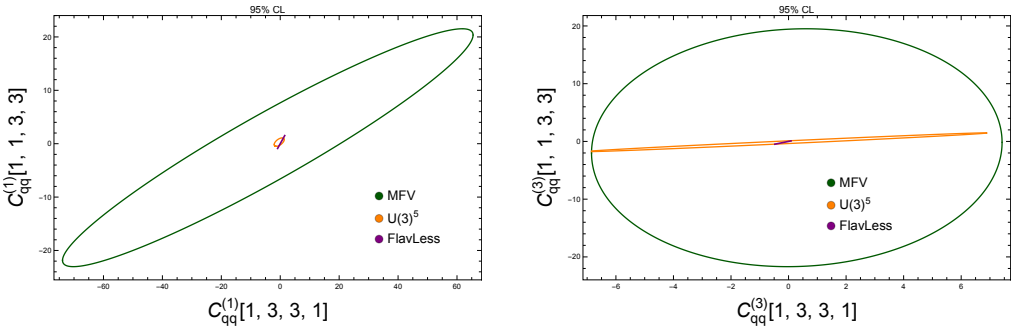

Figure 5.9: 95% CL limits on $C_{qq}^{(1)}$ (left) and $C_{qq}^{(3)}$ (right), in various flavor scenarios with all other coefficients taken to be 0. **On the left** we present $C_{qq}^{(1)}[1331]$ vs. $C_{qq}^{(1)}[1133]$ in the MFV (green), 3^{rd} generation centric (orange) and flavorless (violet) scenarios. **On the right** we present $C_{qq}^{(3)}[1331]$ vs. $C_{qq}^{(3)}[1133]$ in the MFV (green), 3^{rd} generation centric (orange) and flavorless (violet) scenarios. All the independent flavor structures not present in the plots are marginalized over.

rently unavailable. Furthermore, it should be noted that within this approach, we lack projected experimental values, preventing us from performing a fit of the observables. However, we are not interested in the actual possible ranges of the coefficients because our goal is to make an estimation of the *size* of the bounds based on future colliders projections.

USC UNIVERSIDADE DE SANTIAGO DE COMPOSTELA

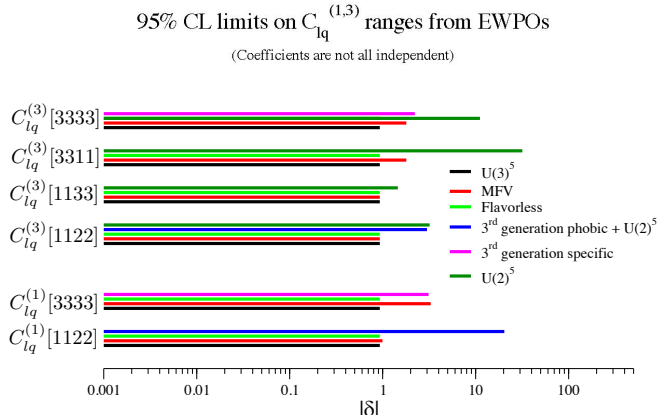

Figure 5.10: Limits on sample of coefficients of Class C 4-fermion operators in various flavor scenarios, with the independent flavor structures of each operator marginalized over. Exact numbers are given in 5.6.

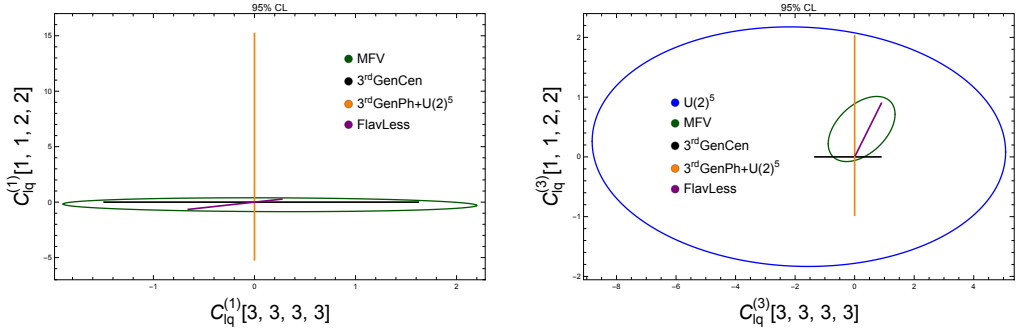

Figure 5.11: 95% CL limits on $C_{lq}^{(1)}$ (left) and $C_{lq}^{(3)}$ (right), in various flavor scenarios with all other coefficients taken to be 0. **On the left** we present $C_{lq}^{(1)}[3333]$ vs. $C_{lq}^{(1)}[1122]$ in the MFV (green), 3^{rd} generation centric (black), 3^{rd} generation phobic + $U(2)^5$ (orange) and flavorless (violet) scenarios. **On the right** we present $C_{lq}^{(3)}[3333]$ vs. $C_{lq}^{(3)}[1122]$ in the $U(2)^5$ (blue), MFV (green), 3^{rd} generation centric (black), 3^{rd} generation phobic + $U(2)^5$ (orange) and flavorless (violet) scenarios.. All the independent flavor structures not present in the plots are marginalized over.

Method

Similarly to the approach used in the previous section, we evaluate only one non zero operator at time and then we explore different flavor scenarios. Due to the previous assumptions, we consider only single parameter limits, marginalizing over the other independent flavor structures. The marginalization is the same described in 5.5. As already mention, since we do not have projected experimental values, we set them to their "best" theoretical SM value, indicated in Table 5.3. In this way, the χ^2 will not depend on the central value of the observables but only on the projected uncertainties. Finally, we do not expect that the theoretical uncertainties will remain the same at

USC UNIVERSIDADE DE SANTIAGO DE COMPOSTELA

Operator	LO $U(3)^5$	NLO $U(3)^5$	LO MFV	NLO MFV	3^{rd} gen centric LO	3^{rd} gen centric NLO
$C_{\phi q}^{(3)}[33]$	[-0.0029,0.020]	[-0.0024,0.020]	[-0.019,0.042]	[-0.019,0.069]	[-0.011,0.045]	[-0.0062,0.069]
$C_{\phi q}^{(3)}[11]$	[-0.0029,0.020]*	[-0.0024,0.020]*	[-0.0093,0.024]	[-0.012,0.020]	0	0
$C_{\phi q}^{(1)}[33]$	[-0.0070,0.060]	[-0.011,0.053]	[-0.0067,0.060]	[-0.027,0.055]	[-0.011,0.045]	[-0.016,0.059]
$C_{\phi q}^{(1)}[11]$	[-0.0070,0.060]*	[-0.011,0.053]*	[-0.032,0.10]	[-0.071,0.18]	0	0
$C_{\phi u}[33]$	[-0.021,0.13]*	[-0.0037,0.11]	-	[-0.042,0.27]	-	[-0.020,0.29]
$C_{\phi u}[11]$	[-0.021,0.13]	[-0.0037,0.11]*	[-0.021,0.13]	[-0.031,0.10]	0	0
$C_{\phi d}[33]$	[-0.21,-0.0024]	[-0.18,0.0036]	[-0.21,-0.0024]	[-0.18,0.0036]	[-0.28,0.012]	[-0.37,0.00083]
$C_{\phi e}[33]$	[-0.0033,0.019]	[-0.0036,0.018]	[-0.0033,0.019]	[-0.0036,0.018]	[-0.040,0.028]	[-0.041,0.022]
$C_{\phi l}^{(1)}[33]$	[-0.011,0.0050]	[-0.012,0.0049]	[-0.011,0.0050]	[-0.012,0.0049]	[-0.026,0.033]	[-0.029,0.029]
$C_{\phi l}^{(3)}[33]$	[-0.015,-0.00041]	[-0.013,-0.00029]	[-0.015,-0.00041]	[-0.013,-0.00029]	[-0.020,0.033]	[-0.022,0.031]
$C_{uW}[33]$	0	0	-	[-0.90,0.15]	-	[-0.90,0.15]
$C_{uB}[33]$	0	0	-	[-0.61,0.061]	-	[-0.61,0.061]

Table 5.4: 95% CL allowed ranges on 2-fermion operators with varying flavor assumptions described in the text. Other flavor structure of a given operator are marginalized over, and different coefficients set to 0. The entries labelled with a "-" correspond to operators that do not contribute, while those labelled with a "*" are not independent. The flavor structures given not in the table can be always derived from those in the table using the relations detailed in the text.

moment the colliders will run. It is logical to hypothesize that they will decrease thus, in this section, we assume that they will be one half of the current ones [38]. Although simplistic, this assumption seems reasonable when considering the time future colliders will operate at full capacity ($T > 20$ years). In Table 5.7 are indicated the data used for this analysis including ILC-GigaZ and Fcc-ee expected experimental uncertainties and expected theoretical uncertainties.

5.6.1 Results

We begin to show the results starting with Class A. We define the expected upgrade as

$$\eta_{\text{Fcc/ILC}}(C_i) = \frac{\delta_{\text{current}}(C_i)}{\delta_{\text{Fcc/ILC}}(C_i)} \tag{5.54}$$

where $\delta_{current}(C_i)$ and $\delta_{Fcc/ILC}(C_i)$ are respectively the current and the projected size of the bounds of a certain coefficient C_i. Table 5.8 shows the obtained the 95% CL limits on some of the coefficients for different flavor scenario and different future colliders. In this class the current size of the bounds is $\mathcal{O}(C) \lesssim 1$ for all the coefficients and in all the scenarios. Considering future colliders bounds we observe a significant improvement for all the operators. The minimum enhancement is observed for the coefficient $C_{\phi l}^{(1)}[11]$ in the 3^{rd} GenPh scenario, when compared to the ILC-GigaZ projected bounds $\eta_{ILC}(C_{\phi l}^{(1)}[11]) = 3.075$. The maximum, again in the 3^{rd} GenPh scenario, is for $C_{\phi u}[22]$ with $\eta_{fcc}(C_{\phi u}[22]) = 63.008$.

USC UNIVERSIDADE DE SANTIAGO DE COMPOSTELA

Operator	$U(3)^5$	MFV	$U(2)^5$	3^{rd} gen specific	3^{rd} gen phobic	3^{rd} gen phobic+$U(2)^5$	Flavorless
$C_{qq}^{(3)}[1133]$	[-0.80,0.81]	[-17.6,15.4]	x	0	0	0	[-0.48,0.09]
$C_{qq}^{(3)}[1331]$	[-4.38,6.42]	[-5.43,6.00]	x	0	0	0	[-0.48,0.09]*
$C_{qq}^{(3)}[1122]$	[-0.80,0.81]*	[-31.2,45.4]	x	0	x	[-303,375]	[-0.48,0.09]*
$C_{qq}^{(3)}[1221]$	[-4.38,6.42]*	[-44.8,26.3]	x	0	x	[-836,672]	[-0.48,0.09]*
$C_{qq}^{(3)}[3333]$	[-5.15,7.21]*	[-89.4,90.5]*	x	[-2.94,20.4]	0	0	[-0.48,0.09]*
$C_{qq}^{(3)}[1111]$	[-5.15,7.21]*	[-60.9,56.6]*	x	0	x	[-460,369]*	[-0.48,0.09]*
$C_{qq}^{(1)}[1133]$	[-0.20,1.84]	[-18.6,17.1]	x	0	0	0	[-0.89,1.52]
$C_{qq}^{(1)}[1331]$	[-1.39,0.94]	[-60.0,51.6]	x	0	0	0	[-0.89,1.52]*
$C_{qq}^{(1)}[1122]$	[-0.20,1.84]*	[-1623,1408]	x	0	x	[-189,169]	[-0.89,1.52]*
$C_{qq}^{(1)}[1221]$	[-1.39,0.94]*	[-1276,1470]	x	0	x	[-109,106]	[-0.89,1.52]*
$C_{qq}^{(1)}[3333]$	[-0.66,1.86]*	[-2.62,3.42]*	x	[-0.26,1.84]	0	0	[-0.89,1.52]*
$C_{qq}^{(1)}[1111]$	[-0.66,1.86]*	[-153,133]*	x	0	x	[-85.0,62.3]*	[-0.89,1.52]*
$C_{ll}[1133]$	[-5.65,2.52]	[-5.65,2.52]	[-46.1,22.2]	0	0	0	[-.0029,.021]
$C_{ll}[1331]$	[-0.076,0.047]	[-0.076,0.047]	[-38.2,65.4]	0	0	0	[-.0029,.021]*
$C_{ll}[1122]$	[-5.65,2.52]*	[-5.65,2.52]*	[-18.4,14.2]	0	[-11.4,17.4]	[-9.3,5.3]	[-.0029,.021]*
$C_{ll}[1221]$	[-0.076,0.047]*	[-0.076,0.047]*	[-0.25,0.22]	0	[-0.16,0.27]	[-0.13,0.088]	[-.0029,.021]*
$C_{ll}[3333]$	[-5.72,2.56]*	[-5.72,2.56]*	[-44.0,191]	[-55.2,41.6]	0	0	[-.0029,.021]*
$C_{ll}[2222]$	[-5.72,2.56]*	[-5.72,2.56]*	[-18.6,14.4]*	0	[-90.2,27.0]	[-9.4,5.4]*	[-.0029,.021]*
$C_{ll}[1111]$	[-5.72,2.56]*	[-5.72,2.56]*	[-18.6,14.4]*	0	[-26.7,26.3]	[-9.4,5.4]*	[-.0029,.021]*
$C_{ee}[1133]$	[-0.80,4.07]	[-0.80,4.07]	x	0	0	0	[-1.07,5.4]
$C_{ee}[1122]$	[-0.80,4.07]*	[-0.80,4.07]*	x	0	x	[-0.67,6.02]	[-1.07,5.4]*
$C_{ee}[3333]$	[-1.60,8.13]*	[-1.60,8.13]*	x	[-36.7,19.7]	0	0	[-1.07,5.4]*
$C_{ee}[1111]$	[-0.80,4.07]*	[-0.80,4.07]*	x	0	x	[-1.34,12.0]	[-1.07,5.4]*
$C_{uu}[1133]$	x	x	x	x	x	x	[-1.67,0.30]
$C_{dd}[3333]$	x	x	x	[-428,5.54]	x	x	[-68.4,2.38]

Table 5.5: NLO results for 95% CL limits on Class B operators when the coefficients of all other operators are set to 0 and the different flavor structures of a given operator are marginalized over. The limits marked with a "*" are obtained using the relations given in the text and do not represent independent coefficients. We label with an "x" the cases where no limit can be derived.

Finally we notice that for some the coefficients, depending on the scenario, the projected upgrade is almost the same for Fcc-ee and ILC-GigaZ. For example, in Fig. 5.12 we show the results for $C_{\phi u}[33]$. For this coefficient, we do not see significant differences between the two future collider projections.

Table 5.9 presents some of the 95% CL limits on 4-fermion coefficients for multiple scenarios. As discussed in the previous section, flavor has a dramatic effect on the

USC UNIVERSIDADE DE SANTIAGO DE COMPOSTELA

Operator	$U(3)^5$	MFV	$U(2)^5$	3^{rd} gen specific	3^{rd} gen phobic $+U(2)^5$	Flavorless
$C_{lq}^{(3)}[1133]$	[0.026,0.90]	[0.03,0.90]	[-0.0078,1.45]	0	0	[0.026,0.90]
$C_{lq}^{(3)}[3311]$	[0.026,0.90]*	[-0.66,1.13]	[-9.62,22.2]	0	0	[0.026,0.90]*
$C_{lq}^{(3)}[1122]$	[0.026,0.90]*	[0.03,0.90]*	[-1.43,1.78]	0	[-0.98,2.02]	[0.026,0.90]*
$C_{lq}^{(3)}[3333]$	[0.026,0.90]*	[-0.66,1.13]*	[-7.43,3.69]	[-1.33,0.88]	0	[0.026,0.90]*
$C_{lq}^{(1)}[1122]$	[-0.66,0.27]	[-0.73,0.27]	x	0	[-5.20,15.2]	[-0.66,0.27]
$C_{lq}^{(1)}[3333]$	[-0.66,0.27]*	[-1.50,1.79]	x	[-1.50,1.62]	0	[-0.66,0.27]*
$C_{lu}[1122]$	[-0.20,0.49]	[-0.20,0.55]	x	0	[-2.6,7.6]	[-0.20,0.49]
$C_{lu}[3333]$	[-0.20,0.49]*	[-1.33,1.13]	x	[-1.35,1.27]	0	[-0.20,0.49]*
$C_{qe}[1122]$	[-0.20,1.06]	[-66.2,142]	x	0	[-25.7,3.34]	[-0.20,1.06]
$C_{qe}[3333]$	[-0.20,1.06]*	[-2.38,6.35]	x	[-2.26,1.25]	0	[-0.20,1.06]*
$C_{ed}[1122]$	[-3.86,15.3]	[-3.86,15.3]	x	0	[-3.29,25.8]	[-3.86,15.3]
$C_{ed}[3333]$	[-3.86,15.3]*	[-3.86,15.3]*	x	[-117,42.8]	0	[-3.86,15.3]*
$C_{ld}[1122]$	[-9.11,3.26]	[-9.11,3.26]	x	0	[-15.2,5.21]	[-9.11,3.26]
$C_{ld}[3333]$	[-9.11,3.26]*	[-9.11,3.26]*	x	[-72.9,59.3]	0	[-9.11,3.26]*
$C_{le}[1122]$	[-7.09,8.13]	[-7.09,8.13]	x	0	[-10.5,14.5]	[-7.09,8.13]
$C_{le}[3333]$	[-7.09,8.13]*	[-7.09,8.13]*	x	[-92.8,55.5]	0	[-7.09,8.13]*
$C_{eu}[1122]$	[-0.81,0.16]	[-0.88,0.11]	x	0	[-12.9,1.66]	[-0.81,0.16]
$C_{eu}[3333]$	[-0.81,0.16]*	[-1.07,1.73]	x	[-1.05,1.95]	0	[-0.81,0.16]*
$C_{ud}^{(1)}[1122]$	[-0.30,7.68]	[-154,90.2]	x	0	[-13.9,75.7]	[-0.30,7.68]
$C_{ud}^{(1)}[3333]$	[-0.30,7.68]*	[-9.3,27.0]	x	[-0.24,18.4]	0	[-0.30,7.68]*
$C_{qd}^{(1)}[1122]$	[-13.3,0.47]	[-202,128]	x	0	[-29.4,139]	[-13.3,0.47]
$C_{qd}^{(1)}[3333]$	[-13.3,0.47]*	[-27.2,8.27]	x	[-24.4,0.11]	0	[-13.3,0.47]*
$C_{qu}^{(1)}[1122]$	[-2.82,0.54]	x	x	0	[-71.0,14.1]	[-2.82,0.54]
$C_{qu}^{(1)}[3333]$	[-2.82,0.54]*	x	x	[-3.07,0.44]	0	[-2.82,0.54]*

Table 5.6: NLO results for 95% CL limits on Class C operators when the coefficients of all other operators are set to 0 and the different flavor structures of a given operator are marginalized over. The limits marked with a "*" are obtained using the relations given in the text and do not represent independent coefficients. We label with an "x" the cases where no limit can be derived.

flavor bounds. In particular, depending on the scenarios, we have seen that some of the coefficients in Class B & C may have a range of values $\mathcal{O}(\delta(C_i)) \gg 10$. It is interesting to check if a coefficient that is not significantly constrained with the current experimental precision, can provide more useful information in future colliders.

In Fig 5.13, we show the results for $C_{qq}^{(1)}[1122]$ and $C_{qq}^{(3)}[1331]$. For $C_{qq}^{(1)}[1122]$, we see that both the scenarios would not constrain the coefficient sufficiently, in order to have significant bounds. Indeed, although we observe $\eta_{Fcc} = 33.50$ in the MFV

USC UNIVERSIDADE DE SANTIAGO DE COMPOSTELA

Quantity	ILC-GigaZ	FCC-ee	Theoretical error
Δm_W (MeV)	0.5(2.4)*	0.25 (0.3)	0.003
$\Delta\Gamma_w$ (MeV)	2*	1.2 (0.3)	0.004
$\Delta\Gamma_z$ (MeV)	0.12	0.004 (0.025)	0.0003
ΔA_e ($\times 10^5$)	1.5 (8)	0.7 (2)	0.0002
ΔA_μ ($\times 10^5$)	3 (8)	2.3 (2.2)	0.0002
ΔA_τ ($\times 10^5$)	3 (8)	0.5 (20)	0.0002
ΔA_b ($\times 10^5$)	9 (50)	2.4 (21)	0.00003
ΔA_c ($\times 10^5$)	20 (37)	20 (15)	0.0001
$\Delta\sigma^0_{\rm had}$ (pb)	33#	0.035 (4)	0.004
δR_e ($\times 10^3$)	0.2 (0.5)	0.004 (0.3)	0.0002
δR_μ ($\times 10^3$)	0.2 (0.2)	0.003 (0.05)	0.0002
δR_τ ($\times 10^3$)	0.2 (0.4)	0.003 (0.1)	0.0002
δR_b ($\times 10^3$)	0.04 (0.7)	0.0014 (0.3)	0.0002
δR_c($\times 10^3$)	0.2 (3.0)	0.015 (1.5)	0.0001

Table 5.7: EWPOs at future e^+e^- colliders: statistical error (estimated experimental systematic error). Δ (δ) stands for absolute (relative) uncertainty, while # indicates inputs taken from current data [38] and * are taken from ILC250 projections [21].

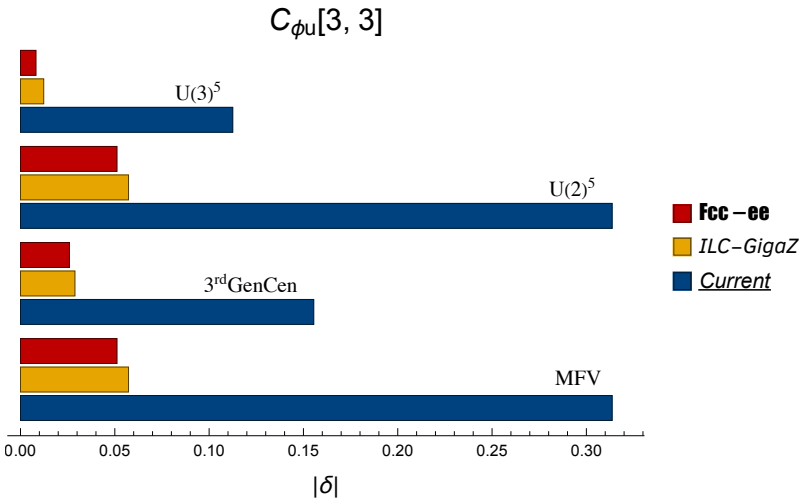

Figure 5.12: 95% CL limits on $C_{\phi u}[33]$ under flavor assumptions and collider predictions, as described in the text.

scenario and $\eta_{Fcc} = 22.04$ in the 3^{rd}GenPh+$U(2)^5$ scenario, the expected ranges would be $\delta_{Fcc} \sim 10$. On the other hand for $C^{(3)}_{qq}[1331]$ we see a complementary situation. Even if the expected upgrades are smaller ($\eta_{ILC} \sim 10$) than the other coefficient, we see that both the scenarios can give more meaningful bounds, already at ILC.

Finally, in Fig 5.14, we show the results for $C^{(1)}_{qd}[1122]$. In this case we see the impact of the flavor scenario on a single coefficient. Indeed, while the $U(3)^5$ scenario would

USC UNIVERSIDADE DE SANTIAGO DE COMPOSTELA

	$U(3)^5$		MFV		$U(2)^5$		3^{rd} Gen Cen		3^{rd}Ph		3^{rd}Ph+$U(2)^5$		FlavLess		
Operator	δ	η	δ	η	δ	η	δ	η	δ	η	δ	η	δ	η	*Colliders*
C_{uW}[33]	0		1.05	//	0		0.53	//	0		0		1.05	//	Current
	0		0.11	9.55	0		0.06	9.55	0		0		0.11	9.55	ILC-GigaZ
	0		0.11	9.69	0		0.06	9.69	0		0		0.11	9.69	Fcc-ee
$C_{\phi l}^{(3)}$[11]	0.013	//	0.013	//	0.013	//	0		0.023	//	0.012	//	0.013	//	Current
	0.002	6.89	0.002	6.89	0.002	6.31	0		0.005	4.70	0.002	7.56	0.02	6.89	ILC-GigaZ
	0.002	7.95	0.002	7.95	0.002	7.94	0		0.003	7.49	0.002	8.09	1.05	7.95	Fcc-ee
$C_{\phi l}^{(3)}$[22]	0.013	//	0.013	//	0.013	//	0		0.023	//	0.012	//	0.013	//	Current
	0.002	6.89	0.002	6.89	0.002	6.31	0		0.005	4.91	0.002	7.56	0.02	6.89	ILC-GigaZ
	0.002	7.95	0.002	7.95	0.002	7.94	0		0.003	7.08	0.002	8.09	1.05	7.95	Fcc-ee
$C_{\phi l}^{(3)}$[33]	0.013	//	0.013	//	0.055	//	0.027	//	0		0		0.013	//	Current
	0.002	6.89	0.002	6.89	0.008	6.71	0.003	8.04	0		0		0.02	6.89	ILC-GigaZ
	0.002	7.95	0.002	7.95	0.006	9.48	0.003	9.65	0		0		1.05	7.95	Fcc-ee
$C_{\phi l}^{(1)}$[11]	0.016	//	0.016	//	0.018	//	0		0.020	//	0.018	//	0.013	//	Current
	0.004	4.46	0.004	4.46	0.004	4.03	0		0.006	3.08	0.004	4.00	0.02	6.89	ILC-GigaZ
	0.002	7.15	0.002	7.15	0.002	6.91	0		0.003	6.26	0.003	6.88	1.05	7.95	Fcc-ee
$C_{\phi u}$[22]	0.113	//	0.135	//	0.135	//	0		0.590	//	0.132	//	0.113	//	Current
	0.012	9.15	0.013	10.3	0.013	9.15	0		0.015	39.2	0.004	10.2	0.012	9.15	ILC-GigaZ
	0.008	13.8	0.008	16.2	0.008	16.2	0		0.009	63.0	0.003	15.9	0.008	13.8	Fcc-ee

Table 5.8: 95% CL allowed ranges on 2-fermion operators with different flavor assumptions and different collider predictions, as described in the text. Other flavor structure of a given operator are marginalized over, and different coefficients set to 0. The flavor structures given not in the table can be always derived from those in the table using the relations detailed in the text.

	$U(3)^5$		MFV		$U(2)^5$		3^{rd} Gen Cen		3^{rd}Ph		3^{rd}Ph+$U(2)^5$		FlavLess		
Operator	δ	η	δ	η	δ	η	δ	η	δ	η	δ	η	δ	η	*Colliders*
C_{ll}[1331]	0.093	//	0.093	//	103.5	//	0		0		0		0.023	//	Current
	0.021	4.39	0.021	4.39	61.52	1.69	0		0		0		0.0028	8.49	ILC-GigaZ
	0.013	7.13	0.013	7.14	14.27	7.25	0		0		0		0.0027	8.74	Fcc-ee
$C_{qq}^{(3)}$[1133]	2.600	//	32.99	//	x		0		0		0		0.564	//	Current
	0.205	12.63	1.612	20.5	x		0		0		0		0.101	5.57	ILC-GigaZ
	0.124	21.0	0.997	33.1	x		0		0		0		0.071	7.96	Fcc-ee
C_{ld}[1122]	12.36	//	12.36	//	x		0		0		20.43	//	12.36	//	Current
	2.975	4.16	2.975	4.16	x		0		0		5.45	3.74	2.975	4.16	ILC-GigaZ
	1.741	7.10	1.741	7.10	x		0		0		3.01	6.77	1.741	7.10	Fcc-ee
$C_{ud}^{(1)}$[3333]	7.98	//	243	//	x		9.46	//	0		0		7.98	//	Current
	1.148	6.96	11.9	20.49	x		0.893	10.6	0		0		1.148	6.96	ILC-GigaZ
	0.614	13.0	7.31	33.4	x		0.394	24.0	0		0		0.614	13.0	Fcc-ee

Table 5.9: 95% CL allowed ranges on 4-fermion operators with different flavor assumptions and different collider predictions, as described in the text. Other flavor structure of a given operator are marginalized over, and different coefficients set to 0. The flavor structures given not in the table can be always derived from those in the table using the relations detailed in the text.

set considerable constraints on this coefficient, the 3^{rd}+$U(2)^5$ and MFV scenarios would give ranges $\delta \geq 10$, thus even at future colliders this coefficient would remain without a meaningful bound.

5.7 Conclusions

Measurements at the Z and W boson poles provide important limits on BSM physics. Using tree level predictions, the fermion-gauge boson interactions are restricted to be

USC UNIVERSIDADE DE SANTIAGO DE COMPOSTELA

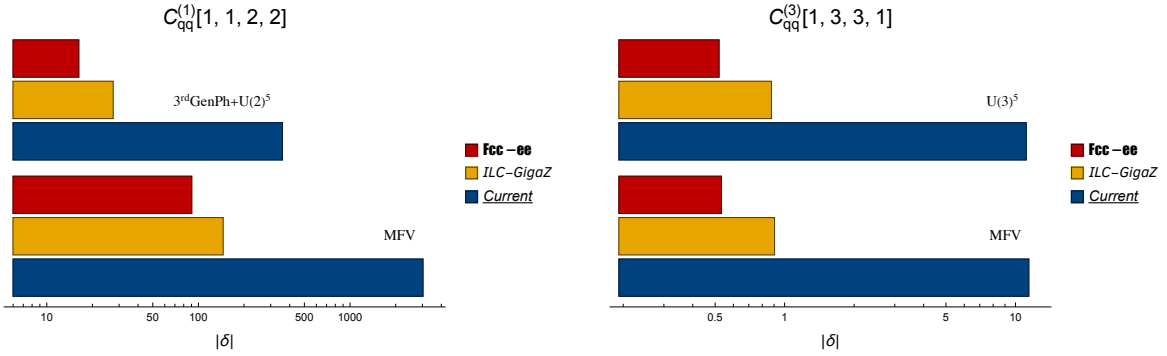

Figure 5.13: 95% CL limits on $C_{qq}^{(1)}[1122]$ and $C_{qq}^{(3)}[1331]$ under flavor assumptions and collider predictions, as described in the text.

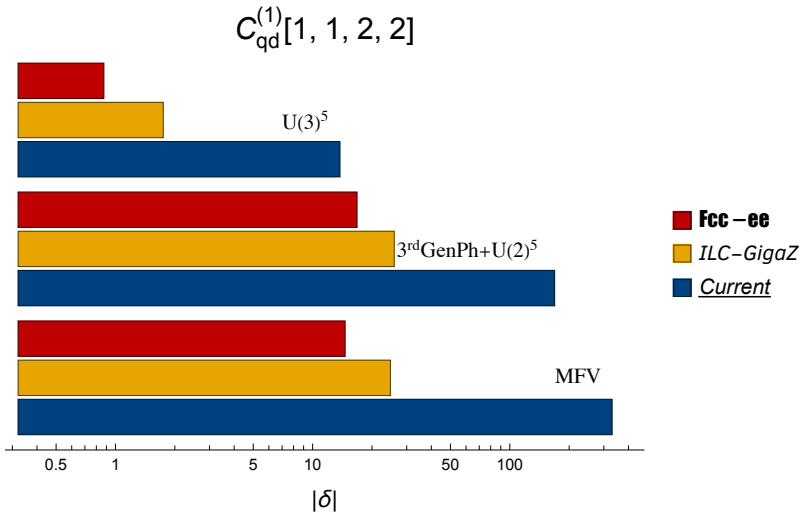

Figure 5.14: 95% CL limits on $C_{qd}^{(1)}[1122]$ under flavor assumptions and collider predictions, as described in the text.

quite close to those of the SM. In the context of the SMEFT, the bounds on anomalous particle couplings can be extended to systematically include NLO QCD and EW effects and interpreted as bounds on dimension-6 SMEFT operators. These bounds were previously derived ignoring the effects of the flavor dependence of the dimension-6 2- and 4-fermion operators. We have re-computed the NLO contributions to EWPOs including an arbitrary flavor structure for the fermion operators. With the exception of C_{ll} (which contributes to muon decay and is quite precisely bounded), the operators that contribute to EWPOs at tree level involve 2 fermions and the NLO corrections are typically quite small relative to the LO results. Comparing the NLO bounds on 2-fermion operators in different flavor scenarios results in factors of $\mathcal{O}(2)$. However, the flavor structure has a dramatic effect on the bounds derived on the 4-fermion operators which first contribute to EWPOs at NLO. We present results for 4-fermion operators when the different flavor structures of an operator are marginalized over and observe large deviations in the fits

USC UNIVERSIDADE DE SANTIAGO DE COMPOSTELA

for different flavor scenarios. These large effects result from the significant correlations between the different flavor structures. We have explicitly demonstrated that ignoring flavor typically leads to much tighter bounds on the SMEFT coefficients than in a general flavor scenario.

We also notice that the presence of a top quark in the internal propagators generally leads to stronger constraints. As we pointed out, the effects coming from the inclusion of NLO contributions are larger for operators where the top quark can contribute in the loop corrections. Furthermore, the limits that can be obtained on the 4-fermion operator coefficients in the $U(3)$ scenario are often orders of magnitude stronger than those obtained in the 3^{rd} generation phobic + $U(2)^5$ scenario. Since these scenarios have the same number of independent coefficients, the difference cannot be attributed to the marginalization procedure. Moreover, in the case of $\mathcal{O}_{ll}$, $\mathcal{O}_{ee}$ and $\mathcal{O}_{le}$, where we do not expect an enhancement due to top loops, the two scenarios produce bounds with similar order of magnitudes.

Finally, considering future colliders perspectives, the size of the expected bounds strictly depends on the flavor scenario considered. In particular, the analyses performed show that using future colliders uncertainties does not guarantee the possibility to put meaningful bounds on the SMEFT. Indeed, even with significant upgrades in measurement accuracy, the BSM flavor structure will have a dominant role.

USC UNIVERSIDADE DE SANTIAGO DE COMPOSTELA

Chapter 6

Drell Yan process

Drell-Yan (DY) production is an excellent path to investigate the EW sector. Indeed, by measuring the cross-section and the kinematic distribution of the produced lepton pairs, it is possible to make precise tests of the SM predictions. In this context, the DY process is a highly sensitive probe for new physics. Indeed, being a well measured process, any deviation between experimental and theoretical results could point at new physics beyond the Standard Model. To enable precise comparisons between theory and experimental data, extensive calculations have been performed in both the electroweak and QCD sectors of the Standard Model.

Following this line of reasoning, the DY scattering has been investigated also in the Standard Model Effective Field Theory (SMEFT) framework, both at LO and NLO. Nevertheless, existing results on this process do not include 4-fermion operators at NLO SMEFT [165, 166]. In this chapter, we extend these calculations in order to include all dimension-6 operators in the SMEFT framework, providing NLO QCD and electroweak contributions for the neutral Drell-Yan process. The chapter is divided as follow. In section 6.1 we present a short introduction about the Drell-Yan process. In section 6.2 we introduce the notation used in this work. In section 6.3, we present our LO calculation for the DY process, showing explicitly the up quark initial states case. In section 6.4 we discuss in detail the calculation of the NLO contributions, explaining how we treated the different Feynman diagrams. In section 6.5 we show the real contributions to the partonic cross section, divided in soft, pdf and collinear terms. Finally in Section 6.6, we provide an initial phenomenological study for $O_{qq}^{(3)}$. This chapter is based on an ongoing project and a paper is in preparation.

6.1 Overview

The measurement of the neutral Drell-Yan (DY) process, $pp \to Z^*/\gamma^* \to l^+l^-$, has played an essential role in validating SM predictions and has been used for various purposes. Among these, we can mention the possibility of testing new physics scenarios, including high mass Z' bosons. Additionally, it has been used as a probe to investigate

USC UNIVERSIDADE DE SANTIAGO DE COMPOSTELA

deviations from the SM in the EFT framework. In all these applications, precise theoretical predictions are crucial, both in the SM and in the EFT context.
The SM results for the neutral DY process, along with NLO QCD and NLO electroweak corrections, were derived many years ago. Subsequent advances in calculations include NNLO QCD results for total cross-section and some differential distributions, and even further to N^{3}LL+NNLO and N^{3}LO [167, 168, 169, 170, 171]. The combination of NNLO QCD and NLO electroweak corrections for high mass DY pairs has also been extensively studied in [172, 173, 174, 175, 176, 177, 178, 179].
The current predictions for DY production are in excellent agreement with experimental results [27, 28], indicating that any potential source of new physics (involved in DY production) either lies at a very high energy scale or shows extremely weak coupling, making it challenging for current experiments to detect. In the context of EFT, new physics effects may appear at the increasing of the partonic energy scales, requiring precision calculations in the EFT, whose are beyond the existing SM results.
As discussed in [108, 110], relevant progresses have been made in the development of simulation tools for the SMEFT. Currently, the inclusion of SMEFT dimension-6 operators at NLO QCD is possible using these tools. Furthrmore, several specific studies have explored individual processes, incorporating NLO QCD, such as $H \to b\bar{b}$ [125, 180, 181], $H \to \gamma\gamma$ [182, 183, 124, 127], $H \to ZZ^*$ [123], $H \to Z\gamma$ [123, 126], $H \to WW^*$ [124], $Z \to f\overline{f}$ [130, 128], and $t \to Wb$ [135]. On the other hand, NLO EW corrections are currently performed on a case-by-case basis. Most of the NLO EW studies have focused on decays, while the only $2 \to 2$ particle scattering process that has been studied at the NLO EW level is the Drell-Yan (DY) process. In previous studies [166, 165], the effect of 2-fermion and bosonic operators in DY were treated. In the following we will consider all dimension 6 operators, including 4-fermion, in the SMEFT framework calculating both NLO QCD and EW contributions. Similarly to Chapter 5, we set the CKM matrix to be diagonal and we set all masses other than the top quark to be 0.

6.2 Notation

We focus on dimension-6 operators, assuming real coefficients and neglecting CP violation effects. We use the Warsaw basis introduced in Chapter 4 and we normalize the coefficients according to Eq. 4.3. Our calculations involve flavor indices and we consider amplitudes up to linear order in the dimension-6 SMEFT coefficients, including 1-loop effects in the QCD and EW couplings.
We use as input parameters for the EW sector M_W, M_Z, and G_μ. As in 5, 4-fermion operators give contributions to the decay of the μ, changing the relation between the vev, v, and the Fermi constant G_μ as

$$G_\mu \equiv \frac{1}{\sqrt{2}v^2} - \frac{1}{2\sqrt{2}\Lambda^2}(C_{ll}[2112] + C_{ll}[1221]) + \frac{\sqrt{2}}{2\Lambda^2}(C^{(3)}_{\phi l,}[11] + C^{(3)}_{\phi l}[22])\,. \tag{6.1}$$

In the dimension-6 truncation of the SMEFT, the amplitude for the DY process to $1-$loop order can be expressed up as follows:

USC UNIVERSIDADE DE SANTIAGO DE COMPOSTELA

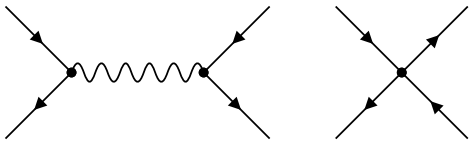

Figure 6.1: LO Feynman diagrams for DY process. Realized with [185]

.

$$A \sim A_{SM} + \Sigma_i \frac{C_i^6}{\Lambda^2} A_{i,LO}^6 + \Sigma_j \frac{D_j^6}{16\pi^2\Lambda^2} A_{j,NLO}^6 \,. \tag{6.2}$$

Here A_{SM}, $A_{i,LO}^6$, and $A_{j,NLO}^6$ represent the SM, dimension-6 tree level, and dimension-6 1−loop contributions, respectively. We define the linear SMEFT result as:

$$\begin{aligned} \mid A \mid_{lin}^2 \equiv & \mid A_{SM} \mid^2 + 2\mathrm{Re}(\Sigma_i A_{SM}^* \frac{C_i^6}{\Lambda^2} A_{i,LO}^6) \\ & + 2\mathrm{Re}(\Sigma_i A_{SM}^* \frac{D_i^6}{16\pi^2\Lambda^2} A_{j,NLO}^6) \end{aligned} \tag{6.3}$$

where we notice that Eq. 6.3 is not positive definite. For our purposes, we define the quadratic SMEFT result as:

$$\mid A \mid_{quad}^2 \equiv \mid A_{SM} + \Sigma_i \frac{C_i^6}{\Lambda^2} A_{i,LO}^6 + \Sigma_j \frac{D_j^6}{16\pi^2\Lambda^2} A_{j,NLO}^6 \mid^2 \,. \tag{6.4}$$

In SMEFT phenomenology studies and global fits, the quantity defined in Eq. 6.4 is commonly used. Nevertheless, it is important to note that we do not include two types of $\mathcal{O}(\frac{1}{\Lambda^4})$ terms in Eq. 6.4: the interference of the dimension-8 operators with the SM result [184], and the double insertions of the dimension-6 operators in the amplitude. In the following we will neglect these terms, because they are beyond the scope of current NLO EW SMEFT calculations.

6.3 LO DY calculations

In this section we show the LO results for $q(p_1)\overline{q}(p_2) \to l^+(p_3)l^-(p_4)$. Fig 6.1 shows the two possible topologies present at LO. In the following, we consider up quark initial states, the down quark case is given in Appendix A.1. In terms of helicity amplitudes we have:

$$M_{XY} = \left[\overline{u}(p_2)\gamma_\mu P_X u(p_1)\right] \cdot \left[\overline{u}(p_3)\gamma^\mu P_Y u(p_4)\right], \tag{6.5}$$

USC UNIVERSIDADE DE SANTIAGO DE COMPOSTELA

with $P_{L,R} = \frac{1\mp\gamma_5}{2}$. At tree level we have

$$A_{LO} = \Sigma_{XY} G_{XY} M_{XY} \tag{6.6}$$

with

$$G_{XY} = G_{XY}^{SM} + \delta G_{XY} \tag{6.7}$$

where the δ term represents the SMEFT contributions.

Therefore, for the up quark initial states we have

$$\begin{aligned} G_{\rm LR}^{SM} &= -\frac{2(s-4m_W^2)(m_W^2-m_Z^2)}{3sv^2(s-m_Z^2)} & G_{\rm LL}^{SM} &= \frac{2sm_W^2+8m_W^4+sm_Z^2-8m_W^2m_Z^2}{3s^2v^2-3sv^2m_Z^2} \\ G_{\rm RL}^{SM} &= -\frac{4(s-2m_W^2)(m_W^2-m_Z^2)}{3sv^2(s-m_Z^2)} & G_{\rm RR}^{SM} &= \frac{8(s-m_W^2)(-m_W^2+m_Z^2)}{3sv^2(s-m_Z^2)} \end{aligned} \tag{6.8}$$

and

$$\begin{aligned} \delta G_{\rm LR} = \frac{1}{\Lambda^2}\Big(&\frac{C_{\phi \rm D}(4m_W^4-sm_Z^2)}{3s^2-3sm_Z^2} + \frac{2C_{\phi \rm WB}m_W^2(-5s+8m_W^2)\sqrt{-1+\frac{m_Z^2}{m_W^2}}}{3s(s-m_Z^2)} - C_{\rm qe}[1122] \\ &+ \frac{(4m_W^2-m_Z^2)C_{\phi \rm e}[22]}{3s-3m_Z^2} + \frac{2(-m_W^2+m_Z^2)C_{\phi \rm q}^{(1)}[11]}{s-m_Z^2} + \frac{2(m_W^2-m_Z^2)C_{\phi \rm q}^{(3)}[11]}{s-m_Z^2} \\ &- \frac{(s-4m_W^2)\,(m_W^2-m_Z^2)}{3s\,(s-m_Z^2)}\Big(-C_{\rm ll}[1221] - C_{\rm ll}[2112] + 2C_{\phi \rm l}^{(1)}[11] + 2C_{\phi \rm l}^{(3)}[22]\Big)\Big), \end{aligned}$$

$$\begin{aligned} \delta G_{\rm RL} = \frac{1}{\Lambda^2}\Big(&\frac{C_{\phi \rm D}(4m_W^4-2sm_Z^2)}{3s^2-3sm_Z^2} + \frac{4C_{\phi \rm WB}m_W^2(-3s+4m_W^2)\sqrt{-1+\frac{m_Z^2}{m_W^2}}}{3s(s-m_Z^2)} - C_{\rm lu}[2211] \\ &+ \frac{4(m_W^2-m_Z^2)C_{\phi \rm l}^{(1)}[22]}{3(s-m_Z^2)} + \frac{4(m_W^2-m_Z^2)C_{\phi \rm l}^{(3)}[22]}{3(s-m_Z^2)} + \frac{(-2m_W^2+m_Z^2)C_{\phi \rm u}[11]}{s-m_Z^2} \\ &- \frac{2(s-2m_W^2)(m_W^2-m_Z^2)}{3sv^2(s-m_Z^2)}\Big(-C_{\rm ll}[1221] - C_{\rm ll}[2112] + 2C_{\phi \rm l}^{(1)}[11] + 2C_{\phi \rm l}^{(3)}[22]\Big)\Big), \end{aligned}$$

$$\begin{aligned} \delta G_{\rm LL} = \frac{1}{\Lambda^2}\Big(&\frac{C_{\phi \rm D}(8m_W^4-sm_Z^2)}{6s^2-6sm_Z^2} + \frac{2C_{\phi \rm WB}m_W^2(-3s+8m_W^2)\sqrt{-1+\frac{m_Z^2}{m_W^2}}}{3s(s-m_Z^2)} - C_{\rm lq}^{(1)}[2211] \\ &+ C_{\rm lq}^{(3)}[2211] + \frac{(4m_W^2-m_Z^2)C_{\phi \rm l}^{(1)}[22]}{3s-3m_Z^2} + \frac{(4m_W^2-m_Z^2)C_{\phi \rm l}^{(3)}[22]}{3s-3m_Z^2} + \frac{(-2m_W^2+m_Z^2)C_{\phi \rm q}^{(1)}[11]}{s-m_Z^2} \\ &+ \frac{(2m_W^2-m_Z^2)C_{\phi \rm q}^{(3)}[11]}{s-m_Z^2} + \frac{2sm_W^2+8m_W^4+sm_Z^2-8m_W^2m_Z^2}{6s^2v^2-6sv^2m_Z^2} \\ &\Big(-C_{\rm ll}[1221] - C_{\rm ll}[2112] + 2C_{\phi \rm l}^{(1)}[11] + 2C_{\phi \rm l}^{(3)}[22]\Big)\Big), \end{aligned}$$

USC UNIVERSIDADE DE SANTIAGO DE COMPOSTELA

$$\delta G_{\rm RR} = \frac{1}{\Lambda^2}\Big(\frac{C_{\phi \rm D}(4m_W^4 - 4sm_Z^2)}{3s^2 - 3sm_Z^2} + \frac{16C_{\phi \rm WB}m_W^2(-s+m_W^2)\sqrt{-1+\frac{m_Z^2}{m_W^2}}}{3s(s-m_Z^2)} - C_{\rm eu}[2211]$$
$$+ \frac{4(m_W^2 - m_Z^2)C_{\phi \rm e}[22]}{3(s-m_Z^2)} + \frac{2(-m_W^2+m_Z^2)C_{\phi \rm u}[11]}{s-m_Z^2}$$
$$+ \frac{4(s-m_W^2)(-m_W^2+m_Z^2)}{3sv^2(s-m_Z^2)}(-C_{\rm ll}[1221] - C_{\rm ll}[2112] + 2C_{\phi \rm l}^{(1)}[11] + 2C_{\phi \rm l}^{(3)}[22])\Big), \tag{6.9}$$

where $s = (p_1 + p_2)^2$.

The SMEFT coefficients contributing at this order are

$$C_{\phi WB},\, C_{\phi D},\, C_{\phi l}^{(3)}[11],\, C_{\phi l,}^{(3)}[22],\, C_{\phi l}^{(1)}[22], C_{\phi e,}[22], C_{\phi q,}^{(3)}[11],\, C_{\phi q}^{(1)}[11],\, C_{\phi u,}[11],$$
$$C_{ll,}[1221],\, C_{ll}[2112],\, C_{lq}^{(3)}[2211],\, C_{lq,}^{(1)}[2211],\, C_{qe}[1122],\, C_{lu}[2211],\, C_{eu}[2211]. \tag{6.10}$$

Summing over helicity amplitudes and averaging over the spin and color we have

$$\begin{aligned} \mid \overline{A}_{LO}(s,t) \mid^2 &\equiv \frac{1}{12}\Sigma_{XY} \mid G_{XY} \mid^2 \mid M_{XY} \mid^2 \\ &\equiv \frac{1}{12} \mid A_{LO} \mid^2 . \end{aligned} \tag{6.11}$$

The partonic cross sections, averaged over spin and color are given by:

$$\begin{aligned} \frac{d\hat{\sigma}}{dt} &= \frac{1}{48\pi s^2}\Big\{(\mid G_{LL} \mid^2 + \mid G_{RR} \mid^2)u^2 + (\mid G_{LR} \mid^2 + \mid G_{RL} \mid^2)t^2\Big\} \\ \hat{\sigma}_{LO} &= \frac{1}{16\pi s^2}\int_{-s}^{0} dt \mid \overline{A}_{LO}(s,t) \mid^2 , \end{aligned} \tag{6.12}$$

where $t = (p_1 - p_3)^2$ and $u = (p_1 - p_4)^2$. The numerical results of the tree level 4−fermion operators has been extensively studied in the literature [186, 163, 187, 188, 189]. According to [190], the Drell Yan process can give useful information not only from the high-energy regime. Indeed, due to its large cross section, it allows us to put significant constraints on the dimension-6 SMEFT coefficients even at relatively low energies, providing a comprehensive understanding of the SMEFT contributions to the neutral DY process. Indeed, even at LHC energies, the one-loop EW contributions to Z decays in the SMEFT can reach $O(10-20)\%$. In previous work [191], where a set of SMEFT contributions to neutral Drell-Yan process were computed, it has been shown that HL-LHC will have significant sensitivity to these effects.

6.4 SMEFT NLO DY calculations: Virtual contributions

In this section, we provide a detailed account of the calculation of virtual NLO corrections within the SMEFT for the Drell-Yan process. The notation follows that of previous works

USC UNIVERSIDADE DE SANTIAGO DE COMPOSTELA

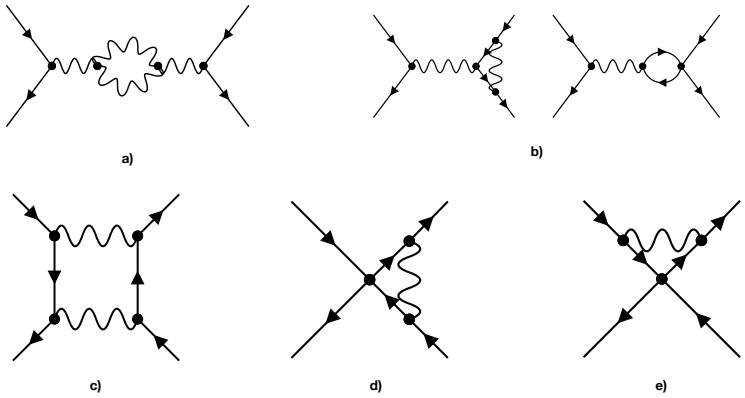

Figure 6.2: Samples of Feynman diagrams contributing at NLO for DY process. Realized with [185]. *a*) Renormalization counterterms, *b*) Vertex,
c) Box, *d*) 4-fermion vertex, *e*) 4-fermion box.

[123, 130, 166, 124]. The relevant operators for the 1−loop amplitudes include those from Eq. 6.10 as well as additional ones listed in Eq. 6.13

$$C_W,\ C_{\phi\Box},\ C_{\phi W},\ C_{\phi B},\ C_{uW}[33],\ C_{uB}[33],\ C^{(3)}_{\phi l}[ii],\ C^{(1)}_{\phi l}[ii], C_{\phi e}[ii], C^{(3)}_{\phi q}[ii],\ C^{(1)}_{\phi q}[ii],\ C_{\phi u}[ii],\ C_{\phi d}[ii],$$
$$C_{ee}[ijkl],\ C_{ll}[ijkl],\ C^{(1)}_{qq}[ijkl],\ C^{(3)}_{qq}[ijkl],\ C_{uu}[ijkl],\ C_{ed}[iijj],\ C^{(1)}_{ud}[iijj],\ C^{(1)}_{qu}[iijj],\ C_{qe}[iijj],$$
$$C^{(1)}_{qd}[iijj],\ C_{lu}[iijj],\ C_{lu}[ijkl], C^{(3)}_{lq}[iijj], C^{(1)}_{lq}[iijj], C_{le}[iijj], C_{ld}[iijj], C_{eu}[iijj], \qquad (6.13)$$

where, as already discussed in Chapter 5, we notice that only operators containing pairs of identical flavor fermions can contribute. In this work, we will start the exploration of the effects in DY production of 4-fermion operators that first arise at 1-loop order as well as the corrections to the 4-fermion operators appearing at LO. The virtual corrections to Drell-Yan encounter both UV and IR divergences, which we handle by working in $d = 4-2\epsilon$ dimensions using the dimensional regularization introduced in Chapter 2. We schematize the contributions to the virtual NLO corrections into box, vertex, 4-fermion vertex triangle, 4-fermion box triangle and renormalization counterterm contributions, as shown in Fig. 6.2. We notice that our computation includes only NLO corrections that interfere with the LO amplitudes. Unlike [165], due to the 4 fermion operators inclusion, we see that also topologies that do not appear at the SM level are involved in the calculation.

We use FeynRules [192] routines to convert R_ξ Feynman rules [100] for the SMEFT into a FeynArts [1] model file, then using FeynCalc [2] we compute amplitudes and we reduce 1-loop integrals to Passarino-Veltman integrals. We do not fix the gauge in the SMEFT Lagrangian and we verify at the end the cancellation of ξ terms, in order to have a further check on our computation. Excluding the renormalization counterterms, we determine the one loop contributions by contracting NLO amplitudes with M_{XY},

USC UNIVERSIDADE DE SANTIAGO DE COMPOSTELA

acting as projectors in the massless fermion limit. To be consistent in the SMEFT expansion, our approach requires to consider Feynman diagrams with at most a single SMEFT operator insertion. This ensures renormalizability by avoiding divergences that cannot be countered without introducing higher-order operators at leading order. As already discussed in Section 2.4.1, the treatment of γ^5 in D dimension requires particular care. Indeed, the complex Dirac traces of the SMEFT raise difficulties in the calculation process. To evaluate the Dirac traces, our choice between the NDR or Kreimer scheme depends on the specific class of Feynman diagrams illustrated in Figure 6.2.

Renormalization counterterms

The propagator contributions are derived directly from the SMEFT gauge boson and fermion 2-point functions [151, 152]. In the renormalization of the LO amplitude, we employed a mixed OS/$\overline{\text{MS}}$ scheme introduced in Chapter 2. SM parameters are renormalized in the OS scheme, while SMEFT operator coefficients are treated as $\overline{\text{MS}}$ objects. We use the $\{G_\mu, M_Z, M_W\}$ scheme for input parameters, with corrections to gauge boson masses defined as

$$M_V^2 = M_{0,V}^2 - \Pi_{VV}(M_V^2), \tag{6.14}$$

where $V = Z, W$, the 0 indicates the bare quantities and $\Pi_{VV}(M_V^2)$ are the 2-point functions of Refs. [151, 152] computed on-shell. As in Chapter 5, the relation of Eq. 6.1 is modified at 1-loop,

$$G_\mu + \frac{1}{2\sqrt{2}\Lambda^2}\Big(C_{ll}[2112] + C_{ll}[1221]\Big) - \frac{\sqrt{2}}{2\Lambda^2}\Big(C_{\phi l}^{(3)}[11] + C_{\phi l}^{(3)}[22]\Big) \equiv \frac{1}{\sqrt{2}v_0}(1+\Delta r) \tag{6.15}$$

where v_0 is the **square** of the minimum of the potential at tree level and the analytic expression for Δr in the SMEFT is given in Ref. [123]. The effective field theory coefficients of the dimension-6 operators are treated as $\overline{\text{MS}}$ quantities, defined at the scale of the measurement, i.e. the EW scale. The poles of the one-loop coefficients C_i are extracted from Refs. [97, 98, 99],

$$C_i(\mu_R) = C_{0,i} - \frac{1}{2\hat{\epsilon}}\frac{1}{16\pi^2}\gamma_{ij}C_j, \tag{6.16}$$

where μ is the renormalization scale, γ_{ij} are the one-loop anomalous dimensions,

$$\mu_R\frac{dC_i}{d\mu_R} = \frac{1}{16\pi^2}\gamma_{ij}C_j, \tag{6.17}$$

and $\hat{\epsilon}^{-1} \equiv \epsilon^{-1} - \gamma_E + \log(4\pi)$.

Vertex

Vertex contributions involve 1PI vertex amplitudes that are extracted by contracting amplitudes with M_{XY}. We notice that the presence of SMEFT operators does not raise

USC UNIVERSIDADE DE SANTIAGO DE COMPOSTELA

the issue of the D-dimensional evaluation of the Dirac trace, because at most 4 Dirac matrices are involved. Thus, in this case we can use the NDR scheme when γ^5 is involved in the calculation.

Box

In this case we considered "SM type" box diagrams, meaning that in this subsection we studied box topologies that appear already at the SM level. As in the previous case we extract the box contributions by contracting amplitudes with M_{XY}, using them as "projectors". In this case, we have fermion chains that involve up to 6 Dirac matrices and therefore we use the Kreimer scheme using a consistent reading point. As discussed in Section 2.4.3, the reading point prescription effectively specifies with which Dirac matrix to start the non-cyclic trace in the Kreimer scheme. Our choice is to begin reading the Dirac traces from the projector insertion.

4-fermion vertex triangle

The diagrams discussed in this subsection are the NLO corrections to the 4-fermion operators appearing at LO; in particular we considered the case where a gauge boson is "connecting" 2 leptons or 2 quarks. The fermion chains appearing in these diagrams have the some form as those in the vertex 6.4 and, after projecting through M_{XY}, we can use the NDR scheme to evaluate the Dirac traces.

4-fermion box triangle

Finally, we discuss NLO 4 fermion feynman diagrams with a gauge boson connecting different type of fermions, e.g quark and lepton. According to the Kreimer scheme when we have more than 5 Dirac matrices and we are dealing with several axial current we should employ a *symmetric* reading point. However, even if we have several γ^5 involved in the calculations we are handling open fermion chains, not closed fermion loops. This means we can reduce the fermion chains using the Dirac algebra *before* we project through M_{XY}. After this operation, the chains appearing in these diagrams will have the same form of 6.4. By the same reasoning, we use the same reading point of the box diagrams, starting to read our Dirac traces from the projector insertion. Finally, we notice that not employing a reading point would not give us the correct results for these diagrams, as expected. Indeed, as explicitly verified, this choice would lead to gauge and chiral violating terms.

USC UNIVERSIDADE DE SANTIAGO DE COMPOSTELA

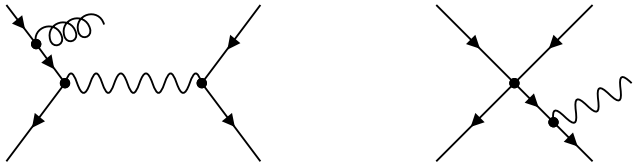

Figure 6.3: Real contributions Feynman diagrams for DY process. Realized with [185].

6.5 SMEFT NLO DY calculations: Real Contributions

The NLO result requires the real contributions from both photon and gluon emission

$$q\overline{q} \to l^+l^-\gamma,\ q\overline{q} \to l^+l^-g\,. \tag{6.18}$$

In Fig 6.3 we show a sample of Feynman diagrams contributing at this order. The IR singularities are regulated using phase space slicing with dimensional regularization $D = 4 - 2\epsilon$, as in Refs. [193, 194, 195, 196]. After regulating the IR singularities by including the collinear and soft limits of the $2 \to 3$ contributions, ϵ can be set to 0.
As discussed in [197, 198], the soft limits of the $2 \to 3$ scattering processes have a universal form that is the same for both the SM and the SMEFT. The soft contribution is characterized by photon or gluon energies with the condition $E_\gamma, E_g < \Delta E$, where ΔE represents a chosen infinitesimally small cutoff. The soft partonic cross section is defined in terms of the lowest order SMEFT cross section of Eq. 6.11,

$$d\hat{\sigma}_{soft} = \quad = \frac{1}{16\pi s^2}\int_{-s}^{0} dt \mid \overline{A}_{LO}(s,t) \mid^2 \left(\alpha\delta^{EW}_{soft}(s,t) + \alpha_S C_F \delta^{QCD}_{soft}(s)\right). \tag{6.19}$$

It is important to point out that α is redefined within the context of the SMEFT. At this order, the factors influencing α arise from the Z mass definition and the $SU(2)/U(1)$ mixing

$$\begin{aligned}\alpha =& \frac{\sqrt{2}G_\mu m_W^2(m_Z^2 - m_W^2)}{\pi m_Z^2} - \frac{1}{\Lambda^2}\frac{m_W^2}{2m_Z^2\pi}\Bigg(m_W^2 C_{\phi D} + 4\sqrt{m_W^2(m_Z^2 - m_W^2)}C_{\phi WB} \\ &+ (m_Z^2 - m_W^2)\Big[2(C^{(3)}_{\phi l}[11] + C^{(3)}_{\phi l}[22]) - C_{ll}[1221] - C_{ll}[2112]\Big]\Bigg).\end{aligned} \tag{6.20}$$

We notice that no adjustments are introduced due to factors like $C_{\phi W}$.

USC UNIVERSIDADE DE SANTIAGO DE COMPOSTELA

The soft functions are

$$\begin{aligned}
\delta_{soft}^{EW} &= Q_q^2 f_q(s) + Q_l^2 f_l(s) + 2Q_q Q_l h(s,t) \\
\delta_{soft}^{QCD} &= f_q(s) \\
f_f(s) &= \frac{\log\left(\frac{\mu^2}{4\Delta \mathrm{E}^2}\right)}{\pi\epsilon} + \frac{2\log^2\left(\frac{\mu^2}{4\Delta \mathrm{E}^2}\right) - \pi^2}{4\pi} + \frac{1}{\pi\epsilon^2} \\
h(s,t) &= \frac{\frac{1}{2}\log^2\left(\frac{\mu^2}{4\Delta \mathrm{E}^2}\right) - \mathrm{Li}_2\left(\frac{s}{t}+1\right) + \log\left(\frac{\mu^2}{4\Delta \mathrm{E}^2}\right)\log\left(-\frac{s}{t}\right) - \frac{\pi^2}{4}}{\pi} + \frac{\log\left(\frac{\mu^2}{4\Delta \mathrm{E}^2}\right) + \log\left(-\frac{s}{t}\right)}{\pi\epsilon} + \frac{1}{\pi\epsilon^2}.
\end{aligned} \tag{6.21}$$

For soft gluons, take $Q_l = 0$ and $\alpha Q_q^2 \to \alpha_s C_F$. Adding the virtual one loop contributions and Eq. 6.21, the ϵ^2 dependences cancel, leaving just the ϵ singular terms.

Consider photons emitted from the initial quark within an angle δ_θ. The initial state collinear contributions are absorbed into the definition of the PDFs [193]. Therefore, in the $\overline{MS}$ scheme, we have

$$\begin{aligned}
\hat{\sigma}_{PDF}^q &= \frac{Q_q^2}{16\pi s^2}\int_{-s}^{0} dt \mid \overline{A}(s,t)_{LO} \mid^2 \alpha\ \delta_{PDF}(s) \\
\delta_{PDF}(s) &= \frac{1}{\pi}\left(\frac{1}{2}\log\left(\frac{\mu^2}{\mu_f^2}\right)\left(4\log\left(\frac{2\Delta \mathrm{E}}{\sqrt{s}}\right)+3\right) + \frac{2\log\left(\frac{2\Delta \mathrm{E}}{\sqrt{s}}\right)+\frac{3}{2}}{\epsilon}\right),
\end{aligned} \tag{6.22}$$

where μ_F is the factorization scale. The QCD contribution is found with the replacement $\alpha Q_q^2 \to \alpha_s C_F$.

When the photons are emitted from the final state lepton,

$$\hat{\sigma}_{coll}^l = \frac{Q_l^2}{16\pi s^2}\int_{-s}^{0} dt \mid \overline{A}(s,t)_{LO} \mid^2 \alpha\delta c^l(s) \tag{6.23}$$

with $\delta c^l(s)$ given by

$$\begin{aligned}
\delta c^l(s) = \frac{1}{\pi}\Bigg(&\frac{1}{6}(-6\log(\frac{2\Delta \mathrm{E}}{\sqrt{s}})(\log(\delta_\theta) - 2\log(2\mu) + \log(s)) + 3(4\log(\frac{2\Delta \mathrm{E}}{\sqrt{s}}) + 3)\log(\frac{2\mu}{\sqrt{s}\sqrt{\delta_\theta}}) \\
&- \frac{9}{2}(\log(\delta_\theta) - 2\log(2\mu) + \log(s)) - 12\log^2(\frac{2\Delta \mathrm{E}}{\sqrt{s}}) - 4\pi^2 + 39) + \frac{2\log(\frac{2\Delta \mathrm{E}}{\sqrt{s}}) + \frac{3}{2}}{\epsilon}\Bigg)
\end{aligned} \tag{6.24}$$

Finally, putting these terms together we have:

$$\hat{\sigma}_a = \frac{1}{16\pi s^2}\frac{1}{12}\int_{-s}^{0} dt \mid A_{LO}(s,t) + \delta A_{NLO}(s,t) \mid^2, \tag{6.25}$$

where

USC UNIVERSIDADE DE SANTIAGO DE COMPOSTELA

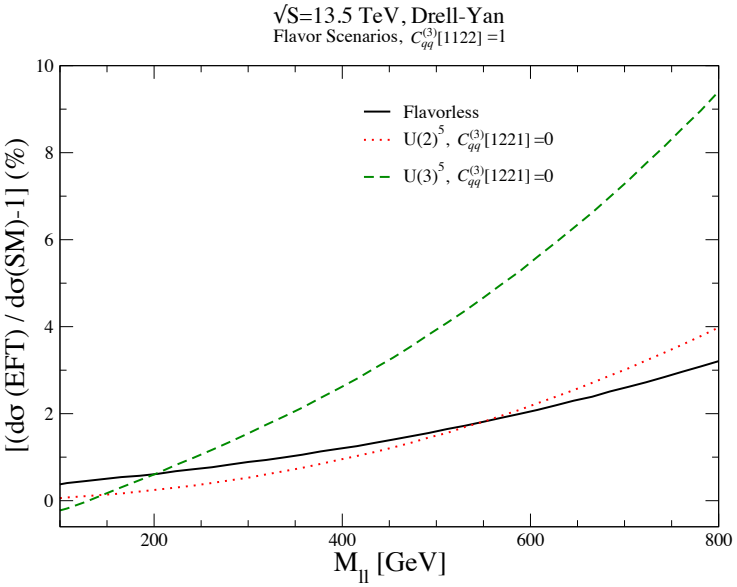

Figure 6.4: $O_{qq}^{(3)}$ in different flavor assumptions, $\sqrt{S} = 13.5$ TeV

$$\delta A_{NLO}(s,t) = \left\{ \delta A_{\text{virt}}(s,t) + \frac{1}{2} A_{LO}(s,t) \left[\alpha \delta_{soft}^{EW}(s,t) + \alpha_s C_F \delta_{soft}^{QCD}(s) + (\alpha Q_q^2 + \alpha_s C_F)\delta_{PDF}(s) + \alpha \delta c^l(s) \right] \right\} \tag{6.26}$$

and $\delta A_{virt}(s,t)$ is the one loop renormalized amplitude calculated in Sect. 6.4 and as always A_{LO} and α are SMEFT quantities. We note that Eq. 6.26 is a finite object and we are free to apply it at linear or quadratic order in the SMEFT following Eqs. 6.3 and 6.4. Indeed, $\hat{\sigma}_a$ has no dependence on ϵ, thus we can take the limit $\epsilon \to 0$.

6.6 Phenomenology

The analytical results obtained in this chapter are going to be implemented in Montecarlo programs, in particular in POWHEG code, in order to include also contributions coming from PDF factorization and hard non-collinear contributions from the $2 \to 3$ process. Being an ongoing project, we can not present a detailed phenomenological analysis at this stage. However, we can provide a preliminary study of the phenomenology involving 4-fermion operators first appearing at NLO. For the flavor scenarios, we use the same notation introduced in Section 5.3.

In Fig 6.4, we show our results for $O_{qq}^{(3)}$ in different flavor assumptions for $\sqrt{s} = 13.5$ TeV. Specifically, we are plotting the percentage difference between the SMEFT and SM differential cross sections as a function of dilepton mass. Assuming $C_{qq}^{(3)}[1122] =$

USC UNIVERSIDADE DE SANTIAGO DE COMPOSTELA

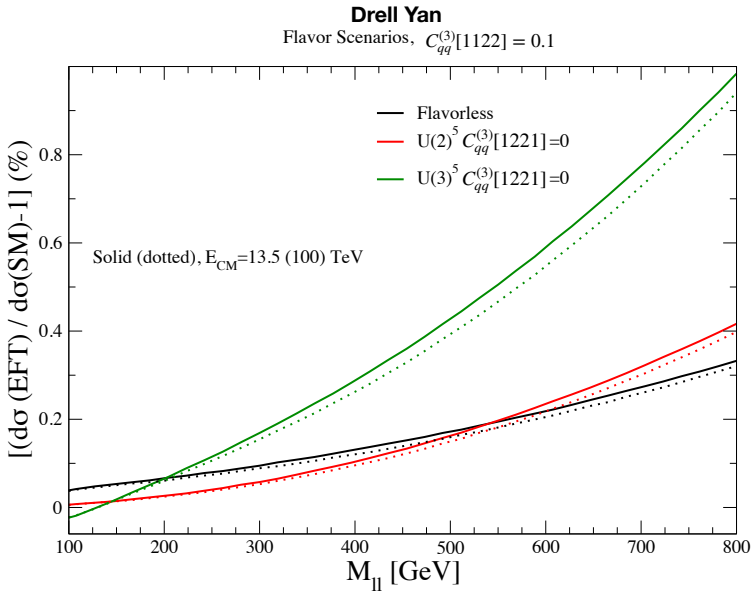

Figure 6.5: $O_{qq}^{(3)}$ different center-of-mass energies.

1 and setting $C_{qq}^{(3)}[1221] = 0$ we notice that in all the flavor scenarios, the SMEFT contribution grows with the dilepton energy, with $U(3)^5$ reaching 9% while the flavorless and $U(2)^2$ remaining below 4%.

In Fig 6.5, we compare different center-of-mass energies: $\sqrt{s} = 13.5$ TeV, which is the energy at which the LHC runs, and $\sqrt{s} = 100$ TeV, the expected energy for the future collider Fcc-ee. We set $C_{qq}^{(3)}[1122] = 0.1$ and $C_{qq}^{(3)}[1221] = 0$. Due to the linear dependence of the SMEFT coefficient on the cross section, this results in a simple rescaling of $\mathrm{d}\sigma_{\mathrm{EFT}}$. We see that increasing the energy scale doesn't significantly affect the contributions in any of the flavor scenarios. However, we do observe a systematic reduction of a few percent between the energy scales.

In Fig 6.6, we show the correlation between the coefficients $C_{qq}^{(3)}[1122]$ and $C_{qq}^{(3)}[1221]$ in the $U(2)^5$ scenario, assuming

$$\left[\frac{d\sigma_{EFT}}{d\sigma_{SM}} - 1\right] > 2\% \text{ or } 10\%, \quad M_{ll} > 500 \text{ GeV}. \tag{6.27}$$

According to [199], the current DY relative uncertainty for muon dilepton mass $M_{ll} > 500$ GeV is $\gtrsim 19\%$. Under these conditions, we can detect BSM events in this channel only if they deviate more than 19% from the SM. It is reasonable to assume that the precision will increase at future colliders and that this upgrade will allow us to measure possible deviations with higher sensitivity. For this reason, in this analysis we considered two scenarios, a "conservative" one at 10% and a more "optimistic" one at 2% .

We notice that, due to the linear approximation, we can not set bounds on the SMEFT

USC UNIVERSIDADE DE SANTIAGO DE COMPOSTELA

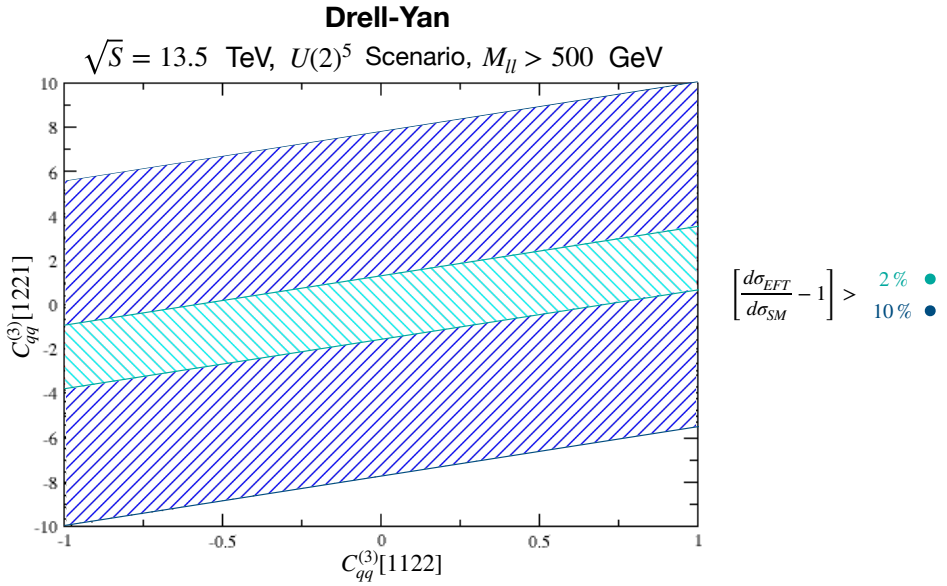

Figure 6.6: Correlation between the coefficients $C_{qq}^{(3)}[1122]$ and $C_{qq}^{(3)}[1221]$ in the $U(2)^5$ scenario.

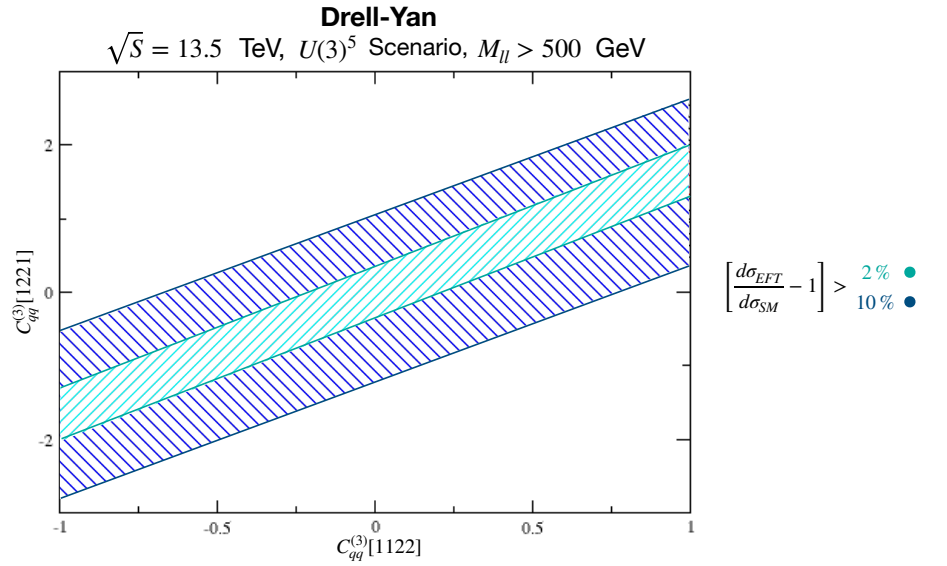

Figure 6.7: Correlation between the coefficients $C_{qq}^{(3)}[1122]$ and $C_{qq}^{(3)}[1221]$ in the $U(3)^5$ scenario.

coefficients, since the area of the allowed values is delimited by two straight parallel lines. Nevertheless, these results can be used to check the consistency of the constraints coming from other sources, for example by studying specific regions. Indeed, it is meaningful to point out that the two parameters show a strong correlation.

USC UNIVERSIDADE DE SANTIAGO DE COMPOSTELA

Finally, in Fig 6.7, we consider a similar plot with $U(3)^5$ symmetry. Comparing with the previous one, we notice a stronger correlation between the coefficients in $U(3)^5$. This happens because in this scenario we have the flavor symmetry $C_{qq}^{(3)}[1122] = C_{qq}^{(3)}[1133]$ and $C_{qq}^{(3)}[1221] = C_{qq}^{(3)}[1331]$, which implies that the coefficients receive contributions $\sim m_t^2$ from the top quark loops.

The constraints on the 4-fermion operators derived from this analysis appear to be less stringent than those obtained, for example, from the EWPOs. However, it should be emphasized that this is still a preliminary study and does not include, for example, NLO corrections to the SM. We expect that the bounds resulting through the DY process can be used to strengthen those from other sources.

USC UNIVERSIDADE DE SANTIAGO DE COMPOSTELA

Chapter 7

Results and Conclusions

"...e si usano segni e segni di segni
solo quando ci fanno difetto le cose."

Umberto Eco
Il nome della rosa

Over the course of centuries, physicists have reached relevant results and conclusions. One of these is probably the fact that even if they are very interested in understanding nature, this does not imply that nature herself is inclined to be studied and comprehended. Regarding high energy particle physics, the last decade has strongly highlighted this concept, since the lack of new physics signals has led particle physicists to reevaluate their assumptions and review their goals. However, looking at the past with a critical point of view, we should not forget how we achieved important results.
In this context, precision physics played a crucial role. Indeed, through an impressive number of confirmed predictions, it brought the SM to be the most rigorously tested theory in history. This result has been obtained by constantly improving the accuracy of both experimental and theoretical values. Following this line of reasoning, experimental physicists continued to upgrade existing colliders and started to plan for new particle colliders. On the other side, theoretical physicists are committed to provide more precise calculations, to ensure that the experimental work is not in vain. This is the perspective we aimed to present in this thesis.

In Chapter 2 we reviewed the SM Lagrangian, analyzing each piece of 2.1 and discussing regularization and renormalization procedures. In Chapter 3, we combined small p_T and HE expansions for $gg \to HH$ and $gg \to ZH$, obtaining accurate results over the entire phase space. In particular, using Padé approximants, we extended the validity ranges of both methods, covering the regions around $|\hat{t}| \simeq 4m_t^2$ effectively. Our method was verified using exact LO analytical results and numerical NLO results, displaying differences below 1%. Additionally, our analytic approach is flexible to changing top quark mass renormalization schemes compared to numerical approaches.

USC
UNIVERSIDADE DE SANTIAGO DE COMPOSTELA

In Chapter 4, we reviewed the EFT method and the key features of the SMEFT, explaining both the advantages and limitations of this framework. Furthermore, we explained how the BSM operators are derived in the *Warsaw basis*, including the list couplings and fields redefinitions.

In Chapter 5, we shown how measurements at Z and W boson poles constrain BSM physics. In particular, we calculated NLO EWPOs contributions, including general flavor structures for fermion operators. Performing global fits, we see that NLO bounds on 2-fermion operators vary by factors of $\mathcal{O}(2)$ between different flavor scenario. Considering 4-fermion operators, flavor structure has a dramatic impact on the constraints of the coefficients. Specifically, neglecting flavor leads to tighter SMEFT coefficient bounds. Finally, the size of expected ranges from future colliders is intricately tied to the specific flavor scenario. Indeed, uncertainties from these colliders can not ensure meaningful constraints on the SMEFT coefficients for all flavor scenarios and the BSM flavor structure remains relevant despite improved measurement accuracy.

In Chapter 6, we calculated NLO QCD and EW contributions for the neutral Drell-Yan process, including all dimension-6 operators in the SMEFT framework with general flavor structure. In particular, studying the Feynman diagrams contributing at this order, we have seen that a careful treatment of the γ^5 was necessary working in dimensional regularization. Additionally, we performed a preliminary phenomenological analysis for the operator $O_{qq}^{(3)}$.

Finally, we mention some possible outlooks for the research line explored here. For instance, the approach discussed in Chapter 3 can be applied to other fundamental processes for the physics programme of the LHC and HL-LHC, such as ZZ and $\gamma\gamma$ gluon fusion production. Additionally, a further step is to calculate the real corrections for $gg \to HH$, as it has been carried out for $gg \to HZ$ in [200, 201]. Including these contributions would allow for the full evaluation of the inclusive cross section.

Regarding the EWPOs analyses, a further development may be to perform global fits keeping more than one operator at time. In particular, considering specific BSM scenarios we know whose specific SMEFT operators will be generated [104]. Therefore, studying the coefficients bounds and correlation in this context would provide meaningful information.

Lastly, for what concerns the Drell Yan scattering, we expect to implement our results into a versatile Monte Carlo program, specifically using POWHEG code. Furthermore, the diagrams calculated for this process are closely related to the diagrams of $e^+e^- \to q\bar{q}$ and therefore, with the necessary adjustments, they can be used to study it. As discussed in previous chapters, this process will be widely explored in future colliders such as Fcc-ee and ILC, demanding precise predictions.

The calculation of sensitive observables is a challenging task and it needs to be carried out to give results for comparison with experimental data. To improve our knowledge of nature, in this thesis we have explored many physical phenomena related to precision physics. We may expect to see the investigation of even more of them in the future.

USC UNIVERSIDADE DE SANTIAGO DE COMPOSTELA

Appendix A

A.1 SMEFT

Recalling dimension 5 operator 4.4.2 we have:

$$C_{\nu\nu}Q_{\nu\nu} = C_{\nu\nu}\epsilon_{jk}\epsilon_{mn}\phi^j\phi^m(l_p^k)^T C l_r^n \equiv C_{\nu\nu}(\widetilde{\phi}^\dagger l_p)^T C(\widetilde{\phi}^\dagger l_r)^T.$$

Setting the Higgs doublet to his vev

$$\phi = \frac{1}{\sqrt{2}}\begin{pmatrix}0\\ v\end{pmatrix},$$

we see that $Q_{\nu\nu}$ gives the Majorana mass term for observed neutrinos

$$\frac{1}{2}m_\nu\epsilon_{jk}\nu_L^j\nu_L^k + h.c. \qquad \text{with} \qquad m_\nu = \frac{C_{\nu\nu}v^2}{\Lambda}.$$

From experimental data $m_\nu \leq 0.5$ eV and assuming $C_{\nu\nu} \sim 1$ we have

$$\Lambda \geq 10^{14} \text{ GeV}.$$

USC UNIVERSIDADE DE SANTIAGO DE COMPOSTELA

A.2 Drell Yan

Drell-Yan LO Amplitude for for down quark initial states:

$$
\begin{aligned}
G_{\mathrm{RR}} &= \frac{4(s-m_W^2)(m_W^2-m_Z^2)}{3sv^2(s-m_Z^2)} \qquad & G_{\mathrm{RL}} &= \frac{2(s-2m_W^2)(m_W^2-m_Z^2)}{3sv^2(s-m_Z^2)} \\
G_{\mathrm{LR}} &= -\frac{2(s+2m_W^2)(m_W^2-m_Z^2)}{3sv^2(s-m_Z^2)} \qquad & G_{\mathrm{LL}} &= \frac{-4m_W^2(s+m_W^2)+(s+4m_W^2)m_Z^2}{3sv^2(s-m_Z^2)}
\end{aligned}
\tag{A.1}
$$

and

$$
\begin{aligned}
\delta G_{\mathrm{RR}} = \frac{1}{\Lambda^2}\Big(&\frac{2C_{\phi\mathrm{D}}(-m_W^4+sm_Z^2)}{3s(s-m_Z^2)} + \frac{8C_{\phi\mathrm{WB}}m_W^2(s-m_W^2)\sqrt{-1+\frac{m_Z^2}{m_W^2}}}{3s(s-m_Z^2)} - C_{\mathrm{ed}}[2211] \\
&+ \frac{2(-m_W^2+m_Z^2)C_{\phi\mathrm{d}}[11]}{s-m_Z^2} + \frac{2(-m_W^2+m_Z^2)C_{\phi\mathrm{e}}[22]}{3(s-m_Z^2)} + \frac{2(s-m_W^2)(m_W^2-m_Z^2)}{3sv^2(s-m_Z^2)} \\
&(-C_{\mathrm{ll}}[1221] - C_{\mathrm{ll}}[2112] + 2C_{\phi\mathrm{l}}^{(1)}[11] + 2C_{\phi\mathrm{l}}^{(3)}[22])\Big)
\end{aligned}
$$

$$
\begin{aligned}
\delta G_{\mathrm{RL}} = \frac{1}{\Lambda^2}\Big(&\frac{C_{\phi\mathrm{D}}(-2m_W^4+sm_Z^2)}{3s(s-m_Z^2)} + \frac{2C_{\phi\mathrm{WB}}m_W^2(3s-4m_W^2)\sqrt{-1+\frac{m_Z^2}{m_W^2}}}{3s(s-m_Z^2)} - C_{\mathrm{ld}}[2211] \\
&+ \frac{(-2m_W^2+m_Z^2)C_{\phi\mathrm{d}}[11]}{s-m_Z^2} + \frac{2(-m_W^2+m_Z^2)C_{\phi\mathrm{l}}^{(1)}[22]}{3(s-m_Z^2)} + \frac{2(-m_W^2+m_Z^2)C_{\phi\mathrm{l}}^{(3)}[22]}{3(s-m_Z^2)} \\
&+ \frac{(s-2m_W^2)(m_W^2-m_Z^2)}{3sv^2(s-m_Z^2)}(-C_{\mathrm{ll}}[1221] - C_{\mathrm{ll}}[2112] + 2C_{\phi\mathrm{l}}^{(1)}[11] + 2C_{\phi\mathrm{l}}^{(3)}[22])\Big)
\end{aligned}
$$

$$
\begin{aligned}
\delta G_{\mathrm{LR}} = \frac{1}{\Lambda^2}\Big(&\frac{2C_{\phi\mathrm{WB}}(s-4m_W^2)\sqrt{m_W^2(-m_W^2+m_Z^2)}}{3s(s-m_Z^2)} - \frac{C_{\phi\mathrm{D}}(2m_W^4+sm_Z^2)}{3s^2-3sm_Z^2} - C_{\mathrm{qe}}[1122] \\
&- \frac{(2m_W^2+m_Z^2)C_{\phi\mathrm{e}}[22]}{3s-3m_Z^2} + \frac{2(-m_W^2+m_Z^2)C_{\phi\mathrm{q}}^{(1)}[11]}{s-m_Z^2} + \frac{2(-m_W^2+m_Z^2)C_{\phi\mathrm{q}}^{(3)}[11]}{s-m_Z^2} \\
&- \frac{(s-2m_W^2)(m_W^2-m_Z^2)}{3sv^2(s-m_Z^2)}(-C_{\mathrm{ll}}[1221] - C_{\mathrm{ll}}[2112] + 2C_{\phi\mathrm{l}}^{(1)}[11] + 2C_{\phi\mathrm{l}}^{(3)}[22])\Big)
\end{aligned}
$$

USC UNIVERSIDADE DE SANTIAGO DE COMPOSTELA

$$\delta G_{\rm LL} = \frac{1}{\Lambda^2}(-\frac{8C_{\phi \rm WB}\sqrt{m_W^6(-m_W^2+m_Z^2)}}{3s^2-3sm_Z^2} - \frac{C_{\phi \rm D}(4m_W^4+sm_Z^2)}{6s^2-6sm_Z^2} - C_{\rm lq}^{(1)}[2211] - C_{\rm lq}^{(3)}[2211]$$
$$- \frac{(2m_W^2+m_Z^2)C_{\phi \rm l}^{(1)}[22]}{3s-3m_Z^2} - \frac{(2m_W^2+m_Z^2)C_{\phi \rm l}^{(3)}[22]}{3s-3m_Z^2} + \frac{(-2m_W^2+m_Z^2)C_{\phi \rm q}^{(1)}[11]}{s-m_Z^2}$$
$$+ \frac{(-2m_W^2+m_Z^2)C_{\phi \rm q}^{(3)}[11]}{s-m_Z^2} + \frac{-4m_W^2(s+m_W^2)+(s+4m_W^2)m_Z^2}{6sv^2(s-m_Z^2)}$$
$$(-C_{\rm ll}[1221] - C_{\rm ll}[2112] + 2C_{\phi \rm l}^{(1)}[11] + 2C_{\phi \rm l}^{(3)}[22])))). \tag{A.2}$$

USC UNIVERSIDADE DE SANTIAGO DE COMPOSTELA

A.3 EWPOs

Other plots for 2-fermion operators

In this subsection, we show a collection of plots involving the 2-fermion operators, as described in Chapter 5.

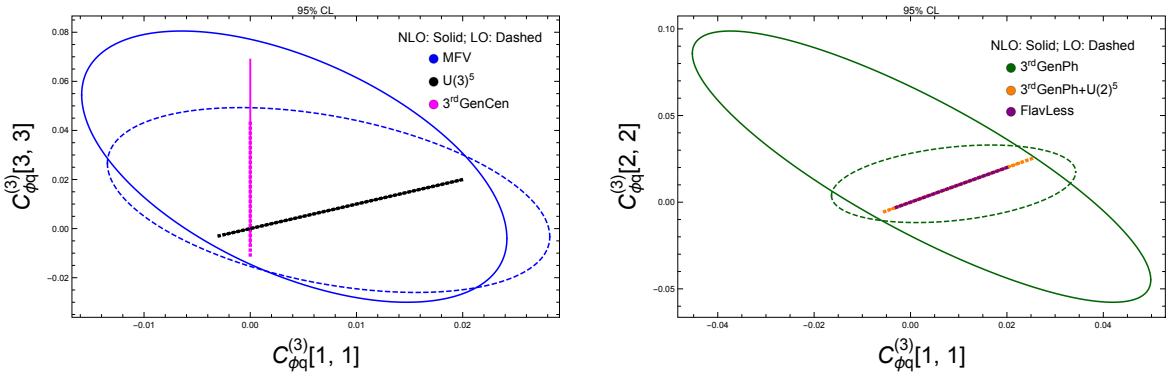

Figure A.1: 95% CL limits on $C_{\phi q}^{(3)}[ij]$ under flavor assumptions described in the text. Results at LO are drawn with dashed lines, results at NLO are drawn with solid lines. **On the left** we present $C_{\phi q}^{(3)}[11]$ vs. $C_{\phi q}^{(3)}[33]$ in the $U(3)^5$ (black), MFV (blue) and 3^{rd} generation centric (magenta) scenarios. In these scenarios $C_{\phi q}^{(3)}[22] = C_{\phi q}^{(3)}[11]$. **On the right** we present $C_{\phi q}^{(3)}[11]$ vs. $C_{\phi q}^{(3)}[22]$ in the 3^{rd} generation phobic (green), 3^{rd} generation phobic + $U(2)^5$ (orange) and flavorless (violet) scenarios. In the first two scenarios $C_{\phi q}^{(3)}[33] = 0$, while in the flavorless scenario $C_{\phi q}^{(3)}[33] = C_{\phi q}^{(3)}[22] = C_{\phi q}^{(3)}[11]$. All other coefficients are set to 0.

USC UNIVERSIDADE DE SANTIAGO DE COMPOSTELA

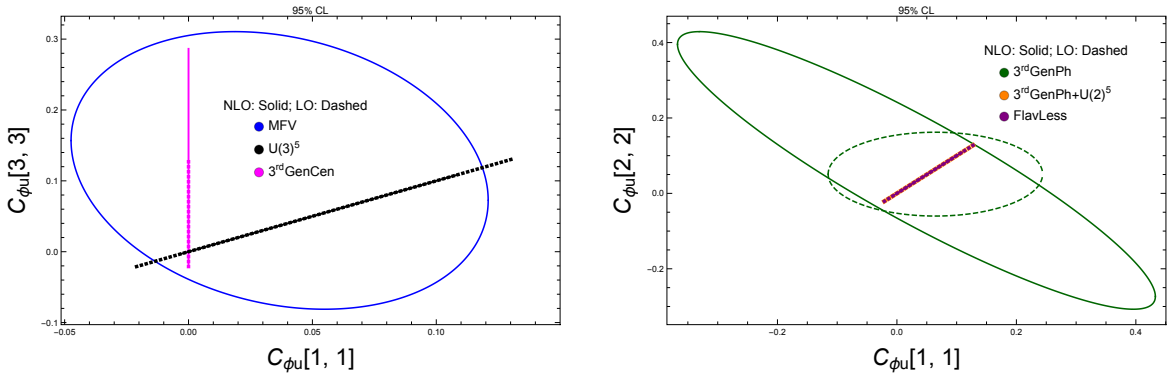

Figure A.2: 95% CL limits on $C_{\phi u}[ij]$ under flavor assumptions described in the text. Results at LO are drawn with dashed lines, results at NLO are drawn with solid lines. **On the left** we present $C_{\phi u}[11]$ vs. $C_{\phi u}[33]$ in the $U(3)^5$ (black), MFV (blue) and 3^{rd} generation centric (magenta) scenarios. In these scenarios $C_{\phi u}[22] = C_{\phi u}[11]$, also notice that for the MFV scenario only the NLO results can be obtained. **On the right** we present $C_{\phi u}[11]$ vs. $C_{\phi u}[22]$ in the 3^{rd} generation phobic (green), 3^{rd} generation phobic $+ U(2)^5$ (orange) and flavorless (violet) scenarios. In the first two scenarios $C_{\phi u}[33] = 0$, while in the flavorless scenario $C_{\phi u}[33] = C_{\phi u}[22] = C_{\phi u}[11]$. All other coefficients are set to 0.

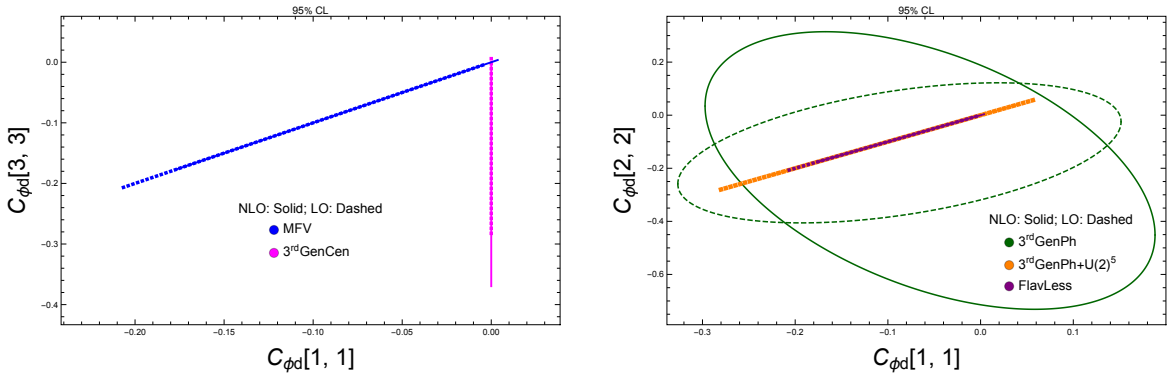

Figure A.3: 95% CL limits on $C_{\phi d}[ij]$ under flavor assumptions described in the text. Results at LO are drawn with dashed lines, results at NLO are drawn with solid lines. **On the left** we present $C_{\phi d}[11]$ vs. $C_{\phi d}[33]$ in the MFV (blue) and 3^{rd} generation centric (magenta) scenarios. In these scenarios $C_{\phi d}[22] = C_{\phi d}[11]$. **On the right** we present $C_{\phi d}[11]$ vs. $C_{\phi d}[22]$ in the 3^{rd} generation phobic (green), 3^{rd} generation phobic $+ U(2)^5$ (orange) and flavorless (violet) scenarios. In the first two scenarios $C_{\phi d}[33] = 0$, while in the flavorless scenario $C_{\phi d}[33] = C_{\phi d}[22] = C_{\phi d}[11]$. All other coefficients are set to 0.

USC UNIVERSIDADE DE SANTIAGO DE COMPOSTELA

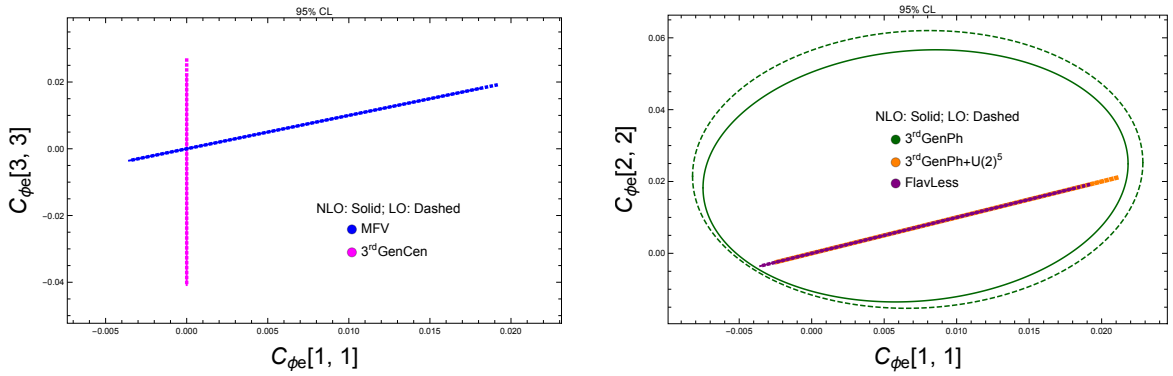

Figure A.4: 95% CL limits on $C_{\phi e}[ij]$ under flavor assumptions described in the text. Results at LO are drawn with dashed lines, results at NLO are drawn with solid lines. **On the left** we present $C_{\phi e}[11]$ vs. $C_{\phi e}[33]$ in the MFV (blue) and 3^{rd} generation centric (magenta) scenarios. In these scenarios $C_{\phi e}[22] = C_{\phi e}[11]$. **On the right** we present $C_{\phi e}[11]$ vs. $C_{\phi e}[22]$ in the 3^{rd} generation phobic (green), 3^{rd} generation phobic + $U(2)^5$ (orange) and flavorless (violet) scenarios. In the first two scenarios $C_{\phi e}[33] = 0$, while in the flavorless scenario $C_{\phi e}[33] = C_{\phi e}[22] = C_{\phi e}[11]$. All other coefficients are set to 0.

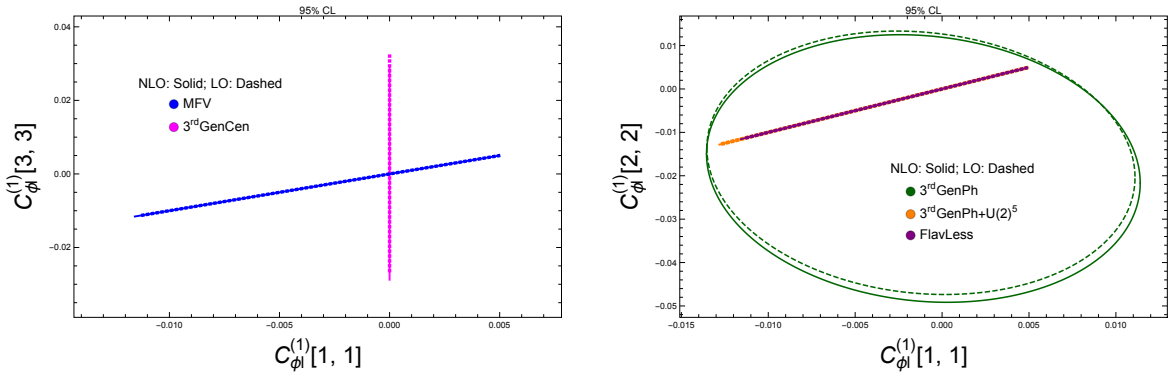

Figure A.5: 95% CL limits on $C_{\phi l}^{(1)}[ij]$ under flavor assumptions described in the text. Results at LO are drawn with dashed lines, results at NLO are drawn with solid lines. **On the left** we present $C_{\phi l}^{(1)}[11]$ vs. $C_{\phi l}^{(1)}[33]$ in the MFV (blue) and 3^{rd} generation centric (magenta) scenarios. In these scenarios $C_{\phi l}^{(1)}[22] = C_{\phi l}^{(1)}[11]$. **On the right** we present $C_{\phi l}^{(1)}[11]$ vs. $C_{\phi l}^{(1)}[22]$ in the 3^{rd} generation phobic (green), 3^{rd} generation phobic + $U(2)^5$ (orange) and flavorless (violet) scenarios. In the first two scenarios $C_{\phi l}^{(1)}[33] = 0$, while in the flavorless scenario $C_{\phi l}^{(1)}[33] = C_{\phi l}^{(1)}[22] = C_{\phi l}^{(1)}[11]$. All other coefficients are set to 0.

USC UNIVERSIDADE DE SANTIAGO DE COMPOSTELA

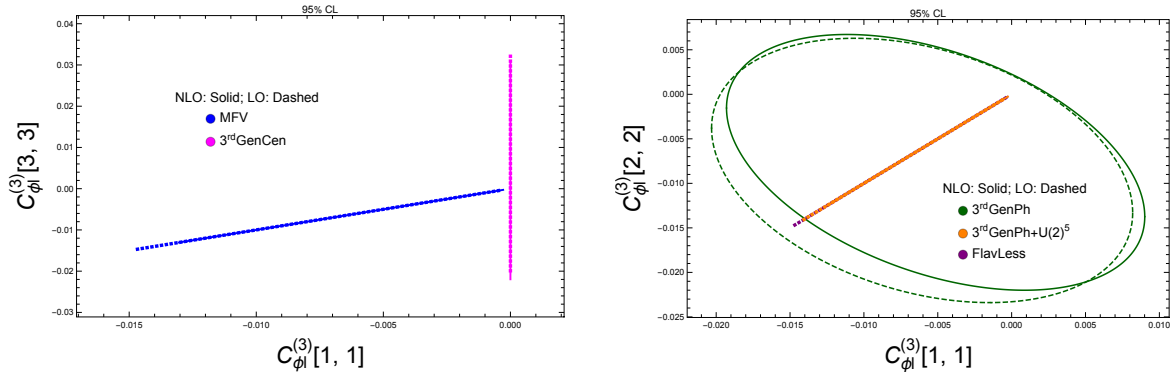

Figure A.6: 95% CL limits on $C_{\phi l}^{(3)}[ij]$ under flavor assumptions described in the text. Results at LO are drawn with dashed lines, results at NLO are drawn with solid lines. **On the left** we present $C_{\phi l}^{(3)}[11]$ vs. $C_{\phi l}^{(3)}[33]$ in the MFV (blue) and 3^{rd} generation centric (magenta) scenarios. In these scenarios $C_{\phi l}^{(3)}[22] = C_{\phi l}^{(3)}[11]$. **On the right** we present $C_{\phi l}^{(3)}[11]$ vs. $C_{\phi l}^{(3)}[22]$ in the 3^{rd} generation phobic (green), 3^{rd} generation phobic $+ U(2)^5$ (orange) and flavorless (violet) scenarios. In the first two scenarios $C_{\phi l}^{(3)}[33] = 0$, while in the flavorless scenario $C_{\phi l}^{(3)}[33] = C_{\phi l}^{(3)}[22] = C_{\phi l}^{(3)}[11]$. All other coefficients are set to 0.

USC UNIVERSIDADE DE SANTIAGO DE COMPOSTELA

USC
UNIVERSIDADE
DE SANTIAGO
DE COMPOSTELA

Bibliography

[1] Thomas Hahn. "Generating Feynman diagrams and amplitudes with FeynArts 3". In: Computer Physics Communications 140.3 (Nov. 2001), 418?431. ISSN: 0010-4655. DOI: 10.1016/s0010-4655(01)00290-9. URL: http://dx.doi.org/10.1016/S0010-4655(01)00290-9.

[2] Vladyslav Shtabovenko, Rolf Mertig, and Frederik Orellana. "FeynCalc 9.3: New features and improvements". In: Computer Physics Communications 256 (Nov. 2020), p. 107478. ISSN: 0010-4655. DOI: 10.1016/j.cpc.2020.107478. URL: http://dx.doi.org/10.1016/j.cpc.2020.107478.

[3] Roman N Lee. "LiteRed 1.4: a powerful tool for reduction of multiloop integrals". In: Journal of Physics: Conference Series 523 (June 2014), p. 012059. ISSN: 1742-6596. DOI: 10.1088/1742-6596/523/1/012059. URL: http://dx.doi.org/10.1088/1742-6596/523/1/012059.

[4] A.V. Smirnov. "FIRE5: A C++ implementation of Feynman Integral REduction". In: Computer Physics Communications 189 (Apr. 2015), 182?191. ISSN: 0010-4655. DOI: 10.1016/j.cpc.2014.11.024. URL: http://dx.doi.org/10.1016/j.cpc.2014.11.024.

[5] Vladyslav Shtabovenko. "FeynHelpers: Connecting FeynCalc to FIRE and Package-X". In: Comput. Phys. Commun. 218 (2017), pp. 48–65. DOI: 10.1016/j.cpc.2017.04.014. arXiv: 1611.06793 [physics.comp-ph].

[6] Roberto Bonciani et al. "Analytical Method for Next-to-Leading-Order QCD Corrections to Double-Higgs Production". In: Physical Review Letters 121.16 (Oct. 2018). ISSN: 1079-7114. DOI: 10.1103/physrevlett.121.162003. URL: http://dx.doi.org/10.1103/PhysRevLett.121.162003.

[7] Lina Alasfar et al. Virtual corrections to $gg \to ZH$ via a transverse momentum expansion. 2021. arXiv: 2103.06225 [hep-ph].

[8] Joshua Davies et al. "Double-Higgs boson production in the high-energy limit: planar master integrals". In: Journal of High Energy Physics 2018.3 (Mar. 2018). ISSN: 1029-8479. DOI: 10.1007/jhep03(2018)048. URL: http://dx.doi.org/10.1007/JHEP03(2018)048.

[9] J. G. Korner, D. Kreimer, and K. Schilcher. "A Practicable gamma(5) scheme in dimensional regularization". In: Z. Phys. C 54 (1992), pp. 503–512. DOI: 10.1007/BF01559471.

USC UNIVERSIDADE DE SANTIAGO DE COMPOSTELA

[10] A. Dedes et al. "Feynman rules for the Standard Model Effective Field Theory in R Ξ -gauges". In: Journal of High Energy Physics 2017.6 (June 2017). ISSN: 1029-8479. DOI: 10.1007/jhep06(2017)143. URL: http://dx.doi.org/10.1007/JHEP06(2017)143.

[11] S. Chatrchyan et al. "Observation of a new boson at a mass of 125 GeV with the CMS experiment at the LHC". In: Physics Letters B 716.1 (Sept. 2012), 30?61. ISSN: 0370-2693. DOI: 10.1016/j.physletb.2012.08.021. URL: http://dx.doi.org/10.1016/j.physletb.2012.08.021.

[12] G. Aad et al. "Observation of a new particle in the search for the Standard Model Higgs boson with the ATLAS detector at the LHC". In: Physics Letters B 716.1 (Sept. 2012), 1?29. ISSN: 0370-2693. DOI: 10.1016/j.physletb.2012.08.020. URL: http://dx.doi.org/10.1016/j.physletb.2012.08.020.

[13] European Strategy. URL: https://europeanstrategyupdate.web.cern.ch/.

[14] High-Luminosity LHC (HL-LHC). URL: https://home.cern/resources/faqs/high-luminosity-lhc.

[15] J. Alison et al. "Higgs boson potential at colliders: Status and perspectives". In: Rev. Phys. 5 (2020). Ed. by Biagio Di Micco et al., p. 100045. DOI: 10.1016/j.revip.2020.100045. arXiv: 1910.00012 [hep-ph].

[16] D. de Florian et al. "Handbook of LHC Higgs Cross Sections: 4. Deciphering the Nature of the Higgs Sector". In: 2/2017 (Oct. 2016). DOI: 10.23731/CYRM-2017-002. arXiv: 1610.07922 [hep-ph].

[17] Laure Berthier, Mikkel Bjørn, and Michael Trott. "Incorporating doubly resonant $W^{\pm}$ data in a global fit of SMEFT parameters to lift flat directions". In: JHEP 09 (2016), p. 157. DOI: 10.1007/JHEP09(2016)157. arXiv: 1606.06693 [hep-ph].

[18] John Ellis et al. "Updated Global SMEFT Fit to Higgs, Diboson and Electroweak Data". In: JHEP 06 (2018), p. 146. DOI: 10.1007/JHEP06(2018)146. arXiv: 1803.03252 [hep-ph].

[19] Jorge de Blas et al. "The Global Electroweak and Higgs Fits in the LHC era". In: PoS EPS-HEP2017 (2017). Ed. by Paolo Checchia et al., p. 467. DOI: 10.22323/1.314.0467. arXiv: 1710.05402 [hep-ph].

[20] Anke Biekötter, Tyler Corbett, and Tilman Plehn. "The Gauge-Higgs Legacy of the LHC Run II". In: SciPost Phys. 6.6 (2019), p. 064. DOI: 10.21468/SciPostPhys.6.6.064. arXiv: 1812.07587 [hep-ph].

[21] Alberto Belloni et al. "Report of the Topical Group on Electroweak Precision Physics and Constraining New Physics for Snowmass 2021". In: (Sept. 2022). arXiv: 2209.08078 [hep-ph].

[22] "The International Linear Collider Technical Design Report - Volume 2: Physics". In: (June 2013). Ed. by Howard Baer et al. arXiv: 1306.6352 [hep-ph].

[23] Philip Bambade et al. "The International Linear Collider: A Global Project". In: (Mar. 2019). arXiv: 1903.01629 [hep-ex].

USC UNIVERSIDADE DE SANTIAGO DE COMPOSTELA

[24] Alexander Aryshev et al. "The International Linear Collider: Report to Snowmass 2021". In: (Mar. 2022). arXiv: 2203.07622 [physics.acc-ph].

[25] G. Bernardi et al. "The Future Circular Collider: a Summary for the US 2021 Snowmass Process". In: (Mar. 2022). arXiv: 2203.06520 [hep-ex].

[26] A. Abada et al. "FCC-ee: The Lepton Collider: Future Circular Collider Conceptual Design Report Volume 2". In: Eur. Phys. J. ST 228.2 (2019), pp. 261–623. DOI: 10.1140/epjst/e2019-900045-4.

[27] Georges Aad et al. "Measurement of the transverse momentum distribution of Drell–Yan lepton pairs in proton–proton collisions at $\sqrt{s}$ = 13 TeV with the ATLAS detector". In: Eur. Phys. J. C 80.7 (2020), p. 616. DOI: 10.1140/epjc/s10052-020-8001-z. arXiv: 1912.02844 [hep-ex].

[28] Albert M Sirunyan et al. "Measurement of the differential Drell-Yan cross section in proton-proton collisions at $\sqrt{s}$ = 13 TeV". In: JHEP 12 (2019), p. 059. DOI: 10.1007/JHEP12(2019)059. arXiv: 1812.10529 [hep-ex].

[29] Roberto Bonciani et al. "Analytical Method for Next-to-Leading-Order QCD Corrections to Double-Higgs Production". In: Phys. Rev. Lett. 121.16 (2018), p. 162003. DOI: 10.1103/PhysRevLett.121.162003. arXiv: 1806.11564 [hep-ph].

[30] Joshua Davies et al. "Double-Higgs boson production in the high-energy limit: planar master integrals". In: JHEP 03 (2018), p. 048. DOI: 10.1007/JHEP03(2018)048. arXiv: 1801.09696 [hep-ph].

[31] Sheldon L. Glashow. "The renormalizability of vector meson interactions". In: Nucl. Phys. 10 (1959), pp. 107–117. DOI: 10.1016/0029-5582(59)90196-8.

[32] Abdus Salam and John Clive Ward. "Electromagnetic and weak interactions". In: Phys. Lett. 13 (1964), pp. 168–171. DOI: 10.1016/0031-9163(64)90711-5.

[33] Steven Weinberg. "A Model of Leptons". In: Phys. Rev. Lett. 19 (21 Nov. 1967), pp. 1264–1266. DOI: 10.1103/PhysRevLett.19.1264. URL: https://link.aps.org/doi/10.1103/PhysRevLett.19.1264.

[34] Murray Gell-Mann. "A Schematic Model of Baryons and Mesons". In: Phys. Lett. 8 (1964), pp. 214–215. DOI: 10.1016/S0031-9163(64)92001-3.

[35] O. W. Greenberg. "Spin and Unitary Spin Independence in a Paraquark Model of Baryons and Mesons". In: Phys. Rev. Lett. 13 (1964), pp. 598–602. DOI: 10.1103/PhysRevLett.13.598.

[36] M. Y. Han and Yoichiro Nambu. "Three Triplet Model with Double SU(3) Symmetry". In: Phys. Rev. 139 (1965). Ed. by T. Eguchi, B1006–B1010. DOI: 10.1103/PhysRev.139.B1006.

[37] G. Zweig. "An SU(3) model for strong interaction symmetry and its breaking. Version 1". In: (Jan. 1964).

[38] R. L. Workman et al. "Review of Particle Physics". In: PTEP 2022 (2022), p. 083C01. DOI: 10.1093/ptep/ptac097.

USC UNIVERSIDADE DE SANTIAGO DE COMPOSTELA

[39] Ling-Lie Chau and Wai-Yee Keung. "Comments on the Parametrization of the Kobayashi-Maskawa Matrix". In: Phys. Rev. Lett. 53 (19 Nov. 1984), pp. 1802–1805. DOI: 10.1103/PhysRevLett.53.1802. URL: https://link.aps.org/doi/10.1103/PhysRevLett.53.1802.

[40] Lincoln Wolfenstein. "Parametrization of the Kobayashi-Maskawa Matrix". In: Phys. Rev. Lett. 51 (21 Nov. 1983), pp. 1945–1947. DOI: 10.1103/PhysRevLett.51.1945. URL: https://link.aps.org/doi/10.1103/PhysRevLett.51.1945.

[41] Giuseppe Degrassi, Paolo Gambino, and Alessandro Vicini. "Two-loop heavy top effects on the mZ-mW interdependence". In: Physics Letters B 383.2 (Aug. 1996), pp. 219–226. DOI: 10.1016/0370-2693(96)00720-4. URL: https://doi.org/10.1016%2F0370-2693%2896%2900720-4.

[42] Riccardo Barbieri et al. "Two-loop heavy-top effects in the Standard Model". In: Nuclear Physics B 409.1 (1993), pp. 105–127. ISSN: 0550-3213. DOI: https://doi.org/10.1016/0550-3213(93)90448-X. URL: https://www.sciencedirect.com/science/article/pii/055032139390448X.

[43] Gerard 't Hooft and M. J. G. Veltman. "Regularization and Renormalization of Gauge Fields". In: Nucl. Phys. B 44 (1972), pp. 189–213. DOI: 10.1016/0550-3213(72)90279-9.

[44] J. G. Korner, D. Kreimer, and K. Schilcher. "A Practicable gamma(5) scheme in dimensional regularization". In: Z. Phys. C 54 (1992), pp. 503–512. DOI: 10.1007/BF01559471.

[45] P. Breitenlohner and D. Maison. "Dimensional renormalization and the action principle". In: Communications in Mathematical Physics 52.1 (1977), pp. 11–38.

[46] Matthias Heller et al. "Mixed EW-QCD two-loop amplitudes for $q\bar{q} \to \ell^+\ell^-$ and γ_5 scheme independence of multi-loop corrections". In: JHEP 05 (2021), p. 213. DOI: 10.1007/JHEP05(2021)213. arXiv: 2012.05918 [hep-ph].

[47] Michael E. Peskin and Daniel V. Schroeder. An Introduction to quantum field theory. Reading, USA: Addison-Wesley, 1995. ISBN: 978-0-201-50397-5.

[48] Steven Weinberg. The quantum theory of fields. Vol. 2: Modern applications. Cambridge University Press, Aug. 2013. ISBN: 978-1-139-63247-8, 978-0-521-67054-8, 978-0-521-55002-4. DOI: 10.1017/CBO9781139644174.

[49] Matthew D. Schwartz. Quantum Field Theory and the Standard Model. Cambridge University Press, Mar. 2014. ISBN: 978-1-107-03473-0, 978-1-107-03473-0.

[50] Stefano Catani et al. "Soft gluon resummation for Higgs boson production at hadron colliders". In: JHEP 07 (2003), p. 028. DOI: 10.1088/1126-6708/2003/07/028. arXiv: hep-ph/0306211.

[51] Valentin Ahrens et al. "Origin of the Large Perturbative Corrections to Higgs Production at Hadron Colliders". In: Phys. Rev. D 79 (2009), p. 033013. DOI: 10.1103/PhysRevD.79.033013. arXiv: 0808.3008 [hep-ph].

USC UNIVERSIDADE DE SANTIAGO DE COMPOSTELA

[52] Armen Tumasyan et al. "Search for Higgs boson pairs decaying to WW*WW*, WW*$\tau\tau$, and $\tau\tau\tau\tau$ in proton-proton collisions at $\sqrt{s} = 13$ TeV". In: JHEP 07 (2023), p. 095. DOI: 10.1007/JHEP07(2023)095. arXiv: 2206.10268 [hep-ex].

[53] Georges Aad et al. "Constraints on the Higgs boson self-coupling from single- and double-Higgs production with the ATLAS detector using pp collisions at s=13 TeV". In: Phys. Lett. B 843 (2023), p. 137745. DOI: 10.1016/j.physletb.2023.137745. arXiv: 2211.01216 [hep-ex].

[54] Elizabeth Brost and Luca Cadamuro. "Searching for Pairs of Higgs Bosons in the LHC Run 2 Dataset". In: Symmetry 14.7 (2022), p. 1467. DOI: 10.3390/sym14071467.

[55] Georges Aad et al. "Measurements of WH and ZH production in the $H \to b\bar{b}$ decay channel in pp collisions at 13 TeV with the ATLAS detector". In: Eur. Phys. J. C 81.2 (2021), p. 178. DOI: 10.1140/epjc/s10052-020-08677-2. arXiv: 2007.02873 [hep-ex].

[56] Lina Alasfar et al. "Virtual corrections to $gg \to ZH$ via a transverse momentum expansion". In: JHEP 05 (2021), p. 168. DOI: 10.1007/JHEP05(2021)168. arXiv: 2103.06225 [hep-ph].

[57] M. Spira et al. "Higgs boson production at the LHC". In: Nucl. Phys. B453 (1995), pp. 17–82. DOI: 10.1016/0550-3213(95)00379-7. arXiv: hep-ph/9504378 [hep-ph].

[58] Robert Harlander and Philipp Kant. "Higgs production and decay: Analytic results at next-to-leading order QCD". In: JHEP 0512 (2005), p. 015. DOI: 10.1088/1126-6708/2005/12/015. arXiv: hep-ph/0509189 [hep-ph].

[59] U. Aglietti et al. "Analytic Results for Virtual QCD Corrections to Higgs Production and Decay". In: JHEP 01 (2007), p. 021. DOI: 10.1088/1126-6708/2007/01/021. arXiv: hep-ph/0611266 [hep-ph].

[60] Charalampos Anastasiou et al. "Two-loop amplitudes and master integrals for the production of a Higgs boson via a massive quark and a scalar-quark loop". In: JHEP 01 (2007), p. 082. DOI: 10.1088/1126-6708/2007/01/082. arXiv: hep-ph/0611236 [hep-ph].

[61] S. Borowka et al. "SecDec-3.0: numerical evaluation of multi-scale integrals beyond one loop". In: Comput. Phys. Commun. 196 (2015), pp. 470–491. DOI: 10.1016/j.cpc.2015.05.022. arXiv: 1502.06595 [hep-ph].

[62] S. Borowka et al. "Higgs Boson Pair Production in Gluon Fusion at Next-to-Leading Order with Full Top-Quark Mass Dependence". In: Phys. Rev. Lett. 117.1 (2016). [Erratum: Phys. Rev. Lett.117,no.7,079901(2016)], p. 012001. DOI: 10.1103/PhysRevLett.117.079901, 10.1103/PhysRevLett.117.012001. arXiv: 1604.06447 [hep-ph].

USC UNIVERSIDADE DE SANTIAGO DE COMPOSTELA

[63] Julien Baglio et al. "Gluon fusion into Higgs pairs at NLO QCD and the top mass scheme". In: Eur. Phys. J. C 79.6 (2019), p. 459. DOI: 10.1140/epjc/s10052-019-6973-3. arXiv: 1811.05692 [hep-ph].

[64] J. Baglio et al. "Higgs-Pair Production via Gluon Fusion at Hadron Colliders: NLO QCD Corrections". In: JHEP 04 (2020), p. 181. DOI: 10.1007/JHEP04(2020)181. arXiv: 2003.03227 [hep-ph].

[65] Long Chen et al. "ZH production in gluon fusion: two-loop amplitudes with full top quark mass dependence". In: JHEP 03 (2021), p. 125. DOI: 10.1007/JHEP03(2021)125. arXiv: 2011.12325 [hep-ph].

[66] S. Dawson, S. Dittmaier, and M. Spira. "Neutral Higgs boson pair production at hadron colliders: QCD corrections". In: Phys. Rev. D58 (1998), p. 115012. DOI: 10.1103/PhysRevD.58.115012. arXiv: hep-ph/9805244 [hep-ph].

[67] Lukas Altenkamp et al. "Gluon-induced Higgs-strahlung at next-to-leading order QCD". In: JHEP 02 (2013), p. 078. DOI: 10.1007/JHEP02(2013)078. arXiv: 1211.5015 [hep-ph].

[68] Jonathan Grigo et al. "On the Higgs boson pair production at the LHC". In: Nucl. Phys. B875 (2013), pp. 1–17. DOI: 10.1016/j.nuclphysb.2013.06.024. arXiv: 1305.7340 [hep-ph].

[69] Jonathan Grigo, Jens Hoff, and Matthias Steinhauser. "Higgs boson pair production: top quark mass effects at NLO and NNLO". In: Nucl. Phys. B900 (2015), pp. 412–430. DOI: 10.1016/j.nuclphysb.2015.09.012. arXiv: 1508.00909 [hep-ph].

[70] Giuseppe Degrassi, Pier Paolo Giardino, and Ramona Gröber. "On the two-loop virtual QCD corrections to Higgs boson pair production in the Standard Model". In: Eur. Phys. J. C76.7 (2016), p. 411. DOI: 10.1140/epjc/s10052-016-4256-9. arXiv: 1603.00385 [hep-ph].

[71] Alexander Hasselhuhn, Thomas Luthe, and Matthias Steinhauser. "On top quark mass effects to $gg \to ZH$ at NLO". In: JHEP 01 (2017), p. 073. DOI: 10.1007/JHEP01(2017)073. arXiv: 1611.05881 [hep-ph].

[72] Roberto Bonciani et al. "A Numerical Routine for the Crossed Vertex Diagram with a Massive-Particle Loop". In: Comput. Phys. Commun. 241 (2019), pp. 122–131. DOI: 10.1016/j.cpc.2019.03.014. arXiv: 1812.02698 [hep-ph].

[73] Joshua Davies et al. "Double Higgs boson production at NLO in the high-energy limit: complete analytic results". In: JHEP 01 (2019), p. 176. DOI: 10.1007/JHEP01(2019)176. arXiv: 1811.05489 [hep-ph].

[74] Joshua Davies, Go Mishima, and Matthias Steinhauser. "Virtual corrections to $gg \to ZH$ in the high-energy and large-m_t limits". In: JHEP 03 (2021), p. 034. DOI: 10.1007/JHEP03(2021)034. arXiv: 2011.12314 [hep-ph].

USC UNIVERSIDADE DE SANTIAGO DE COMPOSTELA

[75] Xiaofeng Xu and Li Lin Yang. "Towards a new approximation for pair-production and associated-production of the Higgs boson". In: JHEP 01 (2019), p. 211. DOI: 10.1007/JHEP01(2019)211. arXiv: 1810.12002 [hep-ph].

[76] Guoxing Wang et al. "Efficient computation of two-loop amplitudes for Higgs boson pair production". In: Phys. Rev. D 104.5 (2021), p. L051901. DOI: 10.1103/PhysRevD.104.L051901. arXiv: 2010.15649 [hep-ph].

[77] Guoxing Wang et al. "Next-to-leading order corrections for $gg \to ZH$ with top quark mass dependence". In: (July 2021). arXiv: 2107.08206 [hep-ph].

[78] Ramona Gröber, Andreas Maier, and Thomas Rauh. "Reconstruction of top-quark mass effects in Higgs pair production and other gluon-fusion processes". In: JHEP 03 (2018), p. 020. DOI: 10.1007/JHEP03(2018)020. arXiv: 1709.07799 [hep-ph].

[79] Joshua Davies et al. "Padé approach to top-quark mass effects in gluon fusion amplitudes". In: PoS RADCOR2019 (2019), p. 079. DOI: 10.22323/1.375.0079. arXiv: 1912.04097 [hep-ph].

[80] Luigi Bellafronte et al. "Gluon fusion production at NLO: merging the transverse momentum and the high-energy expansions". In: JHEP 07 (2022), p. 069. DOI: 10.1007/JHEP07(2022)069. arXiv: 2202.12157 [hep-ph].

[81] Joshua Davies et al. "Double Higgs boson production at NLO: combining the exact numerical result and high-energy expansion". In: JHEP 11 (2019), p. 024. DOI: 10.1007/JHEP11(2019)024. arXiv: 1907.06408 [hep-ph].

[82] Joshua Davies et al. "$gg \to ZZ$: analytic two-loop results for the low- and high-energy regions". In: JHEP 04 (2020), p. 024. DOI: 10.1007/JHEP04(2020)024. arXiv: 2002.05558 [hep-ph].

[83] David Wellmann. "Top Quark Mass Effects in Higgs and Z Boson Pair Production and Higgs Boson Decays". PhD thesis. KIT, Karlsruhe, 2020. DOI: 10.5445/IR/1000105943.

[84] https://www.ttp.kit.edu/preprints/2019/ttp19-018/.

[85] https://www.ttp.kit.edu/preprints/2020/ttp20-041/.

[86] https://github.com/mppmu/hhgrid.

[87] J. Baglio et al. "$gg \to HH$: Combined uncertainties". In: Phys. Rev. D 103.5 (2021), p. 056002. DOI: 10.1103/PhysRevD.103.056002. arXiv: 2008.11626 [hep-ph].

[88] Kirill Melnikov and Timo van Ritbergen. "The Three loop relation between the MS-bar and the pole quark masses". In: Phys. Lett. B 482 (2000), pp. 99–108. DOI: 10.1016/S0370-2693(00)00507-4. arXiv: hep-ph/9912391.

[89] Marcela Carena et al. "Effective Lagrangian for the $\bar{t}bH^+$ interaction in the MSSM and charged Higgs phenomenology". In: Nucl. Phys. B 577 (2000), pp. 88–120. DOI: 10.1016/S0550-3213(00)00146-2. arXiv: hep-ph/9912516.

USC UNIVERSIDADE DE SANTIAGO DE COMPOSTELA

[90] R. L. Workman et al. "Review of Particle Physics". In: PTEP 2022 (2022), p. 083C01. DOI: 10.1093/ptep/ptac097.

[91] Timothy Cohen et al. "Is SMEFT Enough?" In: JHEP 03 (2021), p. 237. DOI: 10.1007/JHEP03(2021)237. arXiv: 2008.08597 [hep-ph].

[92] Howard Georgi. "An Effective Field Theory for Heavy Quarks at Low-energies". In: Phys. Lett. B 240 (1990), pp. 447–450. DOI: 10.1016/0370-2693(90)91128-X.

[93] W. Buchmuller and D. Wyler. "Effective Lagrangian Analysis of New Interactions and Flavor Conservation". In: Nucl. Phys. B 268 (1986), pp. 621–653. DOI: 10.1016/0550-3213(86)90262-2.

[94] Steven Weinberg. "Effective Gauge Theories". In: Phys. Lett. B 91 (1980), pp. 51–55. DOI: 10.1016/0370-2693(80)90660-7.

[95] Bohdan Grzadkowski et al. "Probing anomalous top quark couplings induced by dimension-six operators at photon colliders". In: Nucl. Phys. B 689 (2004), pp. 108–126. DOI: 10.1016/j.nuclphysb.2004.04.006. arXiv: hep-ph/0310159.

[96] B. Grzadkowski et al. "Dimension-Six Terms in the Standard Model Lagrangian". In: JHEP 10 (2010), p. 085. DOI: 10.1007/JHEP10(2010)085. arXiv: 1008.4884 [hep-ph].

[97] Elizabeth E. Jenkins, Aneesh V. Manohar, and Michael Trott. "Renormalization Group Evolution of the Standard Model Dimension Six Operators I: Formalism and lambda Dependence". In: JHEP 10 (2013), p. 087. DOI: 10.1007/JHEP10(2013)087. arXiv: 1308.2627 [hep-ph].

[98] Elizabeth E. Jenkins, Aneesh V. Manohar, and Michael Trott. "Renormalization Group Evolution of the Standard Model Dimension Six Operators II: Yukawa Dependence". In: JHEP 01 (2014), p. 035. DOI: 10.1007/JHEP01(2014)035. arXiv: 1310.4838 [hep-ph].

[99] Rodrigo Alonso et al. "Renormalization Group Evolution of the Standard Model Dimension Six Operators III: Gauge Coupling Dependence and Phenomenology". In: JHEP 04 (2014), p. 159. DOI: 10.1007/JHEP04(2014)159. arXiv: 1312.2014 [hep-ph].

[100] A. Dedes et al. "Feynman rules for the Standard Model Effective Field Theory in R_ξ -gauges". In: JHEP 06 (2017), p. 143. DOI: 10.1007/JHEP06(2017)143. arXiv: 1704.03888 [hep-ph].

[101] Adam Alloul et al. "FeynRules 2.0 - A complete toolbox for tree-level phenomenology". In: Comput. Phys. Commun. 185 (2014), pp. 2250–2300. DOI: 10.1016/j.cpc.2014.04.012. arXiv: 1310.1921 [hep-ph].

[102] Sebastian Bruggisser, Danny van Dyk, and Susanne Westhoff. "Resolving the flavor structure in the MFV-SMEFT". In: JHEP 02 (2023), p. 225. DOI: 10.1007/JHEP02(2023)225. arXiv: 2212.02532 [hep-ph].

USC UNIVERSIDADE DE SANTIAGO DE COMPOSTELA

[103] Ilaria Brivio and Michael Trott. "The Standard Model as an Effective Field Theory". In: Phys. Rept. 793 (2019), pp. 1–98. DOI: 10.1016/j.physrep.2018.11.002. arXiv: 1706.08945 [hep-ph].

[104] J. de Blas et al. "Effective description of general extensions of the Standard Model: the complete tree-level dictionary". In: JHEP 03 (2018), p. 109. DOI: 10.1007/JHEP03(2018)109. arXiv: 1711.10391 [hep-ph].

[105] Johann Brehmer et al. "Pushing Higgs Effective Theory to its Limits". In: Phys. Rev. D 93.7 (2016), p. 075014. DOI: 10.1103/PhysRevD.93.075014. arXiv: 1510.03443 [hep-ph].

[106] Sally Dawson, Samuel Homiller, and Samuel D. Lane. "Putting standard model EFT fits to work". In: Phys. Rev. D 102.5 (2020), p. 055012. DOI: 10.1103/PhysRevD.102.055012. arXiv: 2007.01296 [hep-ph].

[107] Tyler Corbett et al. "EWPD in the SMEFT to dimension eight". In: JHEP 06 (2021), p. 076. DOI: 10.1007/JHEP06(2021)076. arXiv: 2102.02819 [hep-ph].

[108] Ilaria Brivio. "SMEFTsim 3.0 — a practical guide". In: JHEP 04 (2021), p. 073. DOI: 10.1007/JHEP04(2021)073. arXiv: 2012.11343 [hep-ph].

[109] Ilaria Brivio, Yun Jiang, and Michael Trott. "The SMEFTsim package, theory and tools". In: JHEP 12 (2017), p. 070. DOI: 10.1007/JHEP12(2017)070. arXiv: 1709.06492 [hep-ph].

[110] Céline Degrande et al. "Automated one-loop computations in the standard model effective field theory". In: Phys. Rev. D 103.9 (2021), p. 096024. DOI: 10.1103/PhysRevD.103.096024. arXiv: 2008.11743 [hep-ph].

[111] Jacob J. Ethier et al. "Combined SMEFT interpretation of Higgs, diboson, and top quark data from the LHC". In: JHEP 11 (2021), p. 089. DOI: 10.1007/JHEP11(2021)089. arXiv: 2105.00006 [hep-ph].

[112] John Ellis et al. "Top, Higgs, Diboson and Electroweak Fit to the Standard Model Effective Field Theory". In: JHEP 04 (2021), p. 279. DOI: 10.1007/JHEP04(2021)279. arXiv: 2012.02779 [hep-ph].

[113] Anke Biekoetter, Tyler Corbett, and Tilman Plehn. "The Gauge-Higgs Legacy of the LHC Run II". In: SciPost Phys. 6.6 (2019), p. 064. DOI: 10.21468/SciPostPhys.6.6.064. arXiv: 1812.07587 [hep-ph].

[114] Emanuele Bagnaschi et al. "SMEFT analysis of m_W". In: JHEP 08 (2022), p. 308. DOI: 10.1007/JHEP08(2022)308. arXiv: 2204.05260 [hep-ph].

[115] Ilaria Brivio et al. "Truncation, validity, uncertainties". In: (Jan. 2022). arXiv: 2201.04974 [hep-ph].

[116] Aielet Efrati, Adam Falkowski, and Yotam Soreq. "Electroweak constraints on flavorful effective theories". In: JHEP 07 (2015), p. 018. DOI: 10.1007/JHEP07(2015)018. arXiv: 1503.07872 [hep-ph].

USC UNIVERSIDADE DE SANTIAGO DE COMPOSTELA

[117] Adam Falkowski and David Straub. "Flavourful SMEFT likelihood for Higgs and electroweak data". In: JHEP 04 (2020), p. 066. DOI: 10.1007/JHEP04(2020)066. arXiv: 1911.07866 [hep-ph].

[118] Admir Greljo, Ajdin Palavrić, and Anders Eller Thomsen. "Adding Flavor to the SMEFT". In: JHEP 10 (2022), p. 010. DOI: 10.1007/JHEP10(2022)005. arXiv: 2203.09561 [hep-ph].

[119] Darius A. Faroughy et al. "Flavour symmetries in the SMEFT". In: JHEP 08 (2020), p. 166. DOI: 10.1007/JHEP08(2020)166. arXiv: 2005.05366 [hep-ph].

[120] Sebastian Bruggisser et al. "The Flavor of UV Physics". In: JHEP 05 (2021), p. 257. DOI: 10.1007/JHEP05(2021)257. arXiv: 2101.07273 [hep-ph].

[121] Andreas Crivellin et al. "Global Electroweak Fit and Vector-Like Leptons in Light of the Cabibbo Angle Anomaly". In: JHEP 12 (2020), p. 166. DOI: 10.1007/JHEP12(2020)166. arXiv: 2008.01113 [hep-ph].

[122] Andreas Crivellin et al. "Global fit of modified quark couplings to EW gauge bosons and vector-like quarks in light of the Cabibbo angle anomaly". In: JHEP 03 (2023), p. 234. DOI: 10.1007/JHEP03(2023)234. arXiv: 2212.06862 [hep-ph].

[123] Sally Dawson and Pier Paolo Giardino. "Higgs decays to ZZ and $Z\gamma$ in the standard model effective field theory: An NLO analysis". In: Phys. Rev. D97.9 (2018), p. 093003. DOI: 10.1103/PhysRevD.97.093003. arXiv: 1801.01136 [hep-ph].

[124] Sally Dawson and Pier Paolo Giardino. "Electroweak corrections to Higgs boson decays to $\gamma\gamma$ and W^+W^- in standard model EFT". In: Phys. Rev. D98.9 (2018), p. 095005. DOI: 10.1103/PhysRevD.98.095005. arXiv: 1807.11504 [hep-ph].

[125] Jonathan M. Cullen and Benjamin D. Pecjak. "Higgs decay to fermion pairs at NLO in SMEFT". In: JHEP 11 (2020), p. 079. DOI: 10.1007/JHEP11(2020)079. arXiv: 2007.15238 [hep-ph].

[126] A. Dedes, K. Suxho, and L. Trifyllis. "The decay $h \to Z\gamma$ in the Standard-Model Effective Field Theory". In: JHEP 06 (2019), p. 115. DOI: 10.1007/JHEP06(2019)115. arXiv: 1903.12046 [hep-ph].

[127] A. Dedes et al. "The decay $h \to \gamma\gamma$ in the Standard-Model Effective Field Theory". In: JHEP 08 (2018), p. 103. DOI: 10.1007/JHEP08(2018)103. arXiv: 1805.00302 [hep-ph].

[128] Christine Hartmann, William Shepherd, and Michael Trott. "The Z decay width in the SMEFT: y_t and λ corrections at one loop". In: JHEP 03 (2017), p. 060. DOI: 10.1007/JHEP03(2017)060. arXiv: 1611.09879 [hep-ph].

[129] Christine Hartmann and Michael Trott. "Higgs Decay to Two Photons at One Loop in the Standard Model Effective Field Theory". In: Phys. Rev. Lett. 115.19 (2015), p. 191801. DOI: 10.1103/PhysRevLett.115.191801. arXiv: 1507.03568 [hep-ph].

USC UNIVERSIDADE DE SANTIAGO DE COMPOSTELA

[130] Sally Dawson and Pier Paolo Giardino. "Electroweak and QCD corrections to Z and W pole observables in the standard model EFT". In: Phys. Rev. D 101.1 (2020), p. 013001. DOI: 10.1103/PhysRevD.101.013001. arXiv: 1909.02000 [hep-ph].

[131] Sally Dawson and Ahmed Ismail. "Standard model EFT corrections to Z boson decays". In: Phys. Rev. D98.9 (2018), p. 093003. DOI: 10.1103/PhysRevD.98.093003. arXiv: 1808.05948 [hep-ph].

[132] Sally Dawson and Pier Paolo Giardino. "Flavorful electroweak precision observables in the Standard Model effective field theory". In: Phys. Rev. D 105.7 (2022), p. 073006. DOI: 10.1103/PhysRevD.105.073006. arXiv: 2201.09887 [hep-ph].

[133] Ilaria Brivio et al. "O new physics, where art thou? A global search in the top sector". In: JHEP 02 (2020), p. 131. DOI: 10.1007/JHEP02(2020)131. arXiv: 1910.03606 [hep-ph].

[134] Lina Alasfar et al. "B anomalies under the lens of electroweak precision". In: JHEP 12 (2020), p. 016. DOI: 10.1007/JHEP12(2020)016. arXiv: 2007.04400 [hep-ph].

[135] Radja Boughezal et al. "Top quark decay at next-to-leading order in the Standard Model Effective Field Theory". In: (2019). arXiv: 1907.00997 [hep-ph].

[136] G. D'Ambrosio et al. "Minimal flavor violation: An Effective field theory approach". In: Nucl. Phys. B 645 (2002), pp. 155–187. DOI: 10.1016/S0550-3213(02)00836-2. arXiv: hep-ph/0207036.

[137] Andreas Crivellin et al. "First-generation new physics in simplified models: from low-energy parity violation to the LHC". In: JHEP 10 (2021), p. 221. DOI: 10.1007/JHEP10(2021)221. arXiv: 2107.13569 [hep-ph].

[138] Julien Baglio, Sally Dawson, and Ian M. Lewis. "An NLO QCD effective field theory analysis of W^+W^- production at the LHC including fermionic operators". In: Phys. Rev. D 96.7 (2017), p. 073003. DOI: 10.1103/PhysRevD.96.073003. arXiv: 1708.03332 [hep-ph].

[139] Ilaria Brivio and Michael Trott. "Scheming in the SMEFT... and a reparameterization invariance!" In: JHEP 07 (2017). [Addendum: JHEP 05, 136 (2018)], p. 148. DOI: 10.1007/JHEP07(2017)148. arXiv: 1701.06424 [hep-ph].

[140] Thomas Hahn. "Generating Feynman diagrams and amplitudes with FeynArts 3". In: Comput. Phys. Commun. 140 (2001), pp. 418–431. DOI: 10.1016/S0010-4655(01)00290-9. arXiv: hep-ph/0012260 [hep-ph].

[141] R. Mertig, M. Bohm, and Ansgar Denner. "FEYN CALC: Computer algebraic calculation of Feynman amplitudes". In: Comput. Phys. Commun. 64 (1991), pp. 345–359. DOI: 10.1016/0010-4655(91)90130-D.

[142] Vladyslav Shtabovenko, Rolf Mertig, and Frederik Orellana. "New Developments in FeynCalc 9.0". In: Comput. Phys. Commun. 207 (2016), pp. 432–444. DOI: 10.1016/j.cpc.2016.06.008. arXiv: 1601.01167 [hep-ph].

USC UNIVERSIDADE DE SANTIAGO DE COMPOSTELA

[143] G. Passarino and M. J. G. Veltman. "One Loop Corrections for e+ e- Annihilation Into mu+ mu- in the Weinberg Model". In: Nucl. Phys. B 160 (1979), pp. 151–207. DOI: 10.1016/0550-3213(79)90234-7.

[144] Charalampos Anastasiou and Kirill Melnikov. "Higgs boson production at hadron colliders in NNLO QCD". In: Nucl. Phys. B646 (2002), pp. 220–256. DOI: 10.1016/S0550-3213(02)00837-4. arXiv: hep-ph/0207004 [hep-ph].

[145] O. V. Tarasov. "Generalized recurrence relations for two loop propagator integrals with arbitrary masses". In: Nucl. Phys. B502 (1997), pp. 455–482. DOI: 10.1016/S0550-3213(97)00376-3. arXiv: hep-ph/9703319 [hep-ph].

[146] Stephen P. Martin. "Evaluation of two loop selfenergy basis integrals using differential equations". In: Phys. Rev. D68 (2003), p. 075002. DOI: 10.1103/PhysRevD.68.075002. arXiv: hep-ph/0307101 [hep-ph].

[147] Alexander V. Smirnov. "FIRE5: a C++ implementation of Feynman Integral REduction". In: Comput. Phys. Commun. 189 (2015), pp. 182–191. DOI: 10.1016/j.cpc.2014.11.024. arXiv: 1408.2372 [hep-ph].

[148] W. F. L. Hollik. "Radiative Corrections in the Standard Model and their Role for Precision Tests of the Electroweak Theory". In: Fortsch. Phys. 38 (1990), pp. 165–260. DOI: 10.1002/prop.2190380302.

[149] Giuseppe Degrassi, Paolo Gambino, and Pier Paolo Giardino. "The $m_W - m_Z$ interdependence in the Standard Model: a new scrutiny". In: JHEP 05 (2015), p. 154. DOI: 10.1007/JHEP05(2015)154. arXiv: 1411.7040 [hep-ph].

[150] Ilaria Brivio et al. "Electroweak input parameters". In: (Nov. 2021). arXiv: 2111.12515 [hep-ph].

[151] Chien-Yi Chen, S. Dawson, and Cen Zhang. "Electroweak Effective Operators and Higgs Physics". In: Phys. Rev. D89.1 (2014), p. 015016. DOI: 10.1103/PhysRevD.89.015016. arXiv: 1311.3107 [hep-ph].

[152] Margherita Ghezzi et al. "NLO Higgs effective field theory and κ-framework". In: JHEP 07 (2015), p. 175. DOI: 10.1007/JHEP07(2015)175. arXiv: 1505.03706 [hep-ph].

[153] "Review of Particle Physics". In: Phys. Rev. D 98 (3 Aug. 2018), p. 030001. DOI: 10.1103/PhysRevD.98.030001. URL: https://link.aps.org/doi/10.1103/PhysRevD.98.030001.

[154] Ayres Freitas. "Higher-order electroweak corrections to the partial widths and branching ratios of the Z boson". In: JHEP 04 (2014), p. 070. DOI: 10.1007/JHEP04(2014)070. arXiv: 1401.2447 [hep-ph].

[155] Ievgen Dubovyk et al. "Complete electroweak two-loop corrections to Z boson production and decay". In: Phys. Lett. B783 (2018), pp. 86–94. DOI: 10.1016/j.physletb.2018.06.037. arXiv: 1804.10236 [hep-ph].

[156] Ievgen Dubovyk et al. "Electroweak pseudo-observables and Z-boson form factors at two-loop accuracy". In: (2019). arXiv: 1906.08815 [hep-ph].

USC UNIVERSIDADE DE SANTIAGO DE COMPOSTELA

[157] M. Awramik, M. Czakon, and A. Freitas. "Electroweak two-loop corrections to the effective weak mixing angle". In: JHEP 11 (2006), p. 048. DOI: 10.1088/1126-6708/2006/11/048. arXiv: hep-ph/0608099 [hep-ph].

[158] M. Awramik et al. "Two-loop electroweak fermionic corrections to sin**2 theta**b anti-b(eff)". In: Nucl. Phys. B813 (2009), pp. 174–187. DOI: 10.1016/j.nuclphysb.2008.12.031. arXiv: 0811.1364 [hep-ph].

[159] M. Awramik et al. "Precise prediction for the W boson mass in the standard model". In: Phys. Rev. D69 (2004), p. 053006. DOI: 10.1103/PhysRevD.69.053006. arXiv: hep-ph/0311148 [hep-ph].

[160] Jens Erler and Matthias Schott. "Electroweak Precision Tests of the Standard Model after the Discovery of the Higgs Boson". In: Prog. Part. Nucl. Phys. 106 (2019), pp. 68–119. DOI: 10.1016/j.ppnp.2019.02.007. arXiv: 1902.05142 [hep-ph].

[161] Gi-Chol Cho et al. "The MSSM confronts the precision electroweak data and the muon g-2". In: JHEP 11 (2011), p. 068. DOI: 10.1007/JHEP11(2011)068. arXiv: 1104.1769 [hep-ph].

[162] Jose R. Espinosa et al. "Probing for Invisible Higgs Decays with Global Fits". In: JHEP 09 (2012), p. 126. DOI: 10.1007/JHEP09(2012)126. arXiv: 1205.6790 [hep-ph].

[163] Laure Berthier and Michael Trott. "Consistent constraints on the Standard Model Effective Field Theory". In: JHEP 02 (2016), p. 069. DOI: 10.1007/JHEP02(2016)069. arXiv: 1508.05060 [hep-ph].

[164] Yiming Liu et al. "Probing top-quark operators with precision electroweak measurements*". In: Chin. Phys. C 46.11 (2022), p. 113105. DOI: 10.1088/1674-1137/ac82e1. arXiv: 2205.05655 [hep-ph].

[165] Sally Dawson and Pier Paolo Giardino. "New physics through Drell-Yan standard model EFT measurements at NLO". In: Phys. Rev. D 104.7 (2021), p. 073004. DOI: 10.1103/PhysRevD.104.073004. arXiv: 2105.05852 [hep-ph].

[166] S. Dawson, P. P. Giardino, and A. Ismail. "Standard model EFT and the Drell-Yan process at high energy". In: Phys. Rev. D 99.3 (2019), p. 035044. DOI: 10.1103/PhysRevD.99.035044. arXiv: 1811.12260 [hep-ph].

[167] Claude Duhr, Falko Dulat, and Bernhard Mistlberger. "Drell-Yan Cross Section to Third Order in the Strong Coupling Constant". In: Phys. Rev. Lett. 125.17 (2020), p. 172001. DOI: 10.1103/PhysRevLett.125.172001. arXiv: 2001.07717 [hep-ph].

[168] Claude Duhr, Falko Dulat, and Bernhard Mistlberger. "Charged current Drell-Yan production at N^3LO". In: JHEP 11 (2020), p. 143. DOI: 10.1007/JHEP11(2020)143. arXiv: 2007.13313 [hep-ph].

USC UNIVERSIDADE DE SANTIAGO DE COMPOSTELA

[169] Thomas Becher and Tobias Neumann. "Fiducial q_T resummation of color-singlet processes at N^{3}LL+NNLO". In: JHEP 03 (2021), p. 199. DOI: 10.1007/JHEP03(2021)199. arXiv: 2009.11437 [hep-ph].

[170] Emanuele Re, Luca Rottoli, and Paolo Torrielli. "Fiducial Higgs and Drell-Yan distributions at N^{3}LL′+NNLO with RadISH". In: (Apr. 2021). DOI: 10.1007/JHEP09(2021)108. arXiv: 2104.07509 [hep-ph].

[171] Wojciech Bizoń et al. "Fiducial distributions in Higgs and Drell-Yan production at N^{3}LL+NNLO". In: JHEP 12 (2018), p. 132. DOI: 10.1007/JHEP12(2018)132. arXiv: 1805.05916 [hep-ph].

[172] William B. Kilgore and Christian Sturm. "Two-Loop Virtual Corrections to Drell-Yan Production at order $\alpha_s\alpha^3$". In: Phys. Rev. D 85 (2012), p. 033005. DOI: 10.1103/PhysRevD.85.033005. arXiv: 1107.4798 [hep-ph].

[173] Federico Buccioni et al. "Mixed QCD-electroweak corrections to on-shell Z production at the LHC". In: Phys. Lett. B 811 (2020), p. 135969. DOI: 10.1016/j.physletb.2020.135969. arXiv: 2005.10221 [hep-ph].

[174] Maximilian Delto et al. "Mixed QCD⊗QED corrections to on-shell Z boson production at the LHC". In: JHEP 01 (2020), p. 043. DOI: 10.1007/JHEP01(2020)043. arXiv: 1909.08428 [hep-ph].

[175] Radja Boughezal, Ye Li, and Frank Petriello. "Disentangling radiative corrections using the high-mass Drell-Yan process at the LHC". In: Phys. Rev. D 89.3 (2014), p. 034030. DOI: 10.1103/PhysRevD.89.034030. arXiv: 1312.3972 [hep-ph].

[176] Luca Buonocore, Massimiliano Grazzini, and Francesco Tramontano. "The q_T subtraction method: electroweak corrections and power suppressed contributions". In: Eur. Phys. J. C 80.3 (2020), p. 254. DOI: 10.1140/epjc/s10052-020-7815-z. arXiv: 1911.10166 [hep-ph].

[177] Stefan Dittmaier, Timo Schmidt, and Jan Schwarz. "Mixed NNLO QCD×electroweak corrections of $\mathcal{O}(N_f\alpha_s\alpha)$ to single-W/Z production at the LHC". In: JHEP 12 (2020), p. 201. DOI: 10.1007/JHEP12(2020)201. arXiv: 2009.02229 [hep-ph].

[178] Roberto Bonciani et al. "Next-to-Next-to-Leading Order Mixed QCD-Electroweak Corrections to on-Shell Z Production". In: Phys. Rev. Lett. 125.23 (2020), p. 232004. DOI: 10.1103/PhysRevLett.125.232004. arXiv: 2007.06518 [hep-ph].

[179] Matthias Heller et al. "Mixed EW-QCD two-loop amplitudes for $q\bar{q} \to \ell^+\ell^-$ and γ_5 scheme independence of multi-loop corrections". In: JHEP 05 (2021), p. 213. DOI: 10.1007/JHEP05(2021)213. arXiv: 2012.05918 [hep-ph].

[180] Jonathan M. Cullen, Benjamin D. Pecjak, and Darren J. Scott. "NLO corrections to $h \to b\bar{b}$ decay in SMEFT". In: (2019). arXiv: 1904.06358 [hep-ph].

[181] Rhorry Gauld, Benjamin D. Pecjak, and Darren J. Scott. "QCD radiative corrections for $h \to b\bar{b}$ in the Standard Model Dimension-6 EFT". In: Phys. Rev. D94.7 (2016), p. 074045. DOI: 10.1103/PhysRevD.94.074045. arXiv: 1607.06354 [hep-ph].

USC UNIVERSIDADE DE SANTIAGO DE COMPOSTELA

[182] Christine Hartmann and Michael Trott. "Higgs Decay to Two Photons at One Loop in the Standard Model Effective Field Theory". In: Phys. Rev. Lett. 115.19 (2015), p. 191801. DOI: 10.1103/PhysRevLett.115.191801. arXiv: 1507.03568 [hep-ph].

[183] Christine Hartmann and Michael Trott. "On one-loop corrections in the standard model effective field theory; the $\Gamma(h \to \gamma\gamma)$ case". In: JHEP 07 (2015), p. 151. DOI: 10.1007/JHEP07(2015)151. arXiv: 1505.02646 [hep-ph].

[184] Radja Boughezal, Emanuele Mereghetti, and Frank Petriello. "Dilepton production in the SMEFT at O(1/Λ4)". In: Phys. Rev. D 104.9 (2021), p. 095022. DOI: 10.1103/PhysRevD.104.095022. arXiv: 2106.05337 [hep-ph].

[185] R. V. Harlander, S. Y. Klein, and M. Lipp. "FeynGame". In: Comput. Phys. Commun. 256 (2020), p. 107465. DOI: 10.1016/j.cpc.2020.107465. arXiv: 2003.00896 [physics.ed-ph].

[186] Jorge de Blas, Mikael Chala, and Jose Santiago. "Global Constraints on Lepton-Quark Contact Interactions". In: Phys. Rev. D 88 (2013), p. 095011. DOI: 10.1103/PhysRevD.88.095011. arXiv: 1307.5068 [hep-ph].

[187] Michael Carpentier and Sacha Davidson. "Constraints on two-lepton, two quark operators". In: Eur. Phys. J. C 70 (2010), pp. 1071–1090. DOI: 10.1140/epjc/s10052-010-1482-4. arXiv: 1008.0280 [hep-ph].

[188] Adam Falkowski, Martín González-Alonso, and Kin Mimouni. "Compilation of low-energy constraints on 4-fermion operators in the SMEFT". In: JHEP 08 (2017), p. 123. DOI: 10.1007/JHEP08(2017)123. arXiv: 1706.03783 [hep-ph].

[189] Vincenzo Cirigliano, Martin Gonzalez-Alonso, and Michael L. Graesser. "Non-standard Charged Current Interactions: beta decays versus the LHC". In: JHEP 02 (2013), p. 046. DOI: 10.1007/JHEP02(2013)046. arXiv: 1210.4553 [hep-ph].

[190] Víctor Bresó-Pla, Adam Falkowski, and Martín González-Alonso. "A_{FB} in the SMEFT: precision Z physics at the LHC". In: (Mar. 2021). arXiv: 2103.12074 [hep-ph].

[191] Marco Farina et al. "Energy helps accuracy: electroweak precision tests at hadron colliders". In: Phys. Lett. B 772 (2017), pp. 210–215. DOI: 10.1016/j.physletb.2017.06.043. arXiv: 1609.08157 [hep-ph].

[192] Adam Alloul et al. "FeynRules 2.0 ? A complete toolbox for tree-level phenomenology". In: Computer Physics Communications 185.8 (Aug. 2014), 2250?2300. ISSN: 0010-4655. DOI: 10.1016/j.cpc.2014.04.012. URL: http://dx.doi.org/10.1016/j.cpc.2014.04.012.

[193] U. Baur, S. Keller, and D. Wackeroth. "Electroweak radiative corrections to W boson production in hadronic collisions". In: Phys. Rev. D 59 (1999), p. 013002. DOI: 10.1103/PhysRevD.59.013002. arXiv: hep-ph/9807417.

USC UNIVERSIDADE DE SANTIAGO DE COMPOSTELA

[194] U. Baur et al. "Electroweak radiative corrections to neutral current Drell-Yan processes at hadron colliders". In: Phys. Rev. D 65 (2002), p. 033007. DOI: 10.1103/PhysRevD.65.033007. arXiv: hep-ph/0108274.

[195] Stefan Dittmaier and Michael Krämer. "Electroweak radiative corrections to W boson production at hadron colliders". In: Phys. Rev. D 65 (2002), p. 073007. DOI: 10.1103/PhysRevD.65.073007. arXiv: hep-ph/0109062.

[196] Stefan Dittmaier and Max Huber. "Radiative corrections to the neutral-current Drell-Yan process in the Standard Model and its minimal supersymmetric extension". In: JHEP 01 (2010), p. 060. DOI: 10.1007/JHEP01(2010)060. arXiv: 0911.2329 [hep-ph].

[197] Ansgar Denner and Stefan Dittmaier. "Electroweak Radiative Corrections for Collider Physics". In: Phys. Rept. 864 (2020), pp. 1–163. DOI: 10.1016/j.physrep.2020.04.001. arXiv: 1912.06823 [hep-ph].

[198] Ansgar Denner. "Techniques for calculation of electroweak radiative corrections at the one loop level and results for W physics at LEP-200". In: Fortsch. Phys. 41 (1993), pp. 307–420. DOI: 10.1002/prop.2190410402. arXiv: 0709.1075 [hep-ph].

[199] Albert M Sirunyan et al. "Measurement of the differential Drell-Yan cross section in proton-proton collisions at $\sqrt{s} = 13$ TeV". In: JHEP 12 (2019), p. 059. DOI: 10.1007/JHEP12(2019)059. arXiv: 1812.10529 [hep-ex].

[200] Giuseppe Degrassi et al. "On the NLO QCD corrections to gluon-initiated ZH production". In: JHEP 08 (2022), p. 009. DOI: 10.1007/JHEP08(2022)009. arXiv: 2205.02769 [hep-ph].

[201] Lina Alasfar et al. "Virtual QCD corrections to $gg \to$ ZH via a transverse momentum expansion". In: PoS LHCP2022 (2023), p. 343. DOI: 10.22323/1.422.0343.

USC UNIVERSIDADE DE SANTIAGO DE COMPOSTELA

List of publications

In the following pages, we show all the relevant information about the publications used in the thesis. We have reproduced part of their content in Chapters 3 and 5.

Gluon Fusion Production at NLO:
Merging the Transverse Momentum and the High-Energy Expansions

Authors

Luigi Bellafronte[a], Giuseppe Degrassi[b], Pier Paolo Giardino[a],
Ramona Gröber[c], Marco Vitti[b]

(a) Instituto Galego de Física de Altas Enerxías, Universidade de Santiago de Compostela, 15782 Santiago de Compostela, Galicia-Spain
(b) Dipartimento di Matematica e Fisica, Università di Roma Tre and INFN, sezione di Roma Tre, I-00146 Rome, Italy
(c) Dipartimento di Fisica e Astronomia 'G. Galilei', Università di Padova and INFN, sezione di Padova, I-35131 Padova, Italy

PhD Student Contribution

Collaboration in the calculations presented in the paper, as well as in the discussions and writing.

Used in Chapter : 3

Journal and Article Information

Journal name: Journal of High Energy Physics

Publisher: Springer Nature

ISSN: 1029-8479

Year of publication: 2022

DOI: 10.1007/JHEP07(2022)069

Impact factor in 2022: 5.4

The article is distributed under the terms of the Creative Commons Attribution License (CC-BY 4.0), which permits any use, distribution and reproduction in any medium, provided the original author(s) and source are credited.

The Importance of Flavor in SMEFT Electroweak Precision Fits

Authors

Luigi Bellafronte[a], Sally Dawson[b], Pier Paolo Giardino[a],

(a) Instituto Galego de Física de Altas Enerxías, Universidade de Santiago de Compostela, 15782 Santiago de Compostela, Galicia-Spain
(b) High Energy Theory Group, Department of Physics, Brookhaven National Laboratory, Upton, NY 11973, USA

PhD Student Contribution

Collaboration in the calculations presented in the paper, as well as in the discussions and writing.

Used in Chapter : 5

Journal and Article Information

Journal name: Journal of High Energy Physics

Publisher: Springer Nature

ISSN: 1029-8479

Year of publication: 2023

DOI: 10.1007/JHEP05(2023)208

Impact factor in 2022: 5.4

The article is distributed under the terms of the Creative Commons Attribution License (CC-BY 4.0), which permits any use, distribution and reproduction in any medium, provided the original author(s) and source are credited.

USC UNIVERSIDADE DE SANTIAGO DE COMPOSTELA

Permissions of content reuse

In Fig 3.1 we show plots from [15, 16]. The reproduction of these contents is allowed under the Creative Commons Attribution License (CC-BY 4.0), which permits any use, distribution and reproduction in any medium, provided the original author(s) and source are credited.
All the other figures presented in this thesis are original works of the author or they reproduce contents from the papers mentioned in A.3. As already stated, the use these figures is allowed under the Creative Commons Attribution License (CC-BY 4.0).

USC
UNIVERSIDADE DE SANTIAGO DE COMPOSTELA

USC
UNIVERSIDADE
DE SANTIAGO
DE COMPOSTELA

Resumo da tese (en galego)

A investigación dos fenómenos naturais foi unha das forzas impulsoras do avance científico. No que respecta á física de partículas, esta busca levou ao desenvolvemento do Modelo Estándar (SM), un marco teórico extraordinariamente exitoso que describe e clasifica as partículas elementais e as súas interaccións. Isto culminou na descuberta do bosón de Higgs en 2012 [11, 12], marcando un paso esencial cara a unha comprensión satisfactoria do mecanismo que está na base da ruptura de simetría electrofeble (EWSB). A EWSB está na base do SM, xa que é o mecanismo polo cal os bosóns W e Z adquiren a súa masa. Ademais, o acoplamento dos diferentes fermións co bosón de Higgs proporciona a estes as súas masas. Non obstante, a pesar dos seus triunfos, o SM deixa sen resposta moitas cuestións teóricas e experimentais, como as oscilacións dos neutrinosa materia escura, a enerxía escura ou a asimetría entre materia e antimateria no universo. Dende un punto de vista teórico, podemos mencionar a xerarquía das masas dos fermións, o misterio da orixe do potencial de Higgs e a inclusión da gravidade (máis alá do nivel clásico) no marco do SM. Polo tanto, espérase que a unha escala de enerxías máis alta se atope física máis alá do SM (BSM).

Neste contexto, os colisionadores de partículas xogaron un papel crucial na conformación da nosa comprensión das leis fundamentais do universo. Máis alá do descubrimento dos bosón W no Colisionador de Protóns e Antiprotóns, a construción de colisionadores de alta enerxía como o Tevatron, LEP e o Gran Colisionador de Hadrons (LHC) en CERN, o maior acelerador de partículas nunca construído, permitiu aos científicos probar os seus modelos a escalas de enerxía cada vez máis altas, impulsando descubrimentos e confirmando teorías. Tras a descuberta do bosón de Higgs, ningún das observables medidas indicou claramente a escala de enerxía da física BSM. De feito, só se detectaron eventos preditos polo SM nos colisionadores de partículas.

Nos últimos anos, a medida precisa dos procesos do SM tomou un papel destacado como instrumento fundamental na procura de nova física. Anomalías en medidas de precisión, como desviacións dos valores esperados, poden ser unha indicación indirecta de novos fenómenos. De feito, a través de efectos *off shell* e de *loop*, podemos observar a influencia de novas partículas sen producilas directamente.

En xeral, os fenómenos que estamos a buscar teñen unha probabilidade moi baixa de ocorrer, o que fai que o proceso de detección sexa complicada. Este aspecto é especial-

USC UNIVERSIDADE DE SANTIAGO DE COMPOSTELA

mente relevante na física de precisión, xa que a medida de pequenas variacións fronte ás predicións require unha gran cantidade de datos. Unha das motivacións centrais detrás da futura actualización de alta luminosidade (HL) do LHC [13] é o desenvolvemento das capacidades do LHC como máquina de precisión. O aumento de luminosidade facilita a xeración de máis datos, o que non só permite un exame máis completo de mecanismos establecidos, senón que, como xa se mencionou, tamén abre a porta á observación de novos fenómenos inesperados.

Por exemplo, proxéctase que o futuro HL LHC xere un mínimo de 15 millóns de bosóns de Higgs ao ano, un aumento significativo en comparación cos aproximadamente tres millóns recollidos durante o funcionamento do LHC en 2017 [14] que nos permitirá impoñer restricións máis severas sobre moitos parámetros do SM. Neste contexto, a fusión de gluóns, que xa é o mecanismo de produción máis relevante [15, 16] para a producción do bosón de Higgs, será aínda máis significativa. Este proceso xoga un papel importante na produción de dobre Higgs, $gg \to HH$, e tamén é relevante na produción dun bosón de Higgs en asociación cun bosón Z, $gg \to ZH$. Estes dous mecanismos de producción son moi importantes para a física do Higgs: a primeira recibe contribucións da interacción trilineal do Higgs, un dos poucos acoplamentos do SM que aínda non foi medida; a segunda é un dos principais canles para ZH e permite estudar os desintegracións do Higgs a quarks b, un proceso complexo de observar nos colisionadores hadrónicos debido ao fondo de QCD. Por esta razón, nesta tese estudamos as contribucións virtuais de segunda orde (NLO) para estes procesos.
Sen dúbida, o esforzo experimental debe complementarse cun nivel equivalente de traballo teórico. Isto é esencial porque, para que as medidas teñan importancia,as nosas predicións do SM deben ter unha precisión comparable cos resultados experimentais.

Este raciocinio tamén se aplica ás teorías máis alá do SM, e é especialmente importante cando se consideran Teorías Efectivas de Campo (EFT). De feito, sen depender dun modelo BSM, unha extensión do SM con operadores de maior dimensión ofrece unha maneira importante de describir fenómenos indirectos BSM. Un dos métodos máis comúnmente utilizados para estudar os efectos da nova física é a Teoría Efectiva de Campo do Modelo Estándar (SMEFT), que mantén a mesma composición de campos e simetrías que o SM. Neste contexto, investigar as propiedades dos bosóns gauge electrofeble masivos (W e Z) ten un potencial significativo para buscas indirectas de física BSM, tendo en conta que as interaccións que involucran fotóns e gluóns están altamente restrinxidas polas simetrías gauge non rotas. Podemos dividir en dúas clases os procesos que foron estudados para explorar esta dirección. A primeira inclúe os procesos de producción de moitos bosóns (multi-bosón) en colisionadores de alta enerxía; a segunda implica os procesos de dispersión de fermións mediados por bosóns W/Z en canles s ou t, tamén coñecidos como Observables de Precisión Electrofeble (EWPOs). Nesta tese centrámonos nestes últimos.
Nas últimas décadas, os EWPOs ofreceron claras indicacións de que o SM describe de forma precisa a física á escala electrofeble, xa que son sensibles a modificacións dos

USC UNIVERSIDADE DE SANTIAGO DE COMPOSTELA

acoplamentos dos bosóns gauge con fermións e das masas dos bosóns gauge.

Nos últimos anos, a análise destas medidas tamén se estendeu máis alá do marco do SM. De feito, dentro da aproximación SMEFT, a comparación de EWPOs coas predicións teóricas pode poñer límites significativos nos coeficientes asociados á nova física. Neste contexto, a nivel de primeira orde ou árbore (LO) en SMEFT, realizáronse numerosos estudos, extraendo límites nos coeficientes dos operadores de dimensión 6 a partir de axustes globais en EWPOs e outros observables [17, 18, 19, 20]. Dadas estas consideracións, é razoable considerar a extensión dos cálculos ás contribucións de segunda orde (NLO). Nesta tese, calculamos as contribucións de NLO tanto en Cromodinámica Cuántica (QCD) como en teoría electrofeble, considerando unha estrutura de sabor arbitraria para os operadores fermiónicos. Como veremos a continuación, estes cálculos permítennos non só estudar o impacto das correccións de NLO nos coeficientes de LO, senón que tamén nos dan a posibilidade de restrinxir coeficientes que non aparecen a nivel de árbore.
No que respecta ao estudo dos EWPOs, debemos tamén ter en conta que é unha das motivacións detrás da construción planificada de moitos futuros colisionadores [21]. De feito, a investigación destes observables en colisionadores e^+e^- ten as vantaxes derivadas do estado inicial limpo e controlado, mentres que outros colisionadores, como o LHC, están afectados por grandes incertezas sistemáticas debido ás funcións de distribución de partóns e outros efectos de QCD. Polo tanto, colisionadores como o Colisionador Lineal Internacional (ILC) [22, 23, 24] e o Futuro Colisionador Circular ee (Fcc-ee) [25, 26], poden ter potencialmente unha maior sensibilidade para EWPOs que os colisionadores hadrónicos. Como se discutiu en [21], agárdase que as incertezas estatísticas e sistemáticas proxectadas destes futuros colisionadores melloren a precisión dos valores experimentais actuais. Estas máquinas están sendo propostas para a súa construción en distintos lugares do mundo (Xapón e o CERN respectivamente), e teñen un custo tanto material como en termos de traballo moi considerable (da orde de miles de millóns de euros), polo que a motivación precisa das posibilidades de atopar fenómenos físicos interesantes é crucial. Considerado isto, usando os nosos resultados para os EWPOs, realizamos un análise cos valores de erro esperados.

Outro proceso relevante que podemos mencionar para buscas indirectas de física máis alá do SM, é a dispersión de Drell-Yan. En particular, o proceso neutro de Drell-Yan, onde $pp \to Z/\gamma \to l^+l^-$, tivo unha importancia fundamental en confirmar as predicións da SM e, ademais, moi diversas aplicacións. Por exemplo, foi útil para explorar escenarios de nova física, como a presenza de bosóns Z' de alta masa. Os resultados actuais da SM concordan perfectamente cos datos experimentais [27, 28], o que indica que a física BSM, dentro da produción de DY, aparece a unha escala de enerxía alta ou ten un acoplamento moi débil, o que fai da súa detección un desafío difícil para os actuais dispositivos experimentais.
A próxima actualización do HL-LHC espera ter un impacto significativo no estudo do proceso de Drell-Yan. De feito, o aumento da luminosidade incrementará o número de

USC UNIVERSIDADE DE SANTIAGO DE COMPOSTELA

eventos producidos e unha mostra estatística máis grande permitirá medidas máis precisas. Ademais, aínda que o HL-LHC funcionará aproximadamente á mesma enerxía hadrónica ($\sim$ 14 TeV) que o LHC actual, o aumento da luminosidade permitiranos explorar enerxías de colisión máis altas a nivel partónico. O LHC acelera protones, pero as colisións reais ocorren entre quarks e gluóns. Estas partículas internas conteñen só unha porción da enerxía do protón e é moi pouco probable que leven enerxías próximas á totalidade da enerxía do protón, facendo que as colisións de alta enerxía sexan moi raras. Por tanto, un enfoque directo para aumentar o número destas colisións é aumentar a taxa de colisión ou, en outras palabras, aumentar a luminosidade do colisionador. No marco da SMEFT, fenómenos de nova física poden manifestarse á medida que as escalas de enerxía partónica aumentan, esixindo cálculos precisos da SMEFT que están máis alá dos resultados actuais do SM para o proceso de Drell-Yan. Por esta razón, calculamos contribucións de NLO para esta dispersión co obxectivo de estudar a distribución de enerxía asociada.

O obxectivo principal desta tese é probar os fenómenos físicos no LHC e nos futuros colisionadores, proporcionando cálculos precisos de observables sensibles á física BSM. Como xa se mencionou, os cálculos precisos de observables xogaron un papel crucial na nosa busca por comprender a natureza. De feito, permitíronnos probar rigorosamente as teorías formuladas para comprender o universo. Por esta razón, nesta tese calculamos as correccións perturbativas a procesos do SM e da SMEFT que son fenomenoloxicamente relevantes para a física no LHC e nos futuros colisionadores. Estes inclúen:

- A corrección de NLO para a produción dun par de bosóns H e bosóns HZ a través de fusión de gluóns. O cálculo destes procesos é extremadamente importante para a medida experimental das propiedades do Higgs e para medir a súa largura. En particular, a produción dobre de Higgs é significativamente relevante debido ao acoplamento triplo de Higgs involucrado no cálculo, acoplamento nunca medido experimentalemente.
- O cálculo de EWPOs a segunda orde (NLO) en expansións de QCD e electrofebles da SMEFT cunha estrutura de fermións arbitraria para os operadores. Espérase que os axustes numéricos NLO da SMEFT a EWPOs teñan unha forte dependencia das estruturas de sabor asumidas: comprobaremos isto usando diversas suposicións populares sobre simetrías de sabores.
- Producción de Drell-Yan na SMEFT a NLO; este proceso é moi importante para detectar sinais de nova física e polo tanto ter predicións teóricas precisas na teoría efectiva de campos é crucial. Os efectos dos operadores de catro fermións nesta amplitude son un novo desafío e nos darán información esencial sobre a estrutura da física máis alá do SM, en particular sobre a estrutura de sabores.

Todos os cálculos necesarios realizáronse de forma analítica. Aínda que hai métodos puramente numéricos que se poderían usar, as técnicas híbridas numéricas/analíticas

USC UNIVERSIDADE DE SANTIAGO DE COMPOSTELA

xeralmente son máis flexibles e máis fáciles de adaptar para usos máis amplos, como as teorías efectivas de campos, que as puramente numéricas. Ademais, requiren menos recursos computacionais, o que as fai máis axeitadas para construír xeradores de Monte Carlo eficientes. Por estas razóns, os cálculos analíticos son máis convenientes para os nosos obxectivos.

O estudo da física de precisión no SM e nas súas extensións implica a aplicación de ferramentas para o cálculo de procesos relevantes para a fenomenoloxía do LHC e dos futuros colisionadores. A metodoloxía empregada para lograr os nosos obxectivos inclúe o uso de códigos públicos e privados implementados no software Mathematica. As amplitudes relevantes para o espallamento ou a desintegración no análise son xeradas con FeynArts [1] e usamos Feyncalc, LiteRed e Fire [2, 3, 4] para reducir as amplitudes a unha combinación de *Master Integrals* (MI). As integrais de Feynman calcúlanse a través de métodos estándar cando sexa posible e a través de técnicas de expansión de enerxía cando sexa necesario. A nivel dun bucle, usamos as funcións de Passarino-Veltman como base para as MI e as avaliacións analíticas realizáronse a través de FeynHelpers [5]. Usamos os *Padé approximants* para mellorar a converxencia das expansións de enerxía e permitirnos ampliar a validez destas técnicas a rexións do espazo de fases onde estes métodos poderían fallar. Este método aplícase a procesos físicos como $gg \to HZ$ e $gg \to HH$ co obxectivo de mellorar a precisión dos resultados obtidos en [6, 7] e permitirnos reproducir cos resultados de [8]. Desta maneira, podemos facer unha predición en cada punto do espazo de parámetros con alta precisión. Os problemas derivados da presenza de γ^5 e varias matrices de Dirac tratámolos coa técnica de regularización de Kreimer [9], unha ferramenta potente que preserva a simetría quiral do Modelo Estándar en todos os cálculos perturbativos espidos. Todos os cálculos da SMEFT realízanse na base de Varsovia co ficheiro de modelo de FeynArts obtido de [10]. Ademais, usamos gráficos e diagramas de barras para presentar os nosos resultados fenomenolóxicos.

Esta tese divídese do seguinte xeito:

- No Capítulo 2 proporcionamos unha breve revisión do SM, incluíndo procedementos de regularización e renormalización. Comezamos revisando os tensores de forza de campo de gauge e as súas derivadas. A continuación, analizamos con detalle como funciona o mecanismo de Higgs no caso dunha simetría de gauge non abeliana, isto é, no caso da SM. Centrándonos no sector fermiónico, estudamos o problema de xerar masas para quarks e leptóns e as súas interaccións co Higgs e os bosóns de gauge. Lémbrase que, no SM, non está permitido introducir termos de masa renormalizables na lagranxiana posto que os fermións a dereitas e a esquerdas teñen números cuánticos distintos. Por último, analizamos os procedementos de regularización e renormalización, analizando algúns dos métodos que utilizaremos nesta tese.

- No Capítulo 3, analizamos as correccións virtuais do SM á produción de Higgs a través de $gg \to HH$ e $gg \to ZH$ a nivel de NLO; en particular, demostramos que

USC UNIVERSIDADE DE SANTIAGO DE COMPOSTELA

é posible cubrir toda a rexión do espazo de fases mediante a fusión de dúas expansións complementarias presentes na literatura, a expansión en p_T e a expansión de alta enerxía (HE) [29, 30]. Xa que as avaliacións numéricas das dúas expansións son bastante rápidas desde un punto de vista computacional, este método permite unha avaliación rápida das correccións virtuais á produción de Higgs a través da fusión de gluóns que é precisa en todo o espazo de fases. Comezamos cunha visión xeral dos procesos examinados, antes de mergullarnos en aspectos máis técnicos do cálculo. A continuación, introducimos as diferentes expansións, así como o método para combiná-las. Despois, validamos o método a nivel de LO tanto no nivel de factores de forma como no nivel da sección transversal partónica, cun enfoque no proceso $gg \to HH$. Por último, presentamos a fusión das dúas expansións a nivel de NLO. Para mostrar a flexibilidade da nosa estratexia respecto á modificación dos parámetros de entrada, presentamos o resultado da contribución virtual de dous *loops* en $gg \to HH$ e $gg \to ZH$ para dúas escollas diferentes da masa do quark top, en particular a masa *on shell* e a masa $\overline{\text{MS}}$.

- No Capítulo 4, discutimos o método EFT e as principais características da SMEFT, explicando as virtudes e os límites deste marco. En particular, enfocámonos na chamada base de Varsovia para os operadores da SMEFT, usándoa como marco teórico empregado para os cálculos nos Capítulos 5 e 6.

- No Capítulo 5, dentro da SMEFT, presentamos resultados para EWPOs a nivel de NLO tanto en QCD como na expansión EW considerando unha estrutura de sabores arbitraria para os operadores de fermións. Ademáis, asumindo escenarios de sabores específicos, realizamos axustes aos EWPOs incluíndo tamén análises con incertezas proxectadas dos futuros colisionadores. Comezamos cunha visión xeral do estado actual dos cálculos de EWPOs, incluíndo suposicións sobre sabores. Despois, construímos a forma xeral dos coeficientes de fermións de 2 e 4 partículas que ocorren nos cálculos dun *loop* de EWPOs correspondentes a diferentes suposicións de sabor. A continuación, describimos a renormalización a NLO electrofeble e QCD de EWPOs con énfase nos papeis dos operadores fermiónicos de 2 e 4 partículas. Amosamos resultados fenomenolóxicos demostrando o papel importante das suposicións de sabor nos axustes da SMEFT[102]. Vemos que aínda incluíndo suposicións de sabor máis xerais que análises anteriores, moitas direccións sen explorar permanecen nos axustes. Finalmente, estudamos perspectivas futuras considerando as incertezas que se proxectan para os futuros colisionadores.

- No Capítulo 6, proporcionamos contribucións analíticas de NLO QCD e electrofeble para o proceso neutro de Drell-Yan, con todos os operadores de dimensión-6 no marco da SMEFT. Tras unha breve introdución sobre o proceso de Drell-Yan, explicamos a notación usada neste capítulo. A continuación, presentamos o noso cálculo de LO para o proceso DY, mostrando de forma explícita o caso de estados

USC UNIVERSIDADE DE SANTIAGO DE COMPOSTELA

iniciais de quark up. Ademais, analizamos en detalle o cálculo das contribucións de NLO, explicando como tratamos os diferentes diagramas de Feynman e amosamos as contribucións reais á sección transversal partónica, divididas en termos suaves, *Parton distribution functions* (PDFs) e colineares. En particular, neste caso, os termos das PDFs refírense ás contribucións colineares do estado inicial que son parcialmente reabsorbidas na definición de ditas funcións. Por último, proporcionamos un estudo fenomenolóxico inicial para $O_{qq}^{(3)}$.

- No Capítulo 7, presentamos os nosos resultados e conclusións con perspectivas á liña de investigación explorada nesta tese.

O cálculo de observables sensibles é unha tarefa desafiante e debe ser realizada para obter resultados que se poidan comparar con datos experimentais. Para mellorar o noso coñecemento da natureza, nesta tese exploramos moitos fenómenos físicos relacionados coa física de precisión. Poderiamos agardar máis investigación dalgúns deles no futuro.

USC
UNIVERSIDADE DE SANTIAGO DE COMPOSTELA

USC
UNIVERSIDADE
DE SANTIAGO
DE COMPOSTELA

This thesis focuses on precision physics within the Standard Model (SM) and the Standard Model Effective Field Theory (SMEFT) framework. It shows the importance of precise calculations, particularly at high-energy colliders such as the Large Hadron Collider (LHC) and future machines like the Fcc-ee. These predictions are relevant for exploring new physics and understanding the structure of theories beyond the SM. The processes studied are Higgs production from gluon fusion, Drell Yan scattering and electroweak precision observables, with the aim of providing accurate results for testing at future colliders.